Secondary Crystallisation and Degradation During Long Term Aging of P(HB-co-HV)

By

Kate Elizabeth Robbins

UNIVERSITY OF BIRMINGHAM

A thesis submitted to the University of Birmingham

for the degree of

Doctor of Philosophy

School of Metallurgy & Materials

College of Engineering & Physical Sciences

University of Birmingham

December 2016

ABSTRACT

Polyhydroxybutyrate-co-hydroxyvalerate (P(HB-co-HV)) is a bacterially synthesised, and therefore sustainable, copolymer of PHB which biodegrades into H_2O and CO_2. It has similar properties to polymers such as polypropylene just after processing, so has a potential use as a packaging material to replace polymers from petrochemical sources. However, P(HB-co-HV) continues to increase in crystallinity over time in a process known as secondary crystallisation, which causes embrittlement of the polymer. In this work, the temperature dependence of the secondary crystallisation process was studied.

Time-temperature experiments were carried out by conditioning samples at a range of temperatures (–22, 7, 20, 50, 75, 100, 125 and 150 °C), for up to 672 hours. Various mechanical and thermal properties were measured, and changes resulting from storage at 7 to 125 °C can be attributed to the secondary crystallisation process. Generally, higher storage temperatures caused a greater extent of change in the measured variables, showing that the rate of secondary crystallisation is temperature dependent and increases with temperature. Differential scanning calorimetry (DSC) showed that storage at 20 to 125 °C increased the crystallinity (61.1 to 65.6 % at 20 °C, and 64.5 to 78.6 % at 125 °C), and the peak melting temperature (T_m) (172.8 to 173.6 °C at 50 °C, and 171.5 to 179.2 °C at 125 °C). A crystallinity index, generated from infrared spectroscopy (IR) data, generally followed the trends observed in the DSC data. The observed changes in crystallinity corresponded to changes in the mechanical properties of the samples. The Young's modulus and the ultimate tensile strength (UTS) increased over time with storage from 7 to 125 °C (Young's modulus increased from 1346 to 1869 MPa at 20 °C and from 1302 to 1599 MPa at 125 °C, UTS increased from 31.4 to 33.8 at 20 °C and from 31.6 to 32.4 at 125 °C), while the elongation to break decreased (16.9 to 9.3 % at 20 °C, and 14.6 to 6.8 % at 125 °C). Through dynamic mechanical thermal analysis (DMTA) an increase in the

glass transition temperature (T_g) (16.5 to 21.4 °C at 20 °C, and 15.8 to 29.7 °C at 125 °C), a decrease in tanδ peak height (0.09 to 0.05 at 20 °C, and 0.08 to 0.06 at 125 °C), and a re-distribution of the tanδ peak area to a more symmetrical peak were observed in samples stored at 7 to 125 °C.

Following the initial increase in crystallinity, T_m, and T_g of samples stored at 150 °C, the values plateaued then decreased. Crystallinity increased from 64.5 % to 88.7 %, then decreased to 76.8 %, and the T_m increased from 172.9 °C to 180.0 °C then decreased to 169.2 °C. The tanδ peak was seen to decrease in height and broaden over time, and a prominent shoulder emerged on the lower temperature side of the DSC melting peak. After 48 hours, the embrittlement was so severe that tensile testing was no longer possible. Samples stored at 150 °C also discoloured, becoming dark brown, and over 672 hours lost more than 30 % of their original mass. A decrease in molecular weight (M_w), from a unimodal distribution of 215 505 g mol^{-1} to a bimodal distribution of 3373 and 10 100 g mol^{-1}, was also observed. Along with the data from DSC, IR, DMTA and mechanical testing, this indicates that thermal degradation occurred during storage at 150 °C. These results indicate an interesting interplay between the effects of the secondary crystallisation process and degradation (~30 °C below the melting point).

ACKNOWLEDGEMENTS

Firstly, I would like to give my sincere thanks to my supervisor Dr. Mike Jenkins, for all his guidance and encouragement, with which he was always generous throughout the entirety of my PhD.

I would like to express my gratitude to Frank Biddlestone; without his seemingly endless technical knowledge this work would not have been possible.

For all of the support, advice and many constructive discussions, I would like to thank Dr. Catherine Kelly.

I am indebted to Annabel, Joe and Cat for providing continuous encouragement and entertainment, helping me to keep things in perspective, and for making the lab an enjoyable place to work.

I would also like to thank my family and friends for their love, support and unfaltering belief in me; as well as for putting up with me being late, leaving early, or not being there at all, to allow me to put the hours in and get the job done.

Finally, a special mention must go to my husband, Andy, who never failed to make things better. I will be forever grateful.

CONTENTS

CHAPTER 1 – INTRODUCTION

1.1 Polymer microstructure

Thermoplastics are classified as being either amorphous or semi-crystalline materials depending on their microstructure. Amorphous polymers are completely disordered, and semi-crystalline polymers are a combination of highly ordered crystals and disordered amorphous regions.

1.1.1 Amorphous polymers

Amorphous polymers exist in a liquid-like state. At high temperatures, where the viscosity is low and the motion of the chains is high, the polymer chains are continuously rotating and reptating due to conformational changes along the length of the main chain, forming random coils in a disordered material. On reducing the temperature, the viscosity increases, and the polymer cools to a 'rubbery' state as large scale motion is reduced. Amorphous polymers have insufficient structural regularity to allow crystallisation to occur during cooling, so further reductions in temperature decreases the mobility until no further movement of the chains is possible. This is because the "thermal energy is insufficient to overcome the rotational energy barriers in the chain" [1]. The temperature of this change is called the glass transition temperature (T_g), and corresponds to an abrupt change in the properties of the polymer, as it changes from a rubbery, ductile material, to a rigid, brittle one. At this point the chains are 'frozen' in place, in whatever random orientation they were in just above the T_g. The glass

transition is a change in mobility, rather than a change in structure, meaning that the material is still amorphous, just unable to move. In this state, the polymer is said to be glassy.

1.1.2 Semi-crystalline polymers

It is extremely unlikely to attain a perfectly crystalline polymer, as that would require extensive organisation of tangled, highly coiled chains from the melt. Instead semi-crystalline polymers are formed, so called because they are comprised of highly ordered crystalline regions, with disordered amorphous regions trapped between them.

The crystalline regions are made up of aligned and folded chains forming structures called lamellae. Various models have been proposed as to the exact morphology of the lamella. These include the regular folded array, whereby re-entry of the chains into the lamella after folding is adjacent and regular (Figure 1.1a), and the switchboard model, where chain folding is not as extensive and re-entry is random (Figure 1.1b). The regular re-entry model does not account for a significant proportion of the material remaining in the amorphous phase, which is known to be the case when polymers are crystallised from the melt. On the other hand, the random switchboard model allows for chains which loop and re-enter into the same lamella, chains which have free ends extending out of the lamella, and chains which exit one lamella and re-enter into an adjacent lamella (known as tie-molecules), thus accounting for a significant amorphous phase.

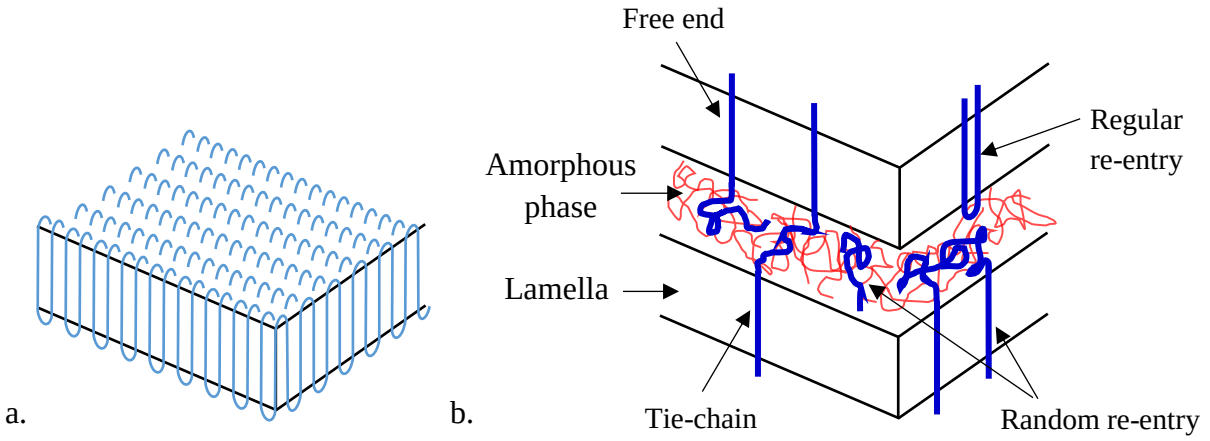

Figure 1.1. Schematics of the possible morphology of a. the regular re-entry model, and b. the switchboard model, indicating examples of chains with free ends, tie-chains, and random and adjacent re-entry into the lamella (the red lines indicate chains entirely within the amorphous region).

Models such as that in Figure 1.1b are favoured, and have been further developed to suggest a 3-phase model. The 3-phase model proposes that the structure should be thought of in terms of a crystalline fraction, a mobile amorphous fraction (MAF), and a rigid amorphous fraction (RAF) (Figure 1.2)

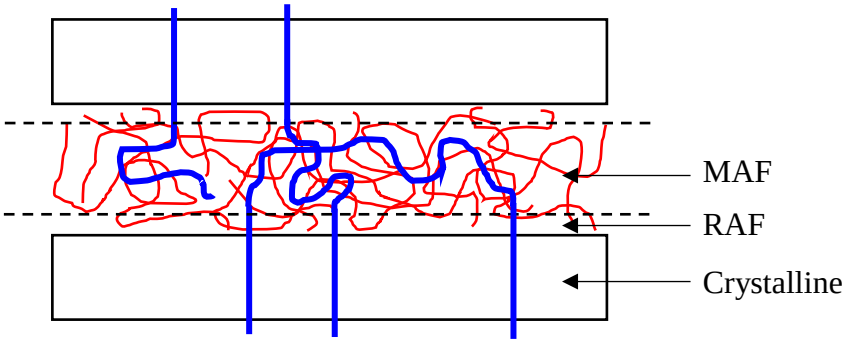

Figure 1.2. Schematic of the 3-phase model, indicating the crystalline, rigid amorphous, and mobile amorphous fractions.

In this model, the MAF is the ‘classic’ amorphous material, where no part of the chain is ordered. The RAF is the material between the crystalline fractions and MAF, which is made up of sections of the chains exiting the crystal lamella. In the RAF, motion of the chains is limited

because part of the chain is held in place in the lamella, so even though the segment of the chain in the RAF is amorphous, it's mobility is restricted.

1.2 Crystallisation

1.2.1 Nucleation and growth during the primary crystallisation process

The primary crystallisation process, of pure polymers from the disordered melt, begins via a process termed homogeneous, or thermal, primary nucleation. This happens when random rotations about the carbon-carbon atoms, which make up the backbone of the polymer chains, happen to aggregate into a structure known as an embryo. Except for very low molecular weight materials, the embryo would not be comprised from an entire polymer chain, but a portion of it [2]. These embryos have been envisaged in varying shapes, including cylinders [3,4] and bundles [2], due to the asymmetry of the polymer molecule. It is noted that the mature crystal structure does not have to mimic that of the nucleus [2].

Due to its positive surface energy, an embryo increases the Gibbs free energy, *G*, of the system. This change in free energy during crystallisation is described by

$$\Delta G = \Delta H - T\Delta S \qquad \text{(Equation 1.1)}$$

where ΔH is the enthalpy change, ΔS is the entropy change and T is the isothermal temperature [5]. At this stage an embryo may either continue to grow, or disappear. If the embryo grows, the surface energy it possesses increases with it, but the surface-to-volume ratio of the embryo decreases, so the overall positive contribution to ΔG reduces the more the embryo grows. If this continues the embryo will reach a point where the overall energy of the system begins to reduce, instead of increasing further. The point at which additional increase in embryo

size turns from increasing ΔG to decreasing ΔG is known as the critical size, and is dependent on the temperature of crystallisation [1]. Beyond the critical size, the embryo is said to be a stable primary nucleus and growth occurs spontaneously, as the decrease in G is thermodynamically favourable. This drives the system towards a negative free energy, compared to that of the original melt. A schematic representation of this process is shown in Figure 1.3.

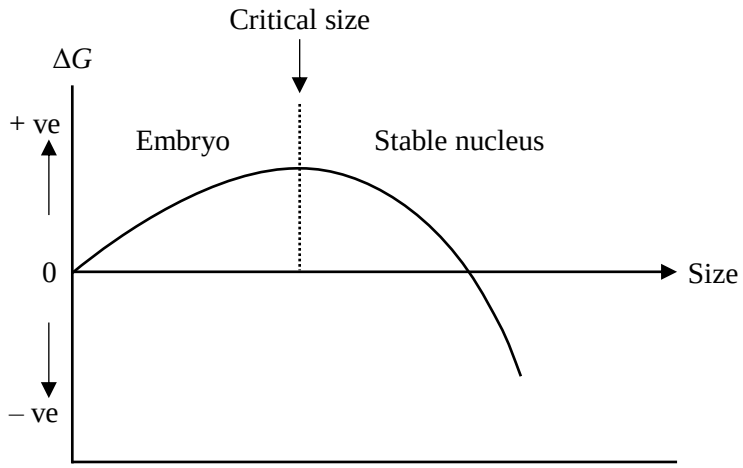

Figure 1.3. A schematic representation of the change in free energy ΔG during the nucleation process.

Once a primary nucleus is formed and stable, a secondary nucleation process onto the surface of this crystal will take place. During this process, molecules stick down onto the surface of the nucleus, causing further growth of the structure. Flexibility of the polymer chains, combined with the interaction of polar bonds, allows for chain-folding and lateral spreading across the growth face. In combination with others, Hoffman and Lauritzen [6-10] carried out extensive work on the subject of chain-folding and the growth of crystal lamella. The additional surface energy introduced when the polymer sticks down onto the primary nucleus is low, due to the smaller increase in surface area compared to increase in volume. This means that the energy barrier to secondary nucleation is lower than primary nucleation [4].

Alternatively, an impurity within the melt may also act as a primary nucleus, termed heterogeneous, or athermal, nucleation. Relatively speaking, there is a smaller energy barrier for growth directly onto an impurity compared to that of a nucleus of critical size formed from an embryo. This is because the additional surface energy introduced when the polymer attaches to the impurity is less, similar to that of the energy barrier to growth described during crystallisation by thermal nucleation.

The crystalline lamella grow radially from the nucleus, with fibrils that spread into the melt, branching out and trapping amorphous regions between them, forming structures known as spherulites. Spherulites grow radially in the melt (Figure 1.4a) until they impinge upon each other, resulting in crystals that are polyhedral in shape (Figure 1.4b).

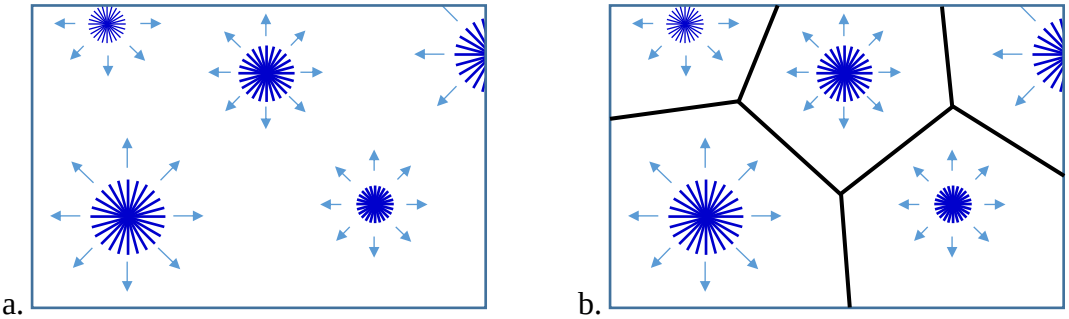

Figure 1.4. Schematic images of a. spherulitic growth from the melt, and b. crystal borders resulting from spherulitic impingement. The arrows indicate the radial growth direction of the spherulites.

At lower crystallisation temperatures, referred to as high degrees of super-cooling, nucleation is thermodynamically favourable, so many spherulites are formed. However, growth is slow as the melt is more viscous, limiting the mobility of the chains which is essential for growth, resulting in large numbers of small spherulites. Conversely, at higher temperatures of crystallisation, or low degrees of super-cooling, the segmental motion is much greater, lowering the chance of stable nucleus formation [1]. At these temperatures growth is favourable due to

the high mobility of chains within the melt, and so fewer, larger spherulites are formed [3]. Hence the rate of crystallisation is said to be growth limited at temperatures near the glass transition temperature (T_g), and nucleation limited near the melting temperature (T_m). As a result, the greatest rate of crystallisation requires a compromise between these two limiting factors, and the shortest crystallisation times are found at an optimum temperature between the T_g and T_m. This compromise impacts other aspects of the material, as it influences the microstructure and is therefore a key factor in determining the mechanical properties. Generally speaking, a polymer crystallised at high degrees of super-cooling, which has a large number of small crystals, will be more ductile, have a greater elongation at break, lower tensile strength, lower modulus, higher toughness and increased impact strength. Conversely, the same polymer crystallised at low degrees of super-cooling, which has a small number of large crystals, will be more brittle, exhibit a lower elongation at break, greater tensile strength, higher modulus, lower toughness and decreased impact strength. Knowledge of the temperature dependence of crystal structure development can, therefore, be exploited in order to obtain particular crystal structures, and consequently mechanical properties, by tailoring the processing temperatures of semi-crystalline polymers.

Differential scanning calorimetry (DSC) can be used to study the kinetics of the isothermal crystallisation of polymers. The polymer sample is first taken into the melt to erase any thermal history, then cooled to the desired crystallisation temperature where it is held until the crystallisation process is complete. Analysis of the crystallisation kinetics follows the established trend of applying the Avrami equation to the data obtained from the crystallisation exotherm.

The relationship between the phase transformation and time is used to describe both the nucleation mechanism and growth rate, by means of the Avrami equation,

$$1 - X_t = \exp(-kt^n) \qquad \text{(Equation 1.2)}$$

and by the creation of double log plots, also known as Avrami plots, plots using

$$\ln[-\ln(1 - X_t)] = \ln k + n \ln t \qquad \text{(Equation 1.3)}$$

where X_t is the fraction of crystallinity, k is the Avrami crystallisation rate constant, n is the Avrami exponent and t is time. The Avrami exponent is the sum of the values attributed to the mechanism and geometry of nucleation. The mechanism is assigned a value of either 0 or 1 for athermal nucleation (also termed heterogenous or instantaneous nucleation) or thermal nucleation (also termed homogenous or sporadic nucleation) respectively. This is due to the assumption that sporadic nucleation is a first order process, and instantaneous nucleation is a zeroth-order process. The geometry of crystal growth is assigned values of either 1, 2 or 3; indicating one dimensional rods, two dimensional discs, and three dimensional spherulites respectively [1]. As it is a combination of these two factors, nucleation mechanism and geometry of growth, *n* should be an integer from 1 to 4, as detailed in Table 1.1.

Table 1.1. Interpretation of Avrami exponent values according to nucleation mechanism and geometry of growth.

Nucleation mechanism	Dimensions of growth geometry	*n*	Resultant morphology
Instantaneous	1	1	Rods
Sporadic	1	2	
Instantaneous	2	2	Discs
Sporadic	2	3	
Instantaneous	3	3	Spheres
Sporadic	3	4	

However, as the Avrami equation makes several general assumptions, experimental data rarely produces and integer value for *n*, and will more commonly produce a non-integer value. Some of the most common assumptions are listed by Verhoyen *et al*. [11] as:

- complete transformation of the sample
- no volume change during phase transformation/crystallisation
- constant radial growth rate
- uniqueness of nucleation
- constant density and shape of the growing nuclei
- no secondary crystallization

There may be variation in the nucleation rate for example, or nucleation resulting from a combination of thermal and athermal sources, which are not accounted for by the Avrami equation.

1.2.2 Secondary crystallisation

Secondary crystallisation is a phenomenon whereby, over time, the polymer continues to increase in crystallinity following impingement of the spherulites (primary crystallisation), resulting in further embrittlement of the polymer. Primary and secondary crystallisation have been differentiated thus "secondary crystallisation takes place in a confined environment from the non-crystalline regions in the presence of existing crystals, whereas primary crystallisation is crystallisation from the free melt" [12]. In literature, the term 'secondary crystallisation' may be used to describe different mechanisms of the same phenomena, therefore readers should be careful to note which mechanism authors are referring to in their work. Secondary

crystallisation may refer to a thickening process of the lamella formed during primary crystallisation [12-14], through incorporation of chains from the amorphous phase, or to infill of smaller crystalline structures within the amorphous regions [15-17].

1.3 Glass transition and melting

Upon heating, a semi-crystalline material first goes through a glass transition temperature (T_g); which, unlike melting, is not a change in structure but a change in mobility [1]. Below the T_g the amorphous regions of a semi crystalline polymer are frozen in place, and are said to behave like a brittle glass. As the material is heated through the T_g, the thermal energy begins to initiate local motions in the amorphous chains. The glass transition occurs over a temperature range, because longer and more entangled chains require more energy to become mobile. Other factors which influence the T_g include the molecular structure, flexibility of the chains, branching, and cross-linking [1]. Above the T_g the amorphous phase achieves large scale co-operative motion, and it behaves like a more rubber. At this point, just above the T_g, the crystalline regions are still intact. However, with further increase in temperature, the highly ordered crystalline regions begin to melt as the thermal energy put into the system breaks the intramolecular bonds holding the structure in place, resulting in a completely disordered material. Just as with the glass transition, melting occurs over a temperature range, as larger, more perfect crystals are more stable and so require a greater amount of energy to break the bonds holding the structure together. Other factors which influence the T_m include flexibility of the main chains, polar groups and intermolecular bonding, chain symmetry, molar mass, branching, and side groups [1,4].

1.4 Polyhydroxybutyrate and polyhydroxybutyrate-co-hydroxyvalerate

Polyhydroxybutyrate (PHB) is a semicrystalline polymer from the polyhydroxyalkanoate (PHA) family. Produced as an intracellular carbon, by bacteria such as *Cupriavidus necator*, it is a form of natural energy storage synthesised in the presence of imbalanced nutrient supplies [18,19]. This means that, unlike those from petrochemical sources, such as polyethylene (PE), polypropylene (PP), and polystyrene (PS), PHB may be classed as a sustainable polymer as it is produced from a renewable source [20,21]. The most commonly studied metabolic pathways for the synthesis of PHB, and various PHB copolymers, are shown in Figure 1.5 [18]. The PHB homopolymer is produced from pathway I, but copolymer production requires pathways II or III for the input of CoA-derivatised monomeric units which have more than 4 carbon atoms [18]. PHB also has an innate biodegradability, degrading into non-toxic products under the correct conditions [21-23]. Owing to the combination of natural synthesis and non-harmful biodegradability, PHB may be considered as a long-term option for sustainability, replacing petrochemical polymers. PHB is currently used in speciality applications, such as drug delivery in the biomedical field, where the high cost of material production is not a limiting factor. Another research avenue for a potential application of PHB is in the coating of surgical sutures to provide antimicrobial properties, again exploiting the inherent biocompatibility and biodegradability of the polymer [24,25]. Chen and Wu reviewed other potential uses of PHAs for tissue engineering applications [26].

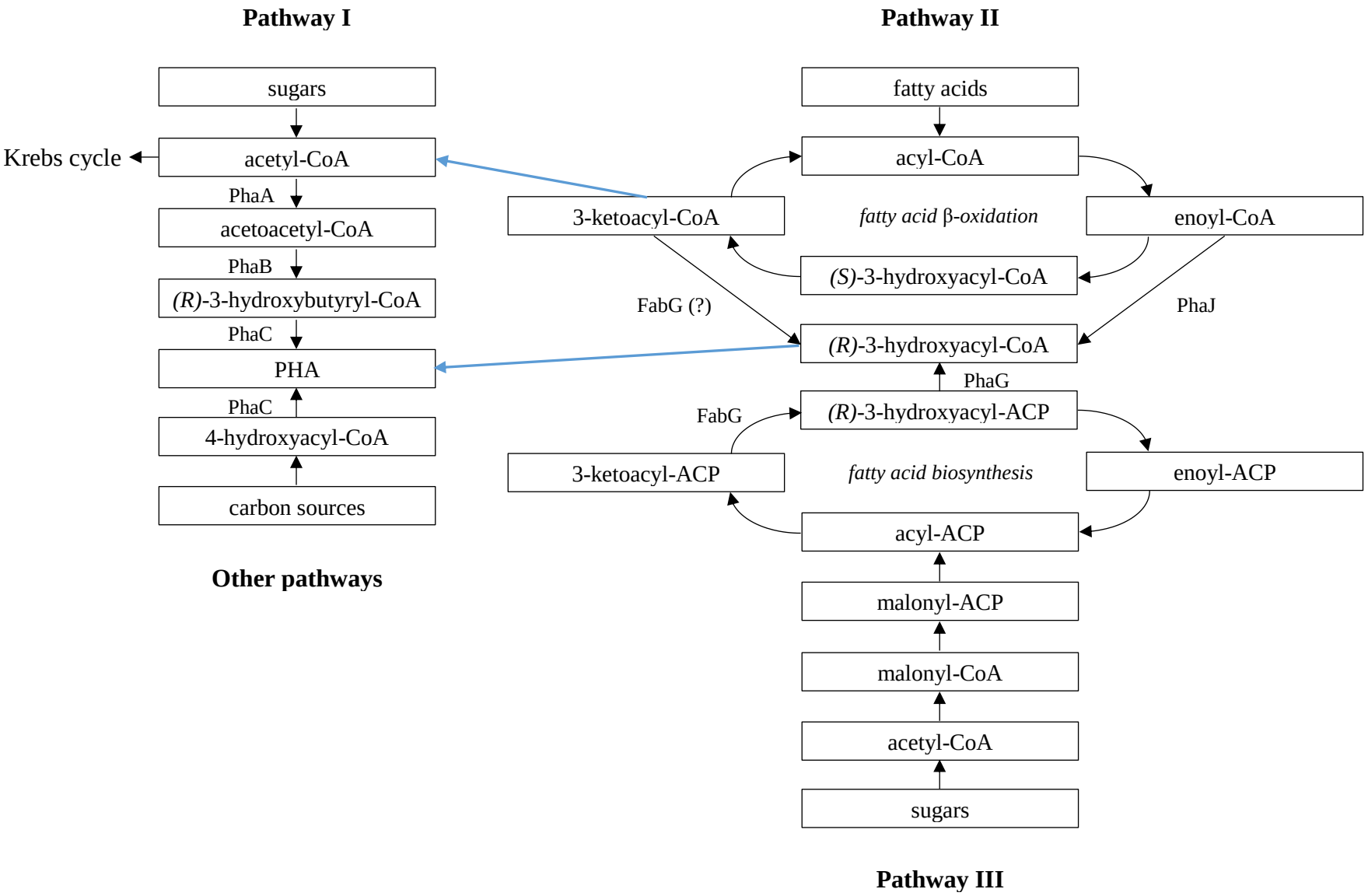

Figure 1.5. Common pathways for PHA synthesis.

The similarity of some properties, including the melting point, tensile strength and, in some cases, crystallinity of freshly processed PHB to polymers such as PP and polyethylene terephthalate (PET) [20,21,27-29], has resulted in PHB being investigated for use within the packaging industry (Table 1.2) [18,30,31]. However, in order to replace currently used polymers, such as PET, PP, PE, PS etc., with PHB, the properties for this purpose must be comparable over the lifetime of the product. A key issue is that the properties (some of which are problematic to begin with, e.g. the low elongation to break) do not remain stable over the lifetime of the material. PHB exhibits secondary crystallisation, which causes the material to become increasingly brittle when stored above its glass transition temperature [32,33]. The T_g of PHB is below room temperature (4 °C) [30], which results in embrittlement at ambient conditions, as chains in the amorphous regions are mobile and are therefore able to crystallise, altering the mechanical properties. These properties have prevented large scale commercial use of the polymer. Clearly PHB is not yet a suitable replacement for petrochemical polymers in the packaging industry, and a solution to improving the properties of PHB is required in order to consider it as being a commercially viable substitute.

Table 1.2. Comparison of the properties of PHB with those of PP and PET.

Property	PHB	PP	PET
Melting point, °C	180	176	267
Glass transition temperature, °C	4	-10	69
Crystallinity, %	60-80	50-70	30-50
Tensile strength, MPa	40	38	70
Elongation to break, %	6	400	100
CO_2 diffusion, g mm m^{-2} day^{-1}	0.09	3.2	0.1
H_2O diffusion, 10^{10} cm^3 STP cm cm^{-3} cm^{-1} Hg^{-1} s^{-1})	1.16	0.59	0.71

Many studies have emphasised that the major cause of problems with the mechanical properties of PHB are due to its high level of crystallinity, which results in brittleness of the polymer [17,29,34-37]. The degree of crystallinity is highly dependent on the polymer chain architecture. In the case of PHB, it has been discussed how the stereoregularity (Figure 1.6), due to natural synthesis, allows ease of crystallisation owing to the isotactic configuration [33].

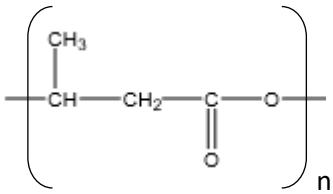

Figure 1.6. Repeat unit of PHB.

Effects of progressive embrittlement on the mechanical properties of PHB over time has been investigated via the use of tensile testing. A decrease in elongation to break of a quenched amorphous P(HB-co-8%HV), from an initial value of over 400 % to less than 10 %, and an increase in yield stress, from 18 MPa to 28 MPa, after a week of storage at room temperature has been reported [32]. The deformation of a quenched amorphous polymer is ductile, exhibiting a higher elongation at break, a lower UTS, and therefore a lower modulus than brittle polymers. This is due to the ability of amorphous chains to uncoil, slip past each other, and align under tension. Left at room temperature, above the T_g of the P(HB-co-8%HV), Biddlestone *et al.* observed a decrease in the elongation to break and an increase in the yield stress as the quenched amorphous material crystallised [32]. This happens because of the reduction in the amount of amorphous material as it forms spherulites. The crystalline chains of the spherulites are not able to uncoil as the amorphous chains do, and can only extend slightly through the bending and stretching of covalent bonds in the crystal lamella, and so the elongation to break is reduced. However, the greater strength provided by the covalent bonds

increases the tensile strength of the material. The increase in crystallinity also constrains the remaining amorphous material, restricting their ability to uncoil and extend, further restricting the extent of elongation to break. The work of de Koning [33] shows that this trend continues with progressive, or secondary, crystallisation of a melt crystallised sample. de Koning observed a logarithmic increase in tensile modulus and a decrease in elongation, from approximately 1500 MPa to 3000 MPa and a maximum of 40 % to less than 10 % respectively. This took place as the material changed from exhibiting a relatively ductile deformation behaviour to a brittle deformation behaviour after 2 weeks of storage at ambient conditions [33]. These changes were also attributed to progressive crystallisation.

In order to improve the properties of PHB for use in packaging, the degree of crystallinity must be prevented from becoming too high so that the material does not become too brittle. This would require decreasing primary crystallisation, preventing/limiting the amount of secondary crystallisation, or a combination of both. Various methods have been trialled including blending with other polymers [27,32,38,39], using nucleating agents [32,37,39,40], and cross-linking [38].

Another method of reducing the degree of crystallinity is to produce copolymers. There are many studies which have focused on the successful production of PHB copolymers; for example, copolymerisation with hydroxyhexanoate (HHx), hydroxyvalerate (HV), and polyethylene glycol (PEG) have achieved a reduction in crystallinity, and a corresponding improvement in mechanical properties above those of pure PHB [16,34,41-43]. It is understood that the addition of the copolymer disrupts the regular close packing of the crystallisation process. Polyhydroxybutyrate-co-hydroxyvalerate (P(HB-co-HV)) is one of the most commonly studied PHB copolymers, and has been commercially available since the 1980s [44]. Hydroxyvalerate (HV) is also formed naturally by bacteria, and the copolymer is easy to

manufacture by alternating the bacteria's feed stock, therefore the copolymer maintains the biodegradability and sustainability aspects of the homopolymer. It has been reported that copolymerisation with HV decreases the rate of primary crystallisation, given as a rate constant k_n, from 1.229 min^{-1} in pure PHB, to 0.224 min^{-1} in P(HB-co-5%HV) and 0.051 min^{-1} in P(HB-co-10%HV) [23]. Increasing the amount of HV present has also been shown to decrease the crystallinity of the copolymer, from 62.0 % in pure PHB, to 47.6 % in P(HB-co-5wt%HV) and 41.6 % in P(HB-co-12wt%HV) [34]. These effects are due to the increased influence of the ethyl group (Figure 1.7), which disrupts the regular close packing of the polymer chains [23]. As a result of the reduced crystallinity the mechanical properties are initially improved over those of the homopolymer, and increasing the content of HV in P(HB-co-HV) copolymers creates a less brittle material [45]. From an elongation to break of 5.6 % and tensile strength of 29.9 MPa recorded from a sample of pure PHB, copolymers with concentrations of 8, 10 and 13 mol% HV increased the elongation to break to 177, 335 and 490 % and decreased the tensile strength to 20.6, 23.4 and 16.4 MPa respectively [45]. However, P(HB-co-HV) still exhibits secondary crystallisation [32], and so the mechanical properties of P(HB-co-HV) will also deteriorate over time. The elongation to break of P(HB-co-8mol%HV) has been shown to decrease from 177 to 52 MPa after a further 18 days storage, at room temperature and to 16 MPa after 224 days [45].

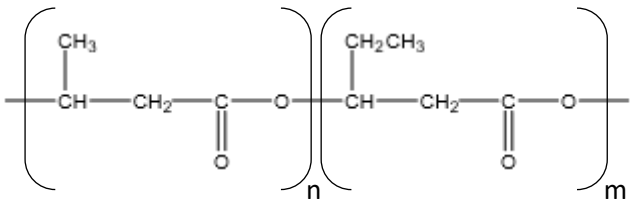

Figure 1.7. The repeat unit of P(HB-co-HV).

Infrared-spectroscopy (IR) has been used both to characterise the functional groups of PHB and P(HB-co-HV) [34,36,38,46-50], and to observe the changes to the carbonyl peak and other functional groups during primary crystallisation [49]. IR studies have been proven to be an effective means of analysing the crystallinity of PHAs as a function of blend ratios [47], copolymerisation [49], and, most significant to this study, to observe the temperature dependence of change in the crystalline and amorphous bands of PHB and P(HB-co-HV) [38,49]. Crystallisation has been found to increase the absorbance intensity of the carbonyl (1724 cm^{-1}) and ether (1275 and 1230 cm^{-1}) bands relating to crystalline material, and to decrease the carbonyl (1741 cm^{-1}) and ether (1182 cm^{-1}) bands relating to amorphous material [49]. while Melting, which occurred between 160 and 180 °C, resulted in the opposite effect [49]. The ratio of the crystalline ether band at 1230 cm^{-1} to the band at 1453 cm^{-1}, corresponding to the deformation of methylene groups which are unaffected by crystallinity, has also been used to successfully provide a crystallinity index in PHB and P(HB-co-HV) [34,49]. This crystallinity index has been used to show the increase in crystallinity resulting from primary crystallisation of solvent cast PHB samples (from 2.17 immediately after solvent evaporation to 2.57 after 12 hours) [49], as well as the increase in crystallinity of P(HB-co-5wt%HV) resulting from annealing at 120 °C (from 3.65 in the unconditioned sample, to 4.09 after 17 hours) [34].

The influence of storage time on the degree of secondary crystallisation of PHB and P(HB-co-HV), corresponding to further embrittlement, has been discussed in many previous studies [14,15,32,33,45]. Crystallinity increase with time has been observed using different techniques, including DSC, Dynamic Mechanical Analysis (DMA) and dilatometry. The melting endotherms produced from DSC have been reported to change shape as a result of further crystallisation over time, developing a low temperature component at approximately 77 °C

[32]. An increase in crystallinity from 55 to 61 % over a period of 200 hours at 25 °C has also been measured by DSC [33]. DMA has also been used to imply an increase in crystallinity by the decrease in height of the tanδ peak of PHB and P(HB-co-8%HV) upon storage at room temperature [13,32]. The work of de Koning and Lemstra used dilatometry, and presented density data as an indication of further crystallisation [33]. An increase, that was more exaggerated with higher temperatures (60 °C > 43 °C > 25 °C), was shown to occur over a time span of 200 hours. The degree of crystallinity has been observed to increase logarithmically with time through the linear correlation in a plot of increase in enthalpy of fusion against log(t) [32]. This correlates well with other findings which observed the influence of storage time, at ambient conditions, on the mechanical properties of PHB; such as a decrease in elongation to break (from ~40 % to less than 10 % after 14 days), a decrease in impact strength (from ~90 J/m to ~62 J/m), and an increase in the tensile modulus (from 15 MPa to 35 MPa) after just over 100 days of storage at room temperature [33]. Biddlestone *et al*. studied the change from quenched amorphous to semi-crystalline P(HB-co-8%HV) and found a yield stress increase from 18 to 28 MPa after 7 days, and a decrease in elongation to break from over 400 % to less than 10 % after 61 days [32]. It is generally accepted that, upon storage at room temperature, the crystallinity rises even further, significantly affecting the mechanical properties.

Whilst many studies show that the length of storage time affects secondary crystallisation, it is likely that temperature will also be an influencing factor on the rate of secondary crystallisation. It is logical that increasing the storage temperature away from the T_g of the polymer will increase the mobility of chains within the amorphous regions, and therefore the rate at which secondary crystallisation can occur. This fits with the work of de Koning and Lemstra, who noted the proximity to the T_g to be a limiting factor in progressive crystallisation [33], and the

later work of de Koning *et al*., where the exposure of injection moulded PHB samples to temperatures ranging from 95 to 147 °C was reported [13]. It was shown that the crystallinity increased with longer exposure times, up to a maximum of 20.5 hours, and the higher the temperature, the greater the increase in crystallinity. The idea of increasing secondary crystallisation rate with increasing storage temperature also fits with the work of Phillipson *et al*., which suggested that secondary crystallisation is a diffusion controlled process [51]. Several studies point out that secondary crystallisation occurs in PHB at room temperature, or at temperatures above the T_g of several other polymers [14,32,33,45,52,53]. Infrared spectroscopy has been used to show an increase in the crystallinity of P(HB-co-5wt%HV) from an original value of 47.6 % to 56.5 % after 17 hours at 120 °C [34]. X-ray diffraction (XRD) has shown P(HB-co-5wt%HV) to increase from an original value of 36.4 % to 36.6, 40.8, 38.2 and 43.7% after 1 hour at 60, 100, 130 and 150 °C respectively [54].

Multiple authors have examined the effects of annealing upon PHB and P(HB-co-HV) using DSC [13,22,32-34,55-58]. What is clear is that exposure to temperatures, greater than ambient, influences the structure of these semi-crystalline polymers even after the completion of primary crystallisation. Many who applied DSC analysis to anneal and subsequently melt samples observed multiple melting endotherms, or shoulders, to the lower temperature side of the main melting peak [13,17,22,34,54,57-61]. These developments are generally attributed to the occurrence of melting-recrystallisation-remelting (MRR) during the DSC scans; resulting from the melting of crystals of different size, perfection or lamellar thickness formed during the annealing process. It has also been discussed how the effects of the heat introduced to the sample, during the melting run, influences the data obtained by DSC; which can also cause the appearance of double melting endotherms produced by MRR. Double peaks may be truly

representative of a sample, or an artefact created by the slow heating rate, in which case a second melting run, or a faster heating rate may provide some clarity as to the cause.

Annealing studies using wide angle X-ray scattering (WAXS) and small angle X-ray scattering (SAXS) revealed an expansion of the crystal lattice with increasing temperature, until reaching such an extent whereby motion of the previously restricted chains was achieved and the lamellar thickening process could ensue [57]. In the same study, lamellar thickening is noted to increase with rising temperatures until whole melting commences. Evidence of a return of some mechanical properties, towards initial values, has been presented upon short term annealing (under 60 minutes at temperatures between 95-128 °C), despite a continued increase in crystallinity [33]. This effect increased with higher temperatures. However, upon annealing for extended lengths of time (115 °C for 1225 minutes) the sample was reported to have deteriorated due to thermal degradation [13]. Similar findings are reported elsewhere [32].

1.5 Thermal instability and degradation

PHB and P(HB-co-HV) are known to be thermally unstable at high temperatures, and to undergo thermal degradation [62-69]. Most literature only reports the thermal degradation at temperatures far above the T_m, or alludes to degradation at temperatures close to the T_m. However, the molecular weight (M_w) of PHB and P(HB-co-HV) has been shown to decrease both above [54,63,65,67,68] and below the T_m [54,67]. The M_w is a measure of chain length, and so a reduction in M_w in this circumstance is therefore an indicator of degradation. While studies that show losses above the melting point, such as the decrease from 270 000 g mol^{-1} to 29 000 g mol^{-1} in PHB held at 200 °C for 10 minutes [68], are common, fewer studies observe the decrease in M_w at lower temperatures. M_w data of PHB and P(HB-co-HV) powders heated

isothermally below the T_m has been reported [54,67]. After 20 minutes at 100 °C, Kunioka and Doi reported a decrease in the number-average molecular weight ($\bar{M}_n$) of P(HB-co-45mol%HV), from 347 000 to 327 000, and from 318 000 to 245 000 at 140 °C [67]. Chen *et al*. observed decreases in the weight-average molecular weight of P(HB-co-5wt%HV) from 620 000 to 395 000 g mol^{-1} after 30 minutes at 130 °C, and from 620 000 to 14 000 g mol^{-1} after 60 minutes at 150 °C [54]. Further increases in storage temperature resulted in greater reduction of $\bar{M}_n$ and M_w.

An increase in M_w is seen first, at very short heating times [65], due to the addition/elimination reaction between the carboxylic acid and alcohol end groups, known as esterification (Figure 1.8). This creates an ester bond between two chains, and causes the increase in M_w. The increase is short lived, however, as the end groups are rapidly used up. Grassie *et al*. reported an increase in M_w in the first 2 minutes, and subsequent decrease within 5 minutes at 170 °C [65].

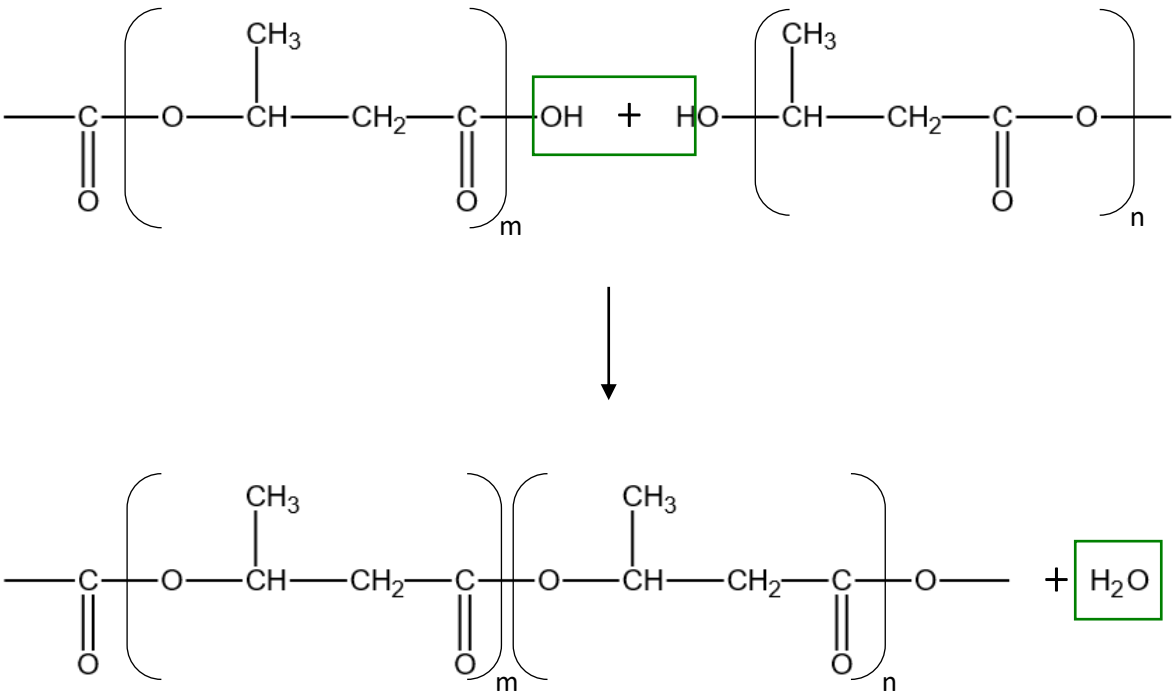

Figure 1.8. Esterification of PHB.

With further increases in time β-elimination reactions occur at the ester linkages, through the formation of a cyclic six-membered ring transition state, resulting in chain scission [28,66,67,70]. If the hydrogen in the methylene group moves in close proximity to the oxygen in the carbonyl group it interacts, causing the formation of a transient cyclic ring. This enables the scission of the ester group, resulting in the formation of two shorter chains (Figure 1.9).

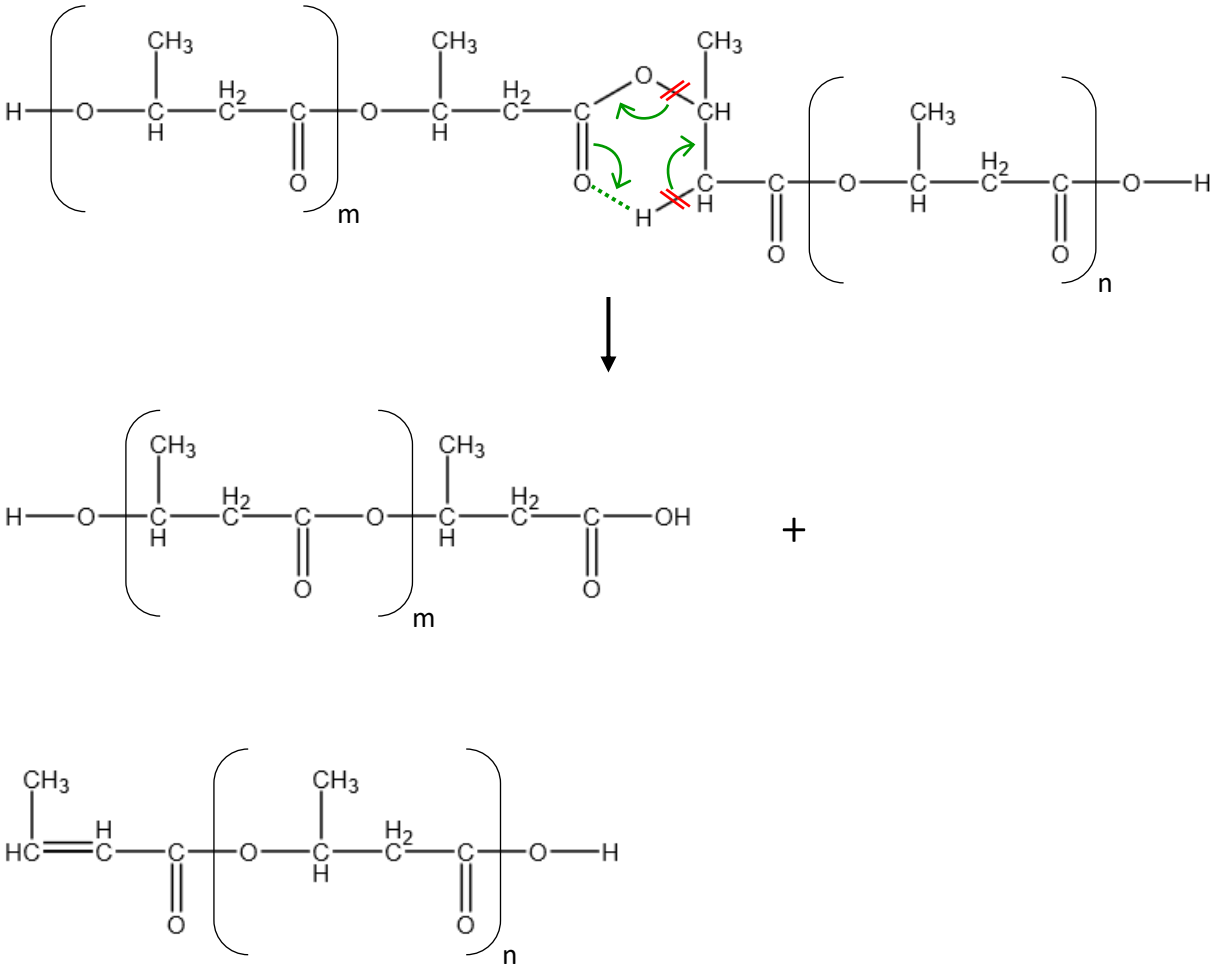

Figure 1.9. Chain scission reaction of PHB in the middle of a long chain. The green dashed line indicates a new Van der Waals bond, green arrows indicate the movement of the electron pairs, red lines indicate points at which bonds are broken.

This chain scission takes place randomly along the length of the chains, resulting either in the formation of two shorter chains, or, in the occurrence of scission at the end of the chain, the production of a shorter chain and crotonic acid (Figure 1.10).

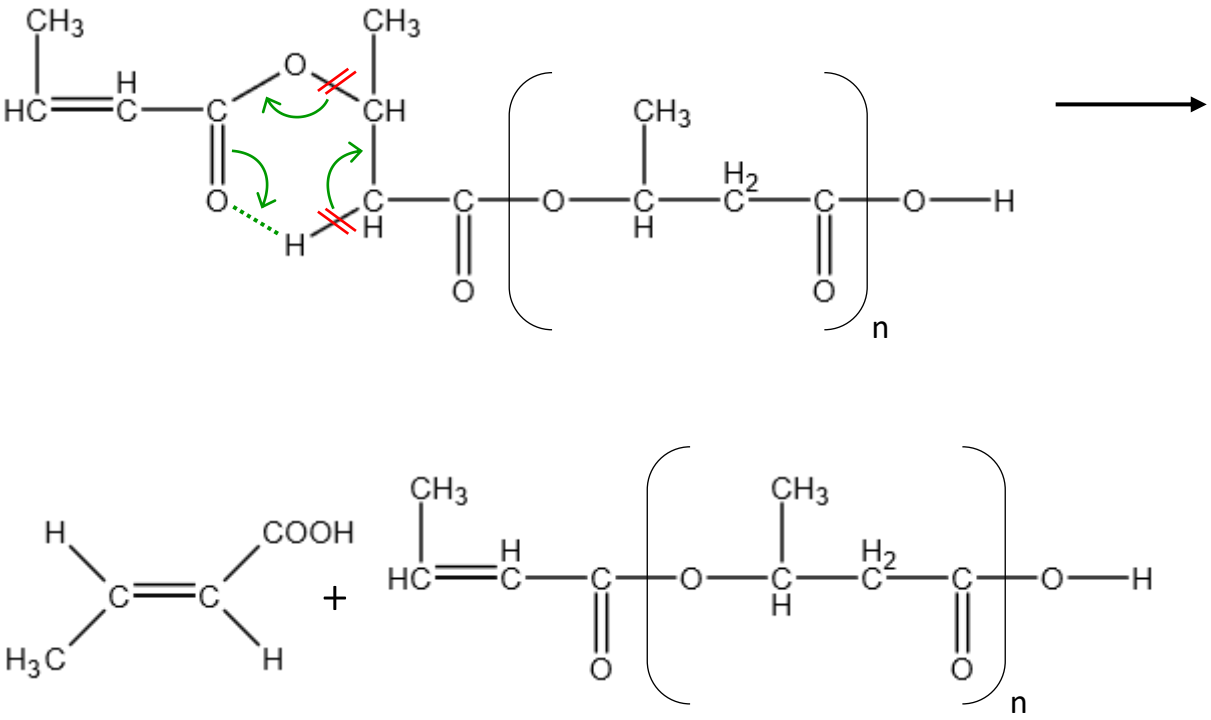

Figure 1.10. Chain scission of PHB at the end of a chain. The green dashed line indicates a new Van der Waals bond, green arrows indicate the movement of the electron pairs, red lines indicate points at which bonds are broken.

One result of the scission being random is that crotonic acid (or 2-pentenoic acid in the case of HV units) can be formed in low concentrations at relatively early stages of degradation. However, as degradation progresses and the average chain length reduces, the chance of scission occurring at the end of a chain and forming crotonic acid increases. At the same time the number of carboxylic acid end groups increases, which catalyses the degradation. Complete breakdown of the polymer results in the formation of propylene, CO_2 and CO [66].

As chain scission requires the polymer chains to be mobile, in order for the cyclic ring to form, degradation takes place in the amorphous regions [71]. At elevated temperatures or time degradation progresses to the least stable crystalline regions, which have more mobility as a result of the breakdown of the amorphous phase. The thermal degradation of PHB above the melting temperature has been studied extensively [33,54,62,64,65,67,68], and the associated effects on the material properties, such as decrease in crystallinity [54,68,69], melting temperature [68,69], molecular weight [65,67,68,72], and mechanical properties [72] are well documented. Many authors focus on thermogravimetric analysis (TGA), studying dynamic heating runs which observe degradation at temperatures far above the melting temperature [48,54,64,73]. As the foundations of most PHA based thermal degradation studies are focused on the thermal instability of PHAs at temperatures above and around the T_m [64,65,68,74,75], the suggestion of thermal degradation manifesting below the T_m is unusual. Some authors claim that the material is thermally stable below 160 °C [68,74]. There is a small amount of evidence to suggest that the number average M_w of P(HB-co-HV) powders may slowly start to decrease at temperatures as low as 100 °C when held isothermally for 20 minutes [67], and in PHB powders at 130 °C within 30 minutes, and 150 °C within 10 minutes [54]. It is widely accepted that at T_m and above**,** a random chain scission (β-elimination reaction) and subsequent auto-acceleration degradation process occurs, resulting in a decrease in molecular weight, M_w [65,67,68,74,75]. A corresponding decline in tensile properties follows the decrease in M_w [68,72]. The decrease in M_w has also been found to result in a shoulder on the lower temperature side of the melting peak of DSC traces [68,75], and to initially increase crystallinity, at the start of the degradation process, due to a combination of the increased mobility and ease of packing characteristic of shorter chains [68]. The thermal instability of PHB and its copolymers has also been studied in terms of processing issues [76,77]. A negative relationship was determined to

exist between increased processing temperature/time, with the molecular weight; and subsequently the mechanical properties of the material [77].

1.6 Summary of the most relevant literature findings

The dominating effect of crystallinity on the performance of P(HB-co-HV) has been discussed, as has the variance of crystallinity upon exposure to different temperatures [13, 32,34,54]. It is also well documented that secondary crystallisation is dependent on storage time of the polymer [13,32-34,54]. However, even the most relevant works to this study [13,32-34,54,67] have limitations on the scope of their results. The work of de Koning and Lemstra, whilst performing an extended study on the development of secondary crystallisation and subsequent effects on the mechanical properties, analysed only the PHB homopolymer, and, apart from short term annealing, the samples were only ever stored at ambient temperature [33]. Later, de Koning *et al*. built on their previous study by increasing the range of annealing temperatures and annealing times to explain the change in mechanical properties [13]. Again, only the PHB homopolymer was studied. The maximum reported length of time the polymer was successfully annealed for was 12.5 hours at 95 °C, and as the annealing temperature was increased, the duration of annealing time was decreased, extending only to 0.5 hours at 147 °C. Biddlestone *et al*. studied the P(HB-co-HV) copolymer for an extended length of time of storage at -13 and 23 °C. They also analysed the crystallisation and mechanical properties [32]. Though once again, apart from short term annealing at temperatures of 95-140 °C, the effects of an extended range of storage temperatures is not investigated. Hong and Chen analysed the effects of storage time and temperature on the development of crystallinity; yet only at two temperatures, ambient and 120 °C, for 0, 17 and 40 hours, so neither an extended range of temperatures or extended storage

times were covered in this work [34]. The effects on mechanical properties were not analysed in the work of Hong and Chen [34]. Kunioka and Doi, and Chen *et al*. both held PHB and P(HB-co-HV) powders isothermally, covering wider temperature ranges of 100 to 200 °C, and 60 to 180 °C (170 °C for P(HB-co-HV)) respectively [54,67]. However, the durations of these studies were very short, with maximums of 20 minutes and 6 hours respectively. The mechanical properties were also not studied in these works.

1.7 Project aims

As P(HB-co-HV) is a potentially desirable option for a packaging material, knowledge of the timescale of the embrittlement process is essential in determining the functional lifetime of the product. Certain applications may require the packaging to maintain its integrity for a matter of days, e.g. fresh food containers, while others may need to last for months, e.g. electrical goods packaging. Therefore, a thorough understanding of how the embrittlement process will respond to different environments is needed, as part of determining the effective lifetime of the product. A prime example of this is the variation in climates of different countries, as the temperature of use may shorten the life-span of the material if it increases the rate of embrittlement. The literature review highlighted that annealing studies of PHB and P(HB-co-HV) are common place, but that there is a distinct lack of research into the effects of long term storage on the secondary crystallisation process, and the resultant properties of the material, at temperatures other than ambient.

The present work aims to combine investigations into the thermal and mechanical properties over the complete temperature range between the T_g and T_m, for an extended length of time, in order to fully investigate the effects of secondary crystallisation on the properties of

P(HB-co-HV). Samples will be stored at 7, 20, 50, 75, 100, 125 and 150°C, as well as -22 °C (below the T_g, to provide a control group) for up to 672 hours, during which time they will be analysed periodically to monitor any change in properties.

As embrittlement is known to be caused by secondary crystallisation, the effects of temperature on the degree of crystallinity will be monitored over time by the use of DSC and IR testing. Thermal properties, including any change in glass transition temperature and melting temperature, will be analysed using DSC and DMTA. The subsequent effects of any crystallinity change on the mechanical properties of the material will be analysed using uniaxial tensile testing.

Analysis of any discolouration, mass loss and GPC will also be carried out to detect any potential thermal degradation of samples stored at higher temperatures.

CHAPTER 2 – MATERIALS AND EXPERIMENTAL METHODS

2.1 Materials

Pellets of Poly(3hydroxybutyrate-*co*-3hydroxyvalerate), P(HB-co-HV), (Tianan ENMAT Y1000P) containing 3 wt% valerate, were provided by Helian Polymers (Venlo, Netherlands) and used as received. The pellets had a T_m of 178 °C and crystallinity of 65 % (as calculated by DSC), density of 1.25 g cm^{-3} (as specified by the manufacturer), M_w of 387 000 g mol^{-1} and polydispersity of 2.70 [78].

2.2 Sample preparation

P(HB-co-HV) plaques were hot pressed from the pellets using a Moore E1127 Hydraulic Press (George E. Moore & Sons Ltd, Birmingham, UK). 8 g of pellets were put in the centre of a polytetrafluoroethylene (PTFE) frame (152 x 158 x 0.266 mm), and sandwiched between two aluminium sheets. This was then enclosed between two stainless steel plates and inserted between the pre-heated platens of the hot press, at 190 °C for 5 minutes, to ensure an even temperature throughout. 10 tonnes of pressure were then added, and held for a further 3 minutes at 190 °C. Subsequently the mould was cooled in the press to room temperature, for 20 minutes, while the pressure was maintained.

Thicker plaques were produced from 43 g of pellets in a frame (150 x 180 x 1 mm), using the same conditions and equipment detailed above.

As all subsequent sample preparation was carried out at room temperature, the time taken to prepare and transfer the samples into the storage conditions was kept to a minimum, to reduce the effect of secondary crystallisation. All samples stayed at room temperature for 30 minutes (the longest preparation time required) before being tested, or transferred into storage, to maintain consistency throughout all samples.

Any samples which were used to provide the unconditioned data, that could not be tested immediately following sample preparation, were kept at -22 °C prior to analysis. This was below the T_g of the material (4 °C) [30], to ensure that no change occurred in the microstructure between processing and testing.

2.3 Storage conditions

The effects of eight different thermal storage conditions were evaluated: -22, 7, 20, 50, 75, 100, 125 and 150 °C. This temperature range was selected as an appropriate scale to study the development of crystallinity over time. It covers temperatures between the T_g and the T_m of P(HB-co-HV), and includes a temperature below the T_g to act as a control. Samples stored at -22 and 7 °C were kept in a freezer and fridge respectively. Samples at 20 °C were at ambient temperature. Samples stored at elevated temperatures of 50 to 150 °C were kept in fan ovens. Thermocouples were used to set the freezer, fridge and oven temperatures.

2.4 Experimental techniques and procedures

2.4.1 Differential Scanning Calorimetry (DSC)

The melting points, degree of crystallinity, and crystallisation kinetics were studied through differential scanning calorimetry (DSC).

Samples for DSC testing were prepared by punching discs, 5 mm in diameter and of mass 4.42 ± 2.37 mg, from the thinner plaques prior to being placed in the relevant storage condition. These samples were removed from the storage condition individually 5 minutes prior to testing. The results from 3 repeats were analysed and averaged to provide the values quoted in the text. Error bars on figures were set to ± 1 standard deviation.

A Mettler Toledo DSC 1, (Mettler Toledo, Schwerzenbach, Switzerland), power compensation differential scanning calorimeter, running STARe software (version 11) was used. Temperature and power calibration were first performed using a known mass of indium and zinc. All DSC runs were carried out using nitrogen as the purge gas with a flow rate of 50 ml min^{-1}. A Mettler Toledo press was used to seal samples in a 40 µL aluminium pan with an aluminium lid (Mettler Toledo). The lid had a small hole pierced in the centre, to allow any gases which may be released during the testing run to escape, preventing a build-up of pressure within the pan and so preventing the pan from warping, which would alter the contact with the sensor and influence the results.

Samples were heated from -40 to 220 °C at a constant rate of 50 °C min^{-1}, in order to minimise any recrystallisation which may occur during the heating scan, which would affect the degree of crystallinity and melting temperature values. Figures of the DSC traces presented in the text are cropped to show only the data from 100 to 220 °C, in order to display the main melting peak

in greater detail. The degree of crystallinity was calculated using the enthalpy of fusion from the area under the melting endotherm using,

$$X_c = \frac{\Delta H_f}{\Delta H_f{}^0} \times 100 \qquad \text{(Equation 2.1)}$$

where X_c is the weight fraction degree of crystallinity, and ΔH_f and $\Delta H_f{}^0$ are the measured enthalpy of fusion from the experimental data, and the theoretical enthalpy of fusion of pure PHB crystals. A $\Delta H_f{}^0$ value of 146 J/g for PHB was taken from the literature [79]; as the samples used in this work contain only 3 wt% HV, the value is assumed to be the same. Various different methods of measuring of the T_m were taken for comparison, including the maximum height of the melting endotherm, the onset of melting and last trace of crystallinity. The normalised heat of fusion was also calculated for all samples. These values were recorded throughout a storage duration of 672 hours.

Figure 2.1 illustrates the various methods of measuring the melting temperature of a sample from a dynamic heating scan; the most commonly used is the temperature corresponding to the peak of the melting endotherm, T_m. Other, less common, methods include the onset of melting and last trace of crystallinity, taken as the temperatures where the endotherm leaves and re-joins the baseline respectively.

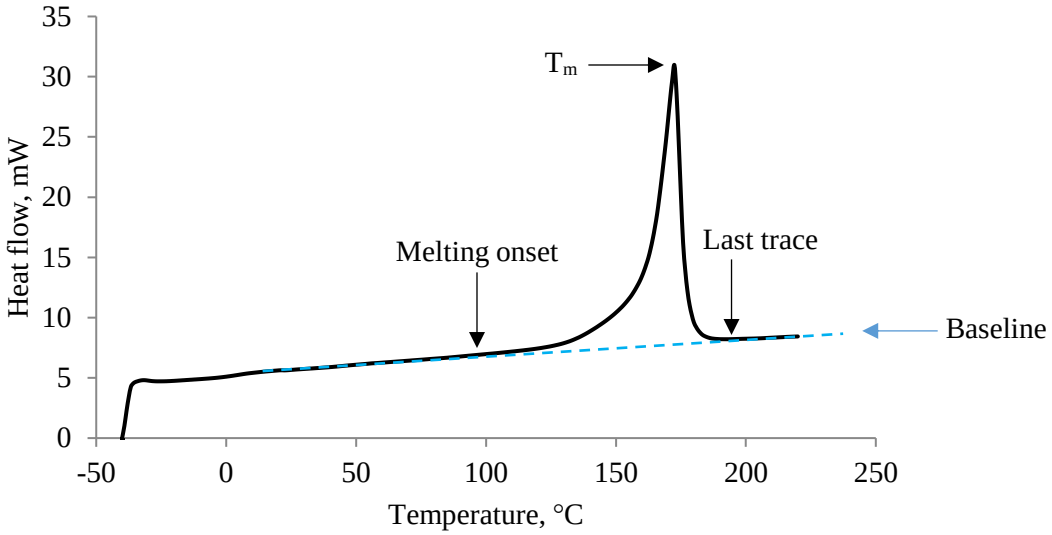

Figure 2.1. An example DSC trace from a dynamic melting run, with various methods of measuring the melting temperature indicated.

Isothermal runs were carried out by heating samples to 190 °C, holding at 190 °C for 3 minutes to erase any thermal history, then rapidly decreasing the temperature at 30 °C min^{-1} to the desired isothermal crystallisation temperature (144-150 °C). Preliminary research indicated that a cooling rate of 30 °C min^{-1} provided the optimum compromise of speed, in order to minimise any crystallisation which might occur prior to the start of the isothermal crystallisation, and control, to prevent overshoot past the desired crystallisation temperature. The samples were held at the crystallisation temperature (T_c) for 120 minutes. Following the crystallisation of the sample, the temperature was then increased from the T_c to 220 °C at 50 °C min^{-1}(again to minimise any recrystallisation which would occur using a slower heating rate), in order to obtain the equilibrium melting temperature, T_m^0, using the Hoffmann-Weeks extrapolation method. The results from 3 repeats were analysed and averaged to provide the values quoted in the text. Error bars on figures were set to ± 1 standard deviation.

Figure 2.2 shows the exothermic peak of an isothermal crystallisation. There is an initial period of time, after the material reaches the crystallisation temperature, before the crystallisation

process begins. It is necessary then to identify the time at which the crystallisation process starts, to improve the accuracy of any further data analysis. The point at which the exothermic peak first diverges from the baseline is taken as t_0. The end of the crystallisation process, t_{end}, is identified as the point where the exothermic peak returns to the baseline. The baseline is superimposed onto Figure 2.2 as a straight line, extrapolated back from the stable heat flow at the end of the isotherm to the stable heat flow at the start of the isotherm, for illustrative purposes.

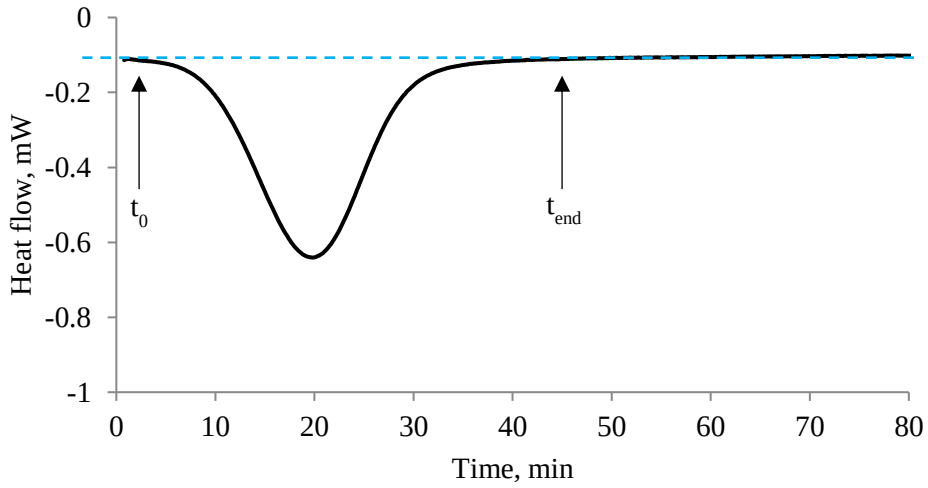

Figure 2.2. An example DSC trace from an isothermal crystallisation run, indicating the start and end of the primary crystallisation process.

Calculation of the area of the crystallisation exotherm was achieved by applying the trapezium rule to the raw heat flow/time data. Figure 2.3 is generated from the cumulative area between the baseline and the exothermic curve at each sequential time point divided by the cumulative area at t_{end}, indicating the fraction of the total material which has transformed to the crystalline state at a given time. The marker $t_{50\%}$ denotes the point at which 50% of the total transformation has taken place, and the time at which this occurs is used to calculate the crystallisation half time, $t_{1/2}$, a commonly quoted measure of the rate of crystallisation. As the crystallisation half

time is the time taken from the onset of the crystallisation process, t_0, to the point where 50% of the material is in the crystalline state,

$$t_{1/2} = t_{50\%} - t_0 \qquad \text{(Equation 2.2)}$$

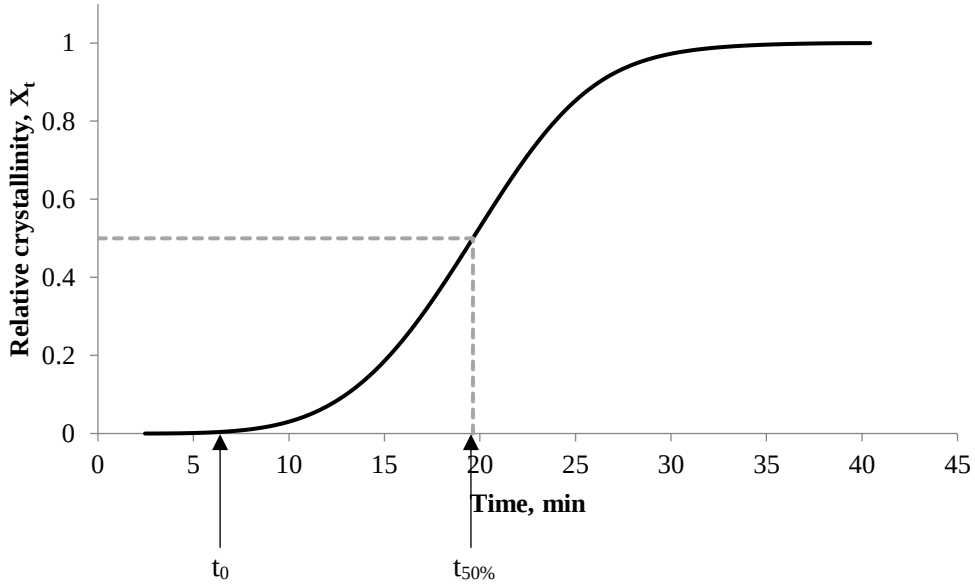

Figure 2.3. Illustrates the timescale over which the material transformed from the amorphous state to the semi-crystalline state.

The crystallisation kinetics were analysed by use of the Avrami equation,

$$1 - X_t = \exp(-kt^n) \qquad \text{(Equation 2.3)}$$

and by the creation of double log plots, also known as Avrami plots, plots using

$$\ln[-\ln(1 - X_t)] = \ln k + n \ln t \qquad \text{(Equation 2.4)}$$

where X_t is the fraction of crystallinity, k is the Avrami crystallisation rate constant, n is the Avrami exponent and t is time. The assumptions of the Avrami equation (Chapter 1.2.1) also mean that, in order for the equation to apply to experimental data, the data must be limited to remove portions during which the rate of transformation is not constant. In this study, the first

20 % and last 15 % were omitted from the analysis. The first 20% is excluded as nucleation and growth is not stable during this time, and the last 15% is excluded to remove the influence of secondary crystallisation [80].

If a plot of $\ln[-\ln(1-X_t)]$ against $\ln(t)$ yields a linear result, the transformation can be described using the Avrami equation (Figure 2.4).

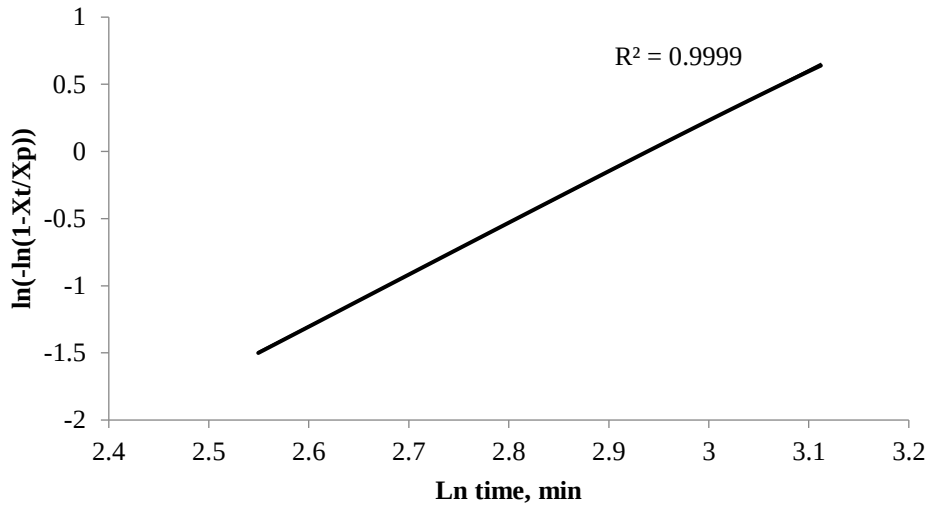

Figure 2.4. An example of a double ln plot of $\ln[-\ln(1-X_t)]$ against $\ln(t)$.

Double log plots of data to which the Avrami equation applies, such as the one presented in Figure 2.4, are used to obtain values of the Avrami rate constant, *k*, and the Avrami exponent, *n*, from the intercept and gradient of the line respectively.

The R^2 value provides an indication about the linearity and the accuracy of the equation to fit the data, as described in Lorenzo (2006) where it was recommended a minimum R^2 value of 0.990 be achieved in order to ensure a good fit of the data. A minimum R^2 value of 0.9999 was recorded in this work [81].

2.4.2 Attenuated Total Reflection Infrared Spectroscopy (ATR-IR)

The development of crystallinity with long term storage was also studied by attenuated total reflection infrared-spectroscopy. Any changes in spectral peaks, such as the absorbance or wavenumber, shape or size, and the appearance/disappearance of peaks were monitored.

Samples for infrared testing were prepared in the same way as for DSC testing, punching samples 5 mm in diameter from the thinner plaques. Samples were removed from the storage conditions 20 to 300 min prior to testing.

A Nicolet 380 FT-IR spectrometer (Thermo Scientific) with Smart Orbit accessory, diamond crystal, DTGS detector, and OMNIC software (Thermo Scientific) provided absorbance spectra used to attain information on crystallinity variance. Spectra were collected using IR wavelengths of 4000-700 cm^{-1}, a resolution of 4 cm^{-1} and 100 scans, an optical velocity of 0.6329 $cm \cdot s^{-1}$, and 2 levels of zero filling. A background spectra was collected prior to the testing of each individual sample, and subtracted from the sample spectra, to remove the effects of atmospheric CO_2 and water vapour. Testing was carried out at ambient temperature. The results from 3 repeats were analysed and averaged to provide the values quoted in the text. Error bars on figures were set to ± 1 standard deviation.

Pellets of P(HB-co-HV) were used as supplied for isothermal infrared testing. This was carried out using a Nicolet 8700 FTIR (Thermo Scientific), also with a diamond crystal, DTGS detector, and running OMNIC software (Thermo Scientific). For this experimental setup, the FTIR was paired with an ATR heated attachment and thermocouple, with Pico Log and OMNIC software. IR wavelengths in the range of 4000-700 cm^{-1} were collected with a resolution of 4 cm^{-1} and 100 scans, an optical velocity of 0.3165 $cm \cdot s^{-1}$, and sampling interval of 180 s. The sample was heated to 190 °C, to obtain a fully amorphous specimen, then cooled to an

isothermal crystallisation temperature of 150 °C. The sample was held at 150 °C until primary crystallisation had ended, determined in this case by the lack of significant variation between the newly obtained spectra and those already collected. A single sample was used to provide the primary crystallisation data, due to issues with maintaining contact between the sample and the crystal.

2.4.3 Dynamic Mechanical Thermal Analysis (DMTA)

DMTA provided information on the storage modulus and tanδ of the samples, which was used to examine the effect of storage on crystallinity through observation of the T_g.

Samples for DMTA were prepared from plaques 1 mm thick. Rectangular samples were cut with a length of 55 mm and a width of 13 mm. Samples were removed from storage 10 minutes prior to testing, during which time the width and thickness was measured as a 3-point average using a Mitutoyo IP65 micrometer. Due to time limitations, single samples were analysed for storage conditions of -22 to 125 °C, and 3 samples were analysed and averaged to provide data for the samples stored at 150 °C. Error bars on figures were set to ± 1 standard deviation.

Dynamic temperature 3-point bend tests were performed using a NETZSCH DMA 242 cell connected to a DMA 242 controller, TASC 414/3 controller and running NETZSCH DMA measurement channel 18 software. Liquid nitrogen was used to cool the sample to -40 °C prior to the start of the run. The temperature was then ramped from -40 to 70-95 °C, at a heating rate of 1 °C min^{-1}.

The target deflection was set to 240 µm for samples stored from -22 – 125 °C, and 120 µm for samples stored at 150 °C due to their elevated brittleness. Each run measured the response of

the samples to three different frequencies, 1.00, 10.00 and 33.33 Hz. The free bending length was 40 mm for all samples.

Figure 2.5 indicates how the tanδ peak height and width were obtained. The peak height was taken as the difference between the maximum height and the starting value. Due to the uneven baseline of some of the tanδ peaks, an adaptation of the Q^{-1} factor,

$$Q^{-1} = \frac{B_t - A_t}{C_t} \qquad \text{(Equation 2.5)}$$

where $A = 0.707 \times C$ and $B = 0.707 \times C$, usually seen in engineering [82], was applied to all samples in order to standardise the point at which the width measurement was taken. In this adaptation, C is the maximum peak height, t is temperature, and A and B are the points at which tanδ reaches $0.707 \times C$, either side of the peak maximum. The peak width values quoted in the text are the widths between points A and B in Figure 2.5. The same approach was taken when calculating the distribution of the peak area, this time using the trapezium rule to calculate the area under the tanδ curves above the line drawn between points A and B. The area was then split into that left and right of the tanδ maximum, indicated by point C.

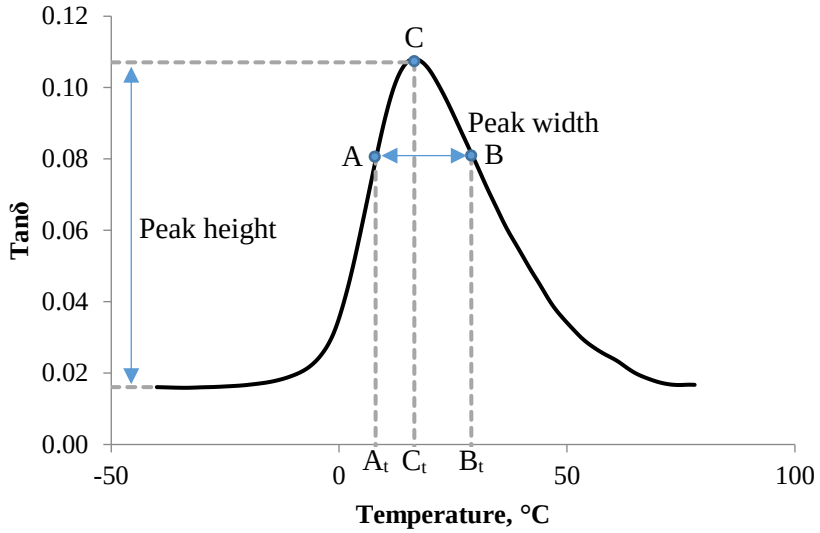

Figure 2.5. An example of a typical tanδ peak with various methods of analysis measurements indicated.

The storage modulus (E′) may also provide a measure of T_g, which is given as the point where the curve begins to deviate away from the initial stable portion, as indicated in Figure 2.6.

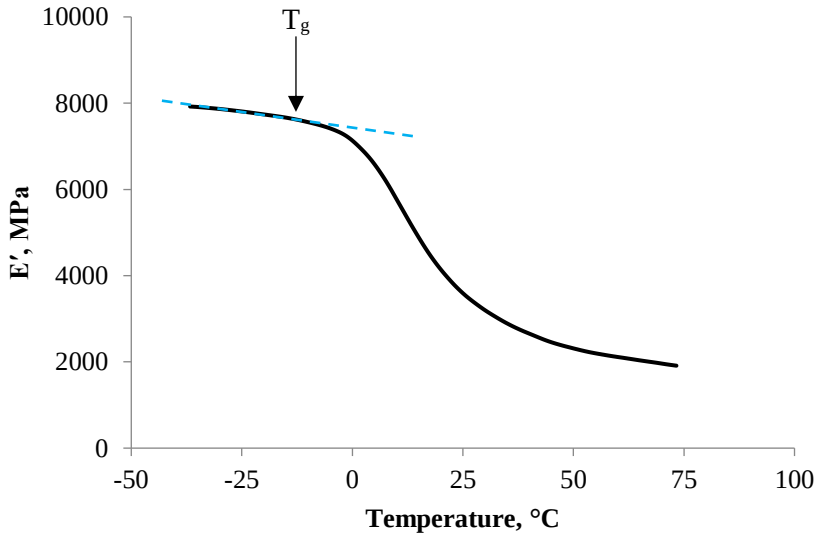

Figure 2.6. An example of a typical E′ curve, with the T_g measurement point indicated.

2.4.4 Mechanical testing

Tensile testing provided stress-strain curves, which were to calculate the mechanical properties of the samples; namely the Young's Modulus, ultimate tensile strength, UTS, and elongation to break.

Dog-bone shaped samples with a gauge length of 26 mm, width of 4 mm, and thickness of 0.214 ± 0.087 μm, were prepared for mechanical testing using a Wallace cutter. The thickness of each sample was measured as a 3-point average using a Mitutoyo IP65 micrometer. Individual dog-bones were removed from each storage condition as required, the edges along the gauge length were smoothed with P800 emery paper, and the samples were tested 10 minutes after removal.

Uniaxial tensile testing was carried out at ambient temperature on an Instron 5566 (High Wycombe, UK) with a 10 kN load cell, using a cross-head speed of 2 mm min^{-1}. Merlin software collected data every 500 ms until failure. The results from 3 repeats were analysed and averaged to provide the values quoted in the text. Error bars on figures were set to ± 1 standard deviation. While the stress measurements of tensile testing are highly accurate, the strain measurements are prone to inaccuracies, the error of which is difficult to quantify. There is also a degree of error associated with the variations in sample thickness. Steps have been taken in an attempt to minimise the effects of experimental error on the data collected, including the use of multiple samples per time point and storage temperature, and the 3-point averaging of thickness measurements. However, as the main objective of this tensile testing is the comparison of samples exposed to the same experimental procedures, the associated error should be equivalent.

Figure 2.7 indicates how the mechanical properties are determined for each sample. The Young's modulus, obtained from the gradient of the linear section at the beginning of the stress-strain curve, is given by

$$E_y = \frac{\sigma}{\varepsilon} \qquad \text{(Equation 2.6)}$$

where the Young's modulus, E_y, is equal to the tensile stress, σ, (force divided by the cross-sectional area) over strain, ε, (change in length divided by the original length). The UTS was taken as the maximum recorded stress value. The elongation to break was the final strain value recorded immediately prior to fracture of the sample.

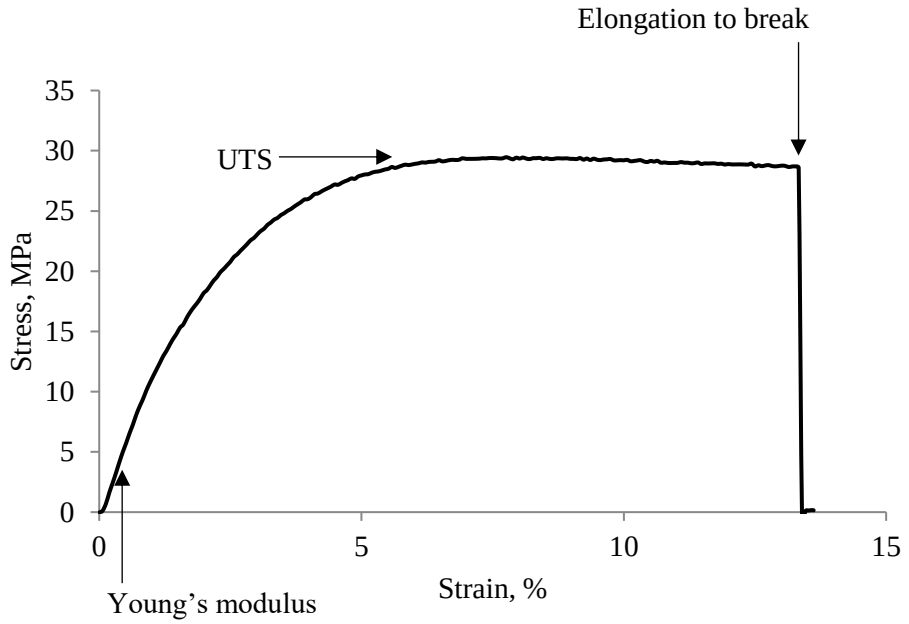

Figure 2.7. An example of a stress-strain plot typical of a brittle polymer.

2.4.5 Discolouration

Photographic evidence of discolouration, of samples from the thicker plaques, was logged as an indication of the degree of degradation.

Digital images of samples (one sample per time point at each temperature), 10 mm x 40 mm x 1 mm, stored from 0 to 672 hours at -22, 20, 125 and 150 °C were recorded using a Fujifilm FinePix S1.

2.4.6 Mass loss

For mass loss studies, square samples were cut from 1 mm thick plaques to have a mass of 30.01 ± 0.51 mg. A mass loss study was also carried out using pellets, as provided from the manufacturer, with starting masses of 28.68 ± 0.24 mg.

A Perkin Elmer Autobalance Ad-2 was used to measure the mass of each sample. Samples were removed from their storage conditions, put onto the balance, and returned to their conditions within 10 minutes. Each sample was left on the balance for 1 minute to stabilise before the mass was recorded. The results from 3 repeats were analysed and averaged to provide the values quoted in the text. Error bars on figures were set to ± 1 standard deviation.

2.4.7 Gel Permeation Chromatography

GPC was used to examine the effect of elevated storage temperatures on the weight average molecular weight (M_w) of the material over time. One repeat was carried out for each time point and storage temperature.

50 mg of sample from the thinner plaques was added to 50 mL of chloroform. Samples were refluxed in the chloroform at 85 °C until dissolved, then passed through a 0.22 μm PVDF membrane into 250 ml duran bottles.

The solutions were given to the University of Warwick. There the analyses were performed on an Agilent Technologies (Berkshire, UK) LC 390-MDS instrument, comprising of two PLgel Mixed-D columns (5 μm) and one PLgel guard column (5 μm) and a differential refractive index (DRI) detector. An injection volume of 100 μL, with concentration of 1 mg/mL, was run at 30 °C in chloroform eluent with a flow rate of 1 ml min^{-1}. Polystyrene standards were used for calibration. Data was collected by Agilent GPC/SEC Software Version 1.2.3182.29519.

As GPC columns contain pores of varying sizes, the polymer chains with smaller molecular weight will take longer to pass through than those with a larger molecular weight. The volume of material exiting the column is recorded and plotted against the retention time, producing a chromatogram (Figure 2.8). Retention times are converted into molecular weight values using the calibration curve generated from the polystyrene standards, producing a molecular weight distribution curve (Figure 2.9).

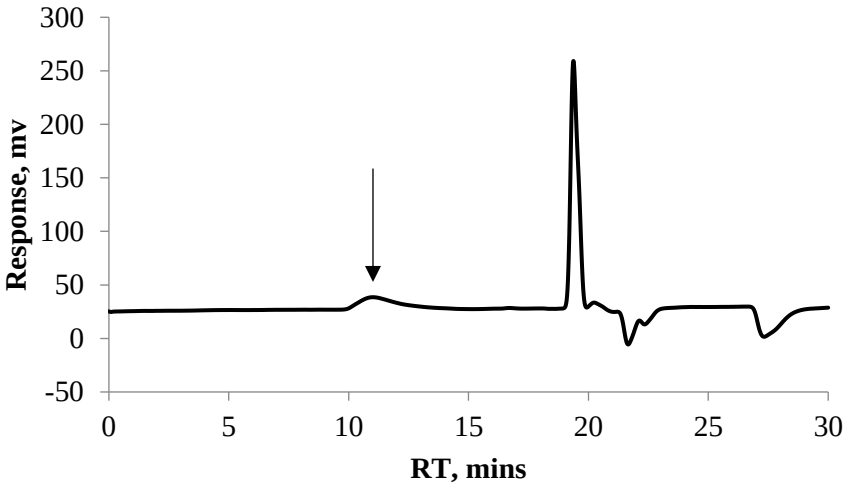

Figure 2.8. An example of a GPC chromatogram obtained from a sample of P(HB-co-HV). The peak relating to P(HB-co-HV) is indicated by the arrow.

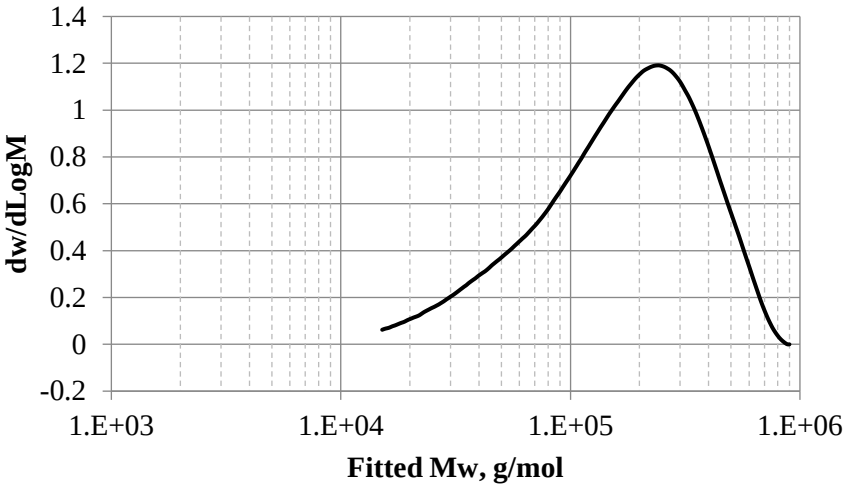

Figure 2.9. An example of a molecular weight distribution curve obtained from a sample of P(HB-co-HV).

CHAPTER 3 – PRIMARY CRYSTALLISATION

3.1 Analysis of primary crystallisation kinetics using Differential Scanning Calorimetry (DSC)

DSC crystallisation exotherms were collected from isothermal crystallisation at temperatures ranging from 144 to 150 °C. Figure 3.1 shows the overlaid traces of these exotherms, to gain a qualitative perspective of the data. Each exotherm in Figure 3.1 represents data limited to within the region of t_0 to t_{end}, as described in Chapter 2.4.1, for visual clarity. An example of the full exotherms which were obtained is presented in Chapter 2.4.1 (Figure 2.2). It is clear that the onset of crystallisation does not proceed immediately when the sample reaches the target crystallisation temperature (T_c), and so the data was normalised according to the induction time, $(t - t_0)$, to make the time at crystallisation onset 0 s.

By overlaying the traces obtained from isothermal crystallisation at varying temperatures, it is immediately obvious that the T_c impacted the crystallisation process (Figure 3.1). Increasing T_c resulted in a smaller decrease in peak heat flow, and an increase in the amount of time taken until primary crystallisation was completed. Gunaratne and Shanks, and Peng *et al*. saw the same with PHB and PHBV 8% respectively [22,44].

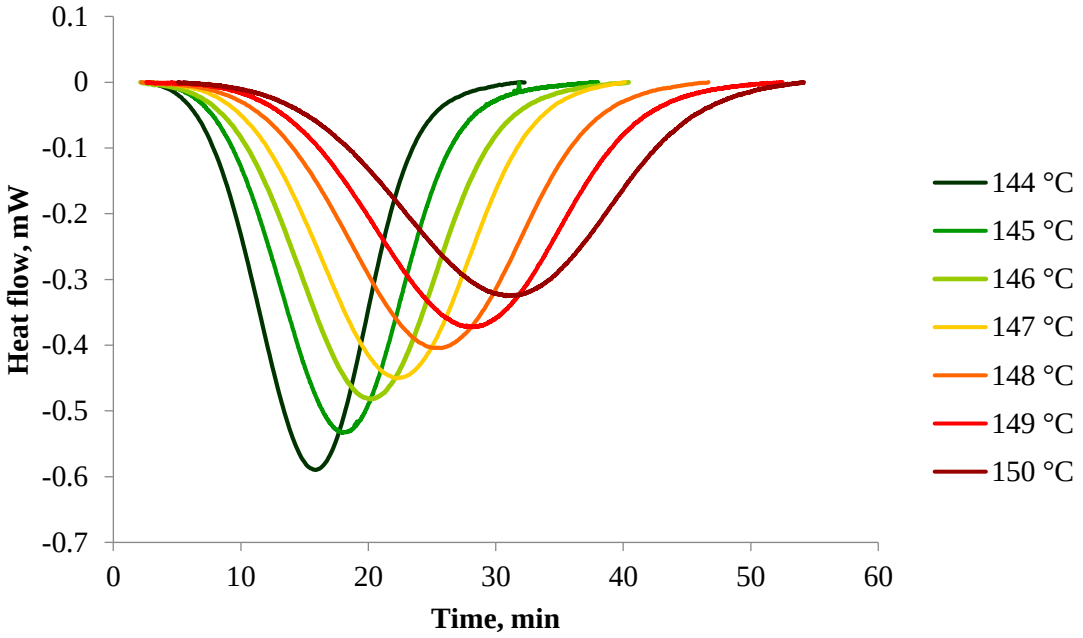

Figure 3.1. DSC traces for isothermal crystallisation temperatures ranging from 144 to 150 °C (which have been limited to the start and end of the primary crystallisation process).

At higher crystallisation temperatures, it also took longer for the crystallisation process to begin, demonstrated in Figure 3.2. At the lower crystallisation temperatures explored in this work, there appeared to be little difference in the time taken between reaching the set T_c and the onset of crystallisation, also known as the induction time, while at higher crystallisation temperatures the time increased (Figure 3.2). At 148 °C samples had an average induction time of 156 seconds, as the crystallisation temperature was increased to 149 and 150 °C the average induction time increased to 224 and 343 seconds respectively. At temperatures near T_m, there is a lower chance of embryos forming and reaching the critical size required for secondary nucleation and growth; hence the time between T_c and t_0 is greater.

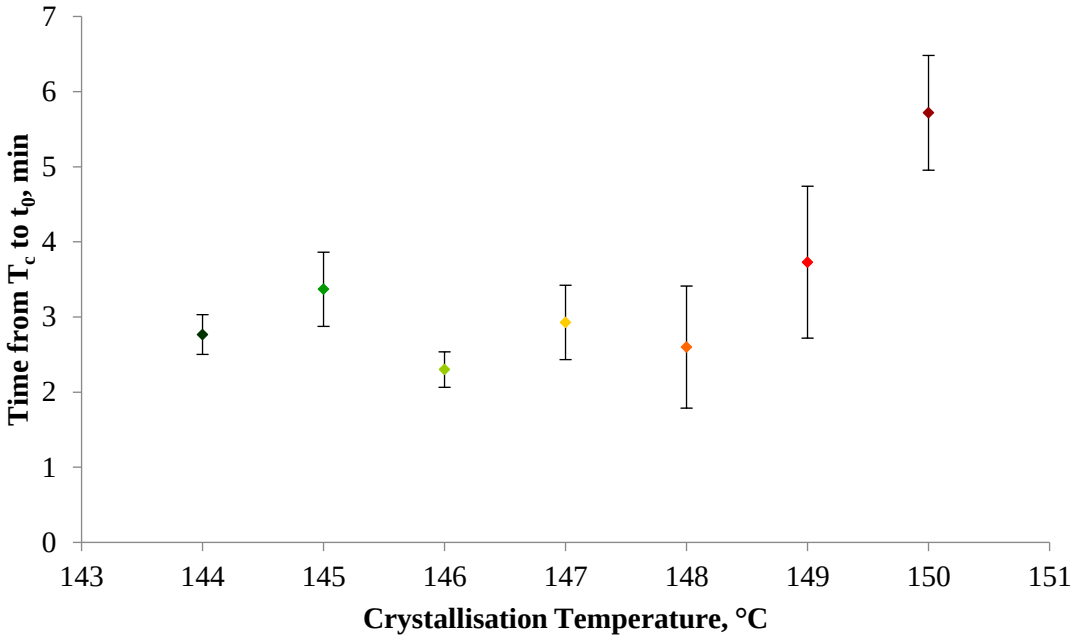

Figure 3.2. Time taken for crystallisation to begin after reaching the sample has reached the crystallisation temperature shown according to the temperature of crystallisation.

The time between the system reaching the desired isothermal crystallisation temperature and the onset of the crystallisation process is often referred to as the induction time, however, it has been claimed that the induction period is improperly named [83]. This is reiterated by Mandelkern, who stated that this observation is in fact an artefact created by the sensitivity of the detector used, and is "more apparent than real" [3]. It is known that DSC is often insensitive to the size of the changes induced by the secondary crystallisation process of polymers following primary crystallisation. It follows that this lack of sensitivity may also apply to the small changes occurring at the start of the primary process during the so-called induction time. If this is the case, then there may be crystallisation taking place within the induction period, but the DSC is not sensitive enough to detect it. Therefore, t_0, or the onset of crystallisation may be interpreted as the first detection of nucleation.

3.1.1 Avrami analysis of experimental DSC isothermal data

Each of the curves displayed the characteristic sigmoidal shape of phase transition curves common to the crystallisation process of PHB. The curve is split into approximate regions in Figure 3.3 to assist in the explanation of the crystallisation process. This sigmoidal shape is a result of 3 stages of crystal formation and growth. At first there is a slow initial transformation as primary nucleation begins, which accelerates as the nuclei reach critical size and crystals start to grow (region 1 of Figure 3.3). This is followed by rapid transformation as the rate of nucleation and growth reaches at a maximum (region 2). Finally, the transformation slows again as the volume of material remaining in the melt decreases, nucleation stops and sufficient impingements occur, halting the growth of primary crystals (region 3). During region 3, another process is active, known as secondary crystallisation. Not be confused with secondary nucleation and growth of a primary nucleus, as detailed in Chapter 1.2.1, secondary crystallisation causes a progressive increase in crystallinity of spherulites following impingement, and is partly responsible for the deviation from the linear response dictated by the Avrami expression [80]. Region 3 can be thought of as a mixed stage, where both primary and secondary processes are active [84]. Secondary crystallisation also continues after the primary crystallisation process has completed, indicated by its own region in Figure 3.3, yet the relatively slow speed at which it progresses means that the DSC lacks the sensitivity to monitor the secondary crystallisation process in real time.

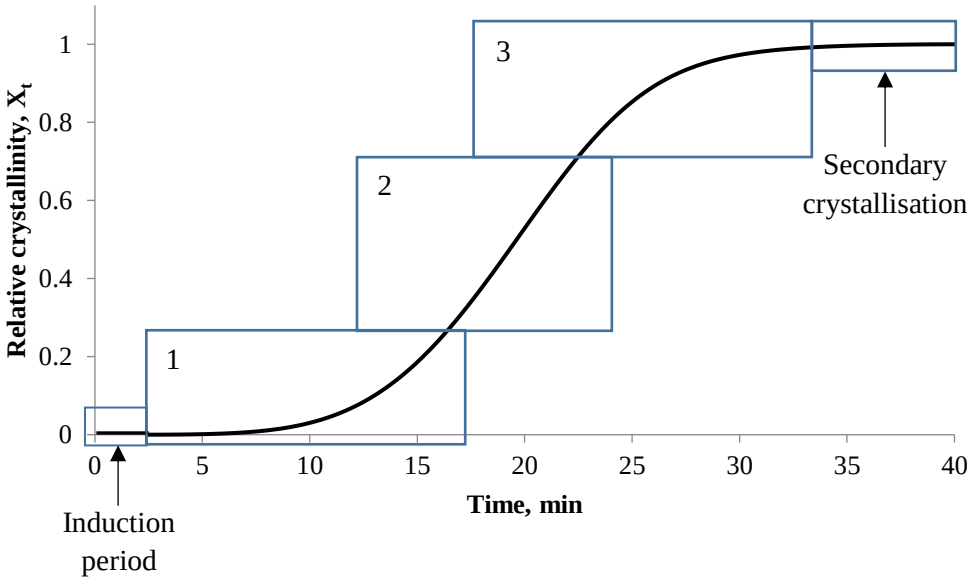

Figure 3.3. An example phase transition curve approximating the different regions of the primary crystallisation process.

Figure 3.4 gives a good visual indication as to how higher crystallisation temperatures reduced the rate of primary crystallisation, seen as an increase in the time taken to reach a completely transformed value of 1.

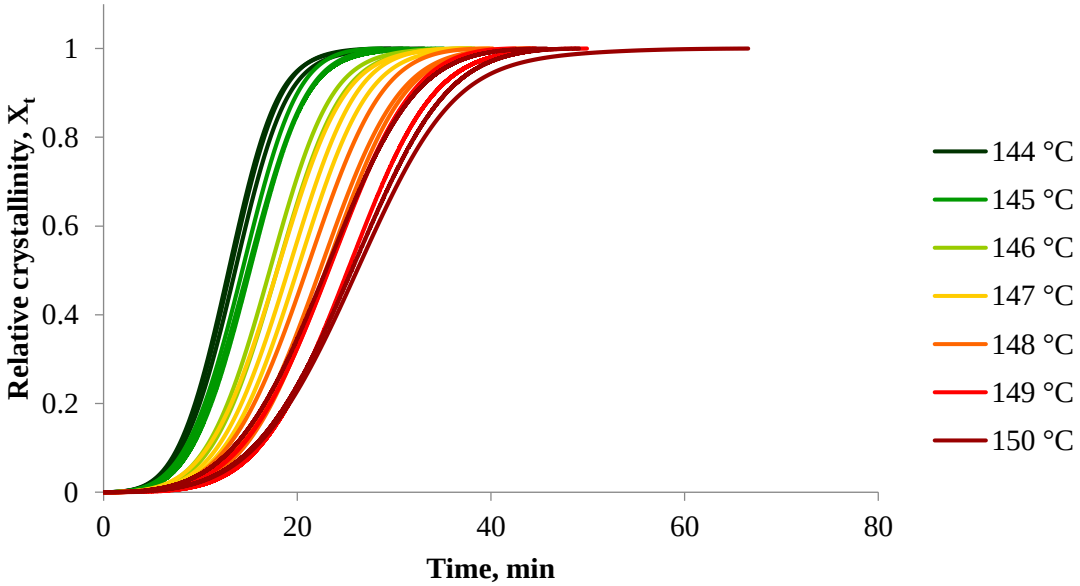

Figure 3.4. Relative crystallinity indicates the fraction of material transformed from the melt over time, according to the isothermal crystallisation temperature, with time zeroed according to the onset of the crystallisation process, $(t - t_0)$.

Another indication is the crystallisation half-life, a standard measure of the rate of primary crystallisation, quoted as the time at which 50 % of the total crystallinity value is reached. The average half-life values presented in Figure 3.5 were measured as the time at which the relative crystallinity values reach 0.5 in Figure 3.4.

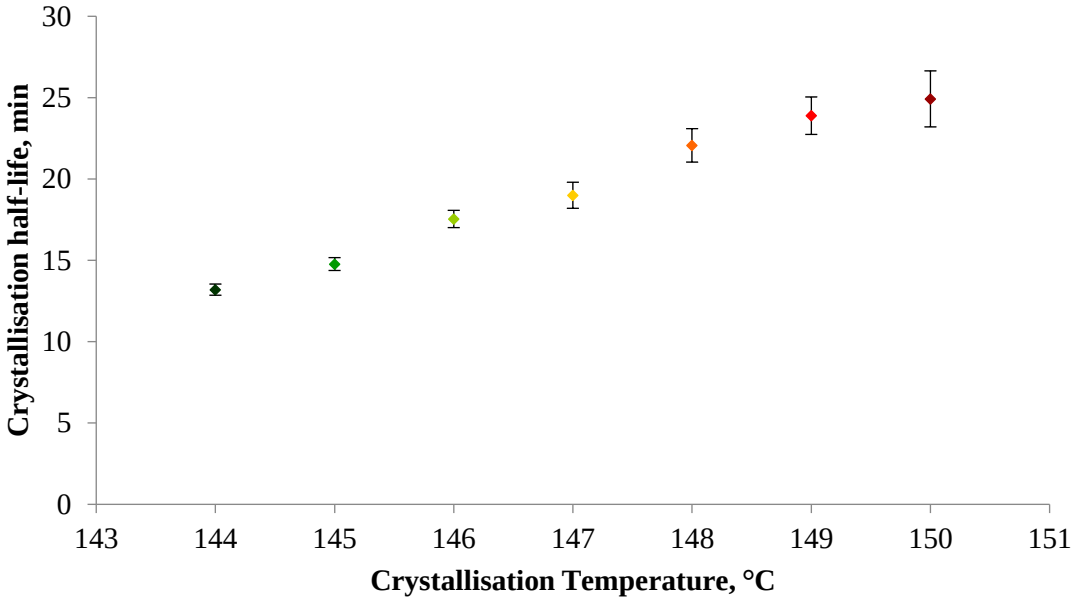

Figure 3.5. Crystallisation half-life according to the crystallisation temperature.

Figure 3.5 illustrates what seems to be a positive linear correlation between the crystallisation temperature and the crystallisation half-life. The shortest average half-life of 792 seconds was observed in the samples crystallised at 144 °C, and the longest average half-life of 1495 seconds seen in the samples crystallised at 150 °C.

It is accepted that the relationship between the crystallisation temperature and half-life for isothermal primary crystallisation follows a parabolic curve, where the optimum balance of nucleation and growth rates produce the shortest crystallisation times. At temperatures close to both the T_g and T_m of the material the crystallisation process is at its slowest, and as the crystallisation moves away from T_g and T_m the rate increases. Yet Figure 3.5 does not show an

obvious exponential increase in half-life with increasing T_c. Samples may have needed to be subjected to a wider range crystallisation temperatures for the trend to become clear.

It was not possible to determine the optimum crystallisation temperature from these isothermal experiments, as at lower temperatures the crystallisation process began before the DSC was able to reach the desired T_c. In other words, the cooling rate of the conventional DSC setup used in this work was not sufficient to accurately record the start of the crystallisation process of these samples at temperatures below 144 °C. As stated by Lorenzo *et al*. "A complete… exotherm must be obtained in order to guarantee the establishment of a good base line and avoid errors associated with the integration of incomplete traces" [81]. Other authors have reported the temperature of maximum crystallisation rate; Righetti and Di Lorenzo and El-Taweel *et al*. quoted temperatures of 80 to 90 °C for PHB [17,85], while the experimental data of Peng *et al*., You *et al*. and Barham *et al*. presented maximums between 55 and 60 °C for P(HB-co-5%HV), and between 75 and 80 °C for PHB respectively [23,44,79]. The samples crystallised at the lowest crystallisation temperature tested in this study experienced the greatest rate of crystallisation, as they would have been closer to the optimum crystallisation temperature. The results of Gunaratne and Shanks also demonstrated an increase in crystallisation rate of PHB and P(HB-co-8mol%HV) with T_c decrease, towards the optimum crystallisation rate temperatures reported by others [22].

The Avrami equation can be used to further analyse the crystallisation process (Chapter 1.2.1). The linearity of the Avrami double log plots, created using Equation 7.1, shows it to be a valid method (Figure 3.6) [44,86]. From the Avrami plots, measurements of the Avrami exponent, *n*, and the crystallisation rate constant, *k*, were determined as the gradient and intercepts respectively.

$$\ln[-\ln(1-X_t)] = \ln k + n \ln t \qquad \text{(Equation 7.1)}$$

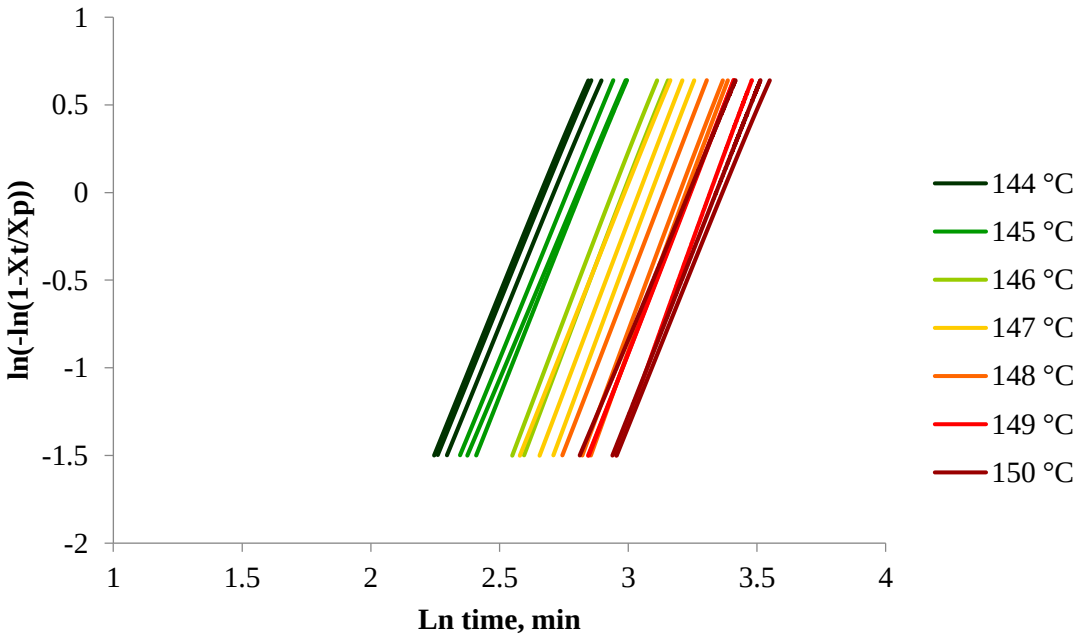

Figure 3.6. Avrami plot of the relative crystallinity for each isothermal temperature.

As may be seen in Table 3.1, Values of *n* between 3.5 and 4 were achieved for all crystallisation temperatures. This potentially indicates that sporadic nucleation and spherulitic crystal growth occurred in all samples across the studied T_c range (as detailed in Chapter 1.2.1). Gunaratne and Shanks, You *et al*. and Peng *et al*. all reported lower *n* values, between 2 and 3, when crystallised at temperatures of 120 °C or less [22,23,44]. Analysis on crystallisation temperatures closer to those used in this work were not found in the current literature. Despite obtaining relatively similar values of *n*, Gunaratne and Shanks, You *et al*. and Peng *et al*. differed in the interpretations of their results. While You *et al*. concluded that their *n* values, of 2 to 3, were indicative of three-dimensional spherulitic growth via heterogeneous nucleation [23], Gunaratne and Shanks believed $n = 2$ to represent heterogenous nucleation and growth of two-dimensional spherulites [22]. Peng *et al*. however, believed P(HB-co-8mol%HV) melts to undergo homogenous nucleation and so suggested that $n \sim 3$ meant that the growth was two-

dimensional [44]. The difficulty in interpretation of *n* is widely recognised, in part because the factors determining *n* may vary during the crystallisation process [4].

Table 3.1. Average values of *n* obtained according to the temperature of crystallisation.

Crystallisation temperature, °C	*n*	Standard deviation
144	3.6	0.01
145	3.6	0.09
146	3.8	0.02
147	3.8	0.13
148	3.9	0.10
149	3.9	0.15
150	3.6	0.09

Figure 3.7 highlights a clear dependence of the rate of crystallisation on the temperature of crystallisation. The rate constant was greatest at an isothermal crystallisation temperature of 144 °C, with an average value of 6.59 $x10^{-5}$, and saw a rapid decline when crystallisation was carried out at 145 and 146 °C, to average values of 4.53 $x10^{-5}$ and 1.20 $x10^{-5}$ respectively. The rate constant values only reduced slightly from those observed from the 146 °C samples with further increase in T_c. Gunaratne and Shanks, and Peng *et al*. also described an observed decrease in the rate constant with higher crystallisation temperatures [22,44].

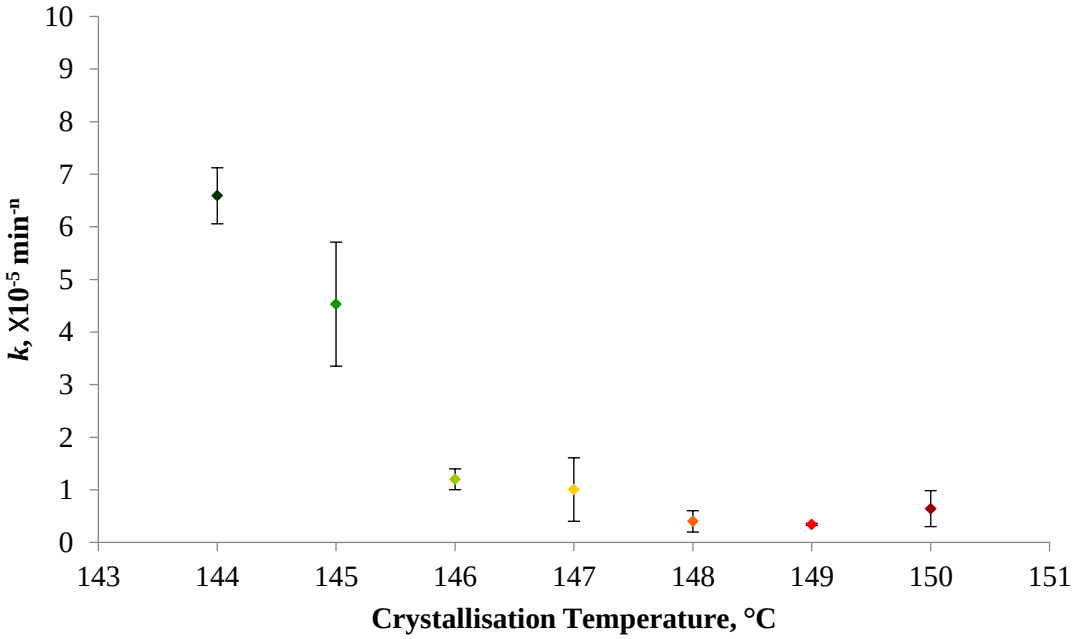

Figure 3.7. Crystallisation rate constant, *k*, according to the temperature of isothermal crystallisation.

The rate constant data in Figure 3.7 decreased in agreement with the data obtained from $t_{1/2}$, as noted by You *et al*. [23], whereby the rate of crystallisation decreases as the temperature of crystallisation approaches the T_m of the material. Further detail of these trends may be found in relation to $t_{1/2}$ discussed previously in this section.

3.1.2 Hoffman-Weeks approach to estimation of the equilibrium melting temperature

One of the simplest definitions of the equilibrium melting temperature, T_m^0, is "the temperature at which a crystal without any surface would melt" [4]. More comprehensively, Hoffman and Weeks define T_m^0 as "the melting point of an assembly of crystals, each of which is so large that size (i.e. surface) effects are negligible, with the provision that each such large crystal is in equilibrium with the normal polymer liquid" [87]. The degree of undercooling from the equilibrium melting temperature to the isothermal crystallisation temperature, $\Delta T = T_m^0 - T_c$, is

known to affect the final crystal structure obtained [88], and therefore to affect the properties of the material (as discussed in Chapter 1.2.1). Many equations used for examination of crystallisation kinetics also require the equilibrium melting temperature [87]. It may be of significant value therefore, to know the T_m^0 when determining the processing conditions of polymers such as PHB, or when investigating the crystallisation kinetics [88].

Determination of the equilibrium melting temperature is hindered by the inability to observe T_m^0 experimentally as, in the majority of cases, polymers melt out below T_m^0 [87]. The experimentally observed melting temperature, T_m(obs) is depressed by the surface energies of relatively small crystals [3]. Hoffmann and Weeks determined a method of estimating T_m^0, via extrapolation of the observed melting temperature according to T_c to the line $T_c = T_m$ [87]. The extrapolation is said to be equivalent to infinite crystal thickness [88], so could be used to estimate T_m^0 according to the definition given by Hoffman and Weeks [87]. Their reasoning was that a relationship existed between the observed melting temperature, the equilibrium melting temperature, and the temperature of crystallisation,

$$T_m = {T_m}^0(1 - 1/2\beta) + T_c/2\beta \qquad \text{(Equation 7.2)}$$

where $\beta = 1$ when no reorganisation takes place during melting [87]. Hence, with no recrystallisation or annealing during the experimental run, a plot of $T_m = T_c$ with a gradient of 0.5 is assumed from Equation 7.2.

Following the isothermal crystallisation, samples immediately underwent a melting run from the crystallisation temperature. The observed melting temperature values, T_m(obs), taken at the maximum height of the endothermic peak, were used to calculate the equilibrium melting temperature, T_m^0. Examples of these endotherms are shown in Figure 3.8.

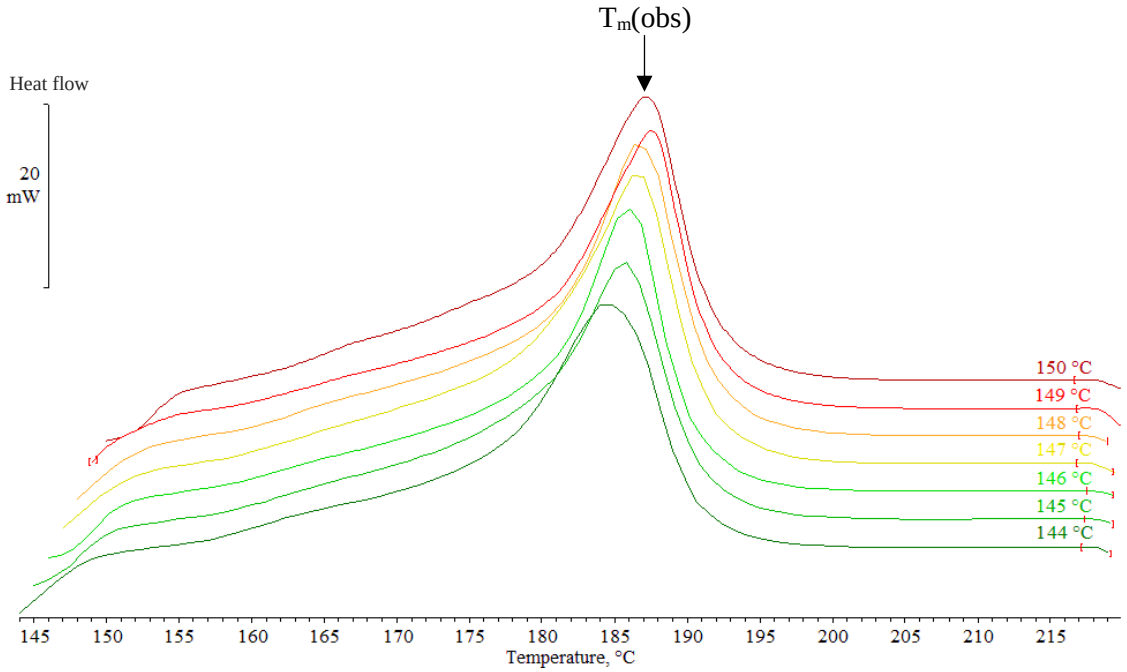

Figure 3.8. Endotherms from the melting runs following isothermal crystallisation at each temperature studied.

Figure 3.9 displays the observed melting temperature data averages, according to T_c, from the post-isothermal crystallisation melting runs. As the T_c increased, so did the average observed melting temperatures; similar trends have been reported previously [23,63].

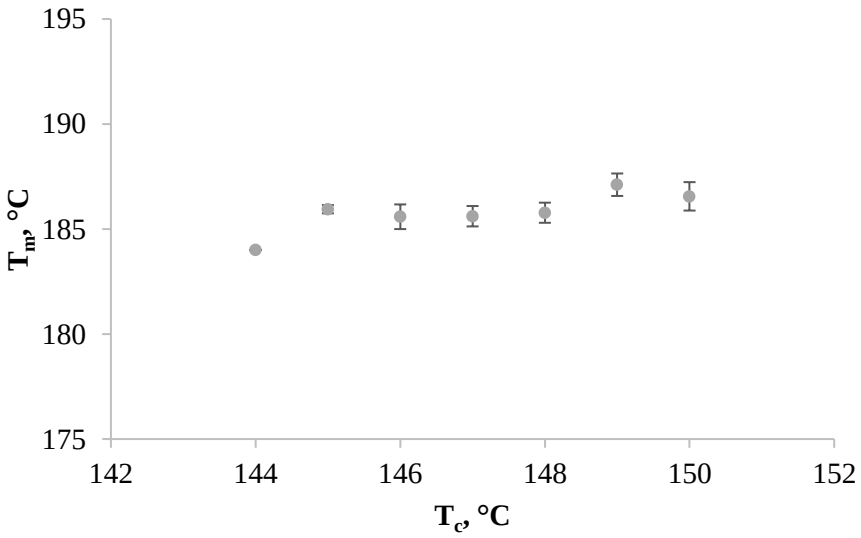

Figure 3.9. Observed peak melting temperature according to temperature of isothermal crystallisation.

The intersection, of the extrapolated line of observed melting temperatures with the line $T_c = T_m$, which provides the equilibrium melting temperature (T_m^0), occurred at 208 °C (Figure 3.10). A gradient of 0.36 was taken from the linear trendline, meaning that some secondary processes must have occurred despite the rapid heating rate of 50 °C min^{-1}.

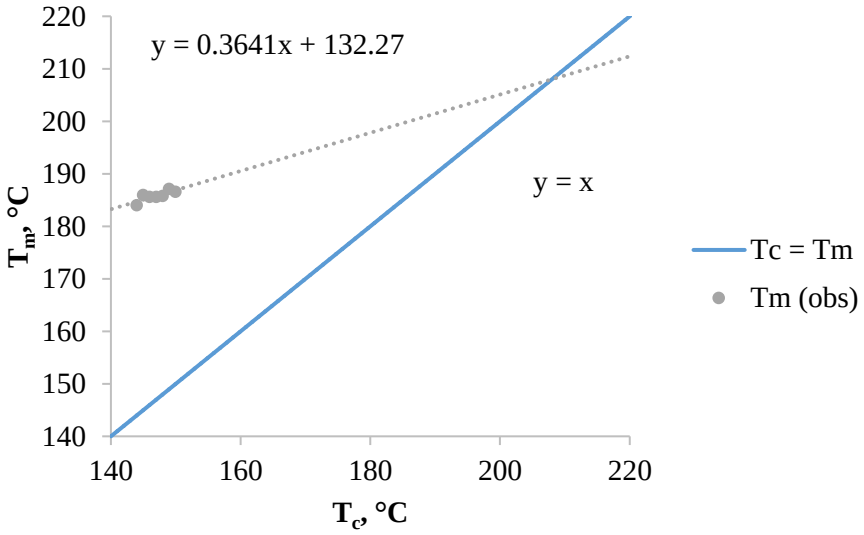

Figure 3.10. Determination of equilibrium melting temperature using Hoffmann-Weeks linear extrapolation of observed melting temperature to the intersection with the line $T_c = T_m$.

Results from several studies using the Hoffman-Weeks extrapolation method are detailed in Table 3.2, along with the experimental parameters used. Lower crystallisation temperatures and slow heating rates are known to affect observed melting temperatures [1], so will influence the value of T_m^0 obtained by the extrapolation method. Crystallisation temperatures with large degrees of undercooling, such as those used by You *et al*. [23] and some of the temperatures used by Barham *et al*. [79] and Organ and Barham [88], decrease the observed melting temperature as a result of the higher interfacial free energies associated with smaller crystals. Slow heating rates allow secondary processes to occur during the experimental run, as evidenced by the gradients of the extrapolated lines of the studies by You *et al*. [23] and Chan *et al*. [63], and the double melting peaks observed by You *et al*. [23] and Organ and

Table 3.2. Equilibrium melting temperatures estimated from the Hoffman-Weeks extrapolation of experimental data, along with details of the experimental methods employed.

Work	Material	T_m^0, °C	Gradient of extrapolated line	Cold- or melt crystallised (CC or MC)	T_c range studied, °C	Heating rate, min^{-1}	Single or double melting peaks
Present study	P(HB-co-3%HV)	208	0.36	MC	144-150	50	Single
You *et al*. [23]	PHB	200	0.34	Not stated, CC assumed due to T_c range	65-110	20	Double
	P(HB-co-5%HV)	195	0.42		50-85		
Barham *et al*. [79]	PHB	195 ± 5	Not shown	Not stated, CC assumed due to T_c range	30-140	Not stated	-
Organ and Barham [88]	PHB	195 ± 2	Unable to determine from data shown	Not stated, CC assumed due to T_c range	80-150	20	Some single, some double
Chan *et al*. [63]	PHB	188	0.18	MC	120-130	5	Single

Barham [88], which are. It is possible that the heating rate employed by Chan *et al*. [63] was slow enough that only one melting endotherm was observed, which corresponded to material which had melted and recrystallised during the melting run [61].

In this work crystallisation temperatures with low degrees of undercooling and high heating rates were used, in an attempt to limit the reorganisation process. The high estimated value of T_m^0 indicates that these precautions may have been successful, but only to a certain extent, as the gradient of the extrapolated line from T_m(obs) was measured at 0.36 suggesting that some secondary processes were active. The value of T_m^0 obtained in this work was higher than those seen by You *et al*. [23], Barham *et al*. [79], Organ and Barham [88] and Chan *et al*. [63], most likely due to a combination of higher crystallisation temperatures and faster heating rates.

3.2 Infrared spectroscopic analysis of spectral changes during primary crystallisation

Figure 3.11 shows the IR spectra taken at the start of isothermal crystallisation at 150 °C, when the sample was amorphous, and at the end of the run when the sample had attained a high degree of crystallinity. Prominent features include the C–H stretching at 3030 to 2845 cm^{-1}, CO_2 at 2390 to 2300, the carbonyl peak at 1770 to 1660 cm^{-1} and the fingerprint region from 1485 to 700 cm^{-1}. As it is separated from the other peaks in the spectra, and is sensitive to change in crystallinity, the carbonyl peak has been of particular interest regarding crystallisation studies. Many authors have examined the carbonyl peak in PHB, identifying a region relating to amorphous material between 1745 and 1739 cm^{-1} [34,36,47,48,89], and a region relating to crystalline material between 1728 and 1718 cm^{-1} [27,34,36,47,89]. The fingerprint region has also been shown to contain peaks sensitive to the crystallinity of PHB. Peaks in the regions of 1280 to 1275 cm^{-1} and 1230-1225 cm^{-1} have been attributed to stretching of the C–O–C

functional group, relating to crystalline material [34,36,48,89]. Peaks between wavenumbers of 1186 and 1183 cm^{-1} are said to represent the C–O–C asymmetric stretching bands of amorphous material [34,38,48,49].

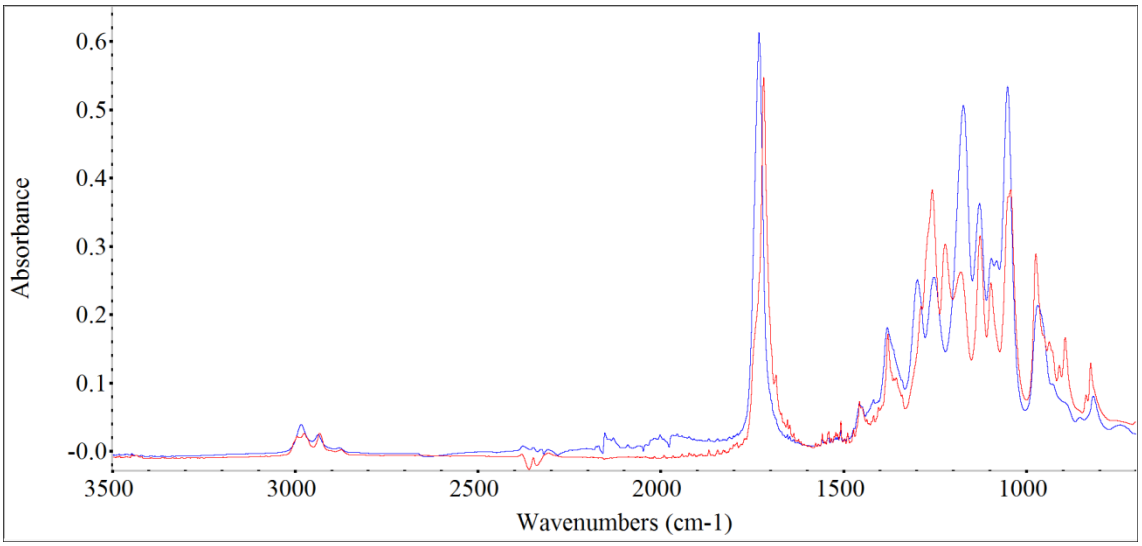

Figure 3.11. Spectral comparison of the start and end of the crystallisation run. Blue spectra = start, red spectra = end.

As it is sensitive to crystallinity, and is clearly resolved and separated from the other spectral peaks, crystallisation studies have often focused on the development of the carbonyl peak during primary crystallisation [41,49]. While Figure 3.12 illustrates the overall change in shape of the carbonyl peak, showing the first and last spectra of the primary crystallisation only, Figure 3.13 documents the transition process over time.

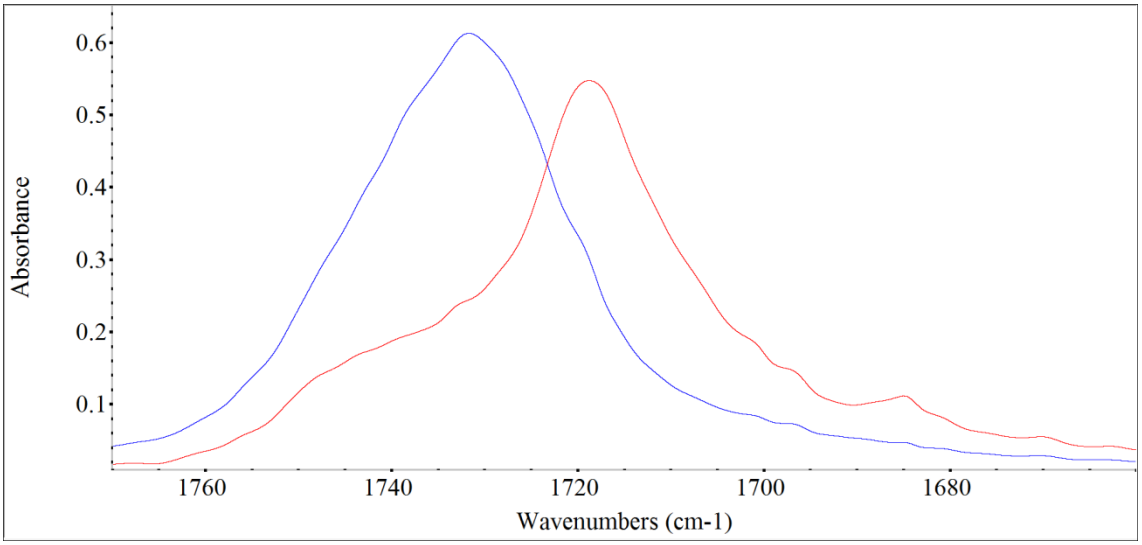

Figure 3.12. Carbonyl peak start and end of run comparison. Blue spectra = start, red spectra = end.

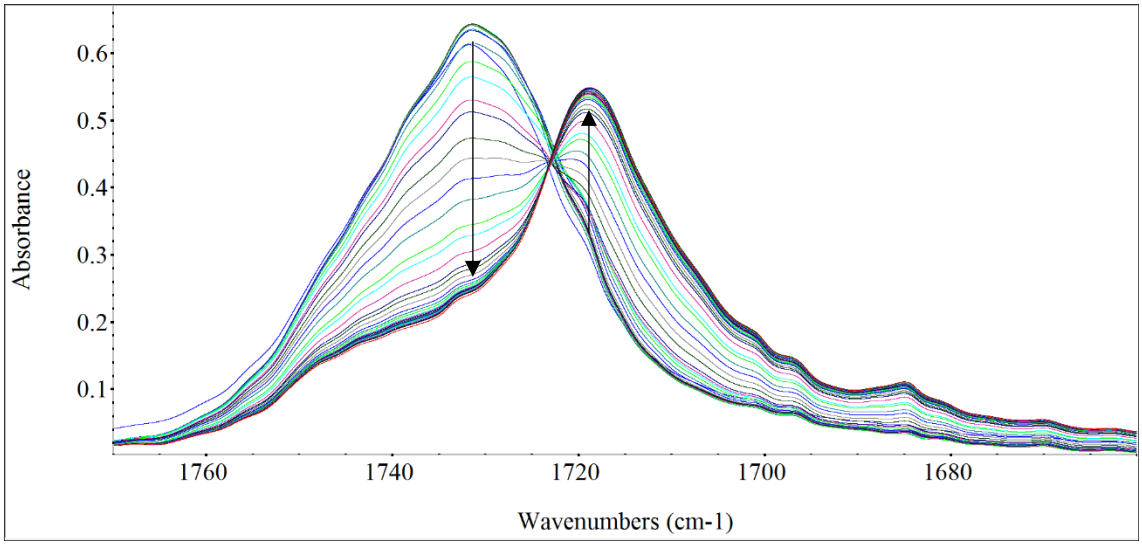

Figure 3.13. Carbonyl peak development over time during isothermal crystallisation. The arrows indicate the direction of change in the peak absorbencies with increasing crystallisation time.

Figure 3.14 illustrates the development of the peak height of the carbonyl band associated with the crystalline phase during primary crystallisation. Generally speaking, the curve has the sigmoidal shape typical of a phase transition, similar to those generated from the DSC isothermal data in Figures 3.3 and 3.4.

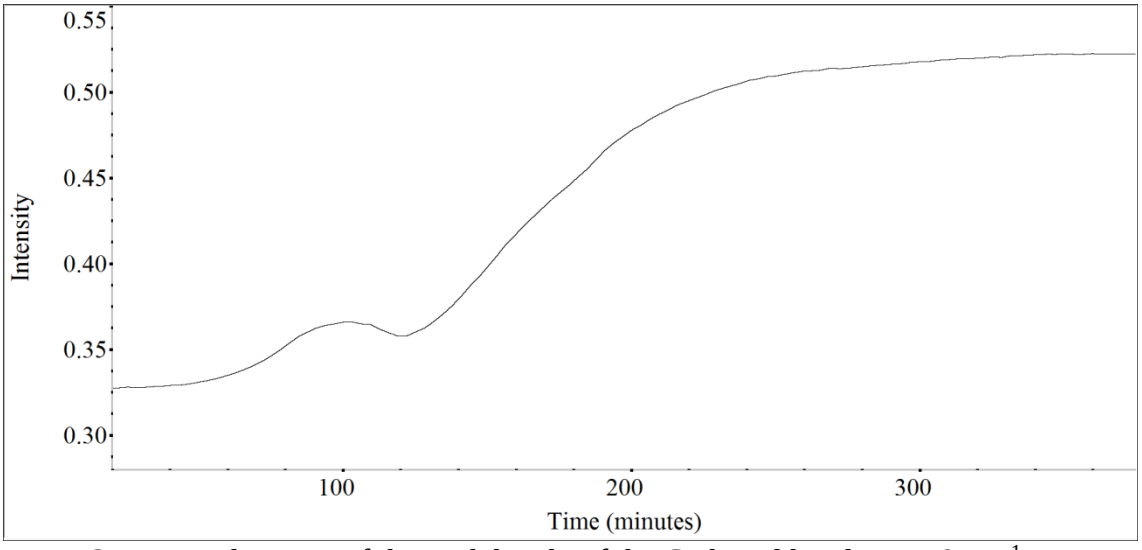

Figure 3.14. Development of the peak height of the Carbonyl band at 1719 cm^{-1} over time.

The fingerprint region has also been shown to contain peaks sensitive to the crystallinity of PHB and P(HB-co-HV). Peaks in the regions of 1280 to 1275 cm^{-1} and 1230-1225 cm^{-1} have been attributed to the C–O–C functional group, relating to crystalline material [34,36,48,89]. Peaks between wavenumbers of 1186 and 1183 cm^{-1} are said to represent the C–O–C asymmetric stretching bands of amorphous material [34,38,48,49]. Figure 3.15 shows the extent of change in the fingerprint region during primary crystallisation as a whole, with the first and last spectra overlaid, while Figure 3.16 depicts the pattern of change over the entire course of the experimental run. As can be seen in Figure 3.15, the crystalline peak at 1221 cm^{-1} is a single peak visible only when the sample is semi-crystalline, and not in the amorphous state. For this reason, the peak at 1221 cm^{-1} was used for analysis. During the primary crystallisation process, the amorphous peak, at 1180 cm^{-1}, decreased from an absorbance of 0.47 to 0.23. The crystalline peak, at 1221 cm^{-1} increased in absorbance from 0.11 to 0.27. At the end of the crystallisation run, the peak at 1180 cm^{-1}, in Figures 3.15 and 3.16, along with the shoulder at 1740 cm^{-1}, in Figures 3.12 and 3.13, demonstrate that the sample still maintained a proportion of the amorphous phase.

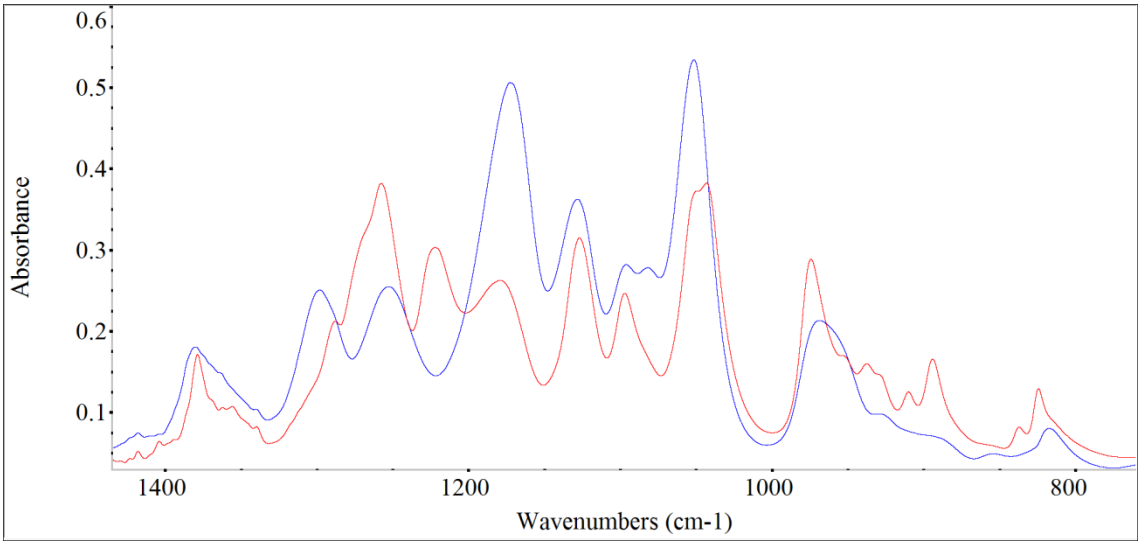

Figure 3.15. FP region start (blue spectra) and end (red spectra) of run comparisons. Blue spectra = start, red spectra = end.

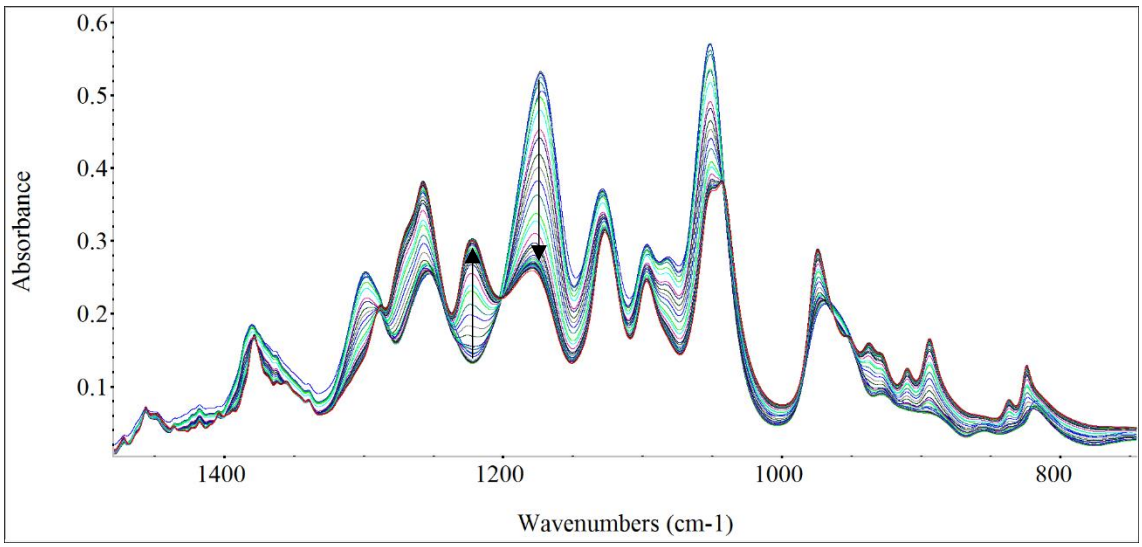

Figure 3.16. FP region development over time.

3.3 Conclusions

Higher crystallisation temperatures resulted in increased induction times and half-life, indicating decreased crystallisation rates as the temperature of crystallisation moved closer to the melting temperature. This agrees with the observed decrease in the Avrami rate constant with higher crystallisation temperatures. It is assumed that the crystallisation temperatures

studied were in the primary nucleation limited region, so the higher the T_c the lower the chance of embryos reaching critical size, therefore the crystallisation process took longer.

Similar values of the Avrami exponent, between 3.5 and 4, were calculated for all temperatures studied. Due to the difficulty associated with the interpretation of *n*, it is tentatively suggested that sporadic growth of spherulites occurred at all crystallisation temperatures in this work.

An equilibrium melting temperature of 208 °C was estimated using the Hoffman-Weeks extrapolation method. Despite the rapid heating rate, the gradient of the extrapolated line was 0.36, meaning some secondary processes must have been active during the melting run.

Analysis of the IR spectra obtained during primary crystallisation enabled identification of peaks sensitive to changes in crystallinity. The peak at 1732 cm^{-1} decreased in height and split into the narrow, more intense peak at 1719 cm^{-1} and broader, less intense shoulder around 1740 cm^{-1} as the crystallinity of the sample increased. Three peaks were highlighted in the fingerprint region, at 1453 cm^{-1}, 1221 cm^{-1} and 1180 cm^{-1}. These peaks were identified as being insensitive to the change in crystallinity, and representative of the crystalline and amorphous material respectively.

CHAPTER 4 – SECONDARY CRYSTALLISATION STUDIES

4.1 DSC dynamic heating runs

As discussed in Chapter 3.1, the DSC lacks the sensitivity required to examine the secondary crystallisation process in real time at isothermal temperatures [32]. It is, however, possible to calculate the resulting degree of crystallinity in samples stored isothermally from a dynamic melting run. Providing a sufficiently fast heating rate is used, to prevent additional crystallisation occurring during the melting run, this method may be used to gain insight into the development of secondary crystallisation.

4.1.1 Qualitative observations of DSC traces

The melting traces of samples stored at -22, 7, 20, 50, 75, 100, 125 and 150 °C are presented in Figure 4.1a-h. Each figure represents a single isothermal storage temperature, and illustrates the effect the storage temperature had on the melting traces of samples over a time span of 672 hours. Two features of note observed in the DSC traces are that there was an increase in the peak melting temperature occurring over time, and that a shoulder is seen to have developed on the lower temperature side of the melting peak when samples were stored at the highest temperatures.

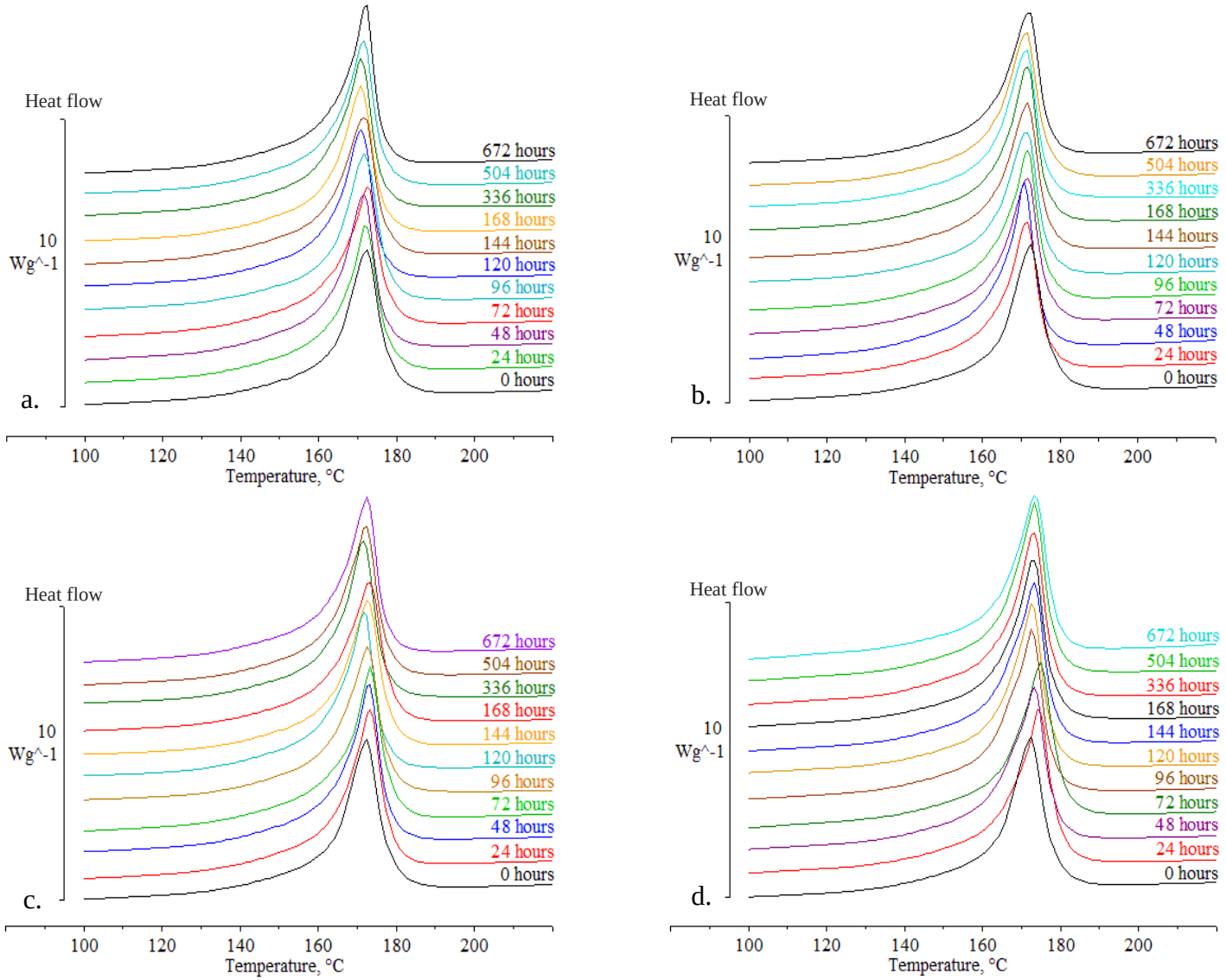

Figure 4.1. DSC traces from samples stored at a. -22 °C, b. 7 °C, c. 20 °C, and d. 50 °C for the durations indicated.

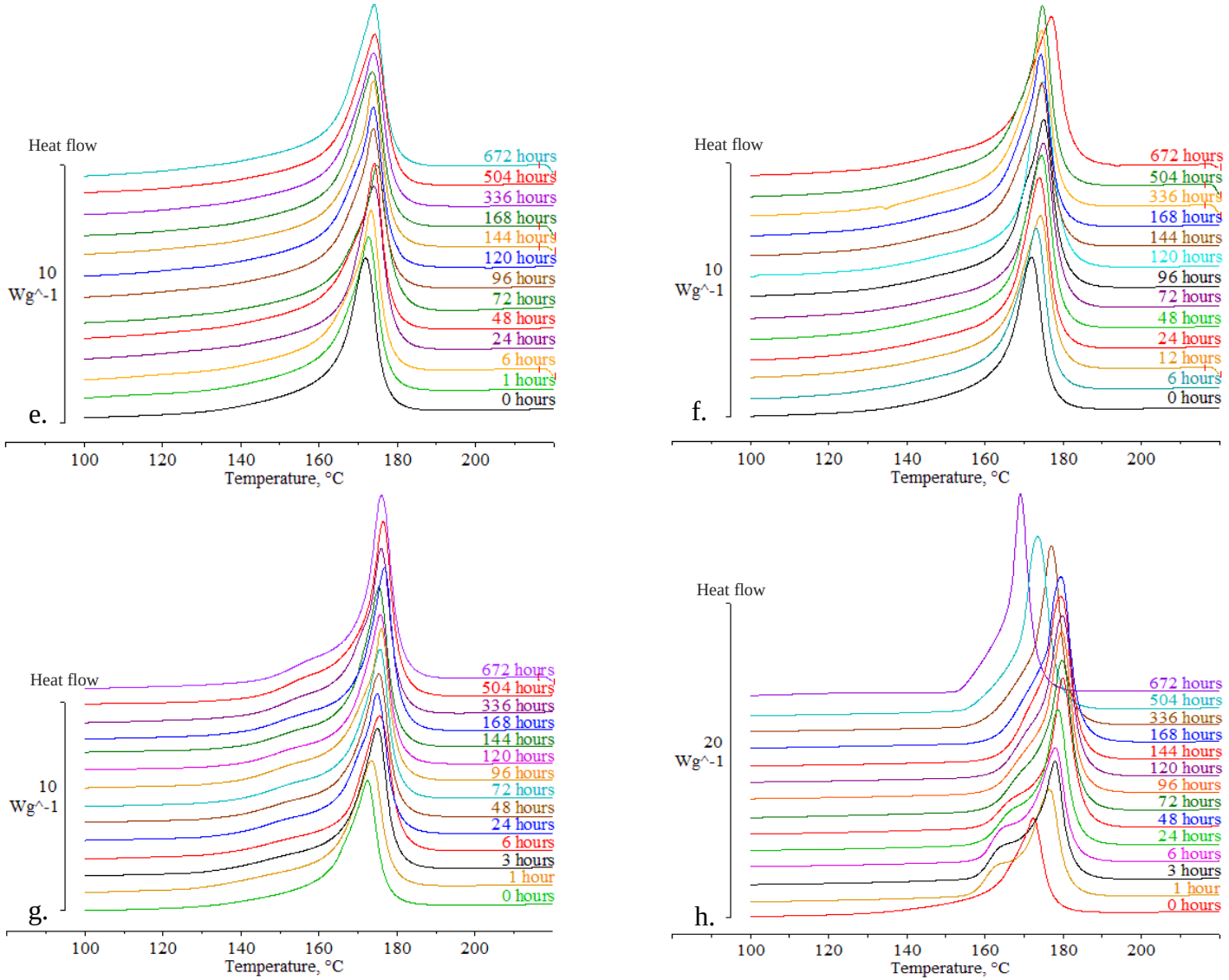

Figure 4.1 continued. DSC traces from samples stored at e. 75 °C, f. 100 °C, g. 125 °C, and h. 150 °C for the durations indicated.

Qualitative analysis of samples stored at -22 to 50 °C, from Figures 4.1a-d, does not reveal any immediately obvious change in the melting traces during storage. When stored at 75 °C there is the first suggestion of change (Figure 4.1e), as the peaks appear to move very slightly towards higher temperatures with increasing storage time. This shift became more definite in the samples kept at 100 °C (Figure 4.1f), and is very obvious in samples kept at 125 °C (Figure 4.1g). From these traces, it is clear that higher storage temperatures produced a change in the samples which meant that the melting peak maximum occurred at higher temperatures, and that this increase became greater with increased lengths of storage time. However, when looking at the traces in Figure 4.1h, obtained from samples held at 150 °C, it is apparent that this trend is only applicable up to a certain point. To begin with, the position of the melting peak did move towards higher temperatures over time in samples stored at 150 °C, however this upward shift halted after around 48 hours. Storage times upwards of 144 hours then resulted in a downward shift back towards lower temperatures. Žagar and Kržan also observed significant change within the DSC traces of samples exposed to high temperatures, which was more severe with longer exposure times [69], and Janigová *et al*. reported a broadening and shift to lower temperatures over time [68]. Both authors attribute these changes to thermal degradation, and while the temperatures they used are higher than the 150 °C used here (190 and 180 °C respectively), it may be possible that the far greater exposure times at 150 °C, up to 672 hours compared to 80 and 300 minutes respectively, produced the same effect. It has been suggested that a decrease in molecular weight, associated with degradative effects (see Chapter 1.5), may occur in P(3HB-co-45%3HV) at temperatures as low as 100 °C [67], so it seems reasonable to suggest that the changes observed at 150 °C in this work are due to degradation. This will be discussed further in Chapter 7.

The first suggestion of a shoulder developing on the lower temperature side of the melting peak may be seen in Figure 4.1f, produced from the traces of samples stored at 100 °C. Not until samples were kept at 125 °C did the shoulder undoubtedly become more prominent with increasing durations of storage. At a storage temperature of 150 °C the development of the shoulder became much more interesting; it grew rapidly at the onset of the study then appeared to merge with the main melting peak over time, as the main melting peak position shifted to lower temperatures.

Many authors have discussed the development of shoulders and/or multiple melting peaks becoming more pronounced over time in regards to PHB and its copolymers. Most commonly these observations are attributed either to the melting, recrystallisation and subsequent remelting of originally less stable crystals, or to the melting of crystals of different sizes, lamellar thickness or degree of perfection [13,17,34,91]. Liu *et al*. discovered that at relatively low heating rates, of 5 and 10 °C min^{-1}, a prominent shoulder was observed that was not present at higher heating rates of 20 and 30 °C min^{-1} [75]. Conversely, Ziaee and Supaphol reported double melting only with higher heating rates (≥ 20 °C min^{-1}) [61]. Taking all of this information into account, it becomes clear that in order to reveal the true properties of the original structure prior to the melting run, a suitably high heating rate must be used to prevent reorganisation. de Koning *et al*. and Righetti and Di Lorenzo suggested 60 °C min^{-1} to be a suitably high heating rate [13,17]. As the samples in this study were subjected to melting runs at 50 °C min^{-1}, it is unlikely that the shoulder is a result of melting, recrystallisation and remelting due to the speed of the heating rate. However, it is possible that at a storage temperature of 150 °C the initial emergence of a very prominent shoulder may be due to the partial melting and recrystallisation of less stable crystal structures upon storage. Evidence supporting this suggestion is shown by the overlaid black and red dashed lines in Figure 4.2; as

the DSC trace of the untreated sample clearly shows that the onset of melting occurred below the storage temperature, and the shoulder of the sample stored for 24 hours emerges above the storage temperature. Further growth of the shoulder may be due to thickening of the lamella, through secondary crystallisation, or because of a decrease in M_w, through chain scission, which created shorter chains that melted at lower temperatures. It could also be a combination of these two processes. This will be discussed in more detail in Chapter 7.

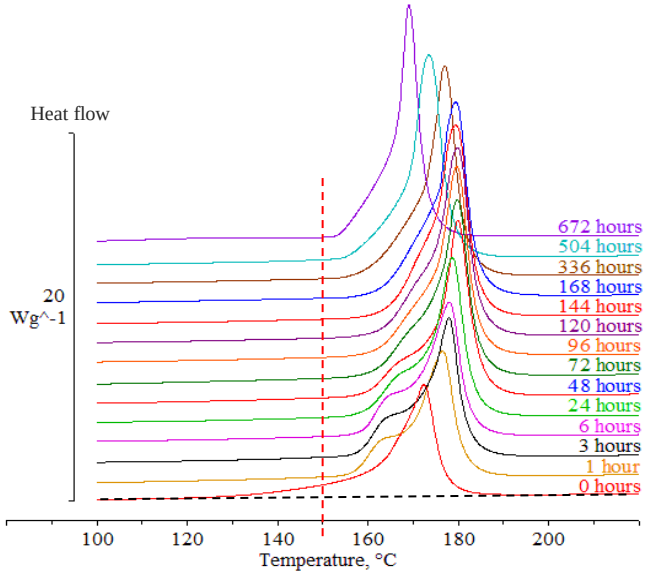

Figure 4.2. DSC traces from samples stored at 150 °C for the durations indicated above the individual traces. The dashed black line indicates the baseline of the untreated sample, the dashed red line highlights the storage temperature.

At storage temperatures of 100 and 125 °C, it is not clear what the cause of the shoulder formation is. Multiple authors have previously attributed the development of a shoulder to the formation of crystals with smaller size, or to lamellar thickening [22,34,57]; which has been shown through wide angle x-ray scattering (WAXS) and small angle x-ray scattering (SAXS) experiments to take place at increased temperatures [57,58]. An alternative suggestion is that the shoulder may be a product of a decrease in the M_w, caused by chain scission. This has been shown to occur isothermally, at temperatures from 100 to 200 °C within 20 minutes, in

P(HB-co-45mol%HV) [67]. Chen *et al*. also reported a decrease in M_w at isothermal temperatures from 100 to 180 °C in PHB and P(HB-co-5wt%HV) within a maximum heating time of 6 hours [54]. Janigová *et al*. studied isothermal degradation of PHB at temperatures of 180 to 220 °C and observed a similar shoulder, which was attributed to chain scission causing changes in the size of the spherulites with decreasing M_w [68]. Numerous authors have stated that thermal degradation is likely to begin in the amorphous regions [69,71,77], which means it is likely that at storage temperatures of 100 and 125 °C chain scission would occur in the amorphous phase only, and not affect the crystalline regions [68].

By comparing the melting traces obtained after 672 hours, the temperature dependence of the shape of the melting peak becomes more obvious (Figure 4.3). The trends of increasing height of the peak and shift towards higher temperatures with increasing storage temperature, up to 125 °C, are clearly visible. The emergence of the shoulder on the lower temperature side of the melting peak only transpired in the samples stored at the higher temperatures. The difference in the peak shape of the 150 °C sample, in comparison to the samples stored at lower temperatures, is striking. Not only did the 150 °C storage peaks become narrower, they are also greater in size, and the transitions at the onset of melting are more abrupt.

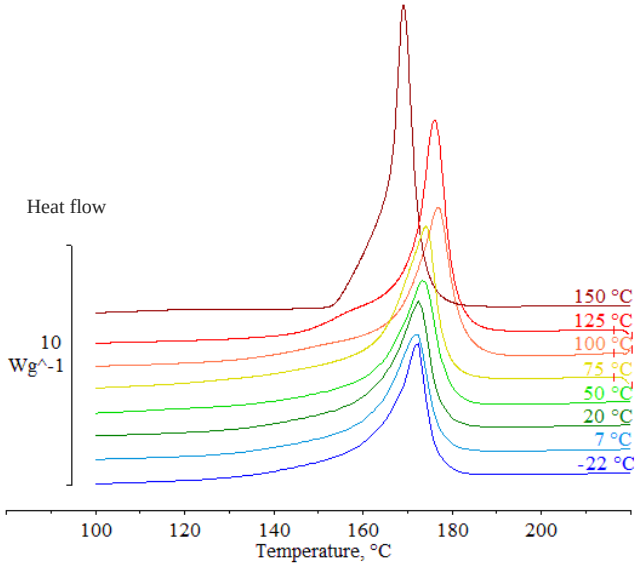

Figure 4.3. DSC traces after 672 hours of storage at the temperatures indicated above each individual trace.

4.1.2 Determination of the degree of crystallinity from the enthalpy of fusion

The enthalpy of fusion values, illustrated in Figures 4.4 and 4.5, were used to calculate the degree of crystallinity using,

$$X_c = \frac{\Delta H_f}{\Delta H_f{}^0} \times 100 \qquad \text{(Equation 5.1)}$$

where X_c is the weight fraction degree of crystallinity, and ΔH_f is the measured enthalpy of fusion from the experimental data and $\Delta H_f{}^0$ is 146 J/g [79], as described in Chapter 2.4.1. The trends in the enthalpy of fusion data will be discussed in terms of the crystallinity values obtained.

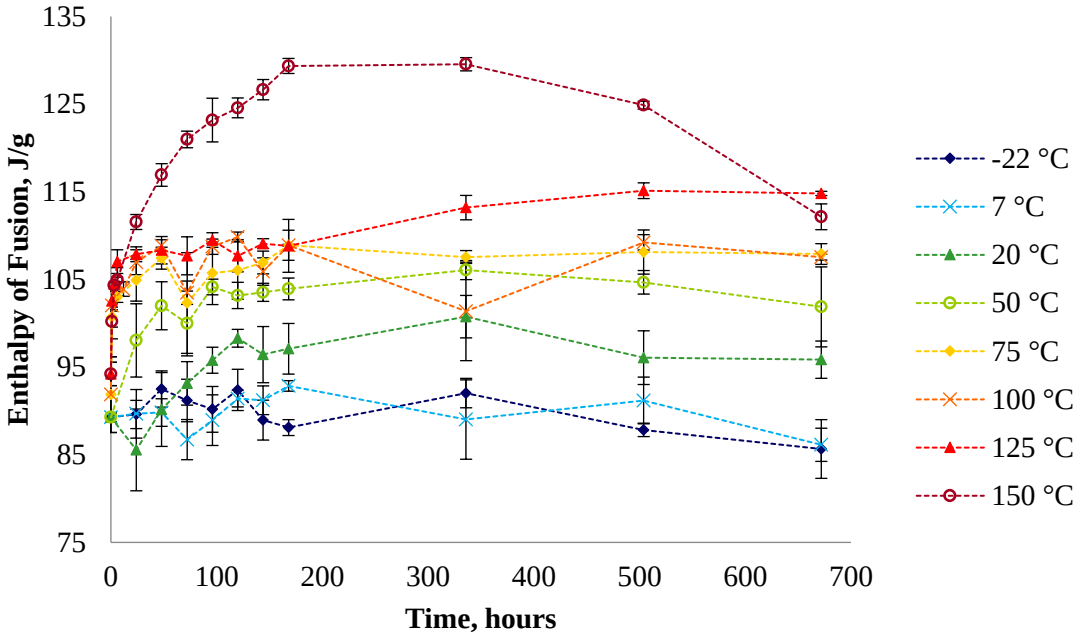

Figure 4.4. Enthalpy of fusion vs. time, according to temperature of storage. Dashed lines have been superimposed between timepoints as a visual aid to guide the eye through the data sets. DSC data tables are in Appendix B.

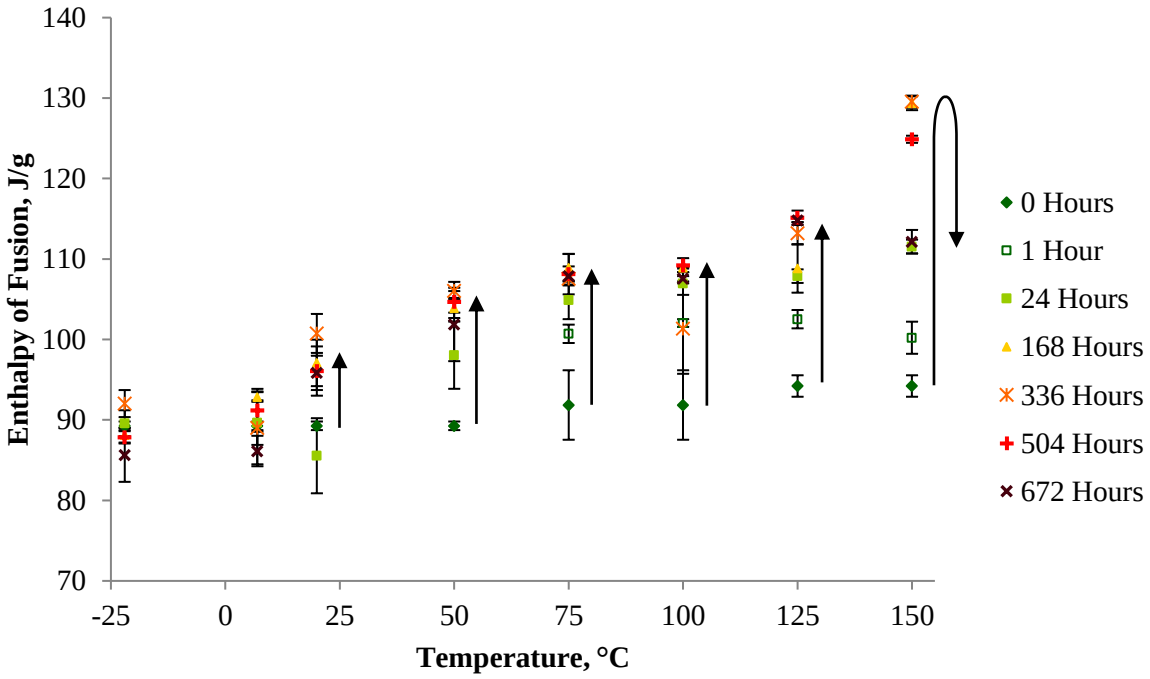

Figure 4.5. Enthalpy of fusion vs. temperature of storage, according to length of storage time.

At storage temperatures of -22 and 7 °C, there were no discernible increases in the crystallinity over time. The work of Righetti and Di Lorenzo discussed the limitations, of reorganisation during secondary crystallisation, imposed by the presence of the rigid amorphous and crystalline phases [17]. This would indeed reduce the degree of secondary crystallisation at temperatures close to the T_g of the material, similar to during the primary process, where the mobility of the polymer chains is low.

In general, at storage temperatures of 20 °C and above, samples stored for longer had higher crystallinities, and the higher the temperature of storage the greater the increase in crystallinity was. The majority of the observed increase in crystallinity occurred within the first 24 hours of the study, as the rate of change was greatest early on and slowed with the increase of time. Biddlestone *et al*. also followed the secondary crystallisation process by observation of the enthalpy of fusion over time, and found that the increase was linear with log(t) when stored at room temperature [32]. This is applicable to the increase in crystallinity, observed at storage temperatures between 20 and 125 °C, over time in Figures 4.6 and 4.7. This logarithmic change happened for two reasons. The first is quite simply that, as secondary crystallisation progresses, there is less material remaining in the amorphous state to undergo crystallisation. The second is that, as the crystallinity increases, the constraints upon the remaining amorphous material become greater, and so the mobility of the chains become more restricted over time. de Koning *et al*. presented similar findings from work with PHB, in terms of the rate and extent of change increasing according to longer exposure times and higher temperatures, although on a much shorter timescale [13]. The increase in the rate of secondary crystallisation with temperature, observed in both this work and the work of de Koning *et al*. results from the increased free volume and mobility introduced into the system at higher temperatures. Unlike the primary crystallisation process, the rate of the secondary crystallisation process is not as limited by the

proximity to the T_m of the material. In the primary crystallisation process, the highest storage temperatures in this study (125 and 150 °C) would be in the nucleation limited region which would reduce the rate of crystallisation. During the secondary crystallisation process, there is no need for the formation of embryos, and therefore the rate of crystallisation is not limited in that way. This means that instead of the temperature-rate dependence in the shape of a parabolic curve seen in primary crystallisation, the temperature-rate dependence of secondary crystallisation follows a relatively linear increase (Figure 4.7). This would agree with the proposal made by Phillipson *et al*. that secondary crystallisation is a diffusion controlled process [51].

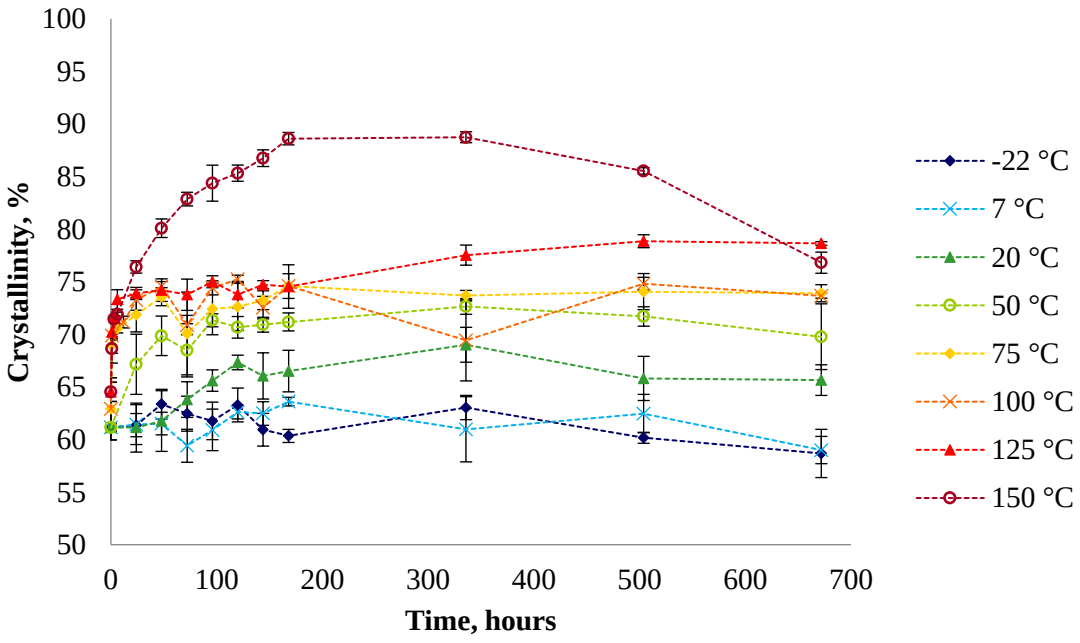

Figure 4.6. Crystallinity vs. time, according to temperature of storage. Dashed lines have been superimposed between timepoints as a visual aid to guide the eye through the data sets. DSC data tables are in Appendix B.

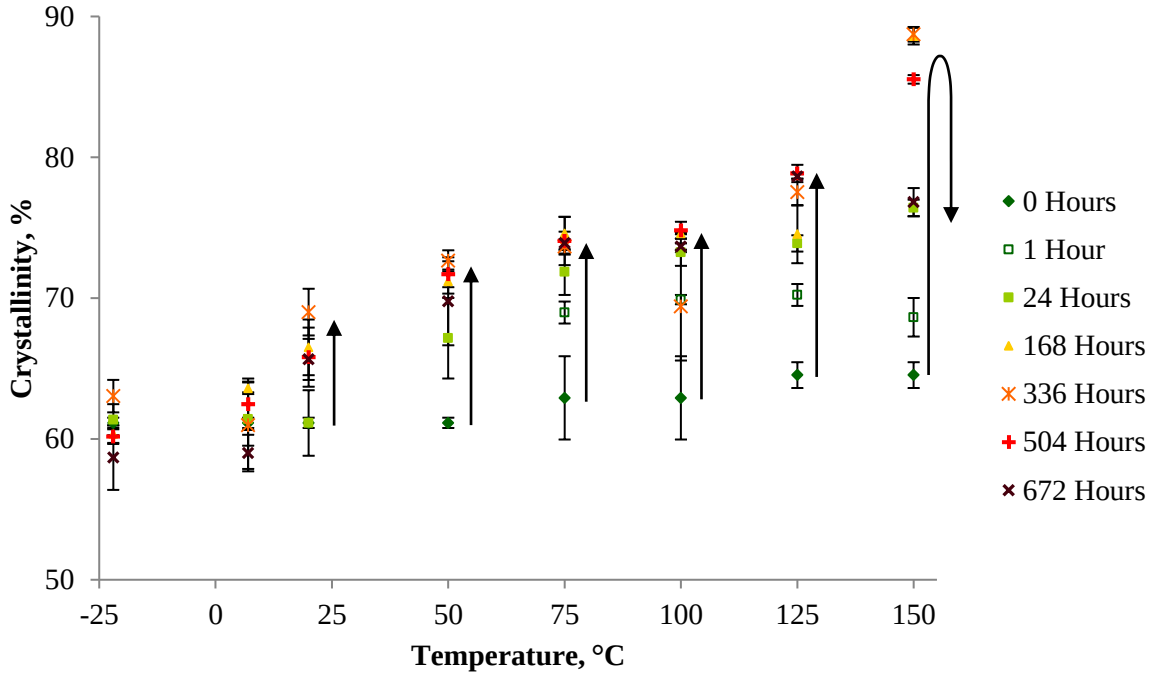

Figure 4.7. Crystallinity vs. temperature of storage, according to length of storage time.

After initially following the trend of increasing crystallinity with increased storage time, from 64.5 % up to 88.6 % after 144 hours, the degree of crystallinity of samples held at 150 °C reached a plateau. The rapid increase in crystallinity which occurred at the beginning of the study could be related to the emergence of the shoulder seen in Figure 4.1h. The prominence of the shoulder, combined with the high storage temperature, led to the belief that there may have been some degree of partial melting and recrystallisation within the samples during storage, which is usually associated with the melting-recrystallisation-remelting often encountered during melting runs. This would allow recrystallisation and reorganisation of less perfect and therefore less stable crystals into a more perfect crystal structure through thickening of the un-melted, more stable lamellae [83]. de Koning *et al*. notes how the rate of reorganisation is rapid within the "well nucleated 'melt' due to the abundance of intact crystals and crystal residues." [13]. After 336 hours of storage, and a maximum value of 88.7 %, the crystallinity then began to drop. Values of 85.5 and 76.8 % were calculated from samples exposed to 150 °C for 504

and 672 hours respectively. A similar pattern of changing crystallinity was presented in the work of Janigová *et al*. and attributed to the thermal degradation of the material [68], which proceeds via the chain scission mechanism detailed in Chapter 1.5. The initial rise in the degree of crystallinity was said to be a result of chain scission producing shorter chains; which have increased mobility and pack more easily into the crystalline structure. The subsequent fall in crystallinity was then assigned to chain scission and the increasing number of free ends of polymer chains with extensive degradation, creating defects within the crystal structure. While Janigová *et al*. observed the same trends that were present in the samples stored at 150 °C in this work, the temperatures in that study were much higher (180 to 220 °C), and the duration was much shorter (up to 80 minutes) [68]. Taking this into account, it is plausible that degradation does not begin as early, or act as rapidly in samples stored at 150 °C as in the work of Janigová *et al* [68]. These factors combine to explain the increase and sustained crystallinity within the first 168 hours of storage. The decrease in crystallinity, associated with extensive degradation, did not occur until much later at 150 °C (504 hours) compared to 190 °C (80 minutes). The findings of Janigová *et al*. also suggest that the degradation process may be active before the decrease in the degree of crystallinity is observed, but the interplay of the secondary crystallisation and thermal degradative effects masks when the first process ends and the second starts [68]. What is shown in Figures 4.6 and 4.7 is which process is dominating over time. The thermal degradation of samples in this work is discussed in more detail in Chapter 7

.

4.1.3 Determination of the onset of melting

As with the crystallinity, there was no change observed in the onset of melting in samples which were held at -22 or 7 °C, which is expected due to the material being held below or very close to its glass transition temperature (Figures 4.8 and 4.9). The samples stored at 20 and 50 °C presented a lower onset of melting temperature than the untreated samples. This change was greater in samples stored at 20 °C than those stored at 50 °C; from 101 °C down to 56 and 67 °C respectively. At these temperatures, almost all the change took place within the first 72 hours of the study, with similar values observed thereafter. Secondary crystallisation is widely acknowledged to be active at room temperature. It is possible that, at these relatively low temperatures, secondary crystallisation results in the formation of new, very thin, lamellae [92]. These structures would have a lower melting point than the more stable primary crystals, and could therefore lower the temperature of the onset of melting. Assuming that secondary crystallisation is a diffusion controlled process, it is likely that this behaviour occurred within the mobile amorphous phase, where diffusion is less restricted, at these low temperatures.

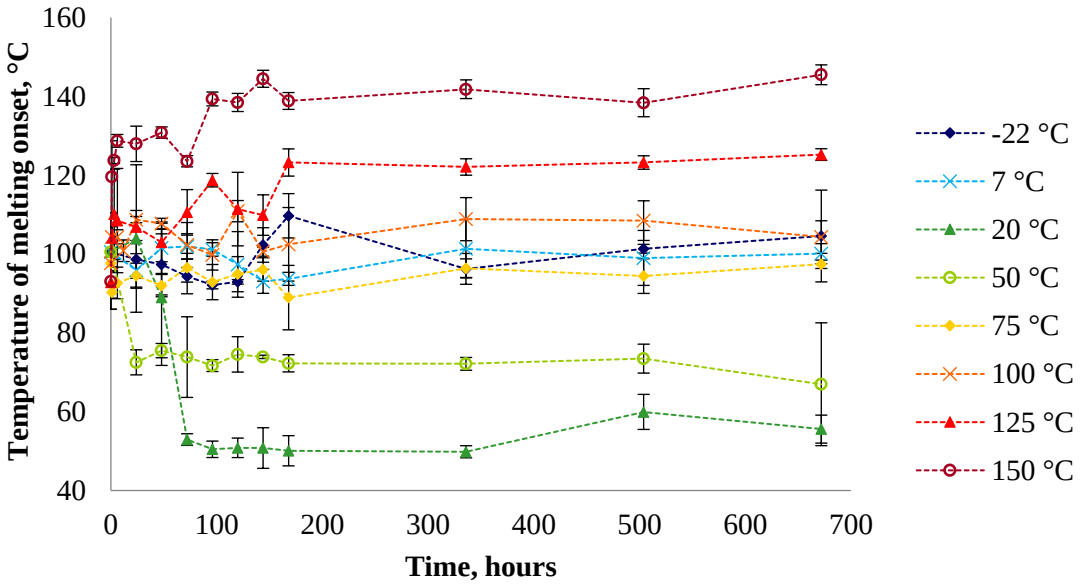

Figure 4.8. Temperature of melting onset vs. time, according to temperature of storage. Dashed lines have been superimposed between timepoints as a visual aid to guide the eye through the data sets. DSC data tables are in Appendix B.

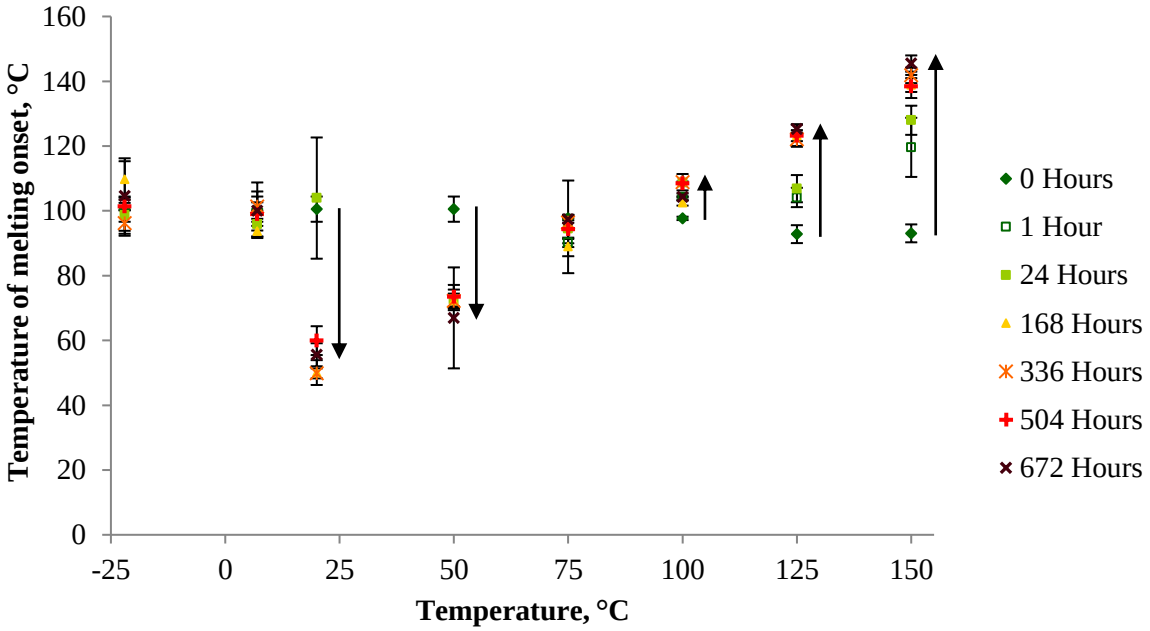

Figure 4.9. Temperature of melting onset vs. temperature of storage, according to length of storage time.

When kept at 75 °C the samples maintained a similar onset of melting temperature throughout the entire duration of the study, with pre- and post-storage measurements of 98 and 97 °C. All temperatures of storage above 75 °C resulted in increased values of onset of melting temperature, with both longer storage times and higher storage temperatures producing greater increases. At all of these temperatures, a plateau appeared to be reached 168 hours into the study. After 672 hours of exposure to the thermal conditions, the onset of melting increased from 98, 93 and 93 °C to 104, 125 and 146 °C respectively when stored at 100, 125 and 150 °C. At these storage temperatures, it is unlikely that new thin lamella would be able to form, as the samples would be above the T_m of these smaller structures. Instead it is more likely is that the secondary crystallisation process acts through the lamellar thickening of the primary crystals, as the higher temperature enables diffusion in the rigid amorphous phase adjacent to the crystalline phase. Fujita *et al*. reported observing an increase in lamellar thickness with temperature increase, above a threshold temperature of 120 °C, which is said to be dependent

on the molecular weight and lamellar thickness of the original sample [57]. Lamellar thickening would cause a rise in the temperature of the onset of melting as the less stable material, which would melt at lower temperatures, is incorporated into the more stable crystal structure, which melts at higher temperatures. Gunaratne *et al*. and Hong and Chen both cite lamellar thickness as an influencing factor of melting temperature [34,59].

The observations, made with regards to Figures 4.8 and 4.9, suggest that there may be two different mechanisms of secondary crystallisation active within the storage temperature range studied, and that each contributes to the increase in crystallinity within a different temperture range. At the lower end, secondary crystallisation is likely to proceed via infill of smaller crystall structures formed in the mobile amorphous fraction (MAF), and at the higher end it proceeds via thickening of the primary crystal lamellar. Infill would decrease the onset of melting, as the smaller stuctures are less stable and melt out at lower temperatures, while thickening would increase the onset of melting, as it creates more stable structures which require more energy to melt. The samples stored at 75 °C may represent a cross over point of these two secondary crystallisation mechanisms, and so no change in the temperature of melting onset was seen within the timescale of this study.

4.1.4 T_m as determined from the temperature of the melting peak maximum

The first definitive change in peak melting temperature over time may be observed in the samples which were stored at 75 °C. At this temperature, there was a very small increase from the unconditioned average value, 172.5 °C, to the samples stored for 24 hours, 173.5 °C. The T_m then stabilised, remaining around this value for the rest of the study where an average value of 173.9 °C was calculated. Storage temperatures of 100 and 125 °C presented very similar

trends to each other, in which the temperature of the melting peak rose over time in a logarithmic manner. The T_m increased from 172.5 to 176.0 °C in samples stored at 100 °C, and from 171.4 to 176.0 °C in samples stored at 125 °C. Mitomo and Doi also reported an increase in T_m when samples of P(3HBco-7mol% 3HV) were held for 120 minutes at temperatures between 100 and 155 °C [58]. This increase was said to be linear with the increase in temperature.

The temperature at which a semi-crystalline polymer melts may be influenced by a number of factors. In this situation, the processing method does not differ, the amount of copolymer does not vary, and the chemical structure of the polymer remains the same, so the degree of crystallinity is the most likely controlling factor of T_m at storage temperatures between -22 and 125 °C. As secondary crystallisation is known to increase the entropy of the system, creating more van der Waals bonds between the chains as they fold and pack together, it follows that a greater degree of secondary crystallisation requires a greater input of thermal energy to de-stabilise the more ordered crystalline regions, raising the T_m. The link between the logarithmic increase in secondary crystallisation with time and melting temperature has also been discussed by Marand and Huang [84]. A follow up paper by Huang *et al*. emphasised that the rate of secondary crystallisation determines the timescale of the change in melting temperature [86]. As seen in Figures 4.6 and 4.7, the higher the temperature of storage, the greater the rate of secondary crystallisation, thus the increase in T_m seen in Figures 4.10 and 4.11.

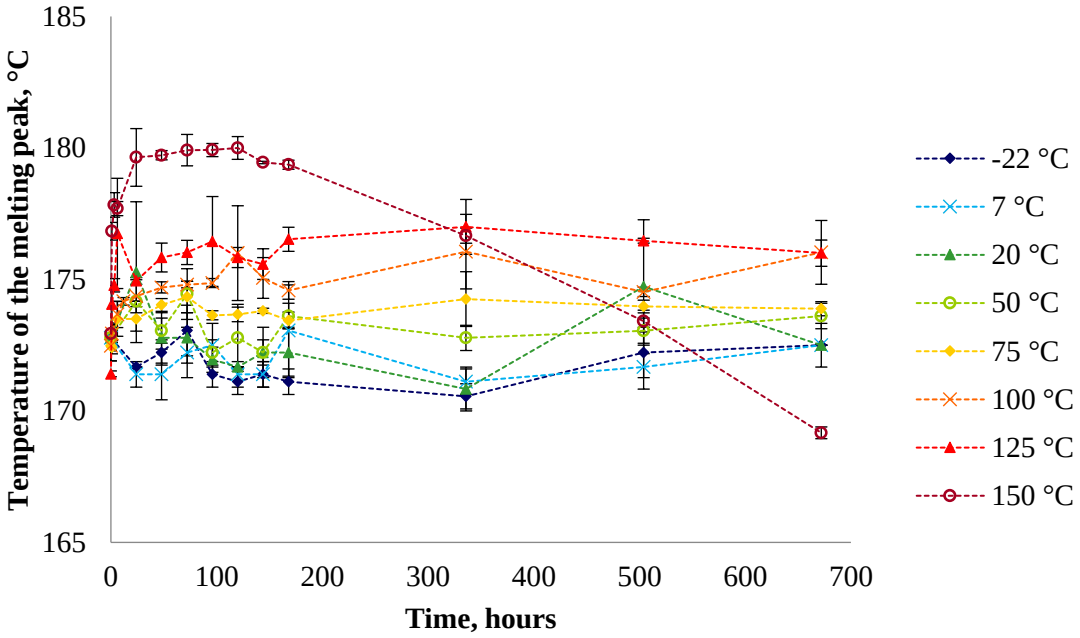

Figure 4.10. Peak melting temperature vs. time, according to temperature of storage. Dashed lines have been superimposed between timepoints as a visual aid to guide the eye through the data sets. DSC data tables are in Appendix B.

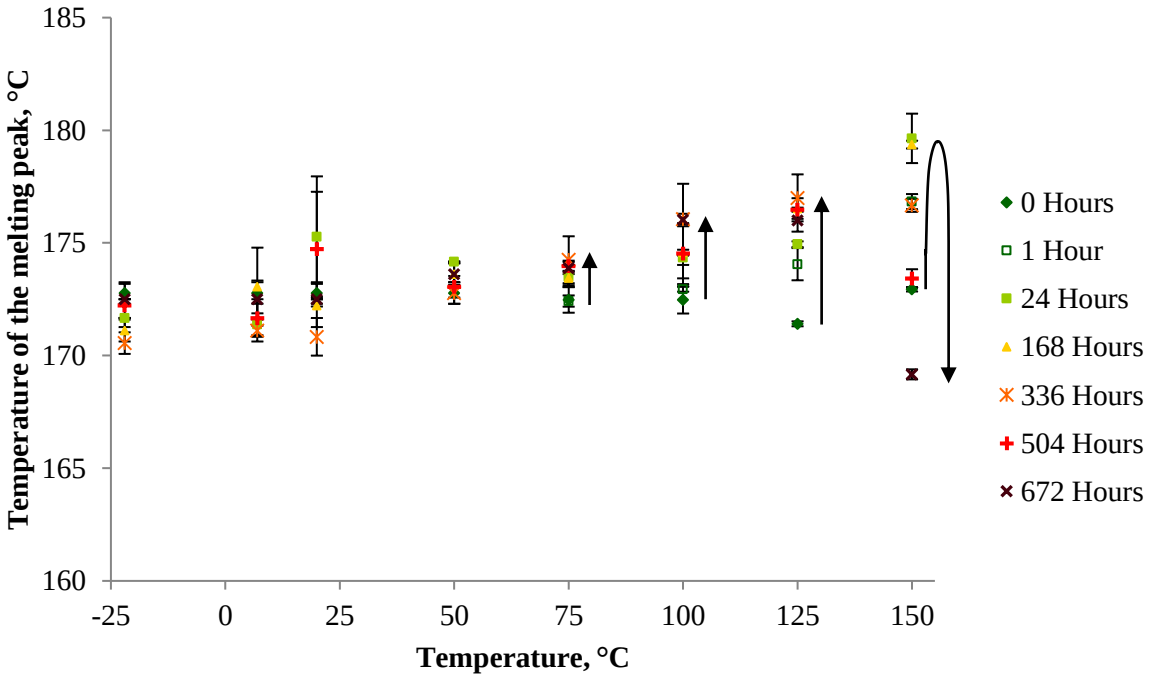

Figure 4.11. Peak melting temperature vs. temperature of storage, according to length of storage time.

The samples held at 150 °C initially underwent the same trend of increase in T_m as the 100 and 125 °C samples, up to a storage time of 120 hours, rising from 172.9 to 180.0 °C. Following this, the melting point began to decrease. After 504 hours of storage the samples had an average peak melting temperature similar to that from the unconditioned samples, at 173.4 °C, and by 672 hours the average value was much lower, at 169.2 °C. If the study had only lasted 120 hours, it might have been thought that these samples were presenting a logarithmic increase in T_m over time, which was accelerated by exposure to the high temperature. However, while the increase in crystallinity, which usually causes a rise in T_m, may have been a factor at the beginning of the study, the subsequent decrease in T_m suggests that is wasn't just the expected slowing down of this process that accounted for the plateau observed between approximately 24 and 168 hours shown in Figure 4.10. It is likely that, if the thermal degradation process postulated earlier is active at 150 °C during prolonged exposure, the chain scission initially aids in the secondary crystallisation process as a result of the easier chain packing [68], and therefore contributes to the increase in T_m. However, as time progresses, and the extent of chain scission increases, the breakdown in the chains reduces the crystallinity of the system, resulting in a material consisting of many short chains with a larger free volume. Accordingly, less energy is required to enable mobility of the chains and the T_m of the samples would decrease, as is presented in Figures 4.10 and 4.11.

4.1.5 Determination of the last trace of crystallinity

The last trace of crystallinity is another measure of the melting temperature, representing the point at which all crystals are completely melted. While the general spread of data, and large degree of error, obtained from samples held at lower temperatures prevents any clear

determination of trends, there may be a trend in the change in last trace of crystallinity over time at storage temperatures of 75 to 125 °C. However, these results were also not very clear or consistent with high margins of error, and it is with hesitancy that a trend of which an increase in temperature causes an increase in the last trace of crystallinity over time is suggested. This agrees with the findings in the previous section, relating the increase in T_m to the increase in degree of crystallinity caused by the secondary crystallisation process. The last trace of crystallinity was measured as 192.6, 192.6 and 197.1 °C prior to storage at 75, 100 and 125 °C respectively, and as 203.9, 202.8 and 200.8 °C after 672 hours. Some of the time points were removed from Figures 4.12 and 4.13 in an attempt to increase the clarity of the data.

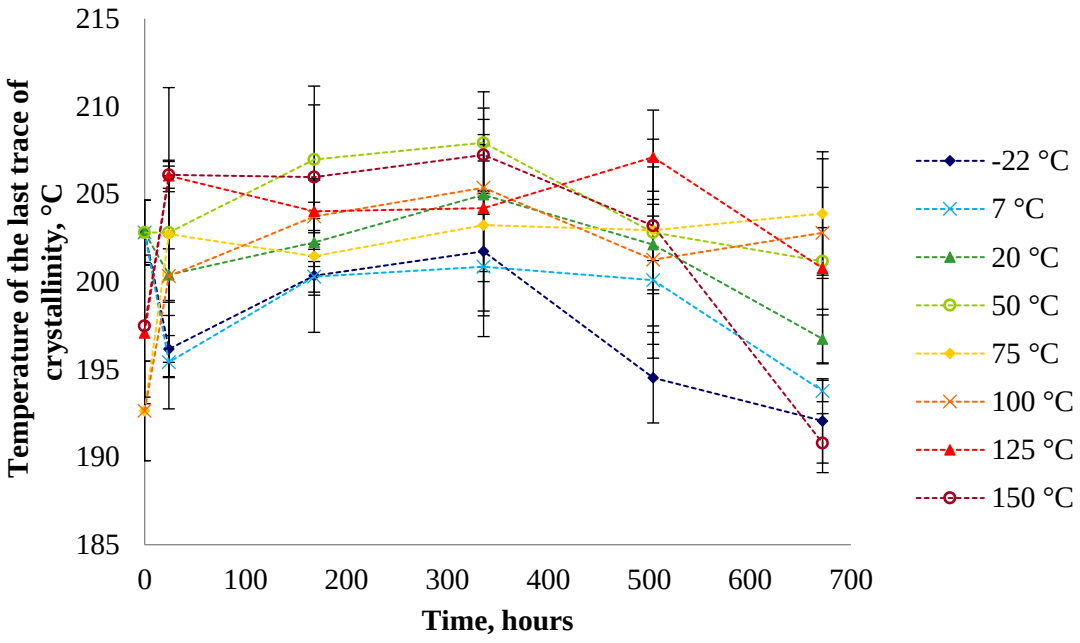

Figure 4.12. Last trace vs. time, according to temperature of storage. Dashed lines have been superimposed between timepoints as a visual aid to guide the eye through the data sets. DSC data tables are in Appendix B.

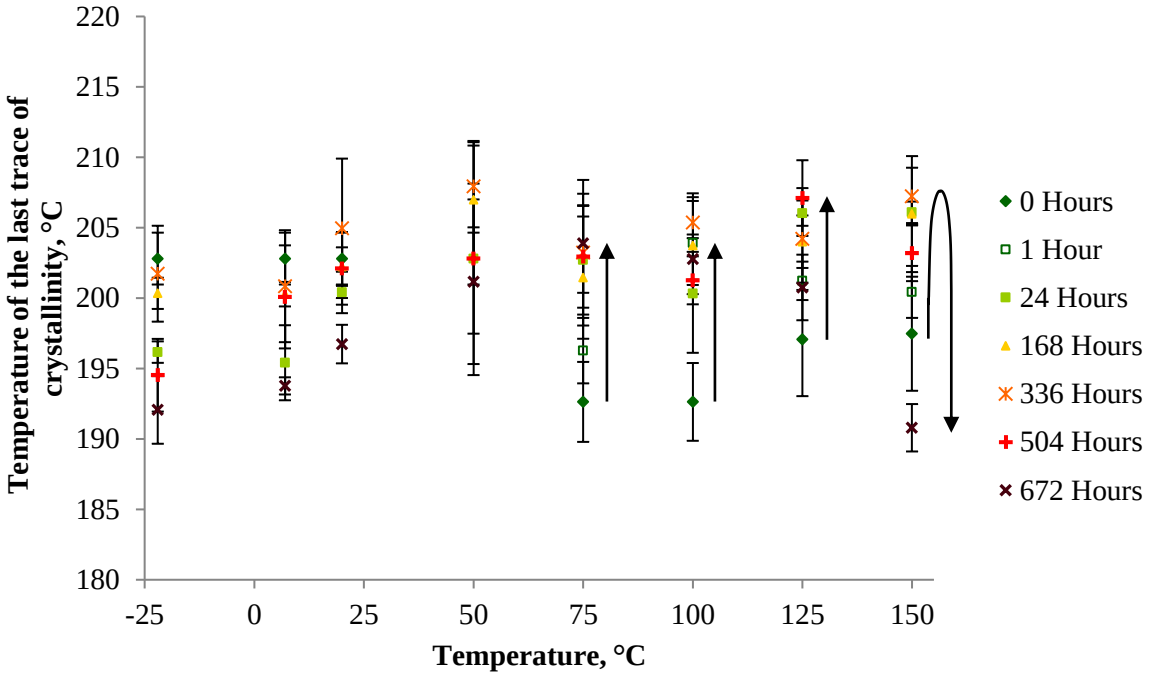

Figure 4.13. Temperature of last trace of melting vs. temperature of storage, according to length of storage time.

The only convincing trend occurred in samples kept at 150 °C. Again, an increase in value was recorded up to a time point of 336 hours (197.5 to 207.2 °C), after which it began to decrease, falling far below the unconditioned value, to 190.8 °C, after 672 hours of storage. As with the T_m measured from the peak maximum of the endotherm, this is most likely due to the increase in crystallinity resulting from secondary crystallisation, followed by the decrease in crystallinity resulting from chain scission, discussed in section 5.1.4.

Due to the large margins of error in the last trace of crystallinity data, compared to those obtained from the melting temperature taken from the peak maximum, it is thought that the peak maximum provides a better representation of the development of melting temperature in this work.

4.2 Infrared spectroscopic analysis of secondary crystallisation

Infrared spectroscopy is another method of determining the degree of crystallinity. It was hoped that the use of IR testing would enable the examination of the secondary crystallisation process, without the further crystallisation issues associated with the heating rate of DSC. Other authors have turned to this method of analysis for the same reason [49].

Figure 4.14 shows an IR spectra taken from an untreated sample. As discussed previously (Chapter 3.2), prominent features include the C–H stretching at 3030 to 2845 cm^{-1}, CO_2 at 2390 to 2300 cm^{-1}, the carbonyl peak at 1770 to 1660 cm^{-1} and the fingerprint region from 1485 to 700 cm^{-1}.

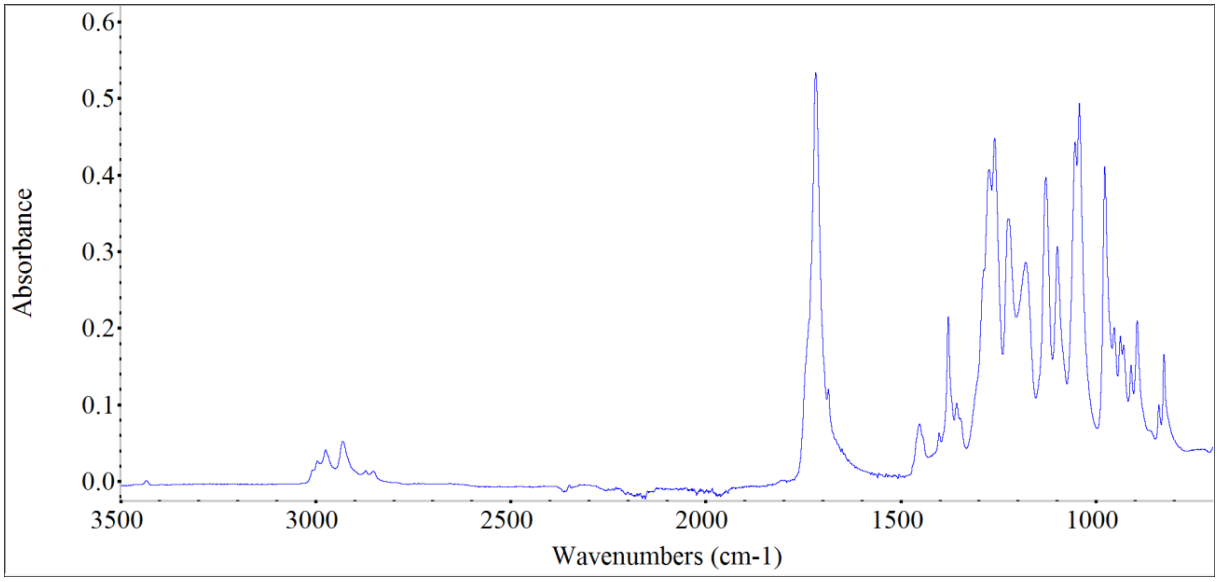

Figure 4.14. Example spectra of an untreated sample.

4.2.1 Crystallinity index generated from the peaks at 1221 cm^{-1} and 1451 cm^{-1}

The timescale of the secondary crystallisation process meant that samples studied by infrared spectroscopy could not be performed on the instrument in real-time, holding the samples at the

selected secondary crystallisation temperatures. Instead the samples were held isothermally at the selected temperatures by means of fridge freezers and ovens, and transferred to the machine for testing after the desired storage time. Ideally, as infrared testing is none-destructive, the same samples would have been used for the entire duration of the study, maintaining the consistency of the data obtained. Unfortunately, the storage places and the infrared instrument were in different buildings, so fresh samples had to be used for each time point of the study. Due to sample to sample variations, and equipment issues with maintaining standardised clamping forces over the duration of the study, the crystallinity could not be monitored simply by means of measuring and comparing the absorbance values of the peaks over time. Vizcaino-Caston *et al*. also highlighted the issues associated with the variance of clamping forces on peak intensities [93]. Examples of these variables on the absorbance values are presented in Figures 4.15 and 4.16. These spectra are obtained from samples stored at -22 °C, below the T_g of the material where there should be no change over time, and a clear difference in absorbance can be seen.

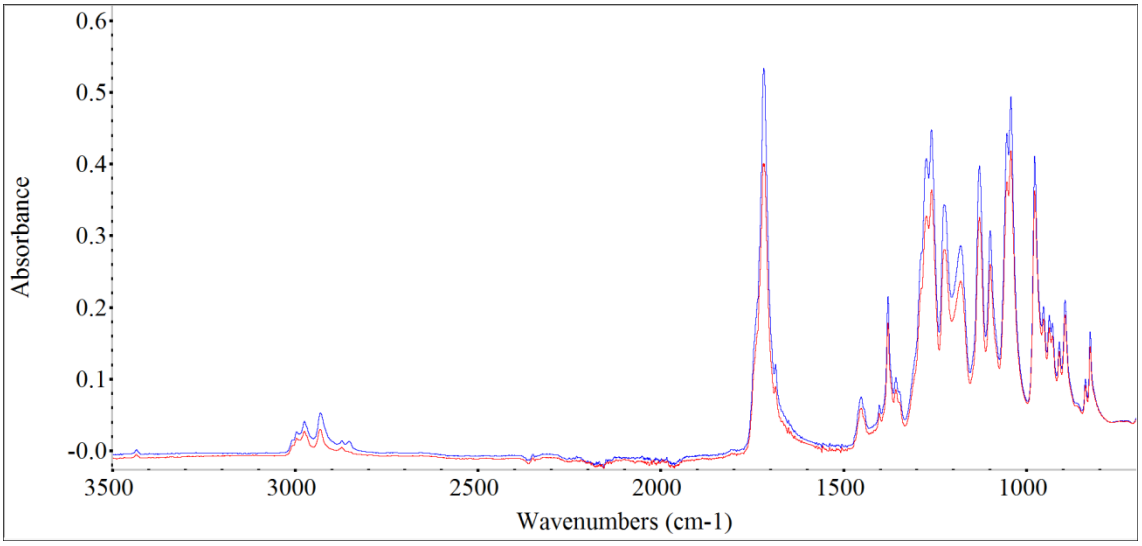

Figure 4.15. Spectral comparison of an unconditioned sample and a sample stored for 672 hours at -22 °C. Blue spectra = unconditioned, red spectra = 672 hours of storage.

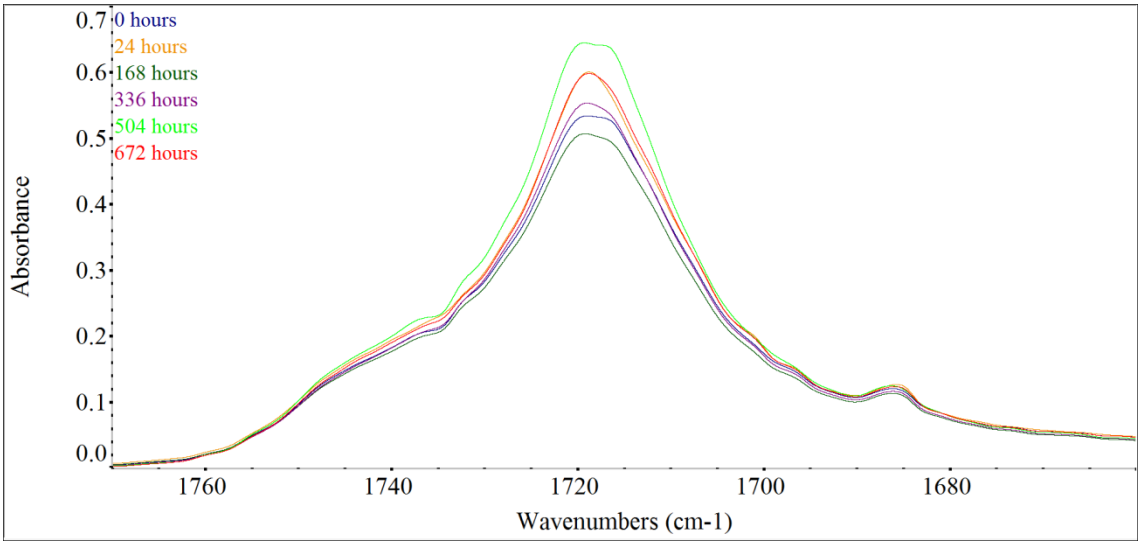

Figure 4.16. Comparisons of the carbonyl peak obtained from samples stored at -22 °C for the durations indicated.

Another method of crystallinity analysis had to be employed in order to determine the effects of the secondary crystallisation process. Cyras *et al*. and Galego *et al*. highlighted a band, at 1382 cm^{-1} (methyl bending) which they said was insensitive to the degree of crystallinity [36,94]. Hong and Chen, and Xu, *et al*. attributed the same characteristic to the peak at 1453 cm^{-1} (methylene bending) [34,49]. As they are insensitive to any change in the degree of crystallinity, these peaks tend to be known as internal references. Various ratios are calculated from combinations of these peaks with peaks which are sensitive to changes in crystallinity. Ratios of the peaks at 1382 to 1185 cm^{-1} (methyl groups, and ether groups relating to amorphous material respectively) [36,94], 1453 to 1186 cm^{-1} (methylene groups, and ether groups relating to amorphous material respectively) [49] and 1453 to 1230 cm^{-1} (methylene groups, and ether groups relating to crystalline material respectively) [34,49] have all been referred to as the crystallinity index, as they do not give a direct measure of the degree of crystallinity of a sample, but instead provide a comparison criterion [94]. As the ratio is generated from within the sample, it provides a measure of change which is independent of the absorbance values.

Calculating a crystallinity index in this manner has a high value in analysing data which contains variance due to the effects of factors such as the clamping force, allowing sample to sample comparisons which would otherwise not be possible.

The peaks at 1221, 1180 and 1451 cm^{-1} (ether stretching relating to crystalline material, ether stretching relating to amorphous material, and methylene bending respectively) from the primary crystallisation experiment (Chapter 3.2) were analysed in more detail. This was done in order to create a picture of how the amorphous and crystalline content of the material varied during an isothermal crystallisation which was unaffected by sample-to-sample variations. The sensitivity of the bands to the changing crystallinity is demonstrated in Figure 4.17, which indicates, in agreement with the literature, that these peaks may be useful in monitoring changes crystallinity. Figure 4.18 is an example of the development of crystallinity determined by a crystallinity index, from the ratio of the peak at 1221 cm^{-1} to the peak at 1451 cm^{-1}, generated from the primary crystallisation data (Chapter 3.2). It displays the characteristic sigmoidal shape inherent to the primary crystallisation of PHB, further validating the use of crystallinity indices for analysis of the crystallisation process.

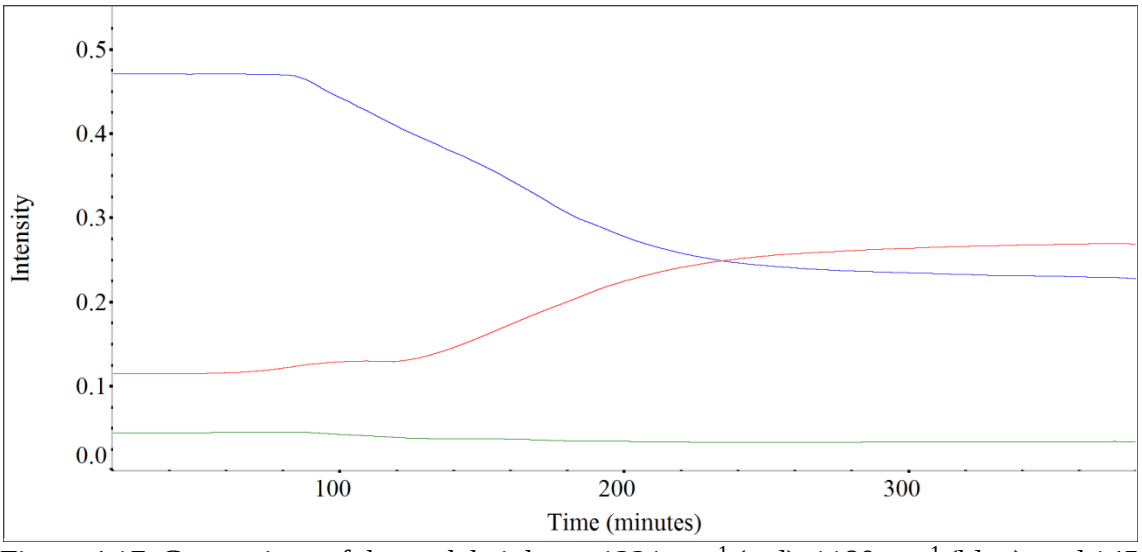

Figure 4.17. Comparison of the peak heights at 1221 cm^{-1} (red), 1180 cm^{-1} (blue), and 1451 cm^{-1} (green) over time.

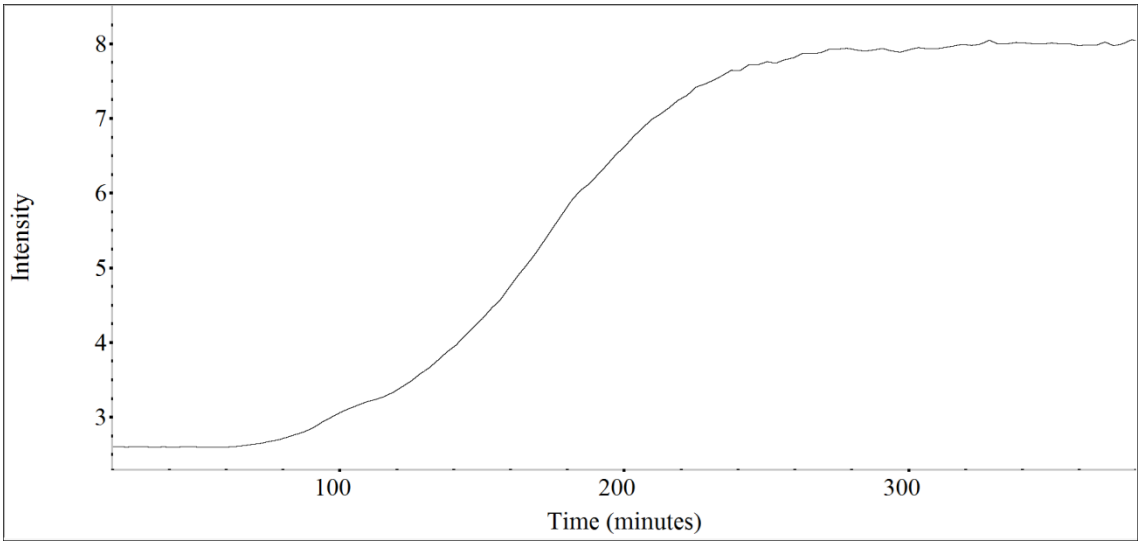

Figure 4.18. Development of the crystallinity index, generated from the peaks at 1221 cm^{-1} and 1451 cm^{-1}, during primary crystallisation.

The crystallinity index used by Xu *et al.* and Hong and Chen, generated from the ratio of the peaks at 1451 and 1221 cm^{-1} (the methylene groups insensitive to the degree of crystallinity, and ether groups relating to crystalline material), was applied to the long-term storage data [34,49]. Figure 4.19 depicts the results obtained from the calculation of the crystallinity index. At storage temperatures of 50 °C and upwards the crystallinity increased over time, and the increase was greater the higher the storage temperature. Hong and Chen held hot pressed PHB and P(HB-co-5wt%HV) samples at the higher temperature of 120 °C, for much shorter durations than the timescale studied in this work, and commented on the increase in the crystallinity index brought about by rearrangement of the chain molecules resulting from the thermal treatment [34]. An increase and decrease in the intensities of bands, relating to crystalline and amorphous material respectively, was also noted by Xu *et al*. as a result of thermal treatment [49]. This was attributed to the improved mobility of the molecules, associated with secondary crystallisation. This corresponds to the DSC work of de Koning *et al*., which linked the increase in the rate of secondary crystallisation to the increase temperature

[13]. Generally, the results in Figure 4.19 seem to follow the trends associated with the secondary crystallisation process as analysed by DSC, noted in Chapter 4.1.2 of this work. However, there is a large amount of noise present in these results, indicated by the size of the error bars, which reduces the degree of confidence in these trends.

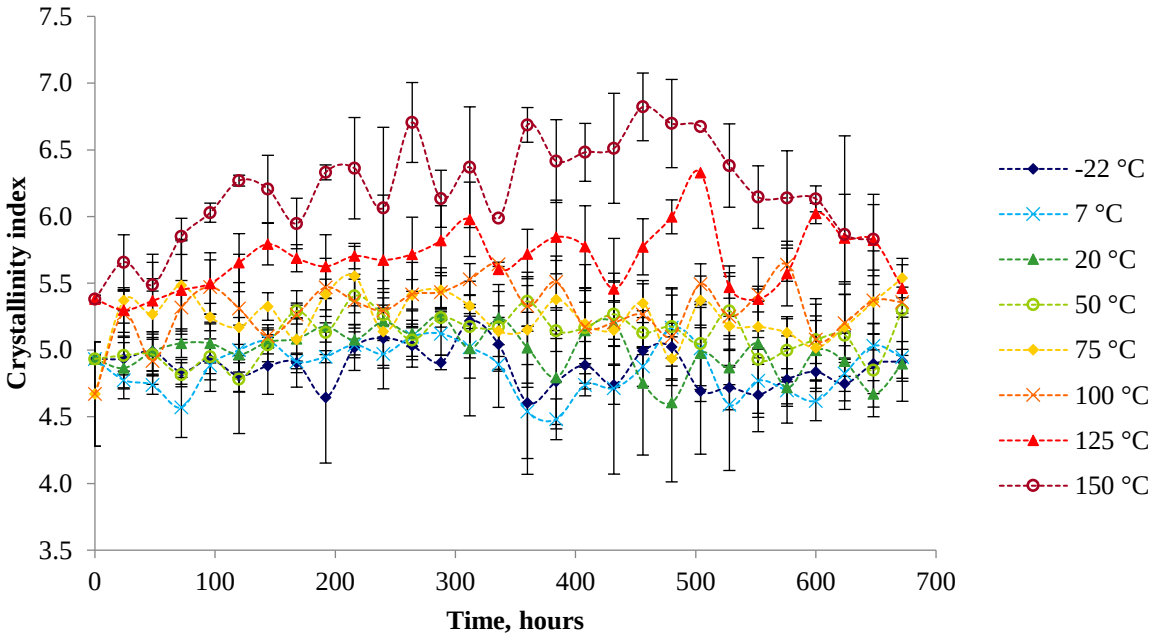

Figure 4.19. Crystallinity index over time, according to the temperature of storage, generated from the peaks at 1221 cm^{-1} and 1451 cm^{-1}. Dashed lines have been superimposed between timepoints as a visual aid to guide the eye through the data sets. A table of the crystallinity index data is in Appendix C.

The level of confidence in the data obtained from the samples held at 150 °C is slightly higher, as the associated error bars overlap less. The crystallinity index is seen to increase initially, until approximately 264 hours of storage, which may also be attributed to the activity of the secondary crystallisation process. There is then a plateau until approximately 456 hours of storage, thereafter the crystallinity index decreased. This indicates the activity of a second process which decreases the proportion of crystalline material, assumed to be chain scission, associated with the early stages of degradation. These trends reflect those observed previously

in the DSC study (Chapter 4.1.2), which were discussed in relation to the work of Janigová *et al*., who also described the changing crystallinity in terms of thermal degradation [68]. Initially the chain scission process aids the secondary crystallisation process, as the shorter chain lengths are able to pack more closely, but there is a cross over point where further scission begins to decrease the crystallinity of the system. Due to the interaction of these processes, it is difficult to judge the point where the first ends and the second begins. The large amount of noise, within the data shown in Figure 4.19, makes pinpointing the changeover times of these processes still less precise.

The general trends picked out from Figure 4.19 are illustrated in Figure 4.20, where temperatures which represent these trends are separated from the rest of the data for visual clarity. Figures 4.12a and 4.12b represent temperatures below (-22 °C) and close to the T_g (7 °C) respectively, where either no increase or minimal increases in crystallinity would be expected. Temperatures where secondary crystallisation increases the crystallinity are represented in Figure 4.12c (100 °C). Finally, the interplay of secondary crystallisation and degradation may be seen in Figure 4.12d (150 °C).

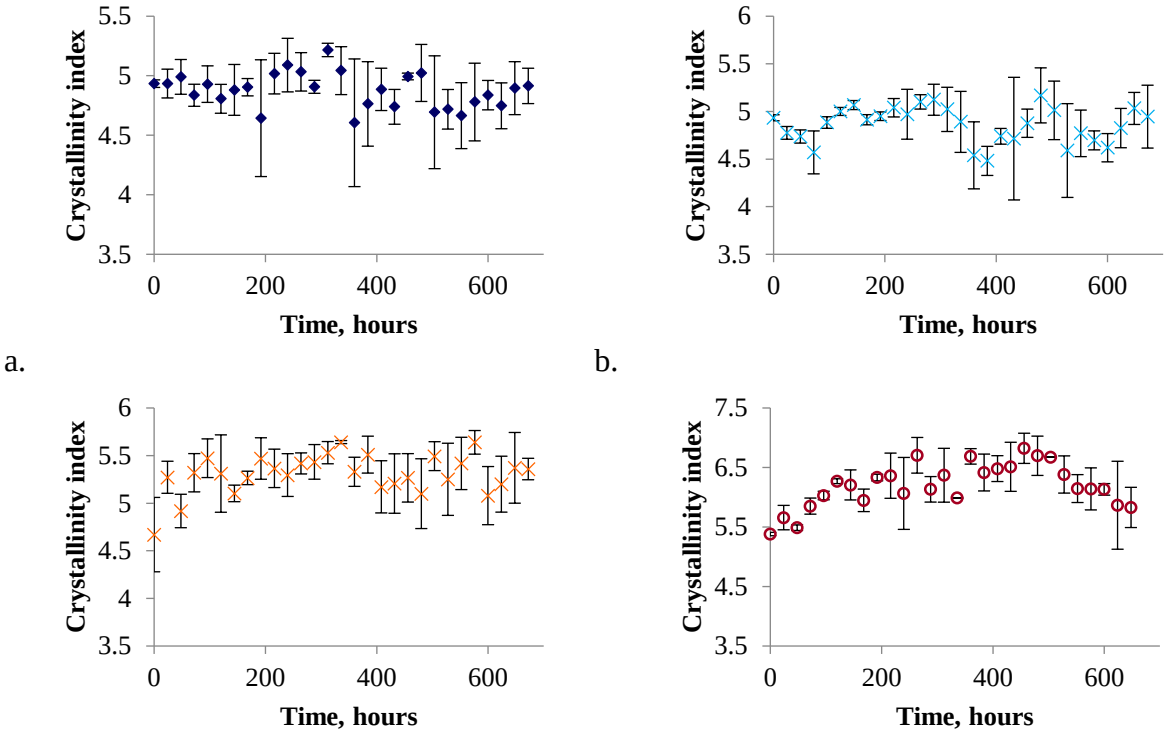

Figure 4.20. Crystallinity index over time, generated from the peaks at 1221 cm^{-1} and 1451 cm^{-1}, at storage temperatures of a. -22 °C, b. 7 °C, c. 100 °C, d. 150 °C.

4.2.2 Observation of the spectral peaks at 1180 cm^{-1} and 1221 cm^{-1}

It has already been stated that there are peaks in the fingerprint region of the spectra, at 1221 and 1180 cm^{-1} (C-O-C peaks), which are sensitive to the crystalline and amorphous material respectively. When examining, in isolation, the peaks at 1221 and 1180 cm^{-1} over time, the changes observed appear to reflect the secondary crystallisation process reasonably well. In Figures 4.21 to 4.28, the peaks at 1221 and 1180 cm^{-1} were normalised to the height of the peak at 1221 cm^{-1} to allow comparisons to be made.

At storage temperatures of -22 and 7 °C (Figures 4.21 and 4.22), the height of the peak at 1180 cm^{-1} relative to that at 1221 cm^{-1} does not vary according to the duration of storage. The change in the peak heights is attributed to inherent sample-to-sample variation; as the samples

were stored below or very close to the T_g of the material, eliminating or vastly limiting the activity of the secondary crystallisation process respectively. In Figure 4.23, there is the suggestion of a decrease in the relative height of the peak at 1180 cm^{-1} with increasing storage duration. This would indicate that the crystallinity has increased and the secondary crystallisation process is active at 20 °C. Cyras *et al*. also commented on the increase of crystallinity over time when the material was kept at room temperature [36]. This corresponds to the DSC work of Biddlestone *et al*., where the increase of crystallinity with time at room temperature was attributed to secondary crystallisation [32], and to the DSC results in this work, where an increase in crystallinity was also observed at a storage temperature of 20 °C.

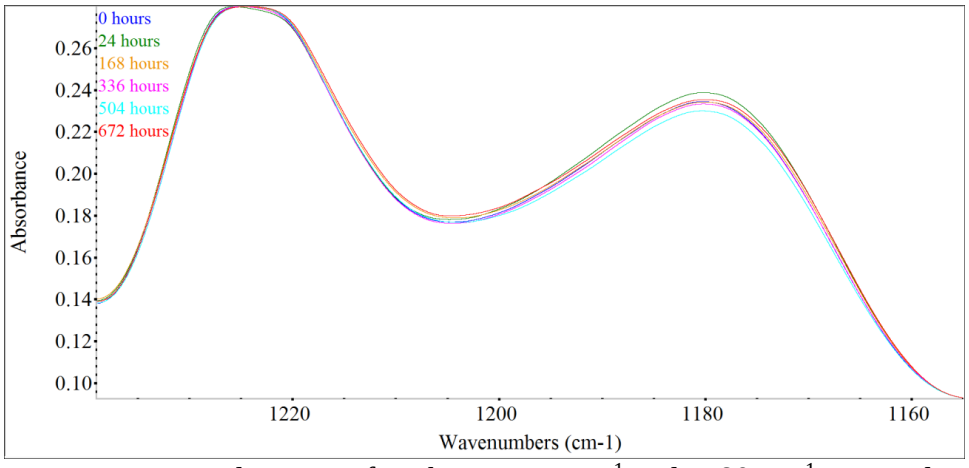

Figure 4.21. Development of peaks at 1221 cm^{-1} and 1180 cm^{-1} in samples stored at -22 °C.

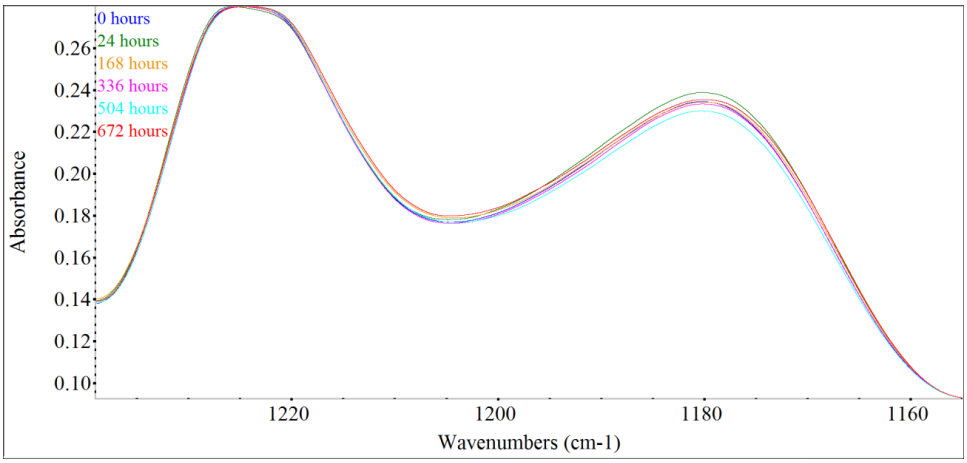

Figure 4.22. Development of peaks at 1221 cm^{-1} and 1180 cm^{-1} in samples stored at 7 °C.

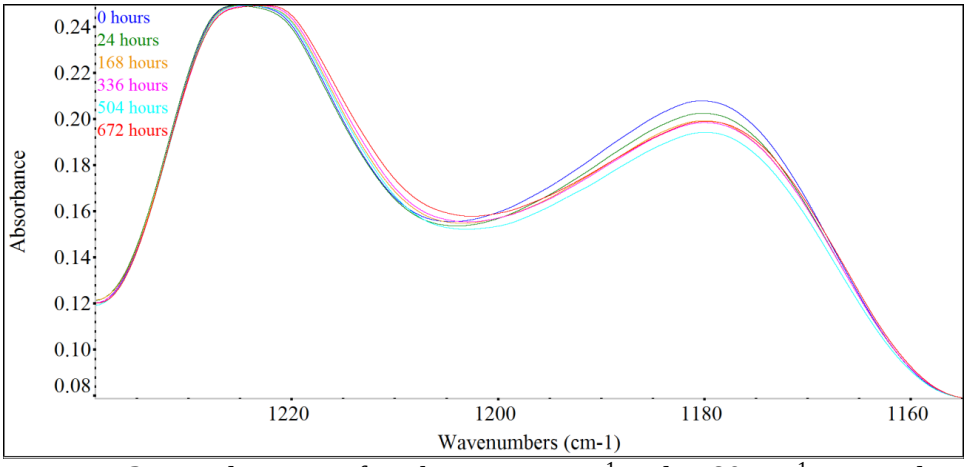

Figure 4.23. Development of peaks at 1221 cm^{-1} and 1180 cm^{-1} in samples stored at 20 °C.

Figures 4.24 to 4.26 depict the changes resulting from storage at 50, 75 and 100 °C. At these temperatures, the figures suggest that a rapid decrease in the amorphous peak happened within the first 24 hours of storage, that the peak height was relatively stable for the remainder of the storage time, and that the extent of change increased with increasing storage temperature. When held at 125 °C, there was again a great change within the first 24 hours. However, as is clearly shown in Figure 4.27, the relative decrease in the amorphous peak continued with further increase in storage duration. These developments suggest the balance between the amorphous and crystalline content in the samples was changing at storage temperatures from 20 to 125 °C due to the secondary crystallisation process. The trends discussed reinforce the developing pattern of increasing rate and extent of secondary crystallisation process with higher storage temperatures, discussed in relation to Figure 4.19.

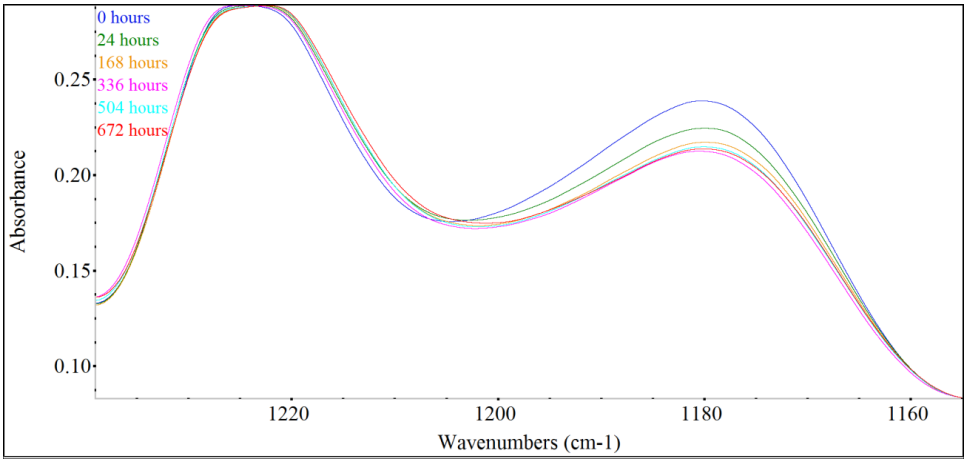

Figure 4.24. Development of peaks at 1221 cm^{-1} and 1180 cm^{-1} in samples stored at 50 °C.

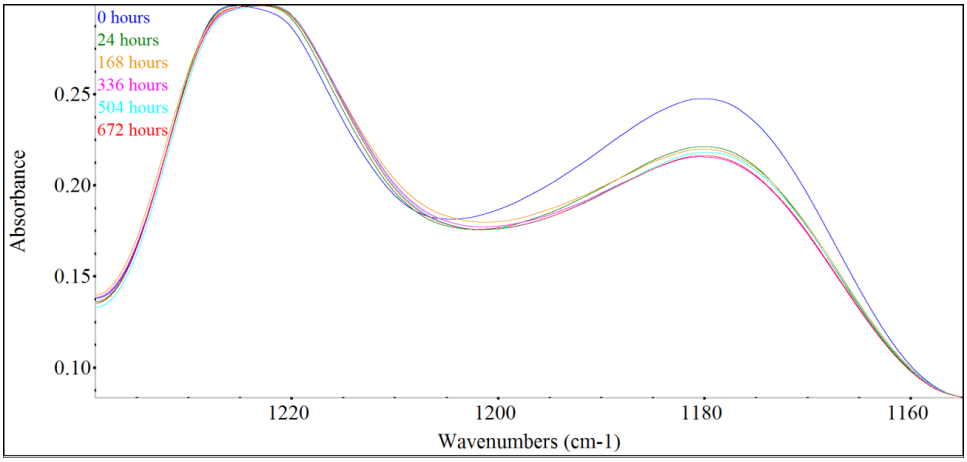

Figure 4.25. Development of peaks at 1221 cm^{-1} and 1180 cm^{-1} in samples stored at 75 °C.

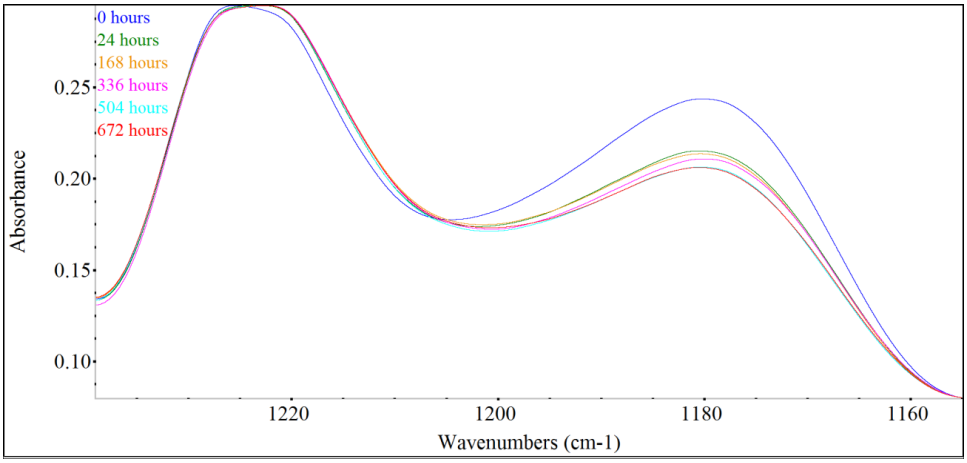

Figure 4.26. Development of peaks at 1221 cm^{-1} and 1180 cm^{-1} in samples stored at 100 °C.

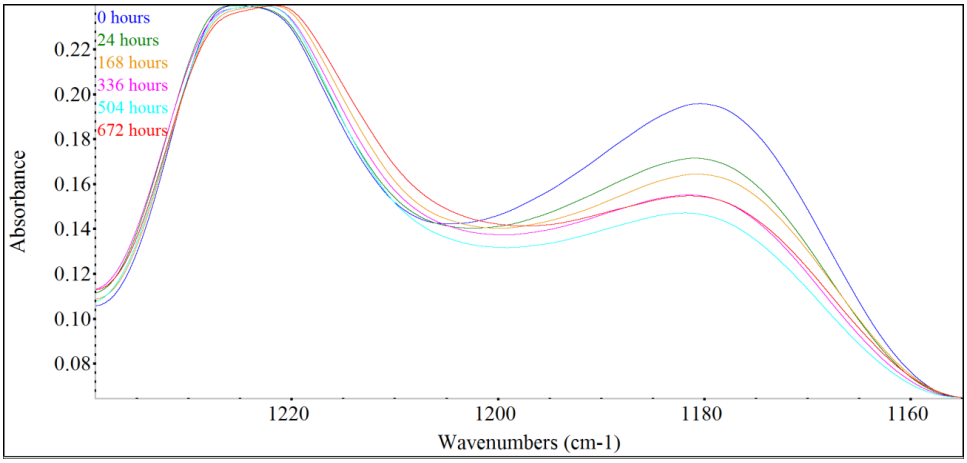

Figure 4.27. Development of peaks at 1221 cm^{-1} and 1180 cm^{-1} in samples stored at 125 °C.

The developments in the spectra stored at 150 °C, shown in Figure 4.28, were the most pronounced of all the storage temperatures analysed in this work. Once again, the results obtained from the 150 °C samples reflect the presence of conflicting processes, as discussed in relation to the DSC results presented earlier in this chapter. The spectra in Figure 4.28 plainly demonstrate the initial relative decrease in the peak at 1180 cm^{-1}, which appeared to halt between 336 and 504 hours, then increase at 648 hours. Again, these trends are attributed to the interplay of the secondary crystallisation and degradation processes, where the dominant process is visible by which trend is being expressed.

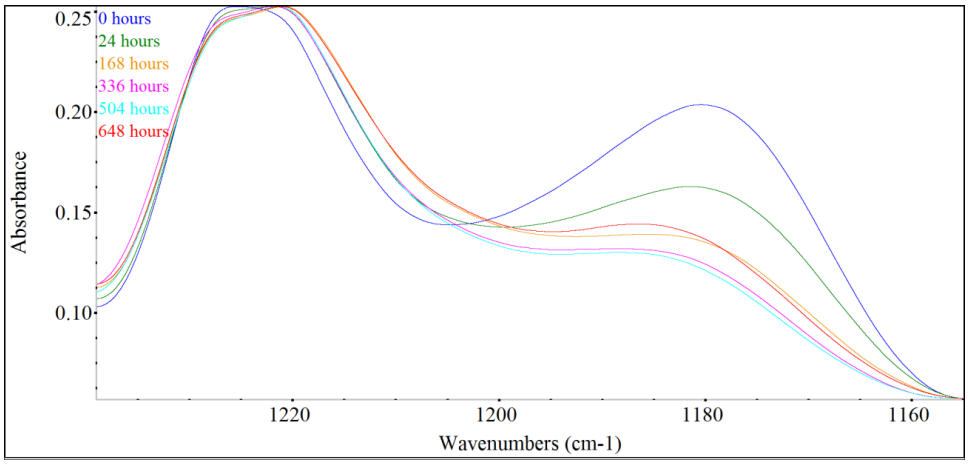

Figure 4.28. Development of peaks at 1221 cm^{-1} and 1180 cm^{-1} in samples stored at 150 °C.

In effect, changes in the crystallinity index presented in Figure 4.19, were illustrated in the full-scale spectra in Figures 4.21 to 4.28. This demonstrates that the use of full-scale spectra for relative comparisons has some value, even if they can't be used directly for quantitative comparisons.

4.3 Conclusions

Storage of samples at temperatures between 20 °C to 150 °C resulted in an increase in the degree of crystallinity, due to the activity of the secondary crystallisation process.

Unlike the measurements of T_m taken from the maximum height of the melting endotherms, and from the last trace of crystallinity, the onset of melting may provide information on which mechanism of the secondary crystallisation process is active. At lower storage temperatures, 20 to 50 °C, the onset of melting occurred at lower temperatures, indicating the melting of newly formed, less stable crystal structures within the amorphous regions (infill). At higher storage temperatures, 100 and 125 °C, the onset of melting increased, which may have been a result of lamellar thickening.

A shoulder emerged on the low temperature side of the melting endotherm in samples stored at 100 to 150 °C. This shoulder may have resulted from lamellar thickening, MRR, or from a decrease in M_w. Additional discussion can be found in Chapter 7.2.

Competing processes of secondary crystallisation and degradation are likely to have been active within the samples stored at 150 °C. Which process dominated the overall change in properties was dependent on how long the samples were stored for prior to testing. Before 168 hours it wasn't immediately obvious that degradation was happening, as the property changes follow

the secondary crystallisation induced trends observed from storage at temperatures below 150 °C. After 336 hours, it is clear from the property changes that another process is active, as the secondary crystallisation trends no longer apply, and effects that would be expected as a result of degradation begin to appear. This will be discussed further in Chapter 7.

The secondary crystallisation process was difficult to follow through IR analysis of multiple samples. A crystallinity index was generated from the peaks at 1221 and 1453 cm^{-1}, where the crystallinity was seen to increase over time, to a greater extent with higher temperatures of storage. It was determined that the crystallinity index, as well as qualitative analysis of spectral peaks, may be used to provide relative comparisons of crystallinity when the absorbance is not standardised from sample to sample. The trends observed at storage temperatures from 7 to 125 °C were attributed to the activity of the secondary crystallisation process. These trends were in agreement with those obtained from DSC studies. Again, an increase in crystallinity, which plateaued then decreased, was observed over time in the samples stored at 150 °C. This will be discussed further in Chapter 7.

CHAPTER 5 – DYNAMIC MECHANICAL THERMAL ANALYSIS (DMTA)

5.1 Analysis of the tanδ peak

5.1.1 Qualitative observations of tanδ

In samples stored below their glass transition temperature (T_g) -22 °C, there was no significant change in the size or shape of the tanδ peak (Figure 5.1). This is to be expected due to the polymer chains inability to move and reorganise at temperatures below the T_g of the material. When stored at a slightly higher temperature, 7 °C, a slight and gradual decrease in the size of the tanδ peak over time was observed (Figure 5.2).

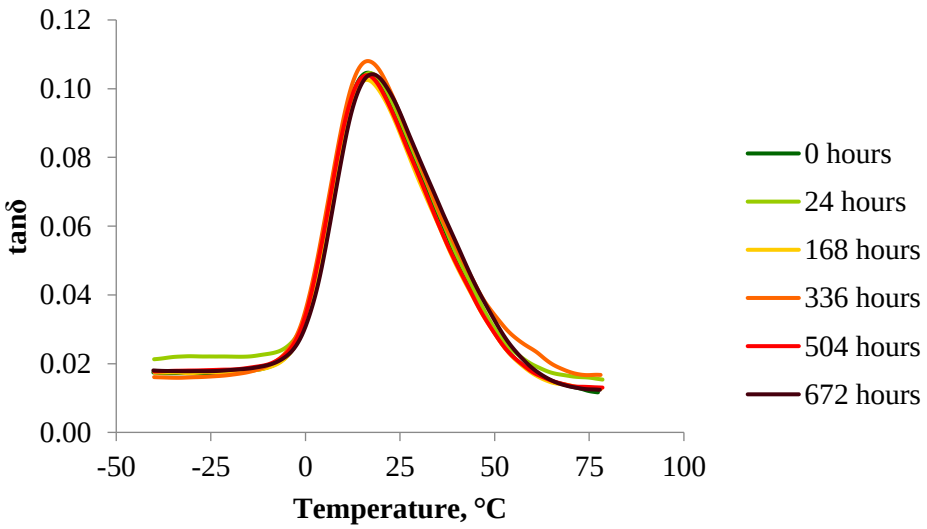

Figure 5.1. Tanδ peaks of samples stored at -22 °C.

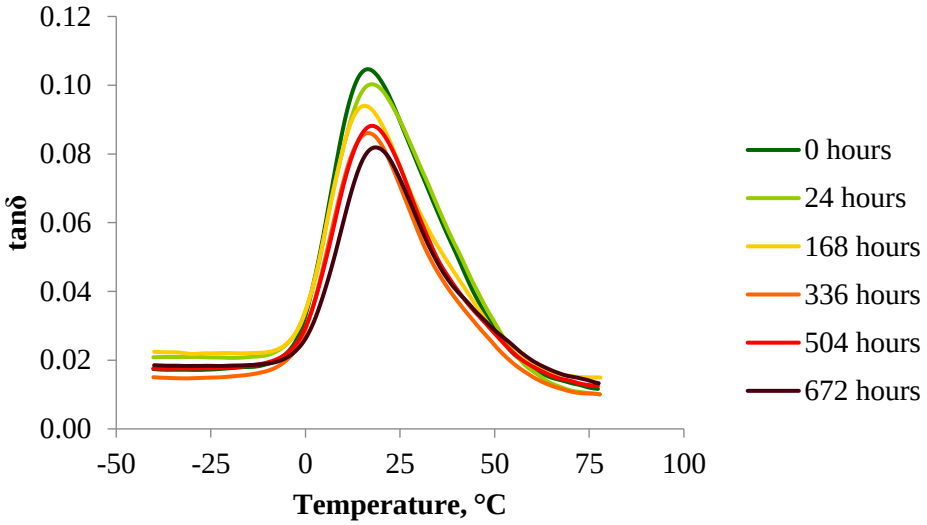

Figure 5.2. Tanδ peaks of samples stored at 7 °C.

At ambient temperatures of 20 °C, where the mechanism of secondary crystallisation is widely reported to be active, the decrease in tanδ peak size over time was more obvious, and it was also accompanied by a small increase in peak temperature (Figure 5.3). This trend became more pronounced as the temperature of storage was further increased to 50 and 75 °C; these samples exhibited a rapid change in tanδ peak size and position, which then appeared to plateau (Figures 5.4 and 5.5 respectively).

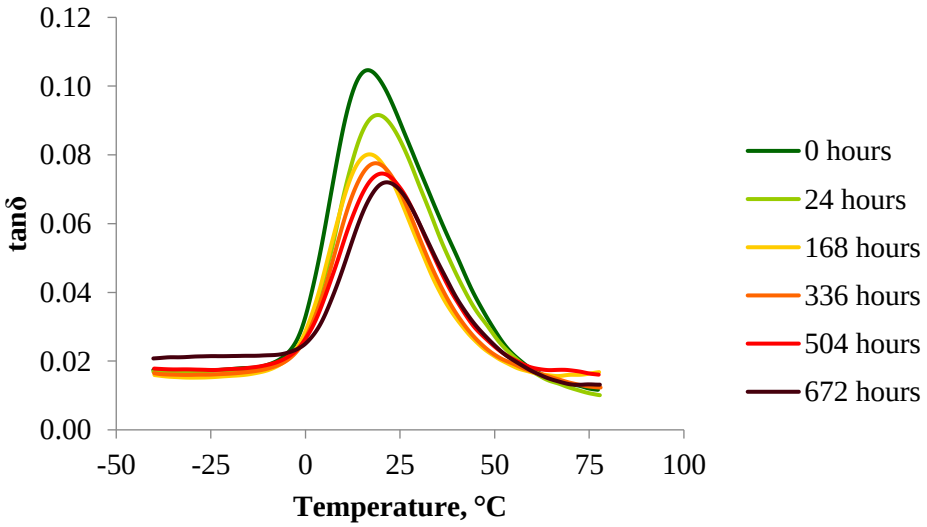

Figure 5.3. Tanδ peaks of samples stored at 20 °C.

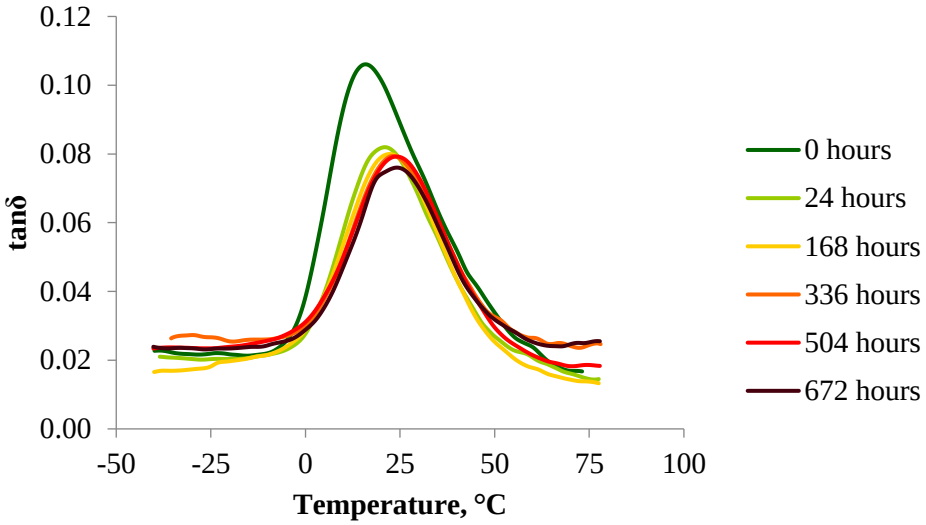

Figure 5.4. Tanδ peaks of samples stored at 50 °C.

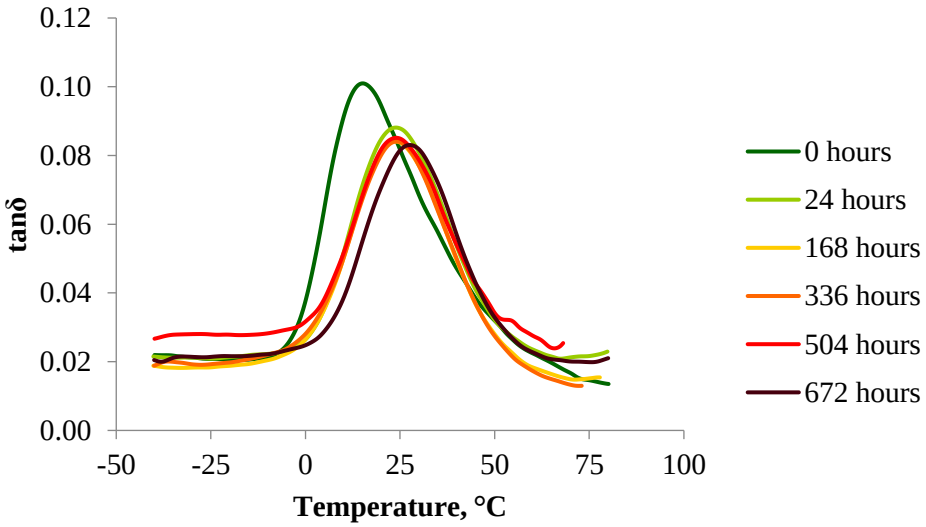

Figure 5.5. Tanδ peaks of samples stored at 75 °C.

While the samples stored at 100 and 125 °C also presented a clear upward shift in peak temperature, at 100 °C the size and shape of the tanδ peak seemed to remain relatively constant over time (Figure 5.6). At storage temperatures of 125 °C, the height of the peak seemed to slightly increased in size initially, before beginning to decrease as the storage time increased (Figure 5.7).

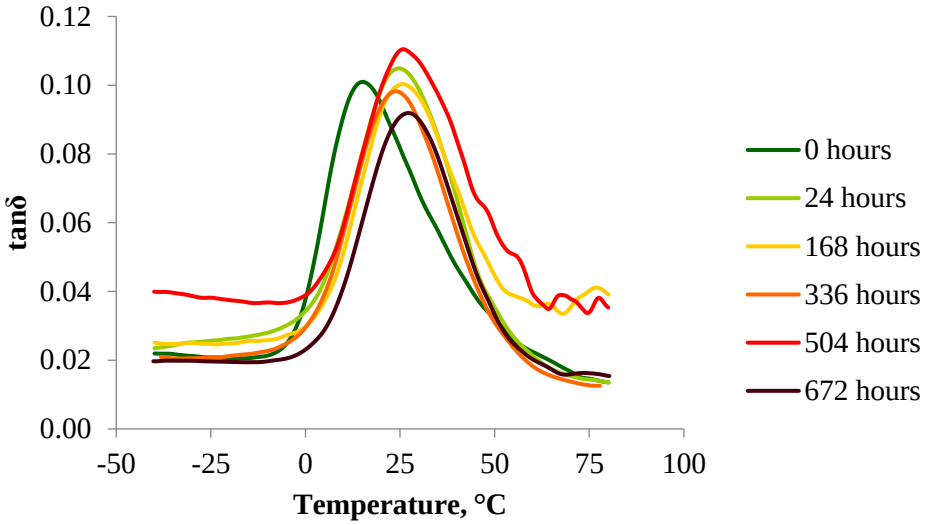

Figure 5.6. Tanδ peaks of samples stored at 100 °C.

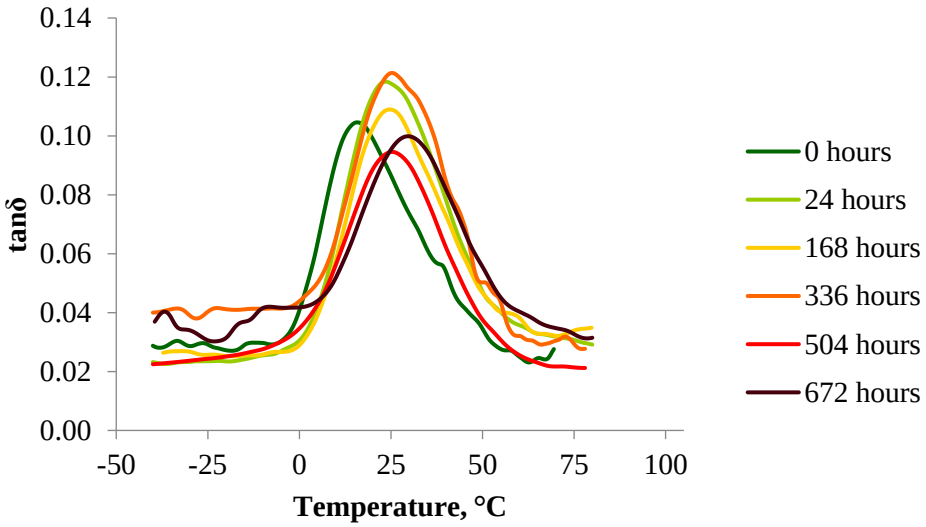

Figure 5.7. Tanδ peaks of samples stored at 125 °C.

Samples which were stored at the highest temperature, 150 °C, showed the most dramatic changes in the tanδ peak over time (Figure 5.8). There was a clear increase then rapid and significant decrease in peak height, an increase then decrease in the temperature at which the peak occurred, and a broadening of the peak.

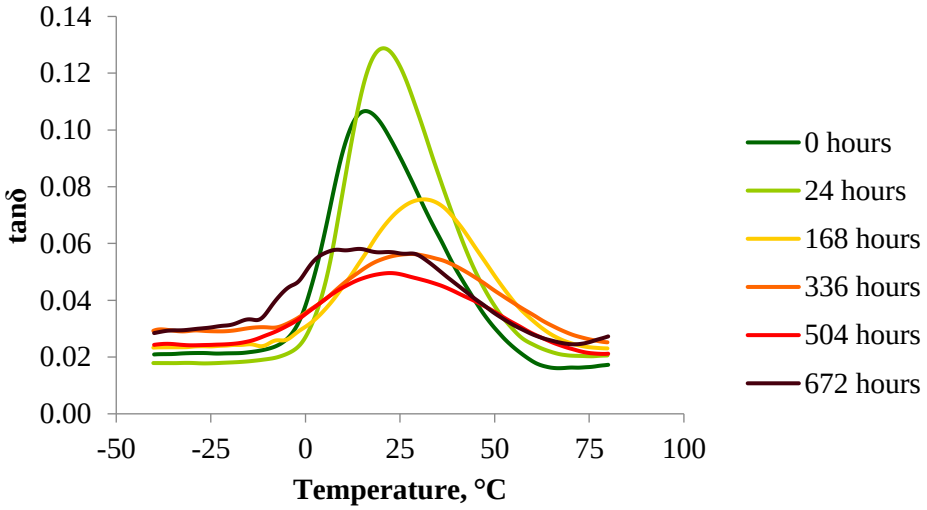

Figure 5.8. Tanδ peaks of samples stored at 150 °C.

Qualitative observation of the tanδ peak revealed two clearly emerging trends. These were changes in the temperature at which the maximum height of the tanδ peak occurred, and a change in height of the tanδ peak.

5.1.2 Determination of T_g from tanδ

The temperature at the tanδ maximum is a measure of the glass transition temperature (T_g); the temperature at which the amorphous content of the material is able to undergo large scale motion about the backbone of the polymer chain. The fact that the tanδ peak is very broad signifies that the glass transition of the material happens over a temperature range [95], and not at a single temperature point, which may be the impression given when quoting the T_g as a specific temperature. Galego *et al*. describes the tanδ maximum as more indicative of the midpoint of T_g [94]. While this would be applicable to symmetrical peaks of tanδ, this author believes that, in order to apply to both symmetrical and asymmetrical tanδ peaks, a more accurate description would be that the tanδ peak maximum represents the mode temperature of the relaxation process.

Figure 5.9 shows the T_g measured over time, according to the different temperatures of storage. No significant change was observed when samples were stored below T_g (-22 °C), and only a very minor change in T_g, from 16.5 °C to 18.5 °C over 672 hours, was seen in samples held at 7 °C. At a storage temperature of 20 °C a steady increase in T_g over time became evident, from a T_g of 16.4 °C in the unconditioned sample, to 21.4 °C after 672 hours of storage. Whereas, at the higher storage temperature of 50 °C, the T_g of the samples was seen to increase rapidly in the first 24 hours, from 15.9 °C to 21.0 °C, after which the rate of increase became much more gradual, reaching 24.1 °C by the end of the study. The same can be said for the samples which were stored at 75, 100 and 125 °C, which presented very similar changes in T_g with rapid increases, from 15.1, 15.1 and 15.8 °C to 23.9, 24.7 and 23.5 °C respectively, within the first 24 hours. The rate of increase was much more gradual for the remaining 648 hours of the study, increasing to final values of 27.6, 27.2 and 29.7 °C. The difference being that the extent of change was greater for higher temperatures of storage within the timescale of the experiment.

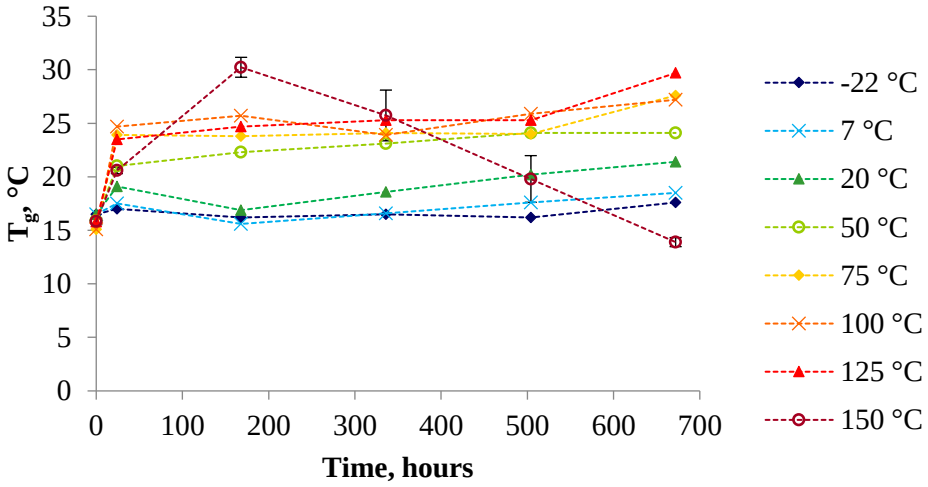

Figure 5.9. Development of T_g over time, comparing the effect of different sample storage temperatures. The value of T_g was taken from the temperature of the peak maximum of tanδ. Dashed lines have been superimposed between timepoints as a visual aid to guide the eye through the data sets. DMTA data tables are in Appendix D.

As noted in Chapter 4, keeping samples at 150 °C resulted in a more complex interaction of storage temperature and duration of storage. In this case, an increase in T_g was observed until 168 hours of storage, from 15.8 °C to 30.2 °C, followed by a steady decrease until 672 hours to a T_g of 13.9 °C. The final observed T_g, of the sample stored at 150 °C for 672 hours, was 1.9 °C lower than the T_g measured prior to storage.

Figure 5.10 allows gross change in the individual temperatures to be seen more clearly as the data points from different storage temperatures don't overlap.

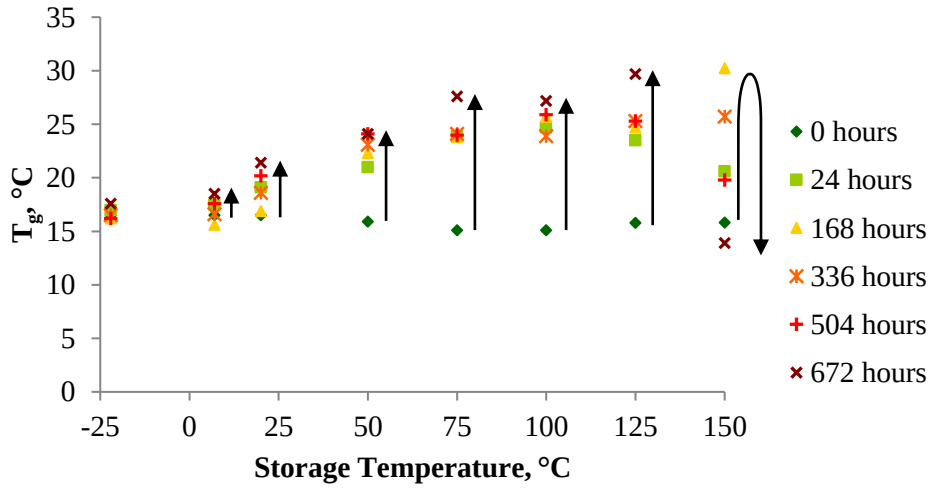

Figure 5.10. Development of T_g according to the temperature at which the samples had been stored, examining the influence of the duration of storage.

Storage of PHB and the copolymer P(HB-co-HV) above its T_g is known to result in secondary crystallisation of the material. As a result of further constraints imposed upon the amorphous material by infill, and the increase of lamellar thickness and rigid amorphous fraction (RAF), motion of the amorphous chains is restricted to a greater degree, therefore a greater amount of energy is required to allow mobility in the amorphous regions of the samples. Thus, secondary crystallisation of the samples stored from 7 to 125 °C is believed to have caused an increase in

the T_g. Other authors have also discussed the increase in T_g recorded from the tanδ peak resulting from a rise in crystallinity [96,97].

Secondary crystallisation has been shown to increase logarithmically with time, in agreement with the work of Biddlestone *et al*. and Vogel *et al*. [32,37]. Within a set period of time, higher temperatures have also been shown to produce a greater amount of secondary crystallisation than lower temperatures [33,34]. This was also shown in Chapter 4, in sections 4.1.2 and 4.2.1. In other words, secondary crystallisation occurs at a greater rate at higher temperatures, so it makes sense that the amorphous content would be the most restricted in those samples, and hence the highest values of T_g would be recorded. The results from this study show that the T_g did increase with the increase in storage temperature, as can be seen in Figures 5.9 and 5.10.

When stored at 150 °C, it is believed that multiple processes may affect the T_g of the samples, in order to produce the curve seen in Figure 5.9. Initially, the same rise in T_g caused by secondary crystallisation was observed. This agreed with the pattern of higher storage temperatures experiencing a greater degree of secondary crystallisation, restricting the mobility of the amorphous chains to a greater extent, and thus possessing higher values of T_g. However, this was subsequently followed by a large, steady decrease in T_g over time. It is possible that these samples were stored at a temperature high enough that the chain scission process of degradation was active with extended storage durations. Chain scission of PHB is known to produce a greater number of chains of lower molecular weight [33,54,68]. The amount of energy required to provide mobility for shorter, and therefore less entangled chains, is lower, and so the T_g of those chains is lower. An increase in free volume is associated with the greater number of chain ends present in material with lower molecular weight, which would also increase the mobility of the system and reduce the T_g. A decrease in the degree of crystallinity, also a result of chain scission, would contribute to the decrease the T_g, as the crystalline phase

and RAF constrain the mobility of the amorphous chains less. The possibility of degradation occurring below T_m is discussed further in Chapter 7.

5.1.3 Analysis of the tanδ peak

Over time, no significant change in tanδ peak height was observed in samples stored at -22 °C, below the T_g (Figure 5.11). The unconditioned sample had a peak height of 0.087, and the sample stored for 672 hours measured 0.086. A slow and steady decrease in tanδ peak height was present in the samples stored at 7 °C. The height measured 0.087 in the unconditioned sample, decreasing to 0.063 in the sample held at 7 °C for 672 hours. The extent of decrease may be seen more clearly in Figure 5.12.

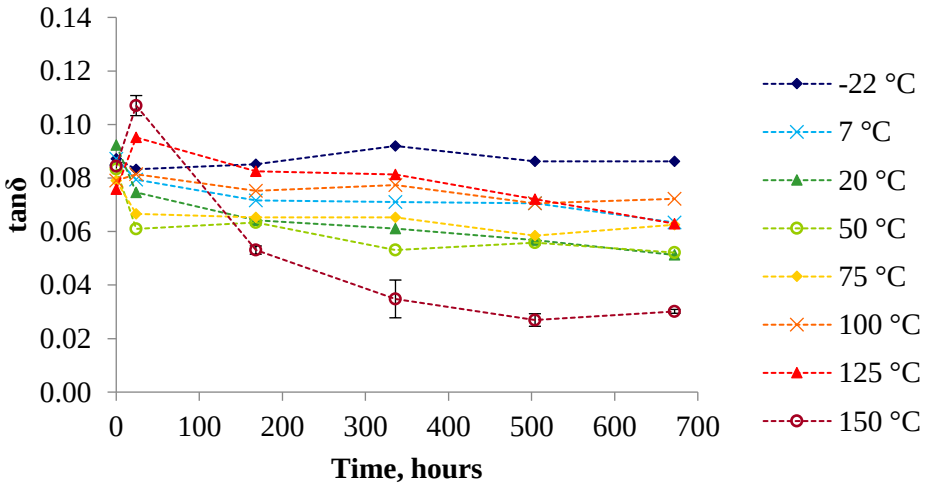

Figure 5.11. Height of the tanδ peak over time, comparing the effect of different sample storage temperatures. Dashed lines have been superimposed between timepoints as a visual aid to guide the eye through the data sets. DMTA data tables are in Appendix D.

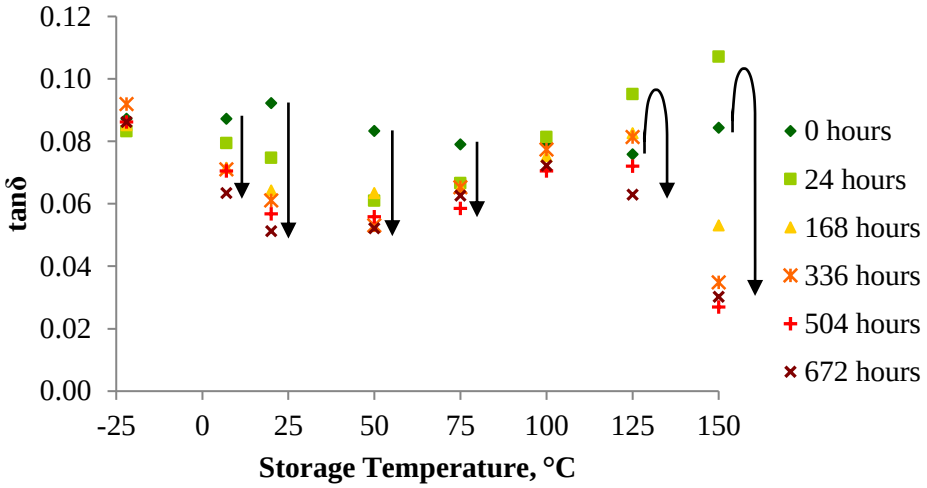

Figure 5.12. Development of tanδ height according to the temperature at which the samples were stored, examining the influence of the duration of storage.

Initially, further increase in the storage temperature again resulted in a greater extent and rate of change. At a storage temperature of 20 °C a decrease in peak height of tanδ, from 0.092 in the unconditioned sample to 0.051 after 672 hours of storage, was observed. However, after 168 hours of storage, the rate of change slowed down. Biddlestone *et al*. found a progressive decrease of tanδ peak height of PHB over time when stored at room temperature [32], and de Koning *et al*. described a logarithmic decrease in the height of tanδ of PHB held at 110 °C for 16 hours [13]. The samples kept at 50 and 75 °C also followed the trend of higher storage temperatures increasing the rate of change as, for both sets of results, the peak height of tanδ decreased to a plateau more rapidly than the 20 °C samples. Decreases from 0.083 and 0.79 to 0.061 and 0.067 were recorded from the 50 and 75 °C samples respectively after 24 hours. After 672 hours, the values of tanδ peak height had dropped to 0.052 and 0.063. However, the total decrease in peak height was not as great in the 75 °C samples as that seen in the 50 °C samples (Figure 5.12). There was an observed peak height difference of 0.031 in the samples stored at 50 °C, and 0.016 in those stored at 75 °C. The trend of decreasing peak height with increasing storage duration was no longer applicable when the storage temperature was 100 °C, as there

did not appear to be a particularly noteworthy decrease in peak height over time. A tanδ peak height of 0.079 was measured from the unconditioned sample, and 0.072 from the sample stored for 672 hours.

The area of the tanδ peak is an indication of the amount of amorphous content in the material. In this study, the height of the tanδ peak therefore provides a relative indication of the amorphous content of the material, as there is negligible change in the peak width. Modi links the decrease in peak height to an increase in stiffness [98]. Renstad *et al*. and Biddlestone *et al*. also note that the tanδ peak height of PHB and P(HB-co-HV) can indicate the degree of constraint on the amorphous material, as the decrease in peak heights were attributed to increased constraints on the amorphous phase by the crystalline phase [32,77]. These effects are caused by the secondary crystallisation process, whereby chains from the amorphous fraction become crystalline, either through an infill process or lamella thickening. This results in a smaller amount of material in the amorphous phase, which is also more constrained. Secondary crystallisation is known to be a logarithmic process [32,37], the rate of which is dependent on the temperature [33,34], as discussed in Chapter 4. This explanation fits well with the data obtained from samples stored at 7 to 50 °C, where higher storage temperatures produced greater extent and rates of tanδ peak height decrease over time. Further increase in the temperature of storage to 75 and 100 °C resulted in a slower reduction in peak height. One possible reason for this is that the crystallinity increase at these temperatures is due to lamellar thickening rather than infilling. Whilst this will reduce the amorphous content, which reduces the height of the peak, it would also constrain the remaining amorphous material to a greater extent. This means that more energy is required for the chains remaining in the amorphous phase to overcome the constraints and achieve large scale motion at these higher temperatures. This results in a greater loss modulus and therefore tanδ, as given by the equation tanδ = loss

modulus/storage modulus, and overall means that the decrease in peak height is less than that seen in the samples stored between 7 and 50 °C.

When stored at 125 °C, there was an increase in tanδ peak height from 0.076 to 0.095 in 24 hours, after which the height of the peak began to fall. At 504 hours of storage the peak height returned to a similar value as that from the unconditioned sample, measuring 0.072, and after 672 hours the peak height was less than that of the unconditioned sample, measuring 0.063. Samples kept at 150 °C exhibited a similar, but more exaggerated, trend to those stored at 125 °C. An increase in tanδ peak height from the unconditioned sample was observed in the sample stored for 24 hours, from 0.084 to 0.107, after which the peak height decreased rapidly. When looking at the average values obtained from the 336, 504 and 672 hour samples, which were 0.035, 0.027 and 0.030 respectively, there is a suggestion that the peak height of tanδ may have been reaching a plateau. By storing samples at 125 and 150 °C, a different pattern in peak height change, to that seen at the lower storage temperatures, was observed over time. Between 0 and 24 hours of storage the peak height increased, but this was followed by a decrease in height for the remainder of the storage duration. The samples held at 150 °C decreased at a greater rate and to a greater extent than those at 125 °C. The molecular weight (M_w) of P(HB-co-45mol%HV) has been shown to decrease at temperatures as low as 100 °C [67], and Chen *et al*. observed a decrease in PHB and P(HB-co-5wt%HV) at times between 10 and 60 minutes [54]. Many authors have used the decrease in M_w to infer the activity of thermal degradation through the chain scission process [54,62,65,67,68,70,71]. Therefore, the decrease in peak height of samples stored at 125 and 150 °C may be a result of the constraints on the amorphous fraction relaxing as chain scission begins to take place. The possibility of thermal degradation being active at these temperatures is discussed further in Chapter 7.

As mentioned previously, the glass transition occurs over a temperature range, rather than at a specific temperature, [95]. This is due to shorter chains, and less constrained sections of chains, which have less entanglement and fewer interactions, becoming mobile at lower temperatures than longer and more constrained chains, which require a greater amount of energy before achieving long range motion. In addition, the rise in temperature applied during the experiment gradually increases the free volume within the material. Shorter chains are able to move in a smaller volume and therefore have lower glass transition temperatures than longer ones which require the greater free volumes brought about by higher temperatures. Hence the width of the tanδ peak, describing the T_g range, provides an indication of the homogeneity of the amorphous phase.

Generally, the storage temperature had minimal effect on the width of the tanδ peak. At lower storage temperatures (7 and 20 °C) the peak width decreased slightly with longer storage durations. When stored at 150 °C, however, there is a clear relationship between the width of the tanδ peak and the duration of storage, as shown in Figures 5.13 and 5.14. Over time, samples stored at 150 °C exhibited an increase in tanδ peak width, from 20.17 °C in the unconditioned sample, plateauing after around 336 hours of storage, at 35.83 °C, an increase of 15.66 °C. Interestingly, no significant change occurred during the first 24 hours of storage at 150 °C. Instead there appeared to be a rapid increase between 24 and 336 hours. This would appear to be inconsistent to the general trends seen in the earlier analysis of the tanδ peak, where the largest changes happened within the first 24 hours.

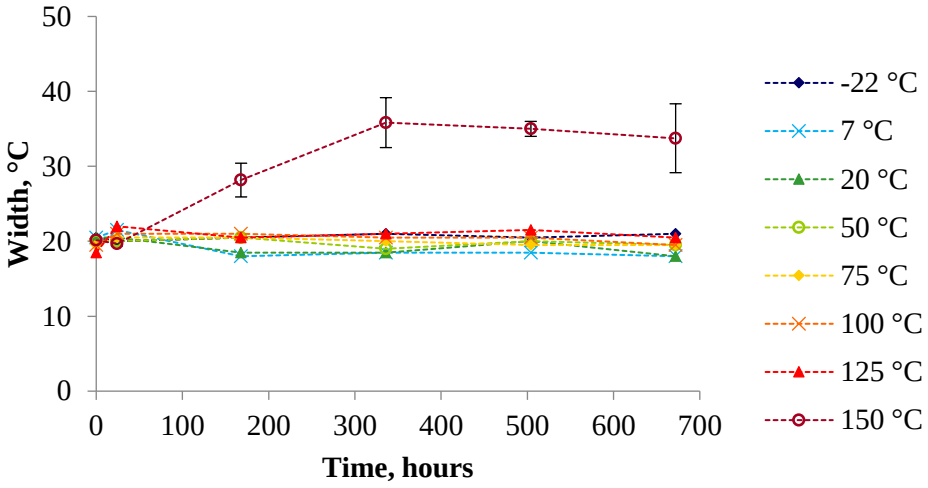

Figure 5.13. Development of tanδ width over time, comparing the effect of different sample storage temperatures. Dashed lines have been superimposed between timepoints as a visual aid to guide the eye through the data sets. DMTA data tables are in Appendix D.

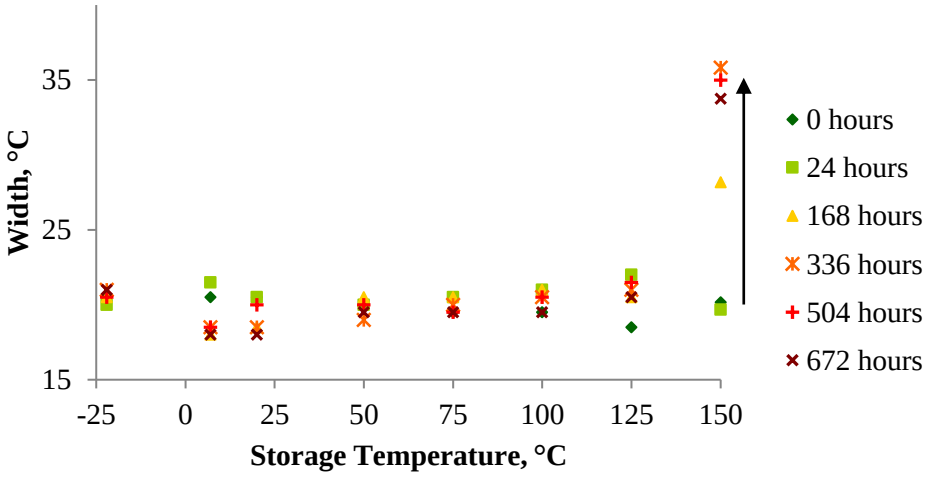

Figure 5.14. Development of tanδ width according to the temperature at which the samples were stored, examining the influence of the duration of storage.

The observed increase in the width of the tanδ peak at 150 °C is an indication that the material is becoming more heterogeneous; in other words, that a greater range of chain lengths were contributing to the relaxation peak [95,98]. While Biddlestone *et al.* and Lizundia *et al.* attributed broadening to an increase in the degree of crystallinity [32,96]. It is possible that both

of these interpretations may be true, depending on whether the peak is extending to the high or low temperature side. An increase in crystallinity could restrict the mobility of the amorphous regions, pushing up the glass transition temperature and increasing the width of the peak to the high temperature side. Whereas a decrease in the molecular weight could lower the T_g, due to shorter, less entangled chains requiring less energy to achieve long range motion, increasing the width of the peak to the lower temperature side. In this case, when samples were stored at 150 °C, both factors may have influenced the tanδ. Initially the width increased to the higher temperature side of the peak, as shown in Figure 5.15, indicating the increased constraint on the amorphous material caused by secondary crystallisation. With longer storage durations, the width of the peak increased further, as the lower limit of tanδ fell (Figure 5.16), indicating that some of the material became more mobile at lower temperatures, potentially as chain scission caused a reduction in the M_w. The sample stored at 150 °C for 672 hours also experienced a fall in the upper limit of tanδ. It may be that, by this time point, chain scission was reducing the constraints imposed by the crystalline regions on the amorphous material.

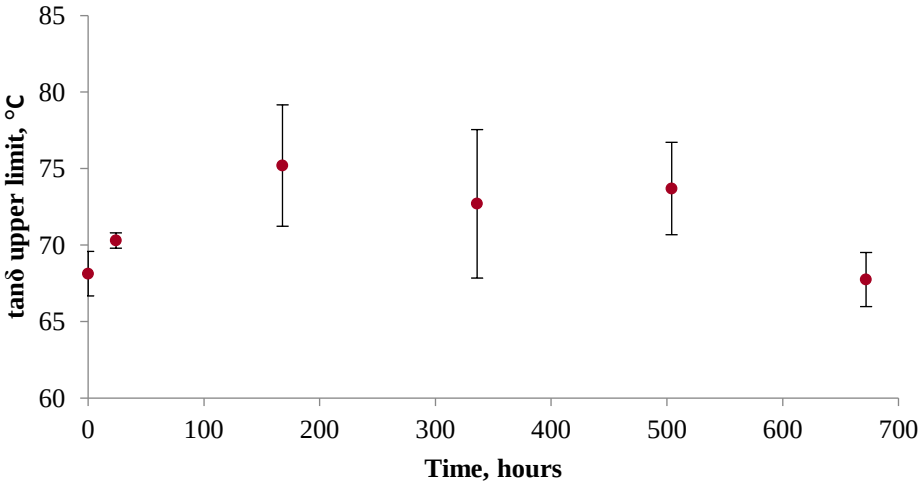

Figure 5.15. The relationship between temperature of the upper limit of the tanδ peak with length of storage time.

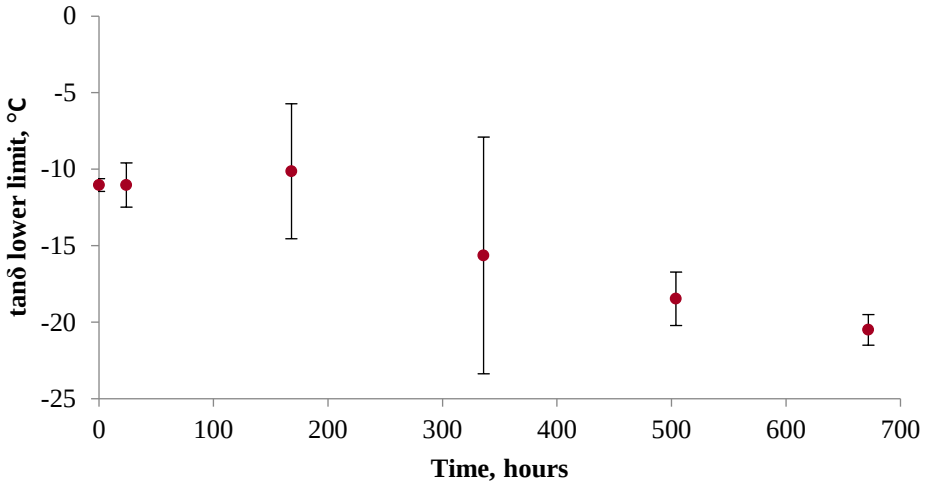

Figure 5.16. The relationship between temperature of the lower limit of the tanδ peak with length of storage time.

It has already been mentioned that the symmetry of the tanδ peak may also contain information relating to the T_g of a material. A completely amorphous material will display a completely symmetrical curve, while a semi-crystalline material will produce an asymmetrical peak. de Koning and Lemstra described how the T_g commonly extends to the high temperature side of the tanδ peak, as a result of crystals constraining the amorphous chains [33]. While many authors discuss the effect of constraints on the amorphous regions [13,17,32], others have described this constraint in terms of a 3-phase model; consisting of the crystalline phase, the mobile amorphous fraction (MAF), and the rigid amorphous fraction (RAF) [96,97], as described in Chapter 1.1.2. Chains which extend from the crystal lamellae into the amorphous phase have lower segmental mobility than chains which exist in the amorphous phase only [96]. The portion of the chain closest to the lamellae, where movement is most restricted, is in the region termed the RAF. Chains in the middle of the amorphous phase, where mobility is the least restricted, are in the region termed the MAF. The asymmetry of the tanδ peak, created by the presence of a rigid amorphous phase, was typical of the samples in this study prior to exposure to the various thermal conditions, as illustrated in Figure 5.17a.

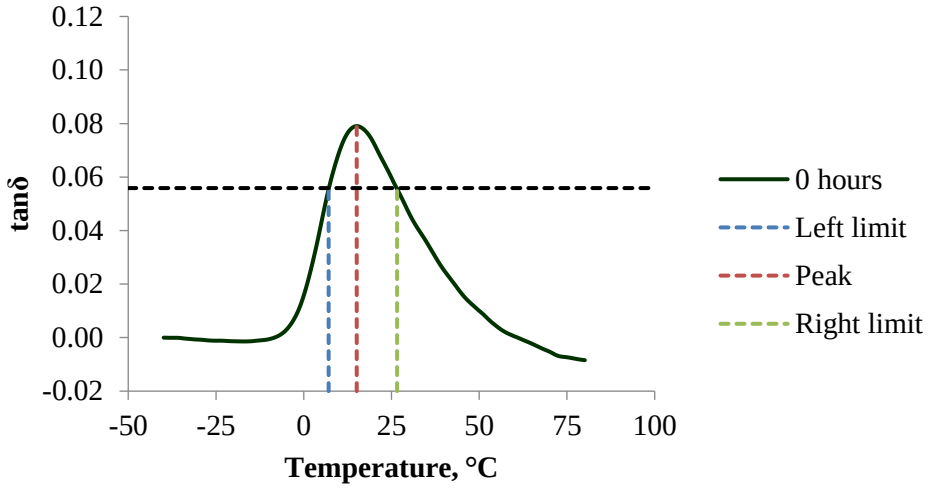

a.

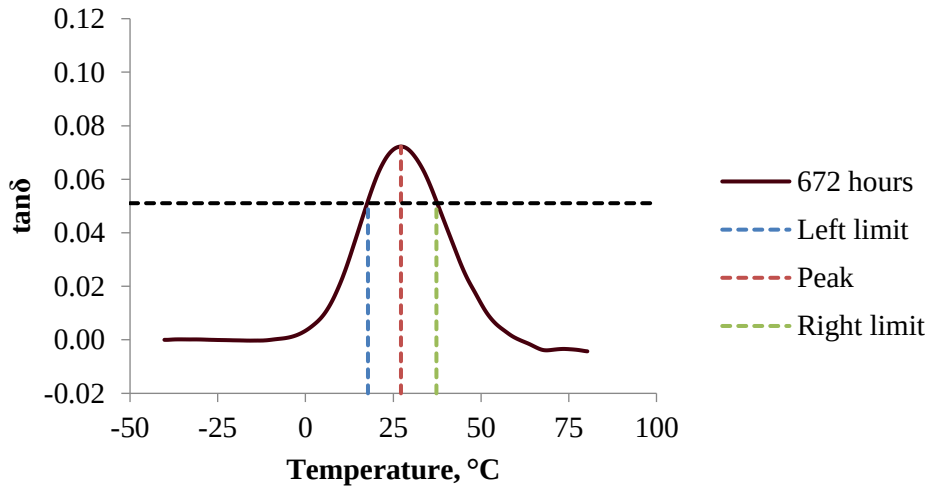

b.

Figure 5.17. Examples of the change in peak area distribution for a sample stored at 100 °C for a. an unconditioned sample, and b. a sample stored for 672 hours. The values quoted in text are taken from the area under the tanδ curve above the black line, as described in Chapter 2.4.3.

While the width of the peak may have remained fairly constant throughout the duration of the study, the distribution of the peak area did change, and was seen to be dependent on both the temperature and duration of storage. Figure 5.17a illustrates the asymmetry of the tanδ peak area prior to storage, described by de Koning and Lemstra [33], and Figure 5.17b illustrates the distribution of the peak area of a sample stored at 100 °C for 672 hours. A clear change occurred within the sample during the storage period, resulting in a much more symmetrical distribution of the tanδ peak area. Secondary crystallisation which thickens the lamellar through movement

of chains in the amorphous region towards the more stable crystalline state, results in smaller amorphous regions comprising of a greater proportion of chains in the RAF than in the MAF. If secondary crystallisation proceeds through an infill mechanism, whereby portions of chains in the MAF form smaller crystal structures, then the movement of chains surrounding these structures becomes more restricted. Consequently, no matter which mechanism of secondary crystallisation is active, the T_g is shifted towards higher temperatures, as it takes a greater amount of energy for amorphous chains to overcome the additional constraints. As the T_g originally extends to the high temperature side of the tanδ peak, and secondary crystallisation decreases the amount of material in the MAF and increases the amount of material in the RAF, it follows that secondary crystallisation would produce in a more evenly distributed tanδ peak, as more amorphous material becomes constrained and requires a greater amount of energy to achieve long range motion.

Consistent with previous findings, the samples which were held at -22 °C remained stable throughout the duration of the study, as below the T_g the polymer chains are immobile (Figure 5.18). Those samples kept at 7 and 20 °C tended towards a more balanced distribution of area over time, starting at 40:60 (left side : right side) and both reaching 45:55 at 672 hours. This re-distribution of peak area became almost equal over time in samples held at 75, 100 and 125 °C, reaching, 49:51 after 672 hours of storage, and samples kept at 50 °C reached a 50:50 split. Secondary crystallisation decreases the amount of material in the MAF and increases the amount in the RAF, shifting the peak area towards higher temperatures.

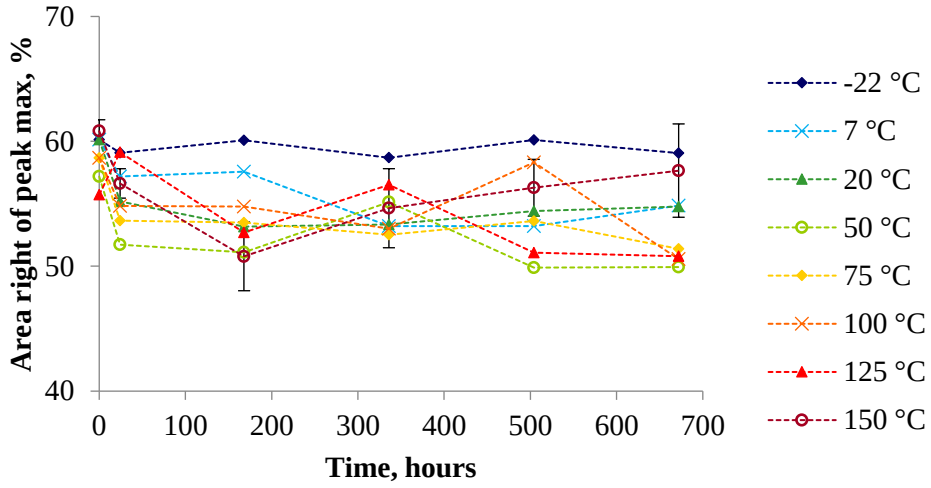

Figure 5.18. Change in the distribution of area of the tanδ peak over time, according to the storage temperature. The percentage of the total area which is to the right of the peak maximum is shown. Dashed lines have been superimposed between timepoints as a visual aid to guide the eye through the data sets. DMTA data tables are in Appendix D.

Samples which were stored at the highest temperature, 150 °C presented a different time dependence to all other storage temperatures. At first, as seen with the other temperatures, there was a clear change to a more balanced distribution around the peak maximum, from 39:61 to 49:51, during the first 168 hours. Together with the observed increases in T_g this would suggest an increase in crystallinity, and further constraint of the rigid amorphous fraction, producing the change in shape of the tanδ peak. However, this was followed by a more gradual redistribution weighted back towards the right side of the peak over the remainder of the study, with an average value of 42:58 recorded from the samples stored for 672 hours.

The re-distribution back to an asymmetrical peak was observed in samples stored at 150 °C with storage lengths upwards of 336 hours. It is likely that the high degree of crystallinity and proportion of material in the RAF, caused by secondary crystallisation, is reducing as the M_w falls due to scission of the polymer chains, which causes a reduction in both chain length, and in the constraints on the amorphous phase. The peak became asymmetrical again as the

temperature of the peak maximum decreased more quickly than the upper and lower limits of the tanδ peak (Figure 5.19). As the upper limit of the peak relates to material in the RAF, most affected by the constraints imposed by the crystalline regions [33,99], then it follows that the rate of decrease in the constraints is slowest in this region, as degradation is thought to begin in the amorphous phase [69,71,77]. The lower limit of the peak relates to material requiring the least amount of energy to move through the glass transition, which is comprised of the least constrained, and therefore less entangled, shortest chains in the MAF. Therefore, the effect of further reduction in length and constraints resulting from chain scission is still small. The peak maximum corresponds to chains which are constrained by the RAF more than those at the lower limit, but less constrained then the material in the RAF itself. It is also likely that these chains are longer, and therefore more entangled, than the material at the lower limit of the peak, as they require a greater amount of energy to achieve long range motion. This means that scission of these longer, partially constrained chains, results in a proportionally greater reduction in temperature required for long range motion, causing the T_g to decrease at a faster rate than the temperature of the lower limit.

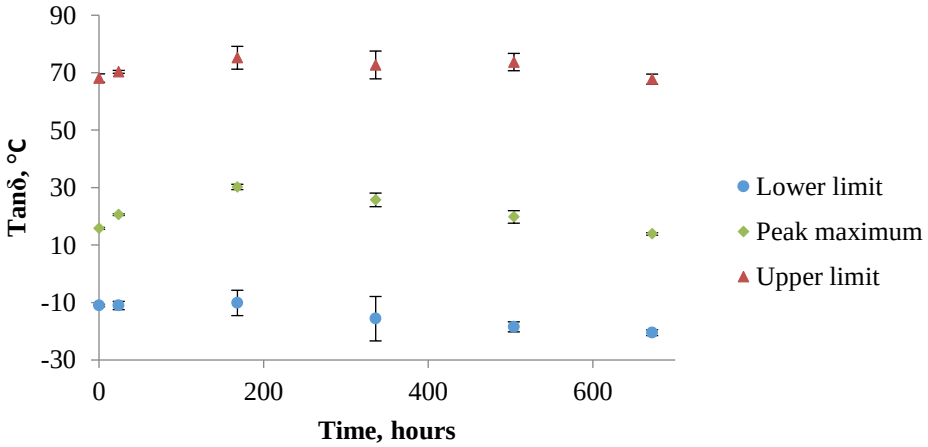

Figure 5.19. The change in the tanδ lower, upper and peak maximum temperatures with increasing duration of sample storage.

5.2 Analysis of the storage modulus (E′)

5.2.1 Qualitative observations of the E′ curves

The storage modulus (E′) is a measure of elastic response of the material. Samples stored at -22 °C had E′ curves which remained relatively constant throughout the duration of the study, as the material was below its T_g where the chains are not mobile (Figure 5.20). Similar results were seen when held at 7 °C, most likely due to the proximity to the T_g (Figure 5.21). Samples stored at 20 °C presented a gradual shift in the onset of the slope to higher temperatures (Figure 5.22). Another interesting feature to draw attention to is that, in both the 7 and 20 °C samples, the development of a second relaxation of E′ was observed as the duration of storage increased. This feature is highlighted within the rings superimposed onto Figures 5.21 and 5.22. However, a secondary relaxation was not observed in the data obtained from samples held at a storage temperatures of 50 °C or above.

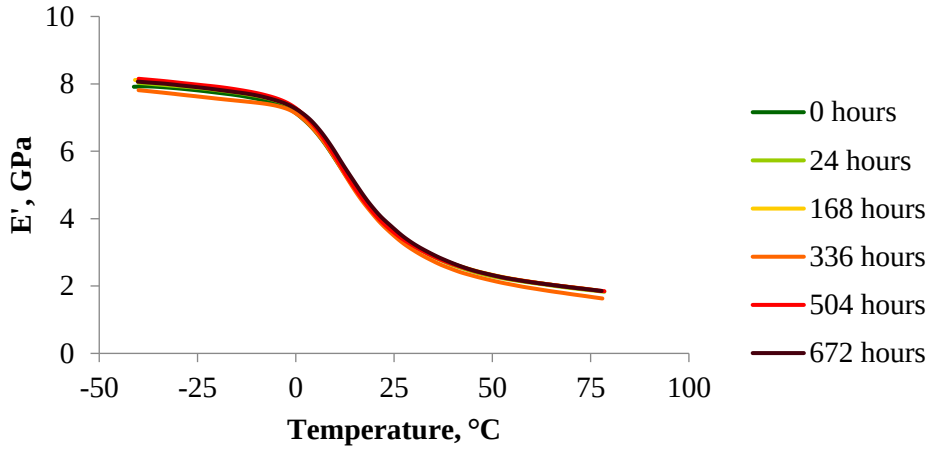

Figure 5.20. E′ curves of samples stored at -22 °C.

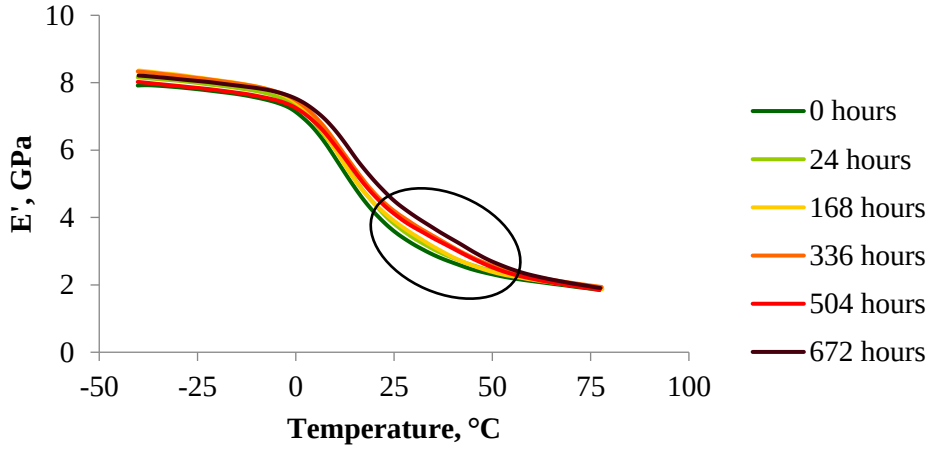

Figure 5.21. E′ curves of samples stored at 7 °C.

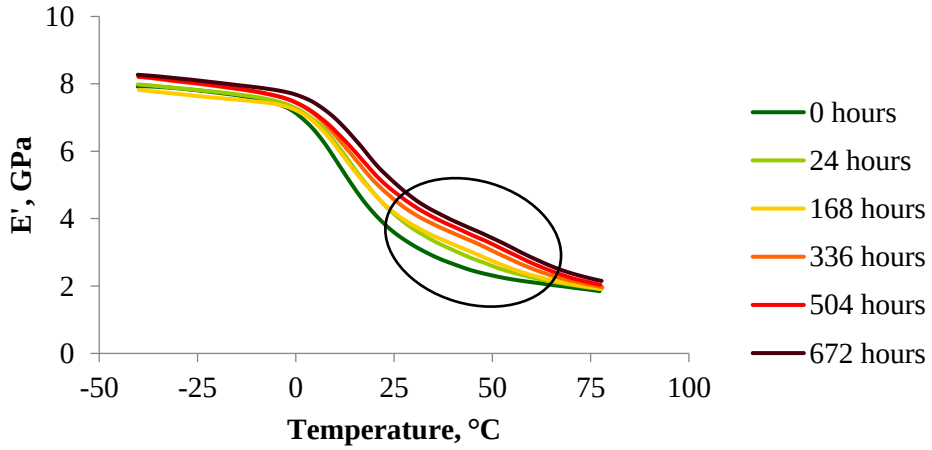

Figure 5.22. E′ curves of samples stored at 20 °C.

At 50 to 125 °C (Figures 5.23 to 5.26) samples exhibited a shift in the onset of E′ decrease to a higher temperature during the first 24 hours of storage, which then remained relatively constant for the remainder of the study.

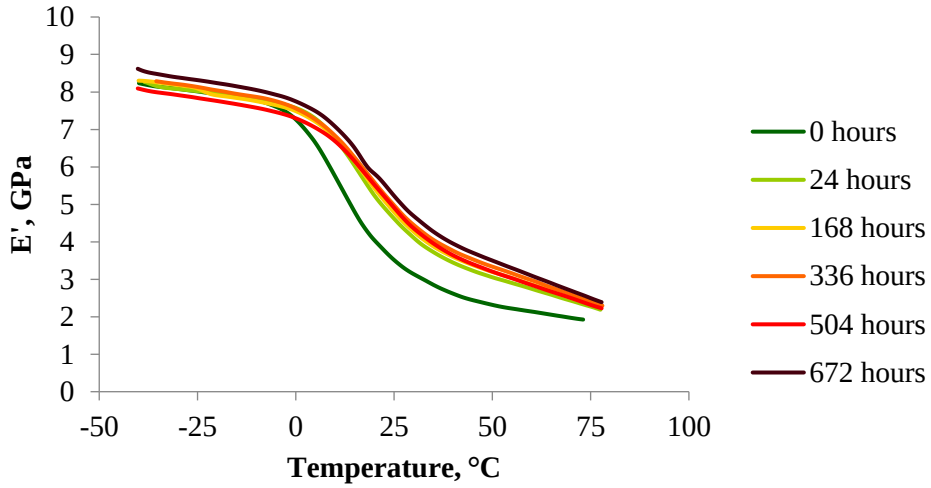

Figure 5.23. E′ curves of samples stored at 50 °C.

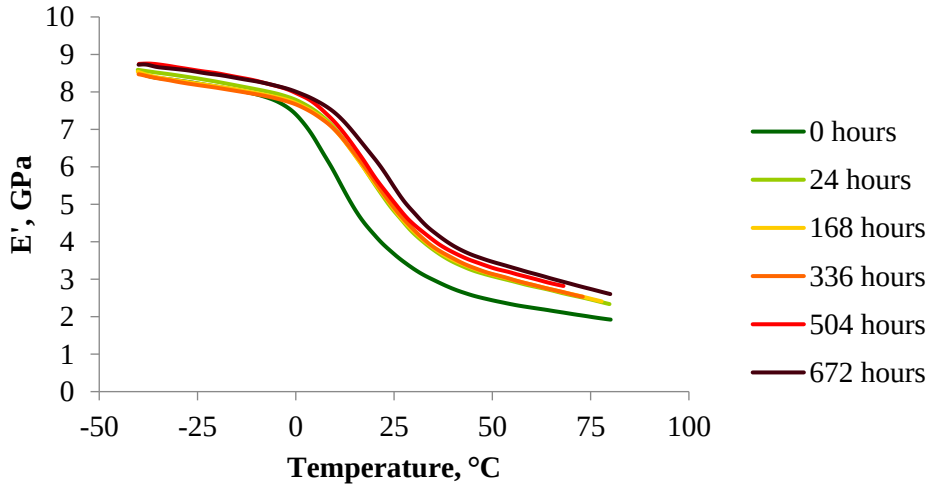

Figure 5.24. E′ curves of samples stored at 75 °C.

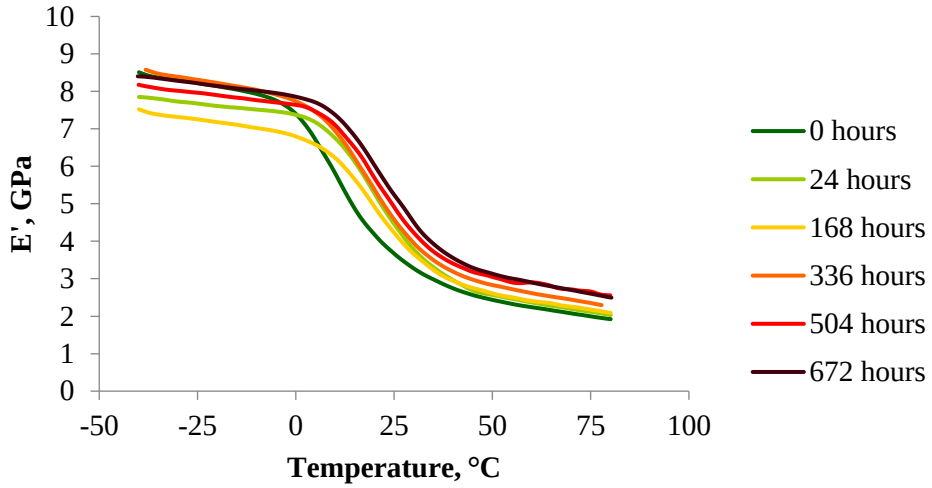

Figure 5.25. E′ curves of samples stored at 100 °C.*

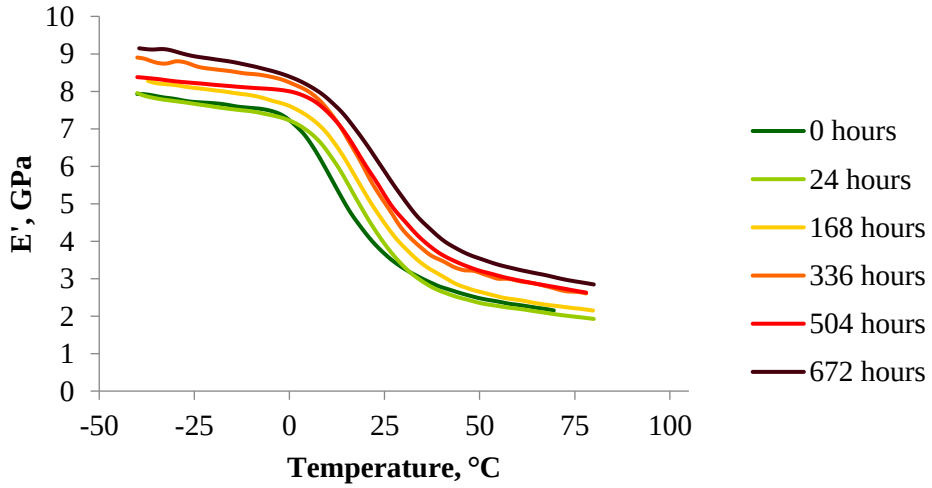

Figure 5.26. E′ curves of samples stored at 125 °C.

**It should be noted that the inconsistency of the sample stored at 100 °C for 168 hours was most likely due to a loading error, whereby the sample was slightly misaligned when inserted into the instrument.*

When stored at 150 °C the temperature of E′ onset increased then decreased with increasing storage time (Figure 5.27). At this storage temperature, the decrease in E′ becomes less with longer storage times, which has been attributed to an increase in chain stiffness [96].

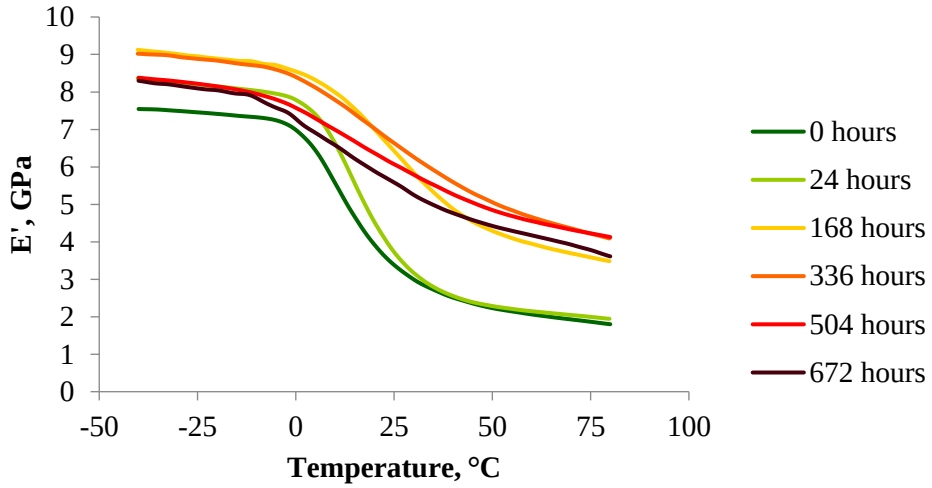

Figure 5.27. E′ curves of samples stored at 150 °C.

Significant trends emerging through qualitative observation of E′ are the change in the onset of E′ decrease, and the emergence of a secondary relaxation at 7 and 20 °C.

5.2.2 T_g measurements from E′

The large drop in E′ with increasing temperature also relates to the T_g of the material [48]. Measuring T_g as the point where the curve begins to deviate away from the initial stable portion provides information on the start of the glass transition process. Figures 5.28 and 5.29 illustrate the development of T_g, at the various storage temperatures, recorded with increasing storage duration.

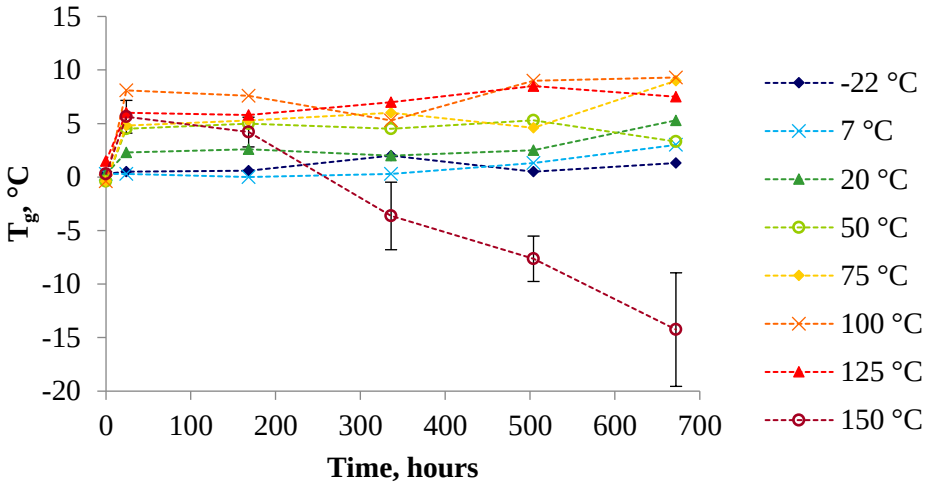

Figure 5.28. Development of T_g over time, comparing the effect of different sample storage temperatures. The value of T_g was taken from the onset of E′ rapid decrease. Dashed lines have been superimposed between timepoints as a visual aid to guide the eye through the data sets. DMTA data tables are in Appendix D.

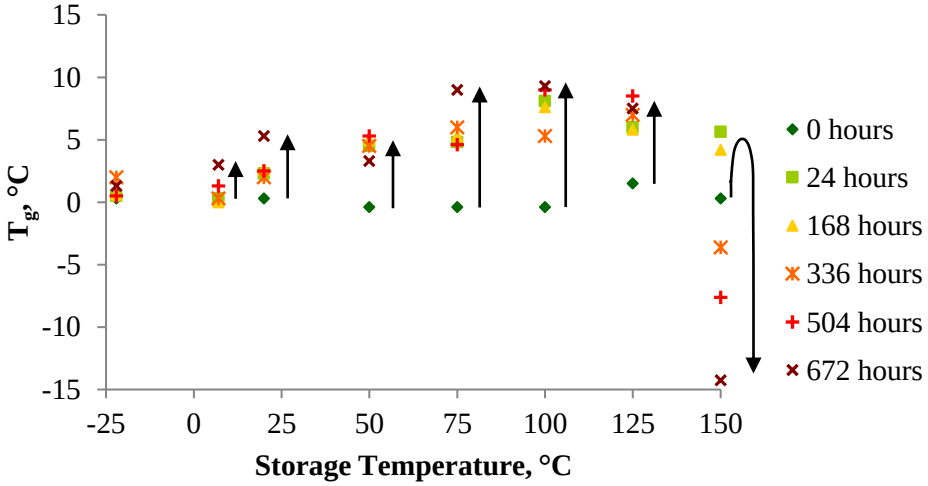

Figure 5.29. Development of T_g according to the temperature at which the samples had been stored, examining the influence of the duration of storage.

The E′ value of T_g, from samples kept at -22 °C, was reasonably stable throughout the study. This lack of change is because of the lack of mobility in the polymer chains when held below the T_g. In samples stored at 7 °C, the T_g did not change for the first 336 hours of the study, at which point it measured 0.3 °C, exactly the same as that obtained from the unconditioned

sample. After 504 hours of storage the T_g showed a minor increase, to 1.3 °C, and a further small increase, to 3 °C, was observed in the sample held for 672 hours.

The results from samples stored at 20 °C indicate a gradual increase in T_g starting from the beginning of the study (0.3 °C), to the sample held for 672 hours, which had a T_g of 5.3 °C. A much more rapid increase in T_g was seen in samples held at 50 °C. Unlike the gradual change seen in samples kept at 20 °C, the change at this temperature seemed mainly to occur within the first 24 hours of storage, where T_g appeared to jump from -0.4 to 4.5 °C, with similar values of T_g observed thereafter. The samples stored at 75 °C exhibited very similar values of T_g to those stored at 50 °C. This was true all the way through the study, apart from the samples which were stored for 672 hours. At this time point the T_g of the sample kept at 75 °C was much greater than that of the sample kept at 50 °C, which were measured as 9 and 3.3 °C respectively. It was also significantly higher than the T_g of the previous time points at 75 °C, with the sample kept for 504 hours giving a T_g of 4.6 °C. The total change in T_g over the entire 672 hours was greatest in the samples held at a storage temperature of 100 °C, with the difference between the unconditioned sample and the sample stored for 672 hours measuring 9.7 °C, from -0.4 to 9.3 °C. Again, most of this change occurred during the first 24 hours of the study, where the T_g jumped to 8.1 °C, followed by a slight increase over the remainder of the storage time.

Samples kept at 125 °C exhibited their greatest and most rapid change in T_g within the first 24 hours, from 1.5 to 6 °C. The T_g then appeared to continue to increase slightly until the end of the study, where it measured 7.5 °C.

After 24 hours at 150 °C a significantly increased T_g, from an average of 0.3 to 5.63 °C, was observed. Though the T_g of the samples stored for 168 hours also had an average value higher than that of the unconditioned sample, at 4.2 °C, it was less than that of the samples held for 24

hours. The average T_g measured from the 336 hour samples, -3.63 °C, confirmed that the T_g was falling, and it continued to do so for the rest of the study, finally reaching an average value of -14.25 °C after 672 hours of storage.

While storage below the original T_g of the samples induced no change in T_g over time, the extent and rate of observed rise in T_g increased with the temperature of storage between 7 and 125 °C. At 150 °C a rapid increase in T_g was followed by a large and steady decrease with storage time. Due to the similarity of these trends to those observed when measuring the T_g as the temperature of the tanδ peak maximum, the reader should refer back to the tanδ peak measurement of T_g for further discussion of trends (Chapter 5.1.2).

5.2.3 E′ secondary relaxation at low storage temperatures

As noted previously, another interesting feature of the E′ data collected in this study is the emergence of a secondary relaxation process over time, some 30 to 50 °C above the onset of the first. Other authors have reported observing similar details in the E′ curves of PHB. Renstad *et al*. described a discontinuity in the storage modulus at temperatures of 30 to 50 °C [77]. Wei *et al*. also described a second thermal relaxation, but at much higher temperatures, around 110 °C [48]. In this study, the secondary relaxation was only apparent in the storage modulus curves produced from samples stored at 7 and 20 °C. Figures 5.30 and 5.31 show the development of the secondary relaxations, indicated by the arrows, with increasing duration of storage.

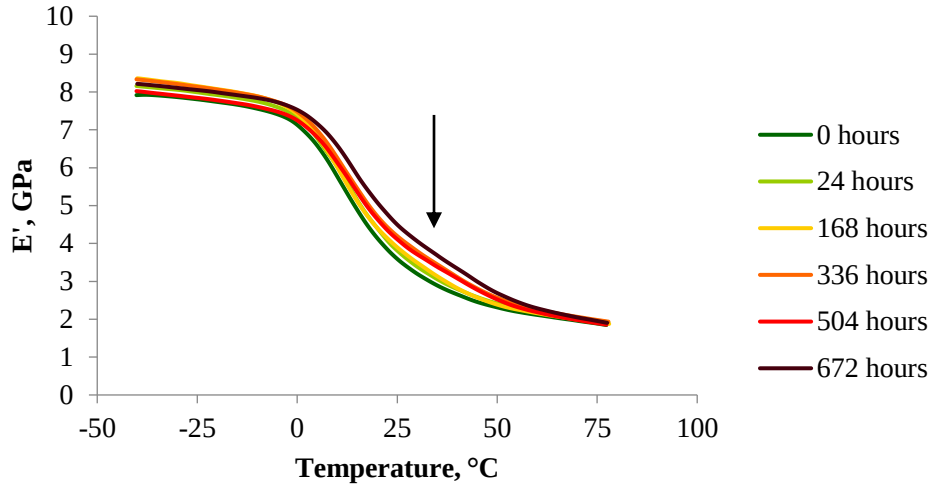

Figure 5.30. E′ of samples stored at 7 °C where a secondary relaxation can be seen to develop over time.

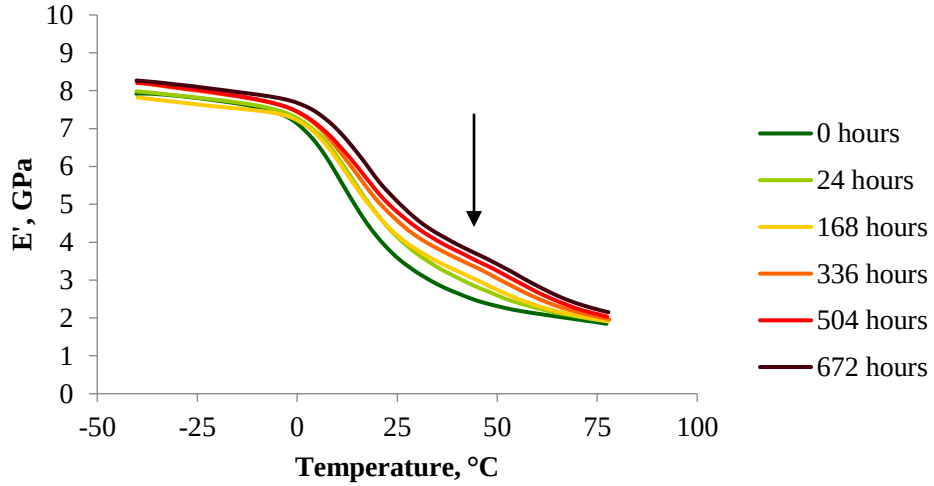

Figure 5.31. E′ of samples stored at 20 °C where a secondary relaxation can be seen to develop over time.

By differentiation of E′ with regards to temperature, it is possible to find at what temperature the peak rate of the secondary relaxation occurred. Figures 5.32 and 5.33 show the resultant first derivative peaks, with the secondary relaxations indicated by the arrows.

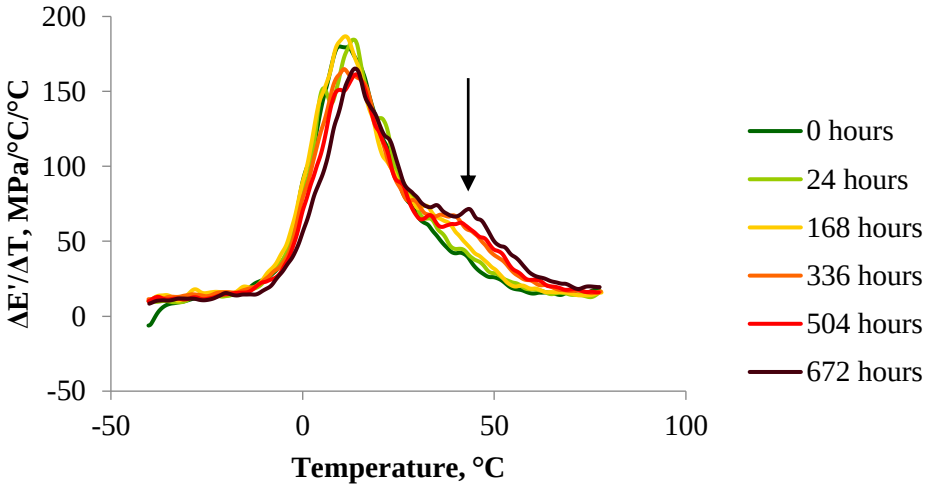

Figure 5.32. The first derivative of E′ of samples stored at 7 °C, where the arrow indicates second peak developing over time relates to the secondary relaxation.

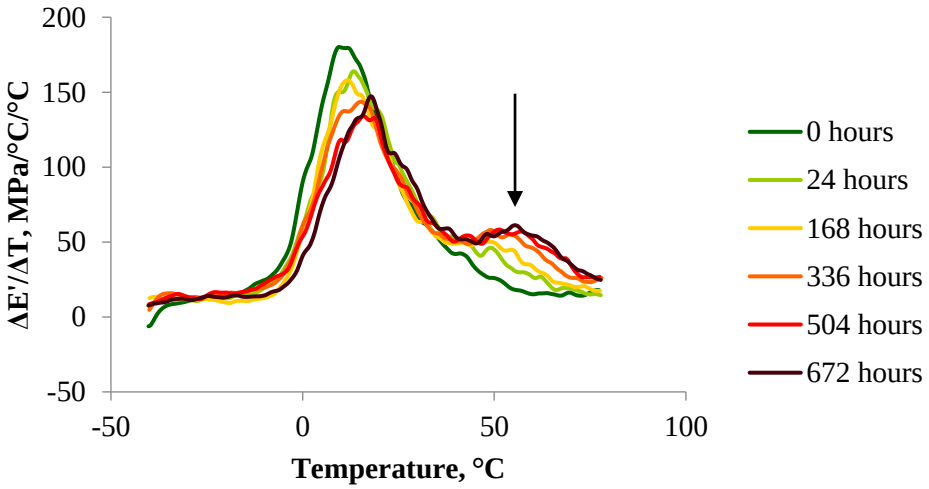

Figure 5.33. The first derivative of E′ of samples stored at 20 °C, where the arrow indicates second peak developing over time relates to the secondary relaxation.

As time progressed the strength of the relaxation, as well as the temperature at which the secondary relaxation was observed, increased in samples stored at both 7 and 20 °C. In the samples kept at 20 °C the secondary relaxation was much more prominent, and was seen to develop much more quickly than in samples held at 7 °C. Figure 5.34 demonstrates the relationship between temperature at which the maximum of the secondary relaxation peak

occurred and the storage duration of the samples. The differentiated data indicates that the higher storage temperature caused the secondary relaxation to take place at higher temperatures.

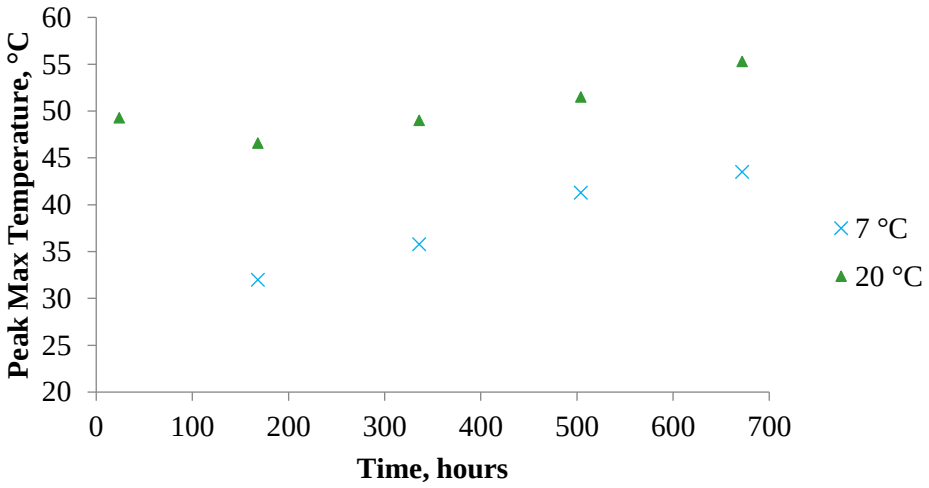

Figure 5.34. Comparing the difference in temperature at which the maximum height of the secondary peak occurs over time, when samples are stored at 7 °C and 20 °C. DMTA data tables are in Appendix D.

As can be seen in Figures 5.30 and 5.32, samples which were kept at 7 °C did not present a secondary relaxation until 168 hours into the study. Figure 5.34 demonstrates that after the secondary relaxation peak appeared, at 32 °C, the temperature at which the peak was observed continued to increase steadily until the end of the study, where the maximum height occurred at 44 °C. In samples stored at 20 °C, the secondary relaxation peak formed at a higher temperature than in samples held at 7 °C, with the first peak maximum being observed at 49 °C. After a slight decrease after 168 hours of storage, the peak temperature also increased gradually over time. The increase occurred at a slower rate than that seen in the samples stored at 7 °C, reaching a value of 55 °C after 672 hours of storage.

The secondary relaxation observed by Wei *et al*. took place at a temperature far above that discussed here; hence the reason presented by Wei, that the relaxation is due to crystal-crystal

slippage prior to melting [48], is unlikely to be the cause of the secondary relaxation observed in this study. There is also evidence within the data collected in this study to disagree with the notion of Renstad *et al*., who attributed the observed secondary relaxation to recrystallisation of the material during the DMTA heating scan [77]. If this were the case, the secondary peak would also be apparent in the storage modulus curves of samples stored at -22 °C, or in those from the unconditioned samples. However, the secondary relaxation was only visible in samples which were held at 7 and 20 °C. Schwarz *et al*. also observed a secondary relaxation process, emerging over time from a quenched amorphous sample of PP held at 20 °C [52]. Starting approximately 20 °C above the annealing temperature, in that work, the relaxation was attributed to the development of a rigid amorphous phase.

Secondary crystallisation at low temperatures has the ability to form new, very thin lamellae within the interlamellar regions [92], which would have melting temperatures far below those grown during primary crystallisation due to their relative instability. It may be possible that, at these low storage temperatures, the secondary relaxation is a result of the melting of these new lamellae. This may explain why the secondary relaxation took place at higher temperatures for the samples stored at the higher temperature, and why it rose over time, as the continuation of secondary crystallisation increased the stability of the new structures, and so the scan reached higher temperatures before the new structures melted out. It could also provide explanations as to why the secondary relaxation is not seen in samples stored at higher temperatures. One of which may be that the continuation of secondary crystallisation, which proceeds at a greater rate at higher temperatures, would increase the size of the newly formed lamellae, increasing their stability and raising the T_m to temperatures greater than the parameters of the experimental run. Another is that the samples would be above the T_m of thin lamellae, so it would not be

possible for them to form at sufficiently high storage temperatures. Instead secondary crystallisation proceeds by lamellar thickening, which does not produce a secondary relaxation.

5.3 Conclusions

Storage at -22 °C did not cause any change in the material. This is due to the lack of mobility of the polymer chains when the material is below its T_g. Over time the secondary crystallisation process, happening during storage of the samples at 7 to 125 °C, resulted in an increase in T_g, a decrease in tanδ peak height, and a re-distribution of the tanδ peak area to a more symmetrical peak. Generally, the higher the storage temperature, the greater the degree of secondary crystallisation and therefore a greater extent of change in the measured variables. The loss of amorphous phase through secondary crystallisation, combined with the increased constraints imposed on the remaining amorphous material, created a stiffer material.

Secondary crystallisation may have also resulted in a secondary relaxation in the E′ curves of samples held at 7 and 20 °C. At these low temperatures, it is possible that smaller lamellae formed within the interlamellar regions, and the softening observed in the E′ related to the melting out of these smaller structures.

At a storage temperature of 150 °C, it is believed that the secondary crystallisation process was active in the early stages of storage, as evidenced by the initial increases observed in the T_g, and the position of the tanδ peak. However, with increasing storage duration it became apparent that a second process may also be influencing the properties of the material. Over time, the rise in T_g, and the tanδ peak position slowed and then the values began to fall. This change in behaviour was attributed to the activation of the chain scission process, which causes a decrease in the molecular weight of the material. The proposed combination of secondary crystallisation

and chain scission would certainly account for the width of tanδ increasing with longer storage times, due to the constrictions imposed on the amorphous material by the increase in crystallinity, and the creation of chains with lower molecular weight which become mobile at lower temperatures. It would also explain the decrease in overall relaxation of E′ with increasing storage duration, as the material became more brittle.

Overall, DMTA proved an effective method of observing the T_g of the samples in this study, which was not possible by conventional DSC methods due to the high degree of crystallinity.

CHAPTER 6 – THE EFFECT OF STORAGE TEMPERATURE ON THE MECHANICAL PROPERTIES

6.1 Stress-strain behaviour

Examples of the stress-strain curves obtained from tensile testing unconditioned samples and samples stored for 24 and 168 hours, at temperatures of -22, 7, 20, 50, 75, 100, 125 and 150 °C, are shown in Figure 6.1. The curves from the original samples, prior to storage, and the curves from samples held at -22 °C, show the characteristics of a relatively ductile material in comparison with those obtained from samples stored at temperatures above the T_g. A decrease in elongation to break over time is seen in all samples stored at temperatures above the T_g (Figure 6.1b-h). An increase in UTS is also observed over time in samples stored between 7 and 125 °C. Samples kept near the lower end of the storage temperature range, at 20 and 50 °C in particular, presented a small amount of yeild before failure, emerging over time. No yield was present in the stress-strain curves from samples stored at the upper end of the tempeature range.

Drastic embrittlement occurred in samples held at 150 °C (Figure 6.1h). This resulted in the inability to perform tensile tests when samples were stored for 48 hours or more, as the samples fractured when being clamped into the instrument.

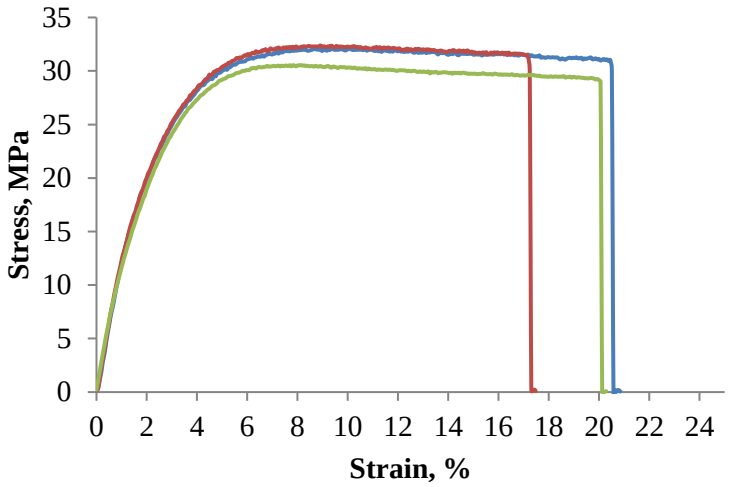

a.

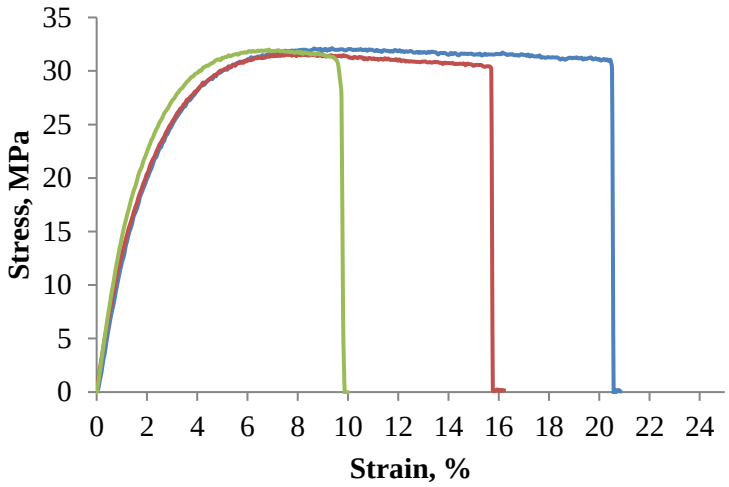

b.

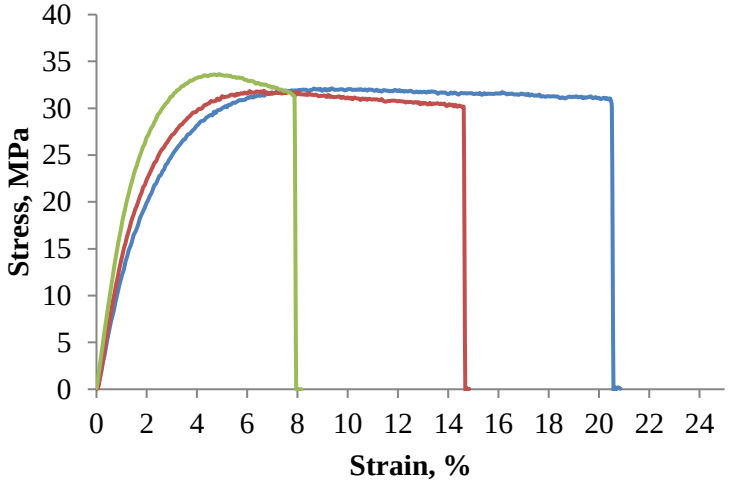

c.

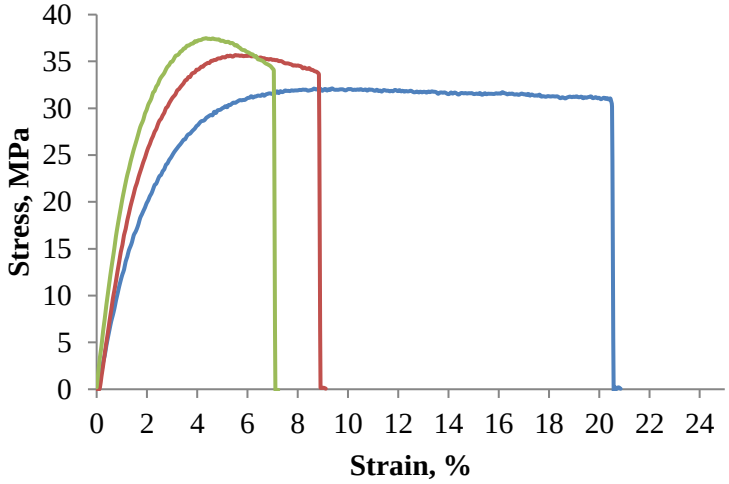

d.

Figure 6.1. Comparison of tensile stress strain curves for unconditioned samples (blue line), for samples stored 24 hours (red line) and 168 hours (green line), at storage temperatures of a. -22 °C, b. 7 °C, c. 20 °C, and d. 50 °C.

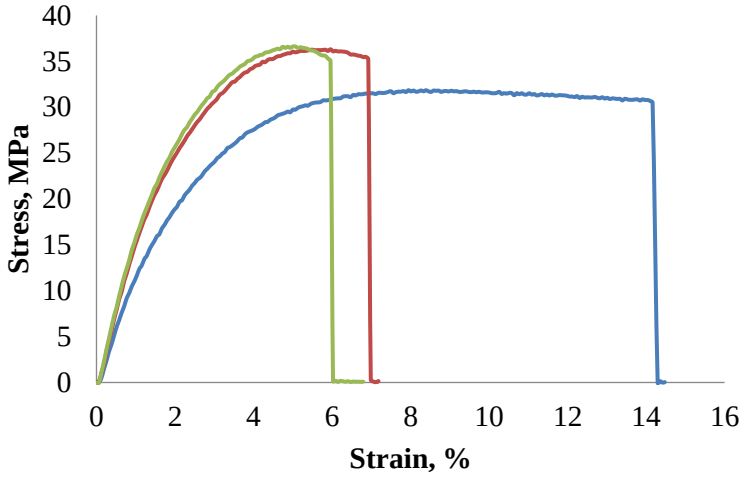

e.

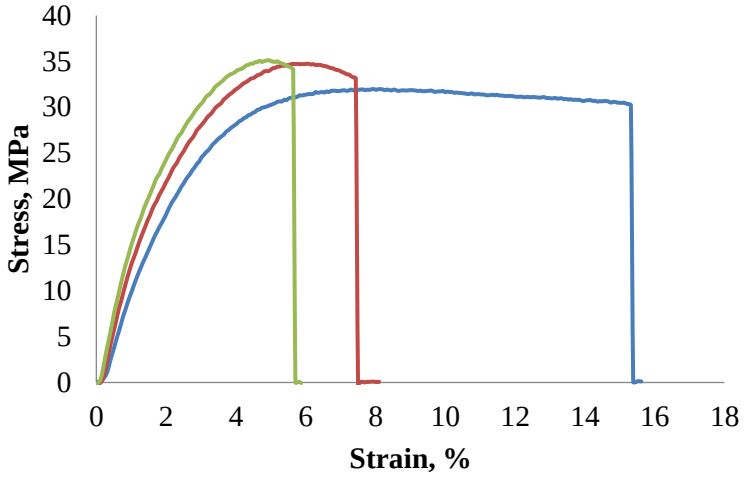

f.

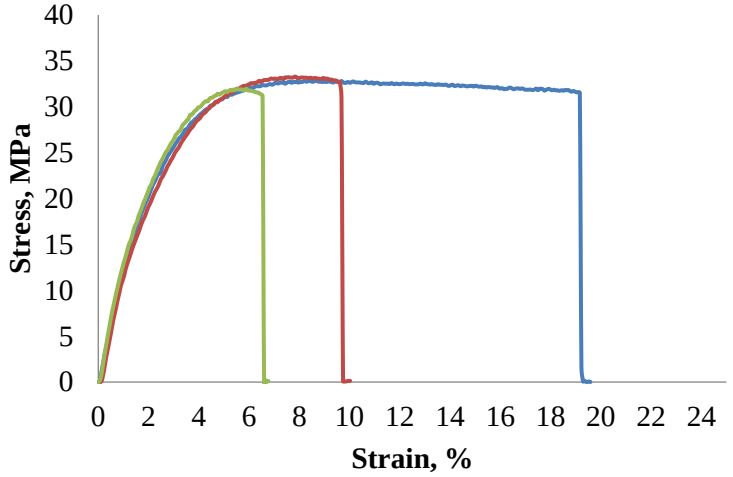

g.

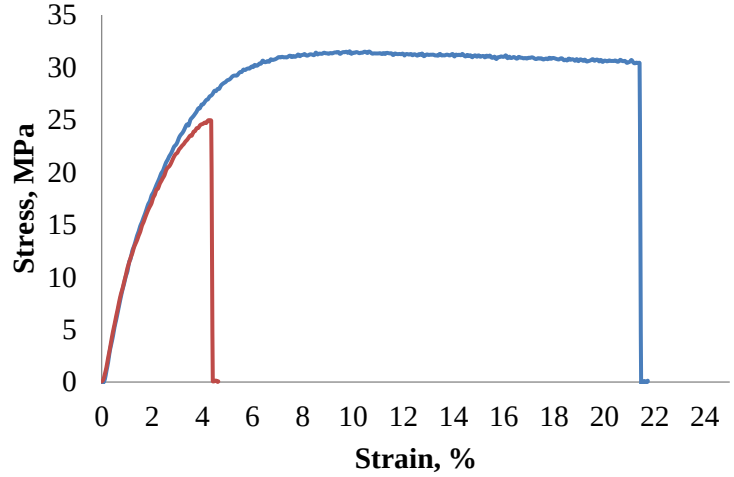

h.

Figure 6.1 continued. Comparison of tensile stress strain curves for unconditioned samples (blue line), for samples stored 24 hours (red line) and 168 hours (green line), at storage temperatures of e. 75 °C, f. 100 °C, g. 125 °C, and h. 150 °C. Note: no data for 150 °C at 168 hours.

6.2 Young's modulus

When stored at -22 °C, below the T_g of the material (Chapter 5.1.2 and 5.2.2), no significant change in Young's modulus was observed throughout the duration of the study (Figure 6.2). This is as expected, due to the inability to crystallise below the T_g, as the polymer chains lack mobility. Samples held from 7 to 50 °C demonstrated a trend of increasing Young's modulus with longer storage duration. Biddlestone *et al*. attributed the change in tensile properties to the occurrence of secondary crystallisation which constricts the mobility of the chains [32]. The increase in crystallinity seen in samples stored at 7 to 150 °C is presented in Chapter 4.1.2 and 4.2.1. As the Young's modulus is an indication of the stiffness of the material, measured from the slope of the initial linear portion of the curve where elastic deformation takes place, it is plausable that the process of secondary crystallisation could cause the increase. During elastic deformation under a tensile load, the molecules within the amorphous regions of the material align, as they are able to uncoil and slip past each other, and the covalent bonds in the crystalline lamella bend and stretch, also allowing a small amount of extension within the crystalline regions [100]. These processes allow the extension of the sample. As the secondary crystallisation process reorganises parts of the amorphous phase into crystalline regions, which in turn increases the constraints on the remaining amorphous material, the amount of extension that the sample can undergo is reduced. The increase in crystallinity also increases the tensile strength of the material, due to the presence of more van der Waals bonds. The combination of this increase in strength and decrease in elongation, resulting from secondary crystallisation, increases the gradient of the linear region of the curve (the Young's modulus) over time.

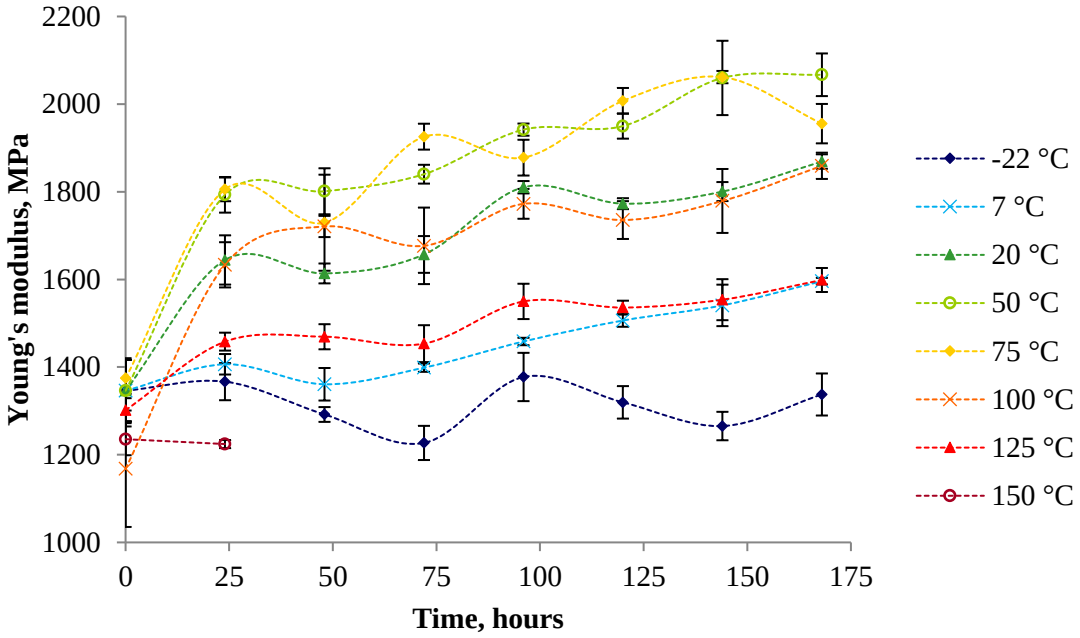

Figure 6.2. Young's modulus over time, according to the temperature of storage. Dashed lines have been superimposed between timepoints as a visual aid to guide the eye through the data sets. Mechanical testing data tables are in Appendix E.

The work of de Koning and Lemstra reported a logarithmic increase in the tensile modulus of PHB, over 100 days of storage at ambient temperature [33]. Generally, a logarithmic-like increase in modulus is also visible in Figure 6.3. The samples which experienced a change in Young's modulus, stored at temperatures from 20 to 125 °C, presented the largest proportion of increase within the first 24 hours of the study, after which the rate of increase slowed over time. de Koning and Lemstra attributed this change to the embrittlement caused by progressive crystallisation of the material, stating that "Progressive crystallization tightly constrains the amorphous chains between the crystals and, as a consequence, the material embrittles" [33]. This is in agreement with the trends of crystallinity increase over time observed during the DSC and IR experiments, presented in Chapter 4. It was also noted that this process is limited at ambient temperatures due to the proximity to the T_g (which in itself is raised due to increasing constraints on the amorphous material resulting from increased crystallinity, see Chapter 5.1.2),

where chain mobility is minimal. This implies that the Young's modulus would increase more at higher temperatures, where the secondary crystallisation process is not limited. Phillipson *et al*. suggest that the secondary crystallisation process is diffusion controlled [51]. As diffusion is limited at lower temperatures where mobility is more restricted, and occurs more easily at higher temperatures, due to the increase in molecular mobility and free volume, the rate of the secondary crystallisation process increases at higher temperatures. The results of this work also indicate that a higher storage temperature leads to higher values of Young's modulus. Samples stored at 7, 20 and 50 °C started with an average Young's modulus value of 1346 MPa and increased to 1596, 1869 and 2067 MPa respectively after 672 hours of storage.

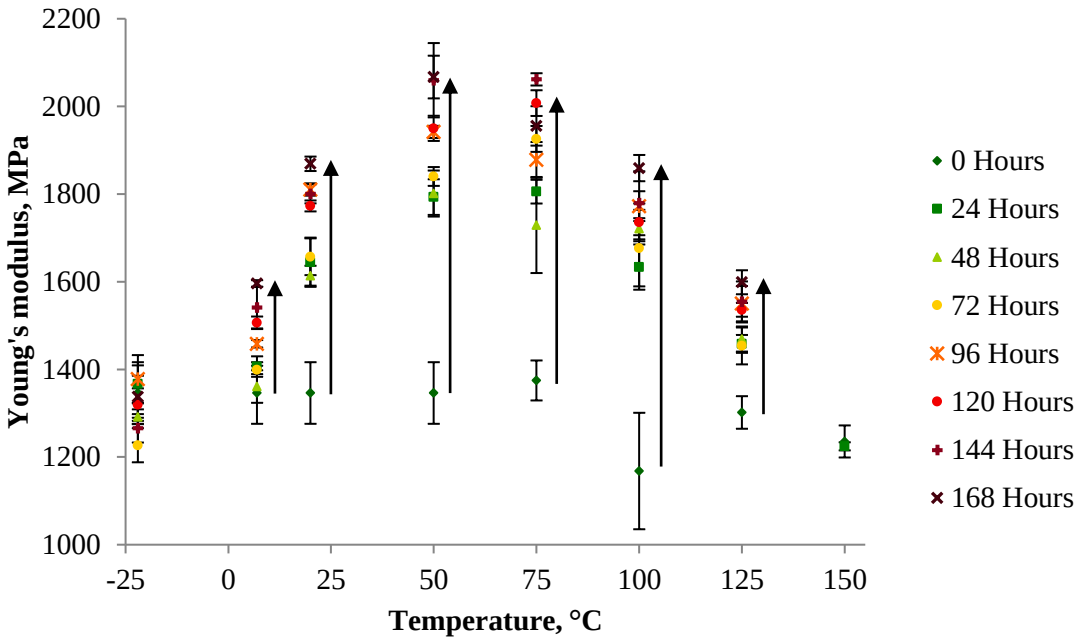

Figure 6.3. Young's modulus versus temperature of storage, according to length of storage time.

While the Young's modulus was also seen to increase with longer storage times at 75 and 100 °C, it appears that the further increase in storage temperature did not continue to increase the Young's modulus to a greater extent, as it did with temperatures from 7 to 50 °C. The average Young's modulus of the 100 °C samples was lower than that of the 75 °C samples after

672 hours of storage. However, the original Young's modulus for the 100 °C samples, prior to storage, was lower than that of the 75 °C samples. The lower starting value skewed the results, as the percentage increase from the original values at the end of the study are similar for the samples at 50, 75 and 100 °C. This suggests that there is a maximum effect of crystallinity increase on the Young's modulus of the samples.

There was also an increase in Young's modulus over time at 125 °C, but both the rate and extent of increase was much slower, and less than that seen in samples with the lower storage temperatures of 50 to 100 °C. After 672 hours of exposure to 125 °C, the Young's modulus only increased by 297 MPa, compared to 691 MPa when stored at 100 °C. There is evidence to suggest that the number average M_w may slowly start to decrease at temperatures of 100 °C and above, when held isothermally for 20 min [67], suggesting a decrease in chain length and potentially degradation of the material. A corresponding decline in tensile properties has been shown to follow the decrease in M_w, through processing experiments carried out above the melting temperature [72,77]. As the present work is over a much longer timescale than the work of Kunioka and Doi [67], and a relative decrease in the tensile properties was also observed, it is possible that the M_w decreased in the samples stored at 125 °C. If the M_w did decrease, and the samples were degrading, this could provide an explanation for the Young's modulus increasing to a lesser extent in samples stored at 125 °C than in samples stored at lower temperatures. This will be evaluated further in Chapter 7.

An increase in Young's modulus was not observed during storage at 150 °C. Within error, the Young's modulus after 24 hours of storage (1224 MPa) remained the same as that of the unconditioned samples (1236 MPa). Further analysis into the effect of storage duration on the properties of samples kept at 150 °C was not possible, as the samples became too brittle and fractured whilst attempting to clamp them into the machine. It is suggested that the samples

stored at 150 °C underwent extensive secondary crystallisation, reaching 80% crystallinity after 48 hours, and thermal degradation during storage, resulting in an extremely fragile material. This is discussed in more detail in Chapter 7.

6.3 Ultimate tensile strength (UTS)

There were no significant changes in the UTS observed in samples held at -22 °C, and no apparent change at 7 °C (Figures 6.4 and 6.5). The average unconditioned value for both storage conditions was 31.4 MPa, and the final average values of UTS measured 30.5 and 31.7 MPa respectively after 168 hours of storage. Again, this is due to the proximity of these storage temperatures to the T_g of the material where the secondary crystallisation process is not active, or is greatly restricted.

A trend of increasing UTS with increasing duration of storage time was present in samples held at 20 to 100 °C (Figures 6.4 and 6.5). A small increase in UTS happened gradually over the entire duration of the study in samples kept at 20 °C. At 50, 75 and 100 °C the increase was large, with the greatest amount of increase at the start of the study and less change towards the end. The average values of UTS increased from 31.4, 31.4 and 32.0 to 33.8, 36.7 and 35.4 MPa respectively. These increases reflect the increase in secondary crystallisation as described previously (Chapter 4.1.2), which is known to increase logarithmically with time, and to a greater extent at higher temperatures [13,32]. The tensile strength is a combination of the strength of the amorphous and crystalline regions of the material. As the crystalline regions are much stronger than the amorphous regions, due to the close packing and van der Waals bonding, the ultimate tensile strength of the material is heavily influenced by the degree of crystallinity. Secondary crystallisation increases the amount of crystalline material, through reorganisation

of the amorphous material, which increases the number of van der Waals bonds and drives up the tensile strength. The yield stress has been previously reported to increase progressively over time, due to the process of secondary crystallisation [32].

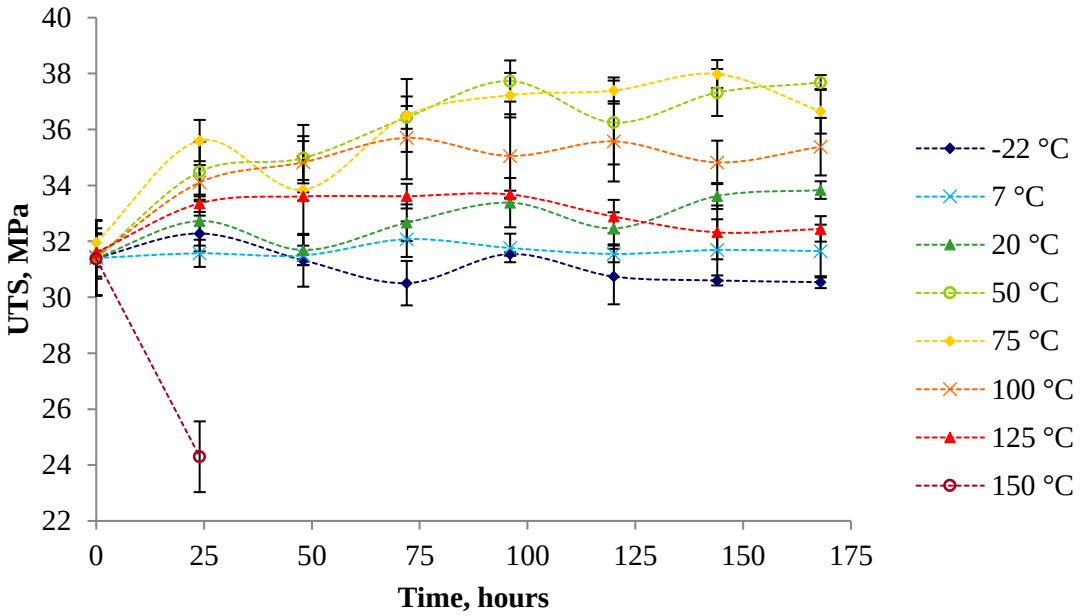

Figure 6.4. UTS over time, according to the temperature of storage. Dashed lines have been superimposed between timepoints as a visual aid to guide the eye through the data sets. Mechanical testing data tables are in Appendix E.

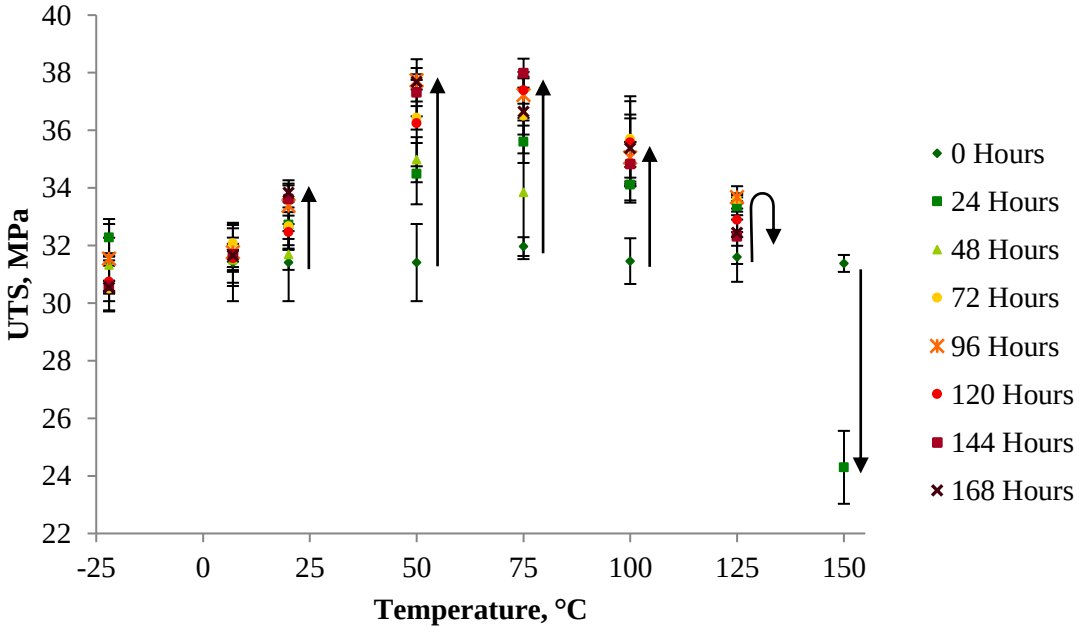

Figure 6.5. UTS versus temperature of storage, according to time.

A notable difference is the change in UTS over time in samples stored at 125 °C. While the UTS increased initially, rising from an average of 31.6 to 33.7 MPa after 96 hours of storage, the first clear decrease in UTS was observed after 120 hours of storage, where it dropped to 32.9 MPa. By the end of the study the UTS had decreased to an average value of 32.5 MPa, less than the average value recorded from samples stored at 20 °C. This trend is visible in Figure 6.4, and is clarified in Figure 6.5 by the arrow representing the direction of change. At a storage temperature of 150 °C, a substantial decrease from the average unconditioned value was recorded in samples held for 24 hours. The UTS dropped from 31.4 to 24.3 MPa.

The decreases in UTS at these temperatures has also been attributed to the decrease in M_w suggested previously, based on the work of Kunioka and Doi [67]. As the UTS is a combination of the strength of both the amorphous and the crystalline regions, it is logical that over time the decrease in the M_w within the amorphous regions would slightly decrease the strength of the overall system. Renstad *et al*. showed that stress at yield decreased with decreasing M_w, and suggested that this could be due to lower M_w causing a reduction in the number of tie-chains [77]. Yang and Liu reported that the decrease in tensile strength of irradiated PHBV samples, compared to control samples, was also due to chain scission within the amorphous regions [71]. This reduction in M_w in the amorphous phase was said to decrease the degree of chain entanglement and cause the loss of tensile strength. However, as the majority of the strength comes from the crystalline regions, the increase in crystallinity brought about by secondary crystallisation initially outweighs the decrease caused by the fall in M_w. As the duration of storage increased, the increase in crystallinity caused by secondary crystallisation slows. At the same time, the fall in M_w becomes greater, resulting in a smaller, weaker amorphous phase and a much more brittle system overall. This explains the decrease in the UTS seen at 125 °C. At a storage temperature of 150 °C, degradation progressed much more quickly. This is evident in

the rapid decrease in UTS, as the effects of the decrease in M_w outweighed the increase in strength resulting from secondary crystallisation within the first 24 hours. Samples stored at 150 °C presented no yield before fracture. In the work of Renstad *et al*. the samples which were processed at the highest temperature and had the lowest M_w did not yield before break [77]. The extent of the degradation experienced within these samples is highlighted by the inability to test them after 48 hours of storage, as they fractured whilst attempting to clamp them into the machine.

6.4 Elongation to break

Within error there was no change in elongation to break in samples stored at -22 °C over the duration of the study (Figure 6.6), again due to being kept below the T_g of the material. Despite the large error bars (discussed in Chapter 2.4.4), it is still possible to see that a gradual decrease in elongation to break took place over time when samples were stored at 7 and 20 °C. From an average unconditioned value of 16.9 %, the elongation to break in the 7 and 20 °C samples decreased to 10.2 and 9.3 % respectively after 672 hours of storage. More rapid and consistent decreases were observed in samples stored at 50, 75, and 100 °C, where the average elongation to break values dropped from 16.9, 13.2 and 11.9 to 7, 5.8 and 5.9 % respectively. The samples stored at these temperatures appeared to reach a plateau after the initial rapid decrease. Results obtained from samples kept at 125 °C were slightly less consistent. However, the general trend of greater reduction in elongation to break with increased length of storage time is still clear, with an average value of 14.6 % from the unconditioned samples to 6.8 % from the samples held for 168 hours. The majority of the elongation shown in Figure 6.1 is due to the aligning of the molecules in the amorphous phase. Secondary crystallisation reduces the amount of material

in the amorphous regions as it reorganises into the crystalline regions, as well as increasing the constraints on the remaining amorphous material, creating a more brittle material which elongates less. de Koning and Lemstra observed a change in PHB, from an initially ductile material to a brittle one after storage at ambient conditions, where the elongation to break decreased from 40 % to below 10 % after two weeks [33]. Biddlestone *et al*. also reported a progressive decrease in the elongation to break over time in P(HB-co-8%HV) at room temperature [32].

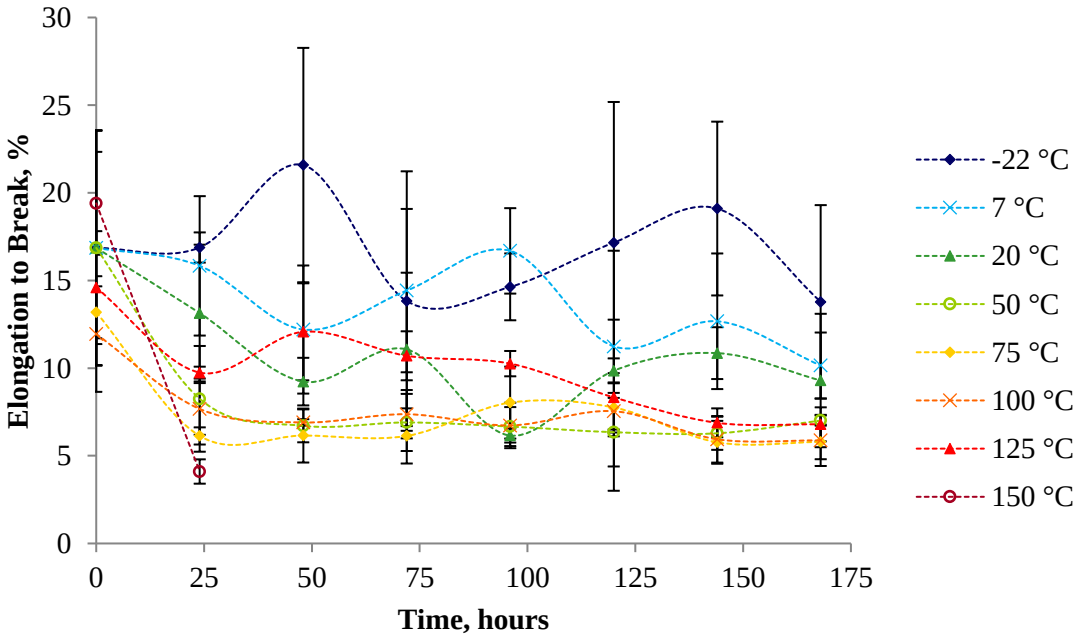

Figure 6.6. Elongation to break over time, according to the temperature of storage. Dashed lines have been superimposed between timepoints as a visual aid to guide the eye through the data sets. Mechanical testing data tables are in Appendix E.

As mentioned previously (Chapter 6.2), Phillipson *et al*. suggest that secondary crystallisation is a diffusion controlled process [51]. If this is the case it seems likely that at the lower end of the temperature range between T_g and T_m, e.g. 7, 20 and 50 °C, the mechanism of secondary crystallisation would be infill of newly formed, smaller crystal structures within the mobile amorphous phase, as diffusion would occur more easily in these less constrained areas. At the

higher end of the temperature range, secondary crystallisation is more likely to proceed via the lamellar thickening mechanism, due to being above the T_m of the smaller crystal structures, and to the increase in free volume which allows diffusion to occur more easily. If infill is the mechanism of secondary crystallisation responsible for the increase of crystallinity at the lower end of the temperature range, this may explain the yield expressed in Figures 6.1c and 6.1d which did not occur after storage at higher temperatures, as it may be easier to break the bonds between the crystalline segments of these smaller structures. Any infill which may have occurred at 7 °C would have been minimal, as the proximity to the T_g limits the mobility of the polymer chains, which would explain why no clear yield is seen in Figure 6.1b. No yield can be seen in Figure 6.1a as no reorganisation of the polymer chains could occur below the T_g.

When observing the elongation to break, after 168 hours of storage, the samples kept at 125 °C produced a similar average value to samples which were stored at 50, 75 and 100 °C, measuring 6.8, 7.0, 5.8 and 5.9 % respectively. This is different to the observations made about the Young's modulus and the UTS, where storage at 125 °C increased to a lesser extent. Further to this, samples stored at 150 °C presented the largest and fastest decrease in elongation to break, clearly shown in Figure 6.7, dropping from an average of 19.4 to 4.1 % within 24 hours. Previously in this chapter, samples stored at 150 °C exhibited a tendency to oppose the general trends observed over time, with property values less than the unconditioned values instead of greater. In this case, the normal trend would be to have values lower than the unconditioned value, and this time the 150 °C sample results followed the trend instead of opposing it. As the elongation to break is a measure of ductility, this is due to the increase in crystallinity, caused by secondary crystallisation, and the decrease in M_w, caused by degradation, both contributing to the brittleness of the material and resulting in abrupt failure after storage at 150 °C. The degradation induced at this temperature will be discussed further in Chapter 7.

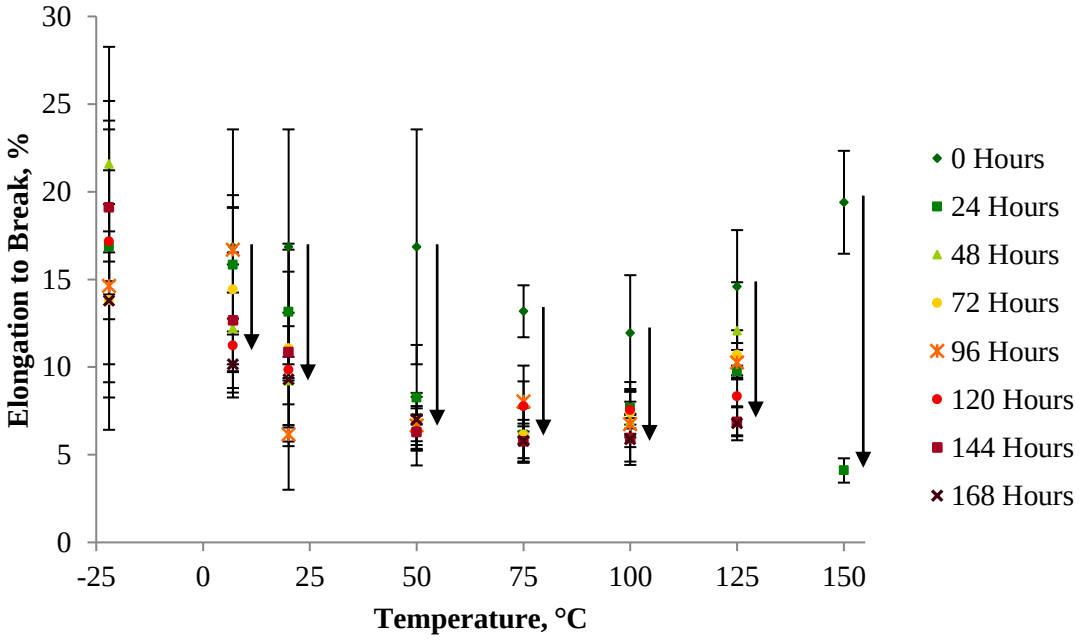

Figure 6.7. Elongation to break versus temperature of storage, according to time.

6.5 Conclusions

Secondary crystallisation caused embrittlement of the samples, due to the reorganisation of the amorphous material into crystalline regions, which in turn increased the constraints on the remaining amorphous material. As the secondary crystallisation process progresses logarithmically, and the rate is increased by an increase in storage temperature, not only did the Young's modulus and UTS increase over time, but they increased to a greater extent at higher storage temperatures, up to 100 °C. The elongation to break exhibited the same trends as the Young's modulus and UTS up to a storage temperature of 100 °C, but with the values decreasing, instead of increasing, over time.

It appears that there were two competing processes active at storage temperatures of 125 and 150 °C; secondary crystallisation and degradation. The large and rapid decreases in UTS and elongation to break after storage at 150 °C for only 24 hours, combined with the fracture of

samples during clamping into the instrument after storage times of 48 hours, indicates a significant embrittlement of the samples. Although the degradation process is less pronounced at 125 °C, the Young's modulus increased to a lesser extent than the samples stored between 20 and 100 °C, and there was a decrease in the UTS observed after 120 hours of storage. Following the work of Kunioka and Doi, Renstad *et al*. and Hoffman *et al*. [67,72,77], it is again proposed that there was a decrease in M_w in the samples stored at 125 and 150 °C for extended durations. This will be discussed further in Chapter 7.

CHAPTER 7 – THERMAL DEGRADATION BELOW THE MELTING TEMPERATURE

7.1 Sample discolouration

Very few authors have discussed the discolouration of PHB with respect to thermal effects. Renstad *et al*. described the change in surface colour of the samples with reference to processing temperatures; with the highest temperatures producing a duller and darker colour [77]. de Koning *et al*. commented on a change in the colour of samples held isothermally at 115 °C for 20 hours, although additional detail on the shade or extent of change is not provided [13]. Both of these authors cite the reason for change in colour as thermal degradation of the material. In this study samples were monitored for discolouration at temperatures of -22, 20, 125 and 150 °C; after first noticing discolouration of the dog-bone samples, used for mechanical testing, stored at 150 °C. These temperatures were selected to provide data for control samples (stored below the T_g), samples kept at ambient temperature (the most commonly studied temperature in the current literature), and samples kept at the elevated temperatures at which degradation has been suggested in this work.

Figure 7.1 shows photographs of the samples stored at -22 °C. While there was very minor sample to sample variation in colour throughout the plaque at the start of the study, there was no significant change in colouration with increasing storage time. This was also true for samples stored at 20 °C (Figure 7.2).

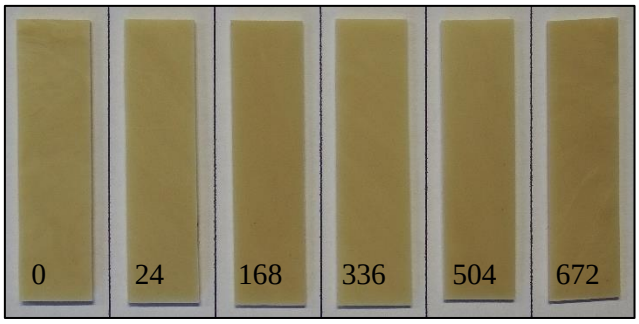

Figure 7.1. Samples stored at -22 °C for the time durations (hours) indicated.

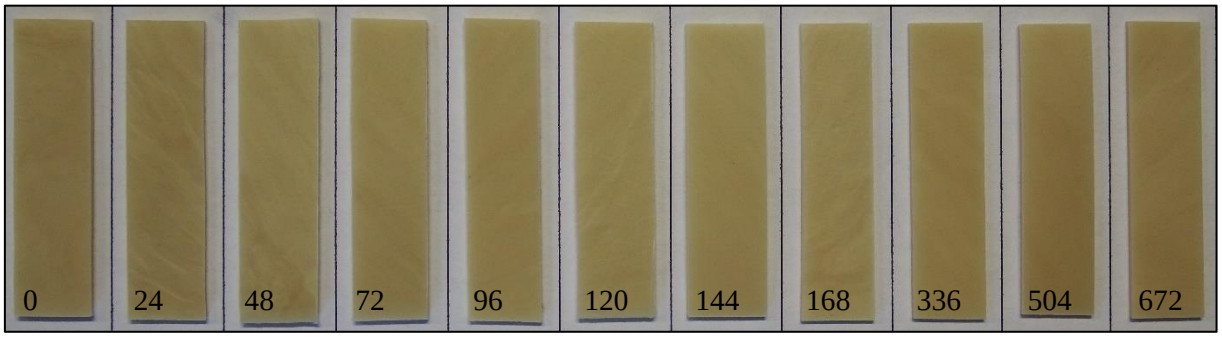

Figure 7.2. Samples stored at 20 °C for the time durations (hours) indicated.

As seen in Figure 7.3, the samples which were held at 125 °C displayed a change in colouration over time. While there was no change during the first half of the experiment, the samples which were stored for 504 hours and 672 hours were darker than those stored for less time. When stored at 150 °C, the change in colouration throughout the whole duration of the study was much more dramatic, with samples darkening from the first 24 hours (Figure 7.4). This process appeared to occur gradually over time; however, once the sample reached 504 hours of storage time no further discolouration was observed.

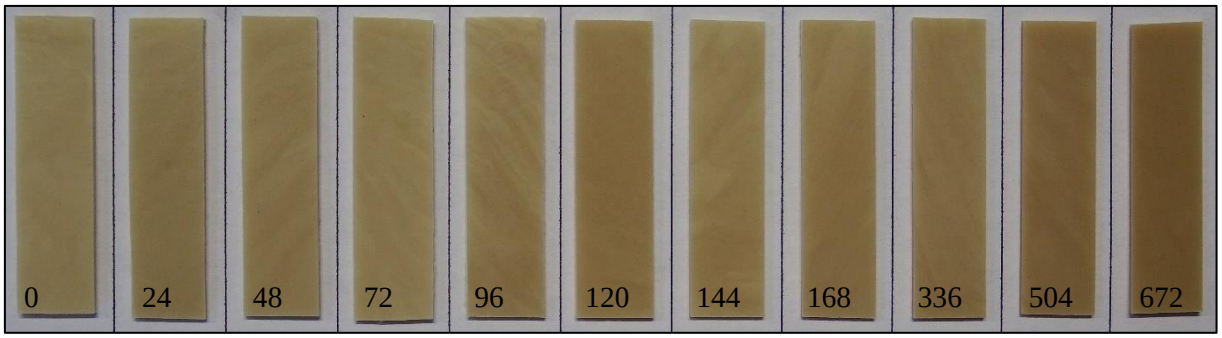

Figure 7.3. Samples stored at 125 °C for the time durations (hours) indicated.

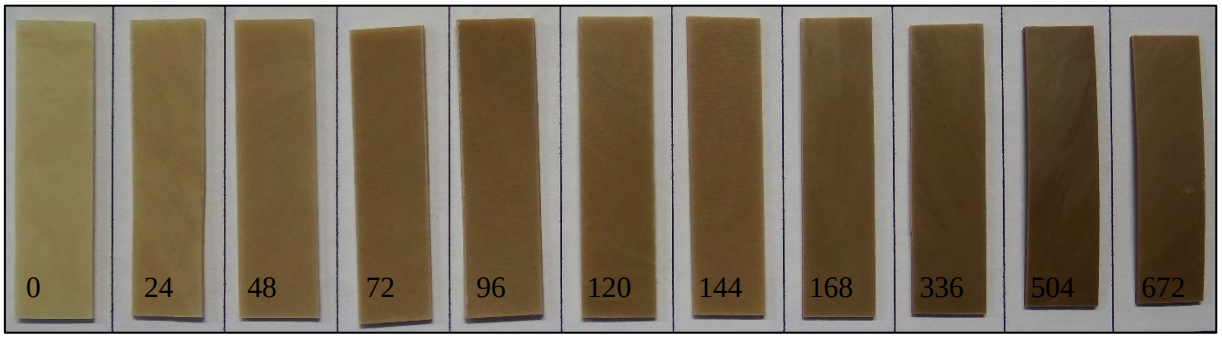

Figure 7.4. Samples stored at 150 °C for the time durations (hours) indicated.

By comparing the images side by side, as in Figure 7.5, it becomes clear that discolouration occured only when samples were stored at elevated temperatures. It also becomes obvious that the process affected the samples which were kept at 125 °C far less than those kept at 150 °C, with much longer storage durations required to produce a similar discolouration to the shortest storage times of the 150 °C samples.

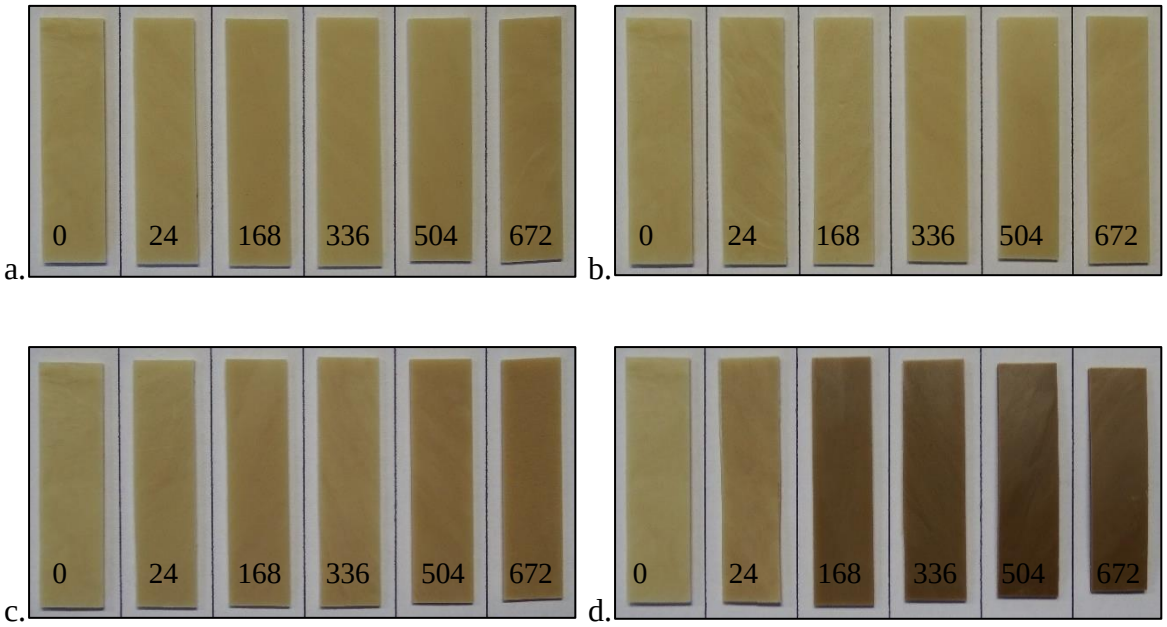

Figure 7.5. Samples stored at a. -22 °C, b. 20 °C, c. 125 °C and d. 150 °C for the time durations (hours) indicated.

This difference in discolouration rate is shown in Figure 7.6. The sample which was held at 125 °C for 672 hours was most similar in colour to the sample stored at 150 °C for only 48 hours.

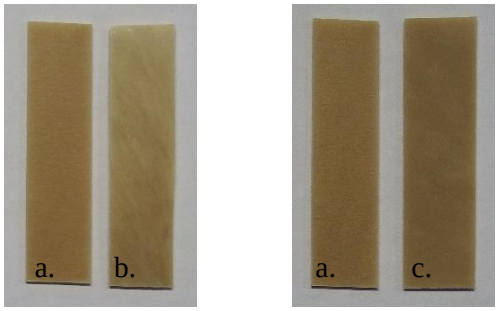

Figure 7.6. Sample a. was stored at 125 °C for 672 hours, sample b. was stored at 150 °C for 24 hours, sample c. was stored at 150 °C for 48 hours.

Primary crystallisation results in the almost transparent, amorphous polymer turning opaque and milky white in colour as it crystallises. As secondary crystallisation is a continuation of the processes occurring during primary crystallisation, it would not be responsible for a change in

sample colour, rather a further decrease in translucence. On the other hand, thermal degradation results in the formation of moieties which are coloured. Extensive work by Grassie, Murray and Holmes in the 1980s investigates the degradation process of PHB, whereby cyclic rings form at the carbonyl and methylene groups, enabling chain scission to occur between the ester linkages [64-66]. A more detailed description of the chain scission process may be found in Chapter 1.5. It is highly likely that thermal degradation of the polymer is active at these high temperatures where the amorphous chains have more mobility, enabling cyclic rings to form and chain scission to occur, and that this caused the discolouration. This agrees with the findings of Renstad *et al*. and de Koning *et al*. [13,77]. Thermal degradation is not possible at the lower storage temperatures due to the lack of chain mobility, meaning it is not possible for the cyclic ring to form, so samples kept at low temperatures do not discolour. The discolouration observed in the samples kept at 150 °C is a clear indication of degradation. After 504 hours of storage at 125 °C a slight change in colour was observed, which may suggest a small amount of degradation took place.

7.2 Differential scanning calorimetry (DSC)

Several indicators of degradation at a storage temperature of 150 °C were observed during the analysis of DSC data (Chapter 4.1), the overall change in shape of the melting endotherm being the most immediately obvious (Figure 7.7). Over time, a shoulder at the lower temperature side of the endotherm developed, and then merged into the main melting peak as the main peak shifted to lower temperatures. Melting and recrystallisation has been reported by other authors, usually referring to that induced during the DSC melting run by low heating rates [13,17,34,91]. As a high heating rate was used for the melting runs (50 °C min^{-1}), the formation of the shoulder

cannot be produced by the experimental run itself. It is believed that, during the first 24 hours of storage, the material experienced a degree of melting and recrystallisation of the least stable crystals into a more perfect crystal structure. The dashed lines superimposed onto the trace of the untreated sample (Figure 7.7) support this, as melting has clearly begun before the storage temperature of 150 °C is reached. Additionally, the trace of the sample stored for 24 hours does not begin to melt until above the storage temperature. As the storage time increased, the shoulder continued to grow, and to merge with the main melting peak, which could be a result of lamellar thickening of the melt-recrystallised crystals. Another process active at this temperature is chain scission (detailed in Chapter 1.5) [54,67], thought to begin in the amorphous regions [69,71,77]. This creates shorter chains which are more mobile, making them able to pack into crystal structures more easily. Initially this process could contribute to the thickening of the lamella. As degradation becomes more extensive, it begins to break down the crystalline regions of the material [68]. Chain scission reduces the molecular weight (M_w) of the chains, and as a result they melt more easily [68]. This is responsible for the reduction in melting temperature of the main peak, and effectively the completion of the main melting peak merging with the shoulder.

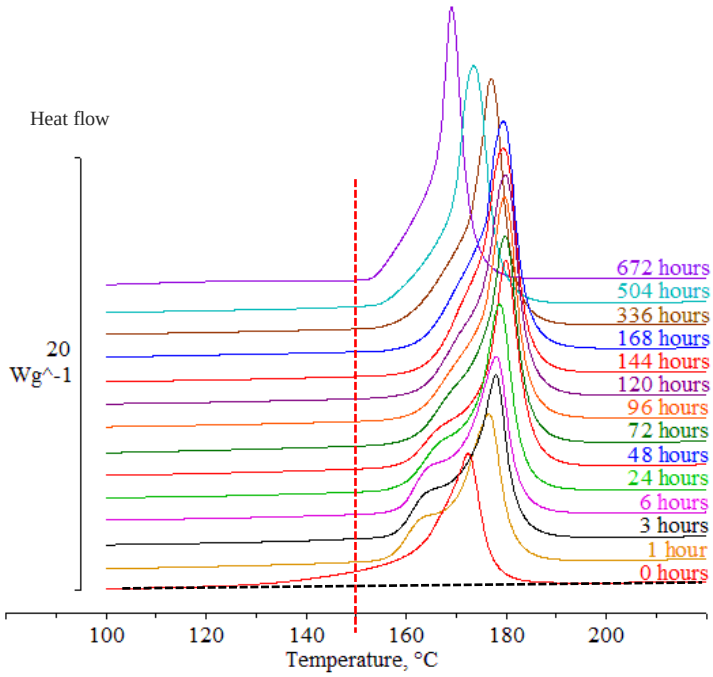

Figure 7.7. DSC traces from samples stored at 150 °C for the durations indicated above each individual trace. The black dashed line indicates the baseline of the sample prior to storage, the red dashed line indicates the storage temperature of the samples.

It has already been suggested that thermal degradation is likely to begin in the amorphous regions [69,71,77], where the molecular mobility is greater, and formation of the cyclic rings occurs more easily. Initially the chain scission process will not cause a decrease in the degree of crystallinity. Instead, it would cause it to increase (Figure 7.8); due to the involvement of the shorter chains in the secondary crystallisation process, which have greater mobility and therefore reorganise more easily into a more perfect crystalline structure [68]. It follows that, as degradation progresses, the degree of crystallinity is maintained for a period of time before it begins to decrease. The interplay of the chain scission and secondary crystallisation processes masks the onset of degradation [54,101]. With extensive degradation, the degree of crystallinity is ultimately reduced [68].

The shift of the main peak after 120 hours of storage pointed to a decrease in the T_m, shown in Figure 7.9, indicating that chain scission after this length of storage began to drastically affect

the stability of the crystalline regions. The rapid decrease in the T_m corresponds to the decrease in the degree crystallinity, pointing towards the dominance of degradation over the secondary crystallisation process with prolonged storage times.

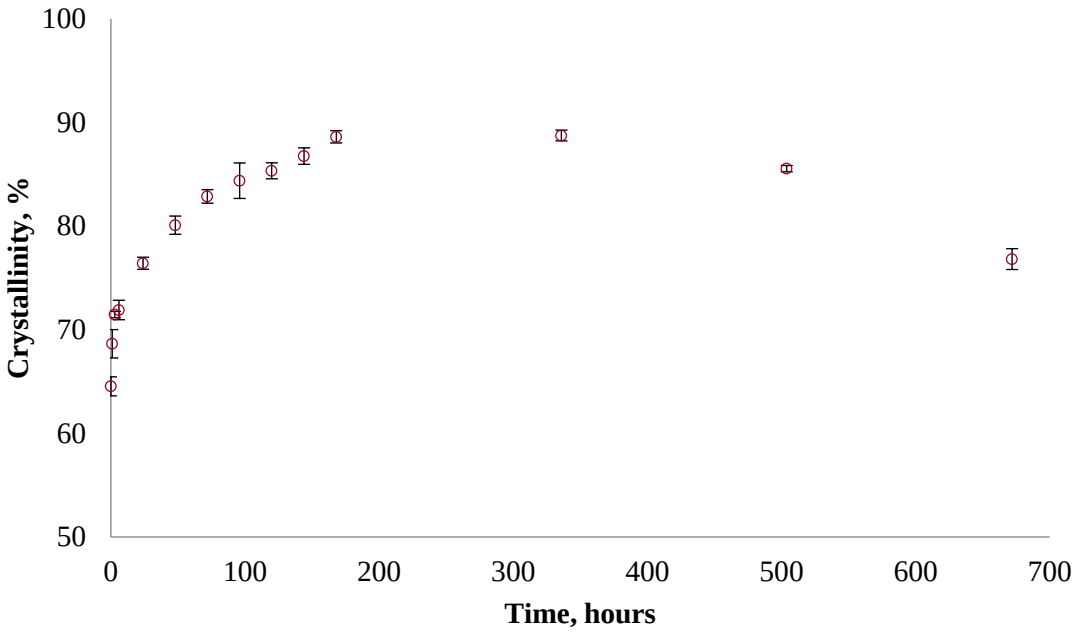

Figure 7.8. Change in crystallinity according to storage time at 150 °C.

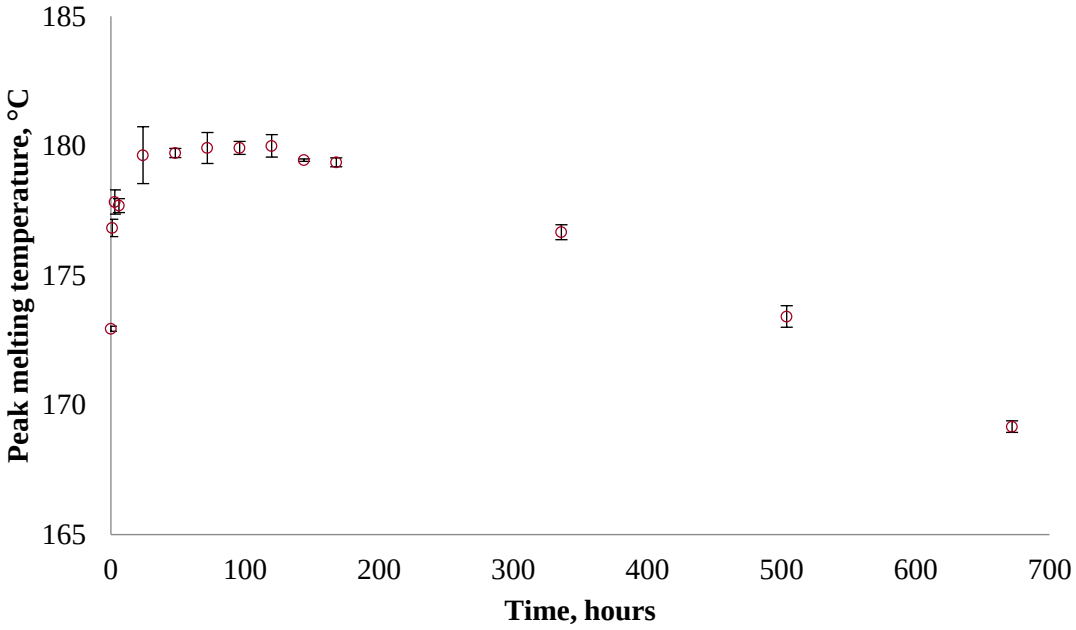

Figure 7.9. Change in peak melting temperature according to storage time at 150 °C.

The traces obtained from samples stored at 125 °C also depict the clear development of a shoulder on the lower temperature side of the melting endotherm (Figure 7.10). In contrast to the samples which were stored at 150 °C, the onset of melting of the untreated sample begins above the storage temperature of these samples, so it is unlikely that melting and recrystallisation caused the initial appearance of the shoulder. It may be that secondary crystallisation caused lamellar thickening, which has been shown by wide angle x-ray scattering (WAXS) and small angle x-ray scattering (SAXS) studies to take place at increased temperatures [57,58]. Previous work has suggested that lamellar thickening could be responsible for the development of a shoulder [22,34,57]; as it incorporates amorphous and smaller, less stable crystal structures which melt at lower temperatures into larger, more stable crystalline regions, which melt at higher temperatures. The other process known to produce a shoulder is chain scission. A decrease in M_w has been reported at temperatures as low as 100 °C [54,67], so it is likely that the chain scission process is active at a storage temperature of 125 °C. However, as it begins in the amorphous regions [69,71,77], it isn't possible for chain scission alone to result in a shoulder. For a decrease in M_w to be sole cause, chain scission would have to take place in the crystalline regions, which would also correspond with a decrease in the melting peak temperature, or a narrowing of the peak, neither of which are seen. Instead, what may have happened is that chain scission of long chains in the amorphous region increased the mobility of the chains, making it easier for them to crystallise and thicken the lamella, as shorter chains rearrange and pack into the crystal structure more easily [68].

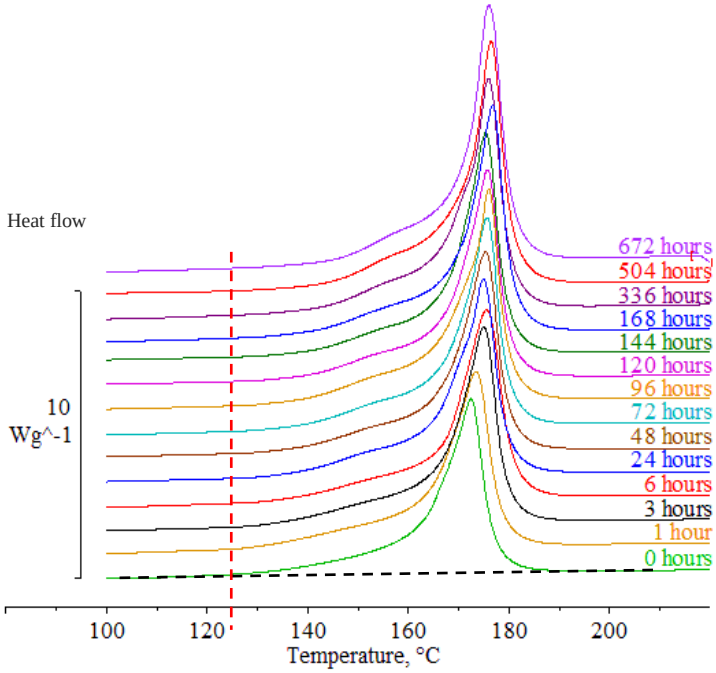

Figure 7.10. DSC traces from samples stored at 125 °C for the durations indicated above each individual trace. The black dashed line indicates the baseline of the sample prior to storage, the red dashed line indicates the storage temperature of the samples.

When held at 125 °C, the crystallinity and the T_m did not decrease over time as is seen in the samples stored at 150 °C (Figures 7.11 and 7.12). This may be because the level of degradation in these samples was very low, with chain scission occurring only within the mobile amorphous fractions (MAF). As described previously this would lead to an increase in the degree of crystallinity and the T_m, as the shorter chains rearrange into the crystal structure more easily [68], and therefore the degradation process is masked by the effects of the secondary crystallisation process. For this reason, it was not possible to determine whether degradation took place in the samples stored at 125 °C from the DSC data alone. The mechanical testing data suggests that, for the longest storage times at 125 °C and for the first 24 hours at 150 °C, degradation was minimal. The DSC data would agree with this, as the degree of crystallinity and the T_m aren't seen to rapidly decrease in those conditions at those times, however, the increase in crystallinity was extensive.

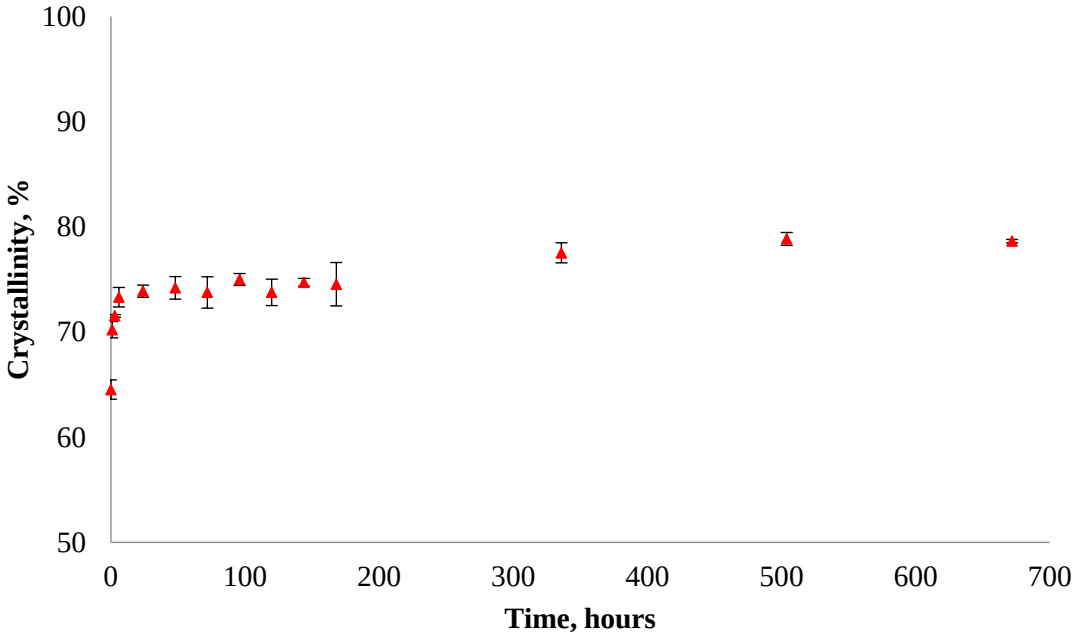

Figure 7.11. Change in crystallinity according to storage time at 125 °C.

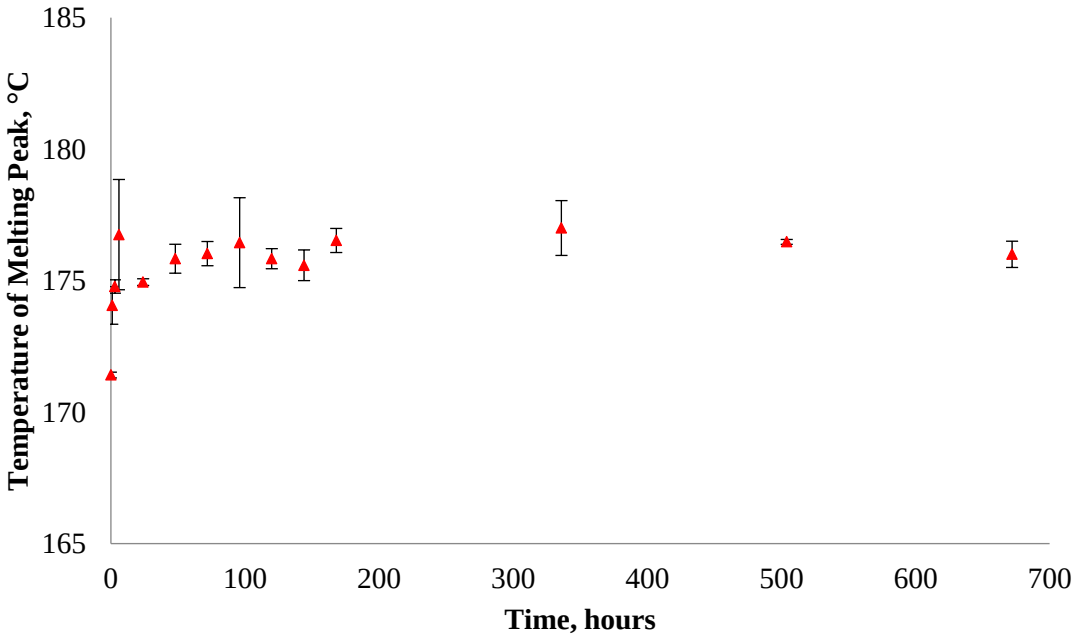

Figure 7.12. Change in peak melting temperature according to storage time at 125 °C.

7.3 Infrared spectroscopy (IR)

Indicators of degradation present within the IR data (Chapter 4.2), includes the change in relative height of the amorphous peak at 1180 cm^{-1} to the crystalline peak at 1221 cm^{-1} (Figure 7.13). Initially, secondary crystallisation causes the height of the amorphous peak to decrease as the crystalline peak increases [34,49]. At first, as degradation begins, it exaggerates this effect, as chain scission of molecules in the amorphous regions creates shorter chains which pack more easily into crystalline structures [68]. This reduces the response of the amorphous peak further. As degradation continues, and begins to breakdown the crystalline phase, the peak at 1221 cm^{-1} begins to decrease relative to that of the amorphous peak. This is seen in Figure 7.13 as a relative increase in the height of the peak at 1180 cm^{-1}.

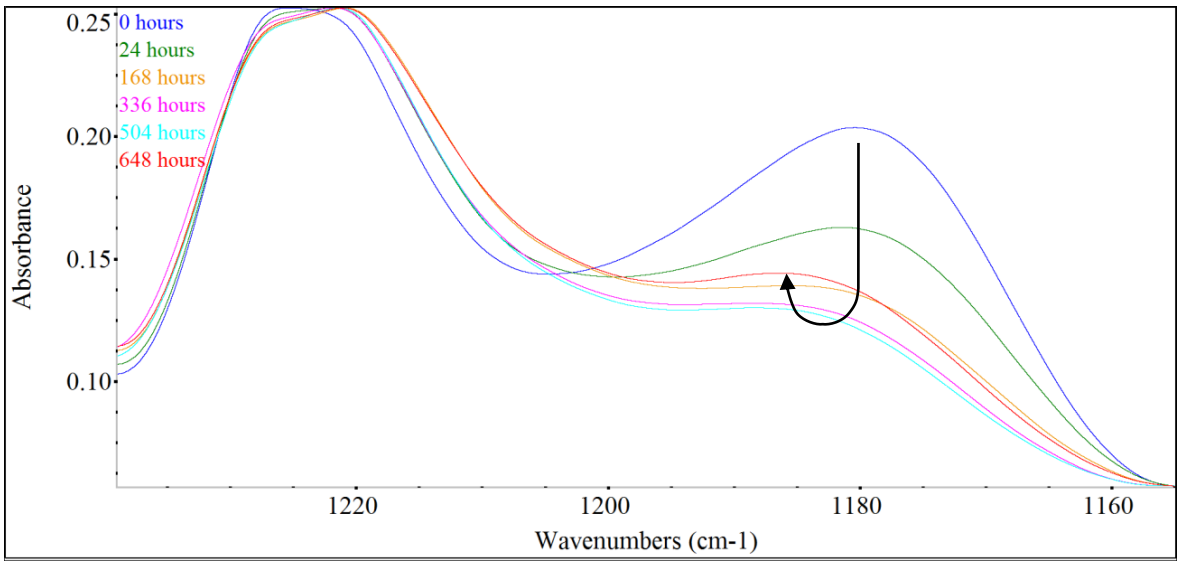

Figure 7.13. Development of peaks at 1221 cm^{-1} and 1180 cm^{-1} (full scale to the peak at 1221 cm^{-1}) in samples stored at 150 °C.

The crystallinity index, calculated from the height of the crystalline peak at 1221 cm^{-1} and the internal reference peak at 1451 cm^{-1}, confirms the initial increase in crystallinity, followed by the decrease after prolonged storage at 150 °C. After approximately 480 hours of storage there was a decrease in crystallinity index, indicating a reduction in the response of the crystalline

peak (Figure 7.14). Hong and Chen also observed an initial increase in the crystallinity index resulting from storage of hot pressed PHB and P(HB-co-5wt%HV) at 120 °C for 40 hours [34]. It is likely that they did not see a subsequent decrease as the storage temperature was too low, and the storage time too short.

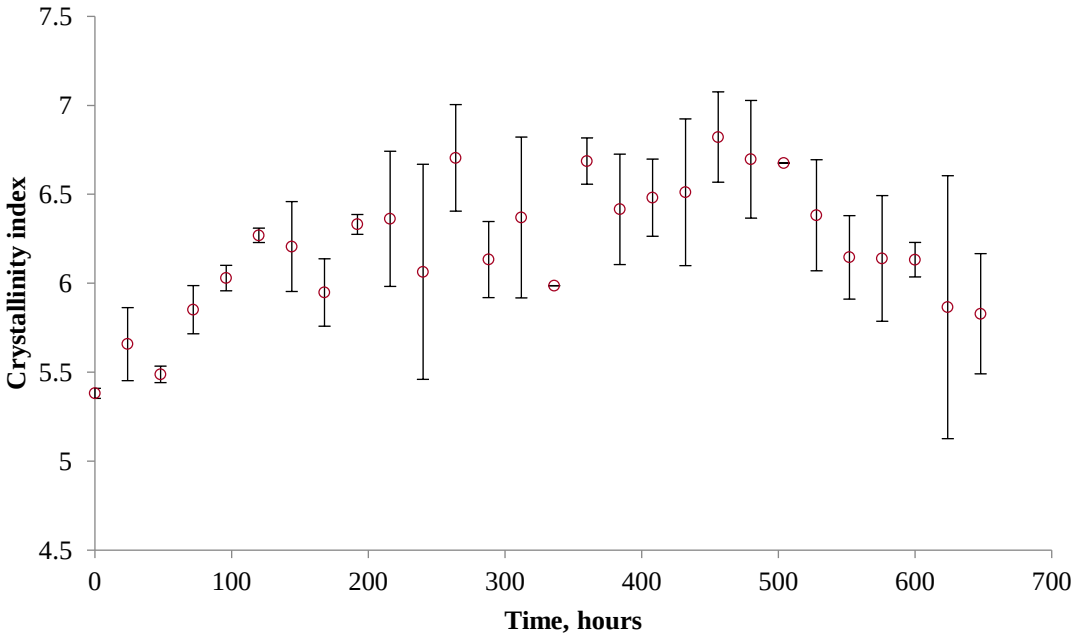

Figure 7.14. Crystallinity index over time, generated from the peaks at 1221 cm^{-1}/1451 cm^{-1}.

There is also a suggestion that crotonic acid is being produced, through chain scission, during storage at 150 °C, by the shoulder emerging at between 1715-1705 cm^{-1} (Figure 7.15). Another peak, also relating to crotonic acid, is present at 1685 cm^{-1}. This peak is better resolved than the shoulder, which is obscured by the carbonyl peak, yet it does not appear to increase with longer storage times. This indicates that crotonic acid is formed, but may be slowly evaporating over time.

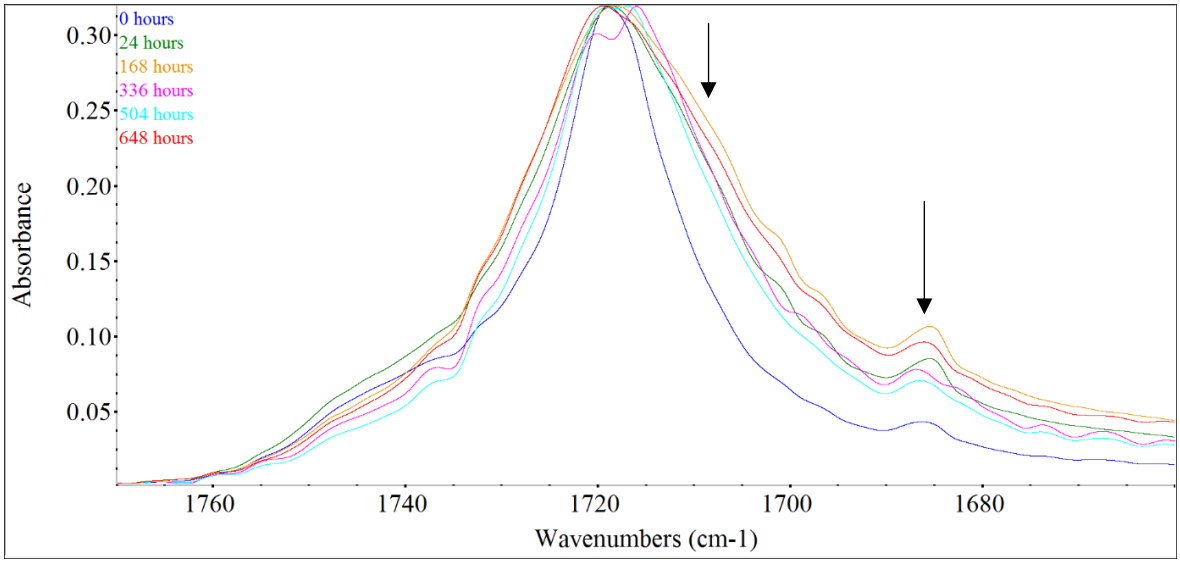

Figure 7.15. Development of the carbonyl peak with time (full scale to the peak at 1719 cm^{-1}). The shoulder and peak relating to crotonic acid are indicated by the arrows.

There may be a hint of crystallinity decrease after 672 hours of storage at 125 °C (Figures 7.16 and 7.17). However, the degree of error in the crystallinity index data is too high to be certain of any degradation within the samples.

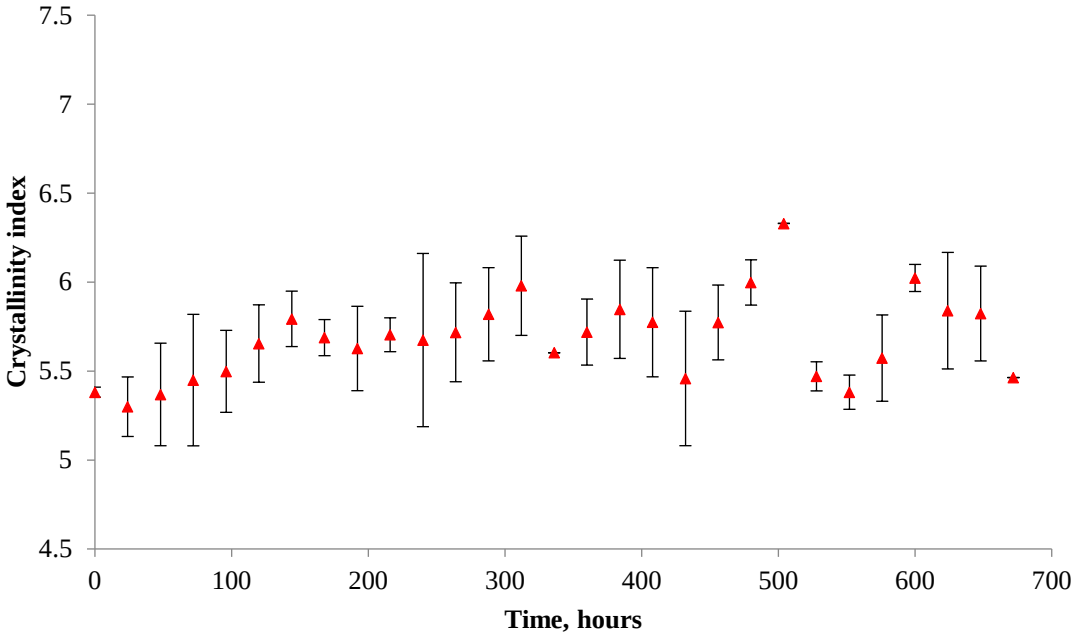

Figure 7.16. Crystallinity index over time, generated from the peaks at 1221 cm^{-1}/1451 cm^{-1}.

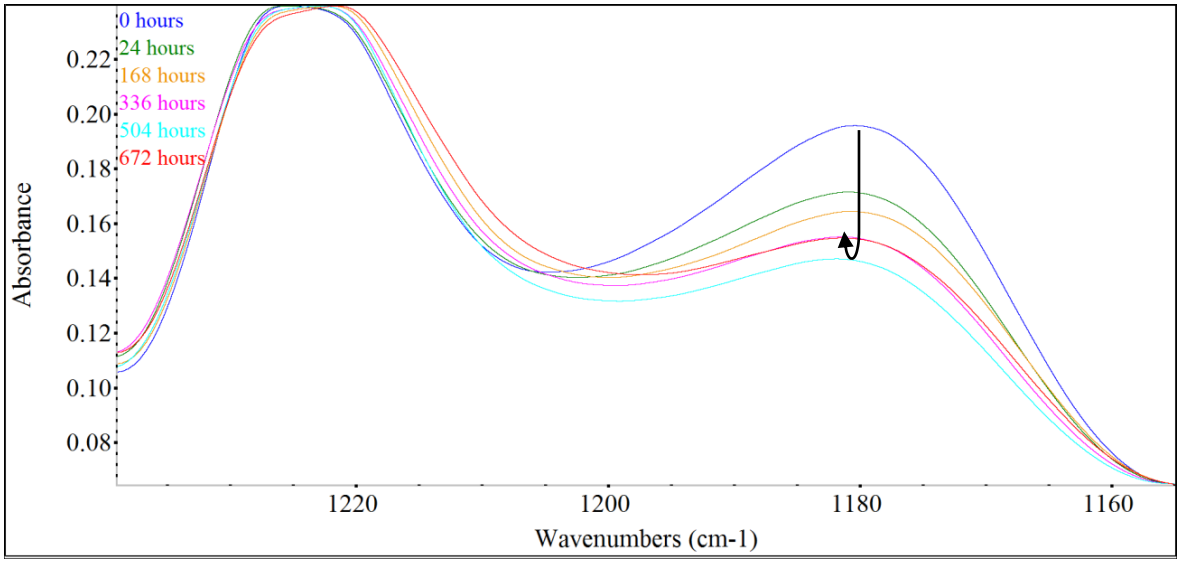

Figure 7.17. Development of peaks at 1221 cm^{-1} and 1180 cm^{-1} (full scale to the peak at 1221 cm^{-1}) in samples stored at 125 °C.

7.4 Dynamic mechanical thermal analysis (DMTA)

Again, the embrittlement of samples stored at 150 °C was revealed during DMTA (Chapter 5). The first indication of degradation of the samples kept at 150 °C, was that, in order to be able to test them, the parameters of the instrument set-up had to be altered. The sample target deflection was lowered from 240 µm to 120 µm, in order to prevent the sample from fracturing during the experimental run.

The second indication of degradation was that the shape of the tanδ peak obtained from samples stored at 150 °C changed extensively as the duration of storage increased. Initially an increase in the peak height and the T_g, taken from temperature at which the peak height maximum occurred, can be seen in Figure 7.18. This is likely to have been caused by the combined activity of the secondary crystallisation and degradation processes. A decrease in M_w, by chain scission in the amorphous phase, will initially drive up the crystallinity through the secondary crystallisation process, increasing the amount of material in the rigid amorphous fraction (RAF)

and putting additional constraints on the material in the mobile amorphous fraction (MAF), which increases both the T_g and the peak height [13,32,96,97]. Over time, Figure 7.18 then shows a decrease in the temperature at which the tanδ peak maximum occurred, a reduction in the height of the peak, a shift in the onset of the peak to lower temperatures and a broadening of the peak. These features relate to a decrease in the T_g, a less constrained fraction of amorphous material, and a broadening of chain length distributions; all of which are indicators of a highly crystalline material undergoing chain scission [33,54,68,98]. The DMTA data is provided in Table 7.1.

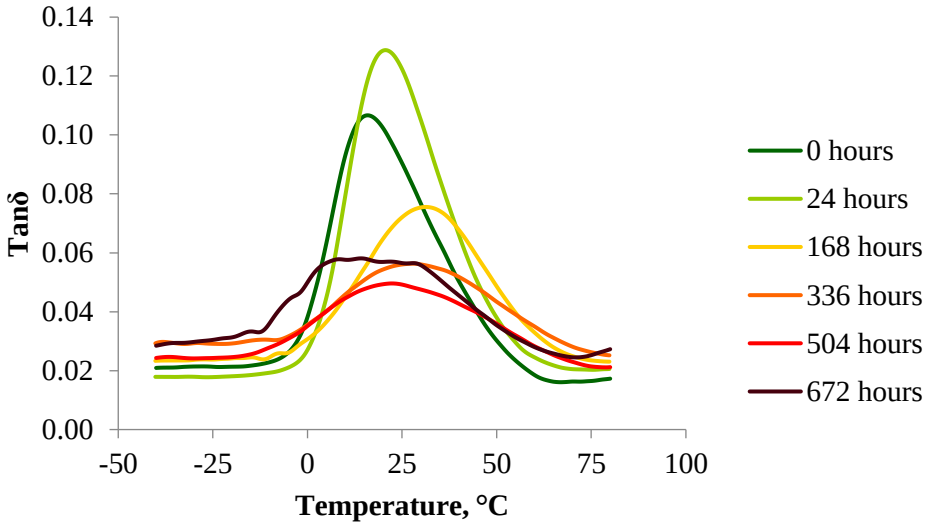

Figure 7.18. Tanδ peaks of samples stored at 150 °C.

Table 7.1. Changes in DMTA property values resulting from storage at 150 °C. Error is to ± 1 standard deviation.

Time, hours	T_g, °C	Peak height	Peak onset, °C	Peak width	Peak distribution, left area:right area
0	15.8 (± 0.3)	0.084 (± 0.001)	-11.0 (± 0.4)	20 (± 0.3)	39:61 (± 0.9)
24	20.6 (± 0.3)	0.107 (± 0.004)	-11.0 (± 1.4)	20 (± 0.3)	43:57 (± 1.2)
168	30.2 (± 0.9)	0.053 (± 0.002)	-10.1 (± 4.4)	28 (± 2.3)	49:51 (± 2.8)
336	25.7 (± 2.4)	0.035 (± 0.007)	-15.6 (± 7.7)	36 (± 3.3)	45:55 (± 3.2)
504	19.8 (± 2.2)	0.027 (± 0.002)	-18.5 (± 1.7)	35 (± 1.0)	44:56 (± 2.3)
672	13.9 (± 0.4)	0.030 (± 0.001)	-20.5 (± 1.0)	34 (± 4.6)	42:58 (± 3.7)

Unlike the data obtained from mechanical testing, the DMTA data from samples held at 125 °C did not appear to show any obvious signs of degradation. The T_g and the onset of the tanδ peak increased over time, the distribution of the peak area became more balanced, and the peak width remained fairly constant throughout (Figure 7.19 and Table 7.2). The only slight indication of degradation may be that the height of the tanδ peak decreased in samples stored for 168 hours or more.

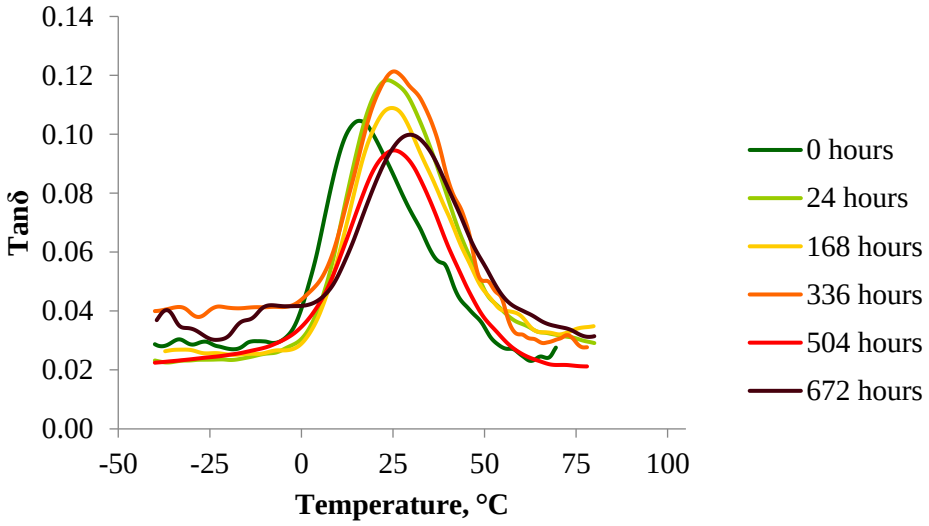

Figure 7.19. Tanδ peaks of samples stored at 125 °C.

Table 7.2. Changes in DMTA property values resulting from storage at 125 °C.

Time, hours	T_g, °C	Peak height	Peak onset, °C	Peak width	Peak distribution, left area:right area
0	15.8	0.076	-6.5	19	44:56
24	23.5	0.095	-7.5	22	41:59
168	24.7	0.083	-2.7	21	47:53
336	25.3	0.081	-3.5	21	43:57
504	25.3	0.072	-9.0	22	49:51
672	29.7	0.063	0.5	21	49:51

7.5 Mechanical properties

The mechanical testing work revealed multiple indicators of thermal degradation during storage at 150 °C (Chapter 6). These include the lack of increase in Young's modulus, and the extensive decreases in UTS and elongation to break, after the first 24 hours of storage (Table 7.3). Perhaps more significantly, there was an inability to test samples stored for 48 hours or more, as the samples became much too brittle, and fractured upon being clamped into the instrument. After 72 hours of storage at 150 °C, some of the mechanical testing samples had fractured whilst still in the oven.

There was also a suggestion that a small amount of degradation occurred within the samples stored at 125 °C. During storage, the UTS increased until 96 hours, plateaued, then decreased after 120 hours. Neither the Young's modulus, nor the UTS values increased as much when stored at 125 °C compared to the samples held between 50 and 100 °C, and even the samples kept at 20 °C presented a greater increase in Young's modulus.

Table 7.3. Changes in mechanical property values resulting from storage at 125 and 150 °C. Error is to ± 1 standard deviation.

Property	Storage at 125 °C			Storage at 150 °C	
	Unconditioned	24 hours	168 hours	Unconditioned	24 hours
Young's modulus, MPa	1302 (± 37.1)	1458 (± 20.4)	1599 (± 27.4)	1236 (± 36.6)	1244 (± 9.2)
UTS, MPa	31.6 (± 0.9)	33.4 (± 0.3)	32.4 (± 0.5)	31.4 (± 0.3)	24.3 (± 1.3)
Elongation to break, %	14.6 (± 3.2)	9.7 (± 0.3)	6.8 (± 1.0)	19.4 (± 2.9)	4.1 (± 0.7)

As mentioned in Chapter 6, the M_w of P(3HB-co-45%3HV), has been shown to slowly start to decrease at temperatures of 100 °C and above, when held isothermally for 20 minutes [67]. Links have been made between decreasing M_w and the decline in tensile properties including loss of tensile strength, elongation to break, and loss of yield before break [68,71,77]. The decrease in M_w is a result of the chain scission process, widely accepted as the mechanism of thermal degradation in PHB [54,62,65,67,68,71]. Chain scission begins in the amorphous phase, reducing the degree of chain entanglement and the number of tie-chains, as well as creating a higher proportion of free end groups, which have greater steric hindrance [69,71,77]. This reduces the strength of the amorphous phase, as well as making it more brittle.

The mechanical testing data indicates that the increase in strength, resulting from the secondary crystallisation process thickening the lamellae, initially outweighs the decrease in strength from chain scission in the amorphous phase. At the early stages the chain scission process has even been thought to contribute to the lamellar thickening process, due to the greater mobility and ease of packing inherent to shorter chains [68]. This contributes further to the brittleness of the system. As the storage time increases, the extent of degradation also increases and begins to outweigh the effects of secondary crystallisation. It is at that point that the trends associated with degradation are displayed in the data.

7.6 Mass loss

It is common for mass loss of PHB and P(HB-co-HV) to be discussed as a process which takes place at temperatures considerably higher than the melting temperature of the polymer, often during thermogravimetric analysis [64,71,73], although mass loss has also been shown to occur in P(HB-co-1.05mol%HV) at temperatures from 210 to 270 °C when held isothermally [70].

However, most authors agree that there is no significant reduction in mass when samples are stored below their melting temperature, usually based on isothermal studies of 30 minutes or less [62,65,67,70]. Generally, Figure 7.20 agrees with these findings, showing that there was very little change in sample mass for all samples which were stored at temperatures below 150 °C, over the entire duration of the study. It is clear though, that prolonged storage at 150 °C did produce a significant decrease in the sample mass. This decrease was highly consistent, as indicated by the small error bars in Figures 7.20, 7.21 and 7.22.

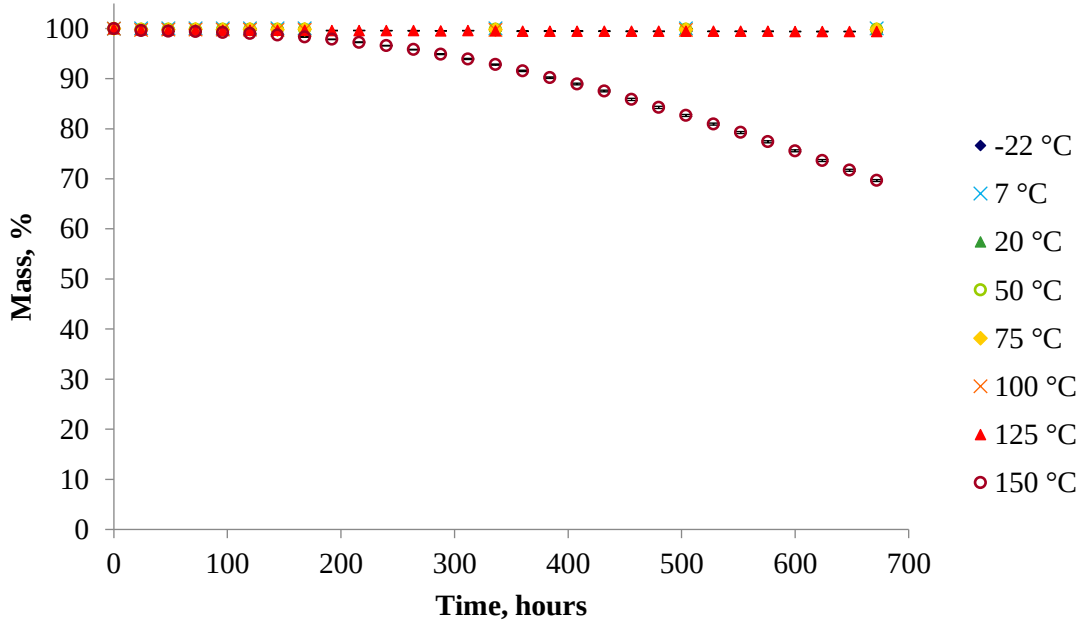

Figure 7.20. Mass loss as a percentage of the original mass *(hot pressed samples)*.

Samples stored at -22, 7 and 20 °C presented no significant change after 672 hours. This was expected due to the limitations resulting from the proximity to the T_g, below which molecular motion, and therefore reorganisation, is not possible (Figure 7.21). Mass loss data tables are in Appendix F.

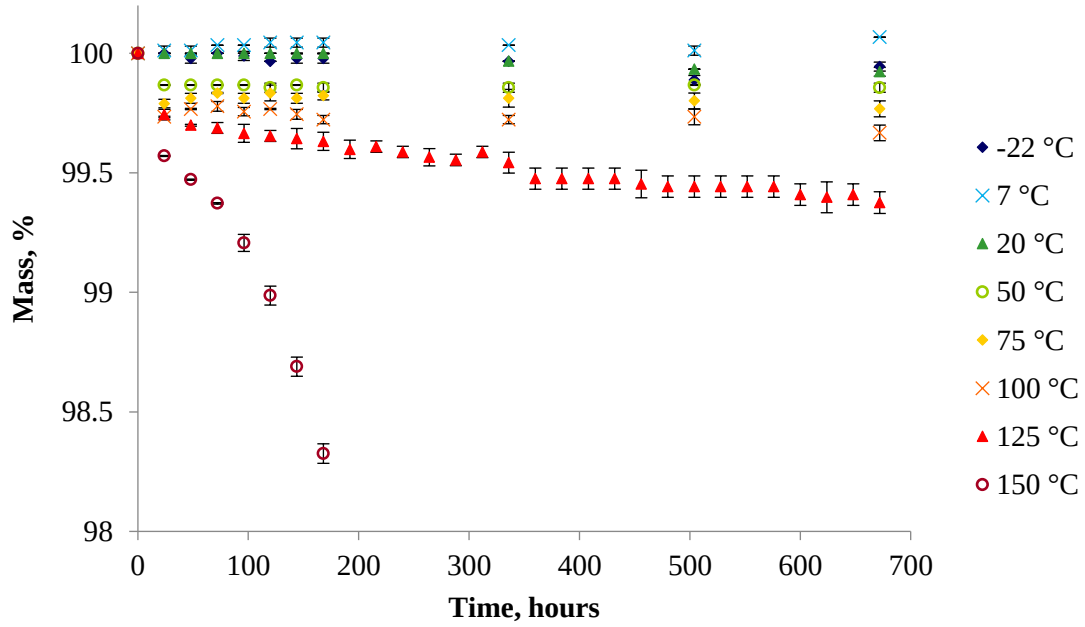

Figure 7.21. Mass loss as a percentage of the original mass, with y-axis magnified *(hot pressed samples).*

When kept at 50, 75 and 100 °C, samples exhibited very similar trends of mass loss. At each of these temperatures, the greatest change in mass occurred within the first 24 hours of the study, with no significant further losses. Higher storage temperatures resulted in a greater loss of mass, with temperatures of 50, 75 and 100 °C losing an average of 0.14, 0.23 and 0.33 % respectively by 672 hours of storage. It is likely that the mass loss at these temperatures is related to the evaporation of surface moisture [48]. The greater free volume at higher storage temperatures would allow more water to evaporate, resulting in larger losses in mass with temperature increase. Samples held at 125 °C again showed a similar but more exaggerated trend of a relatively large loss in mass in the first 24 hours of storage followed by a further steady decrease, losing an average of 0.63 % over the course of the study. The initial loss is again likely to be the evaporation of moisture on the surface of the sample. Subsequent losses may be an indication that degradation is active at 125 °C, but at a very low rate when compared with the rate of degradation observed at 150 °C.

Only when the temperature of storage was set to 150 °C did the loss in mass become much more substantial. As seen in the samples stored at lower temperatures, there was a reduction in mass in the first 24 hours of the study (Figure 7.21). The mass loss proceeded more slowly after the first 24 hours, and then accelerated over the remaining storage time, with samples losing an average of 30.35 % of their original mass after 672 hours. When chain scission occurs at the end of the chains crotonic acid is produced. The melting and boiling points of crotonic acid are 72 °C and 184.7 °C respectively [102], so it is possible that crotonic acid is being formed and is evaporating at a storage temperature of 150 °C, and this is responsible for the mass loss seen at this temperature. As chain scission is random, and can occur at any of the ester linkages along the chain length, crotonic acid is formed in lower concentrations at the onset of degradation, when the chains are long and the chances of scission occurring at the end of the chains is relatively low. This means that mass loss is slow at the start of degradation, when the concentrations of crotonic acid forming and evaporating is low. When the chains split, it results in the formation of carboxylic acid end groups which will catalyse the reaction. With further degradation, scission continues to create shorter chains, meaning crotonic acid forms and evaporates in higher concentrations as the chances of scission occurring at the chain end increases. This explains the exponential mass loss seen in Figure 7.20. Crotonic acid was detected in the IR spectra (Figure 7.15), but was not seen to increase over time, which combined with the observed mass loss confirms the evaporation theory. Xiang *et al*. observed a dramatic mass loss of 17.4 % when holding P(HB-co-1.05mol%HV) isothermally at 230 °C for 30 minutes [70]. At 150 °C the samples reached the equivalent of this mass loss after 504 hours, but had nearly doubled the mass loss reported by Xiang *et al*. after 672 hours of storage.

Pellets of the sample material were also subjected to storage at 150 °C, and exhibited a similar trend of accelerating mass loss with increasing storage time (Figure 7.22). The pellets were

tested as received, sometime after being supplied from the manufacturers, so the duration of storage at ambient temperature was unknown. This means that the secondary crystallisation process would have been active in these pellets for an unknown amount of time prior to storage at 150 °C. However, as demonstrated in Figure 7.20, any previous mass loss as a result of the storage at ambient temperature is likely to have been minimal. As the pellets also exhibited a decrease in mass, down to 80.94 % of the original mass after 672 hours compared with 69.65 % observed in the hot-pressed samples, the loss seen in the hot-pressed samples cannot be entirely due to the additional processing step.

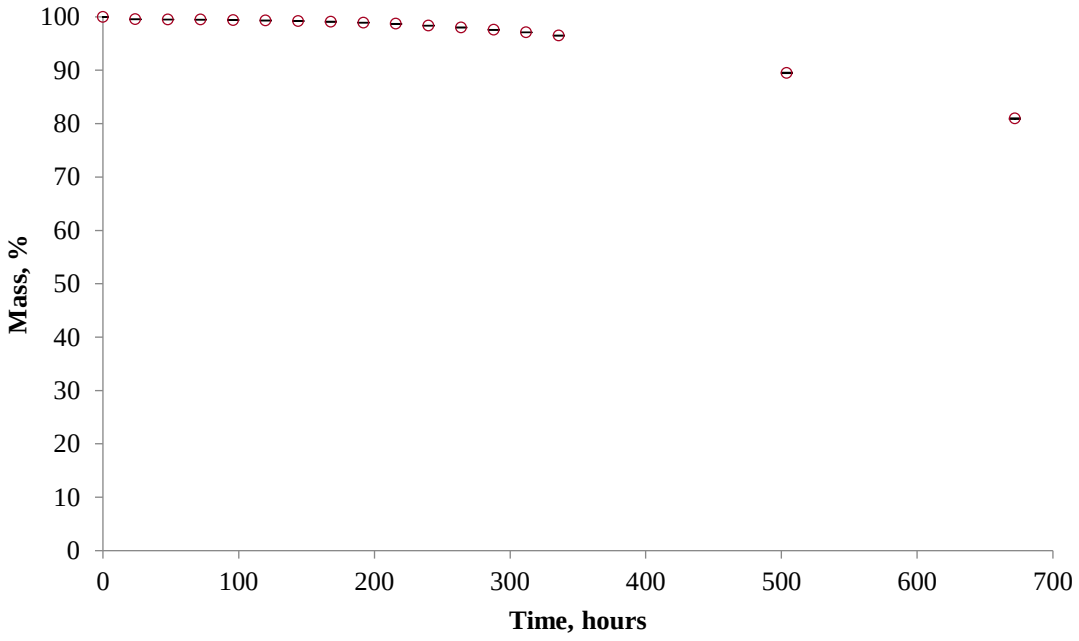

Figure 7.22. Mass loss as a percentage of the original mass, when stored at 150 °C *(Pellets)*. Mass loss data tables are in Appendix F.

The data obtained from the mass loss studies revealed that prolonged storage below the T_m, at a temperature of 150 °C, produced a significant loss in mass. Previous works have not observed mass losses at temperatures below the T_m, however, the isothermal experiments were much shorter in duration compared to those carried out here. The decrease in mass of samples stored at 150 °C is an indication that the degradation process is active below the T_m at this temperature

during prolonged storage times. Data from IR testing has shown that crotonic acid is present within the samples. Crotonic acid boils at a temperature of 184.7 °C [102], meaning it isn't volatile at a storage temperature of 150 °C; however, the melting point is 72 °C [102], so with prolonged storage it is likely that it will evaporate slowly over time, resulting in the loss in sample mass.

7.7 Gel permeation chromatography (GPC)

Suggestions made earlier in this chapter to explain the change in properties include a reduction in M_w. Many authors have used decrease in molecular weight of PHB and P(HB-co-HV) to infer the activity of thermal degradation through the chain scission process [54,62,65,67,68,70,71]. Figure 7.23 shows peaks relating to the samples eluting between 9 and 17 minutes, the M_w distributions of the peaks are presented in Figure 7.24. The distribution of the sample stored at 125 °C for 24 hours was slightly narrower than that of the original sample. When stored at 150 °C for 24 and 168 hours, the distributions became broader than that of the original sample, and after 672 hours the M_w distribution was bimodal, and the response was much greater.

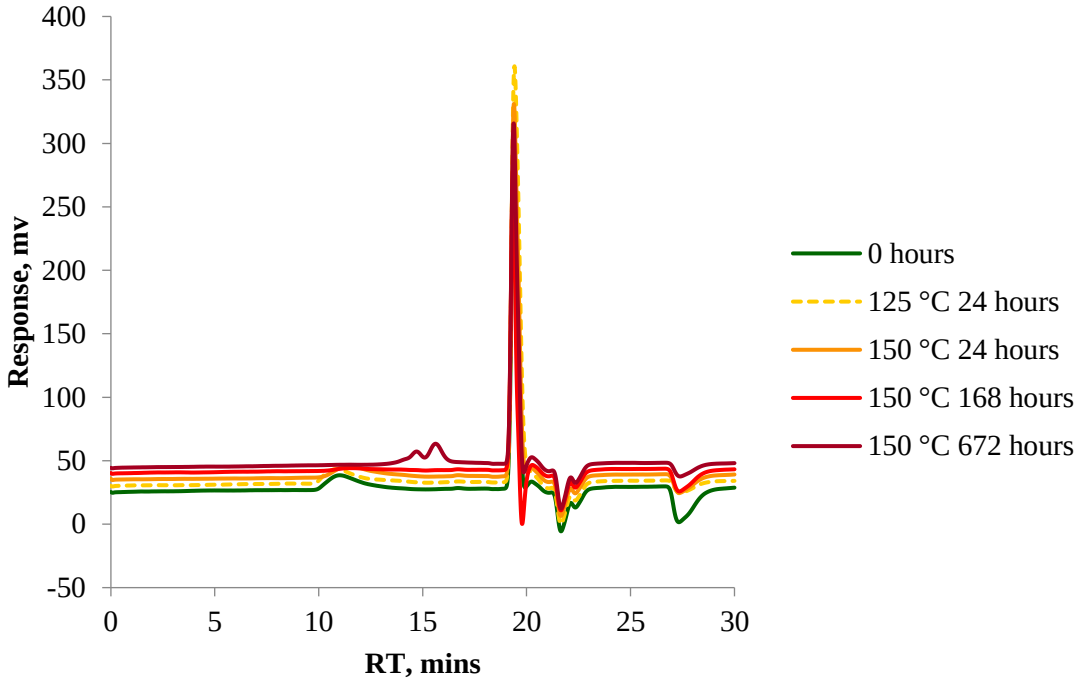

Figure 7.23. Elution times of samples held at 125 °C and 150 °C for different durations.

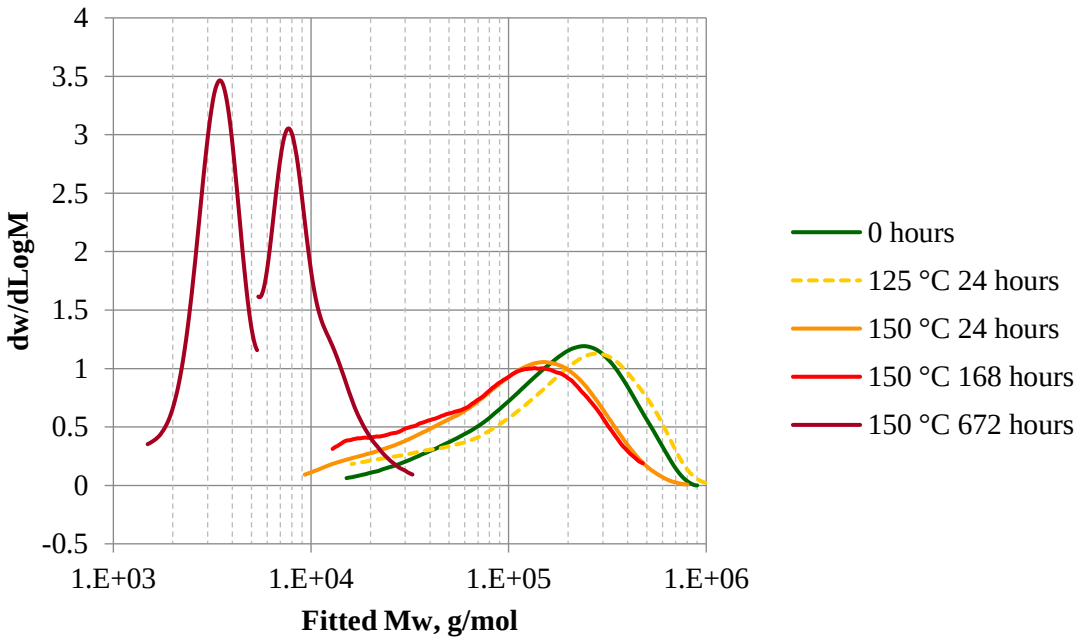

Figure 7.24. Molecular weight distributions of samples held at 125 °C and 150 °C for different durations.

An increase in M_w to 239 985 g mol^{-1} from the original value of 215 505 g mol^{-1} was observed in the sample stored for 24 hours at 125 °C (Figure 7.25). It is possible that the M_w initially increased through an esterification process, known to be active at the onset of degradation, which is discussed in Chapter 1.5 [65]. During esterification, there is a condensation reaction between carboxylic acid and alcohol end groups, causing an increase in molecular weight, until all the OH units have been used up, and subsequently chain scission causes the M_w to decrease [65].

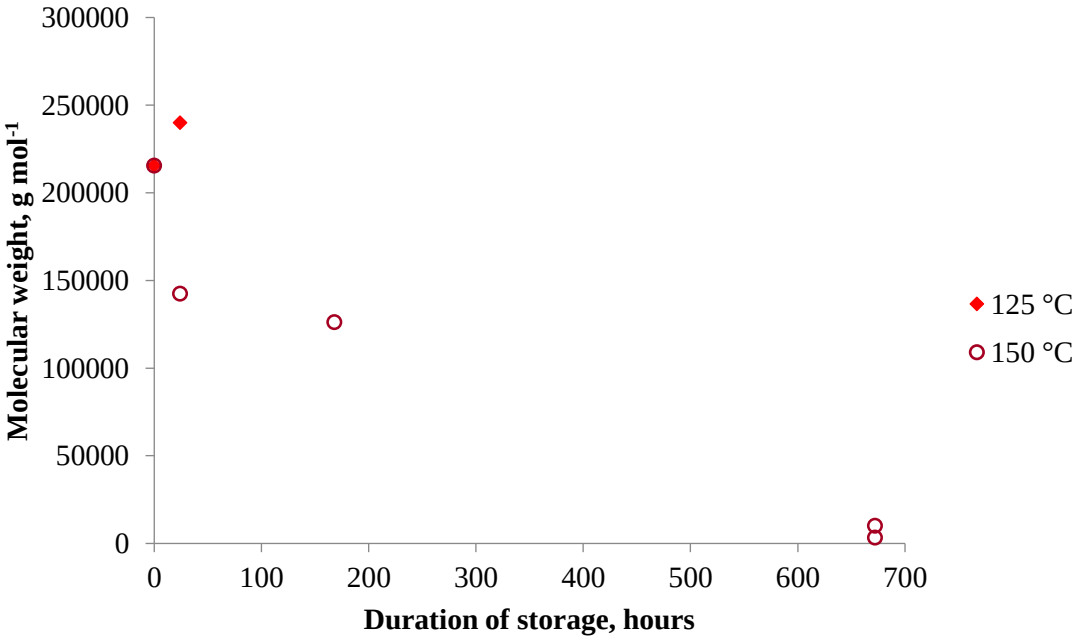

Figure 7.25. Weight average molecular weight.

Samples stored at 150 °C all showed a decrease in M_w from the original value of 215 505 g mol^{-1}. 24 hours of storage suggests a value of 142 570 g mol^{-1}, and after 168 hours the M_w appeared to drop to 126 150 g mol^{-1}. However, it is possible that the samples which were held at 150 °C for 24 and 168 hours may not have fully dissolved. After dissolution the samples were filtered, prior to analysis by GPC, and some residue was visible on the filter paper. This means that the true M_w of the samples, prior to dissolution, may have been greater than

the M_w of the sample that was run through the GPC (Figure 7.25). Terada and Marchessault, and Žagar and Kržan noted how PHB has poor solubility in chloroform at room temperature [69,103]. Later, Chen *et al*. also reported a decrease in solubility after 30 minutes of heating PHB and P(HB-co-HV) at 150 °C, and attributed it to the increase in crystallinity [54]. The DSC data, shown previously in this chapter, revealed an increase in crystallinity from 64.5 % to 76.4 % after storage at 150 °C for 24 hours. It is therefore likely that the increase in crystallinity was responsible for the incomplete sample dissolution.

When stored for 672 hours at 150 °C the sample was able to fully dissolve, and it did so in the shortest amount of time. GPC of this sample revealed not one, but two overlapping peaks in Figure 7.24. This bimodal distribution indicates that differing molecular weights are present within the sample. The first peak appeared after 12.6 minutes, with a M_w of 10 100 g mol^{-1}, and the second peak emerged after 15.1 minutes with a M_w of 3373 g mol^{-1}. It may also be inferred from the size of the peaks that there was a greater amount of material with lower M_w in this sample. Janigová *et al*. also saw a decrease in the M_w of PHB and a bimodal distribution, and described it as being a result of differing crystal sizes produced during chain scission [68]. A similar result was found in P(HB-co-HV) by Leroy *et al*. from thermal degradation induced by processing conditions [76].

In the samples, which were stored at 150 °C for 672 hours, chain scission reduced the crystallinity of the material, enabling complete sample dissolution, and drastically reducing the molecular weight (from 215 505 g mol^{-1} to 10 100 g mol^{-1} and 3373 g mol^{-1}). This agrees with the work of Chen *et al*., where a decrease in the M_w of PHB and PHBV (5wt%) was recorded after samples were held at 150 °C for times between 10 and 60 minutes [54].

7.8 Combined figures

The degradation data has been combined in Figures 7.26a-c, to approximate the region of interplay between the secondary crystallisation and degradation processes. It was necessary to split the data into 3 figures, due to the required number of different y-axis scales. The blue dashed lines have been added as a visual aid, enclosing the secondary crystallisation region, the timescale of which has been estimated to finish at the timepoint where the crystallinity was first seen to decrease (Figure 7.26a).The red dashed lines enclose the region where the degradation process is thought to be active, the start of which has been estimated as the timepoint where the rate of mass loss begins to increase (Figure 7.26b). The overlap of the two boxes indicates the region where the two processes are thought to interact, between approximately 96 and 336 hours of storage at 150 °C, as indicated by the black dashed lines and arrow beneath Figure 7.26c. It has already been stated that the chain scission of the degradation process may initially contribute to the effects of secondary crystallisation, as the shorter chains have greater mobility and are able to pack more easily into the crystalline structure. This interplay, between the effects of secondary crystallisation and degradation, means that the timescales determining the end of the secondary crystallisation process and the start of degradation is difficult to pinpoint accurately. The accuracy could be increased with improved M_w data. If all of the samples could be dissolved fully for GPC testing, then it would be possible to observe the timepoint at which the M_w starts to decrease, indicating the onset of chain scission.

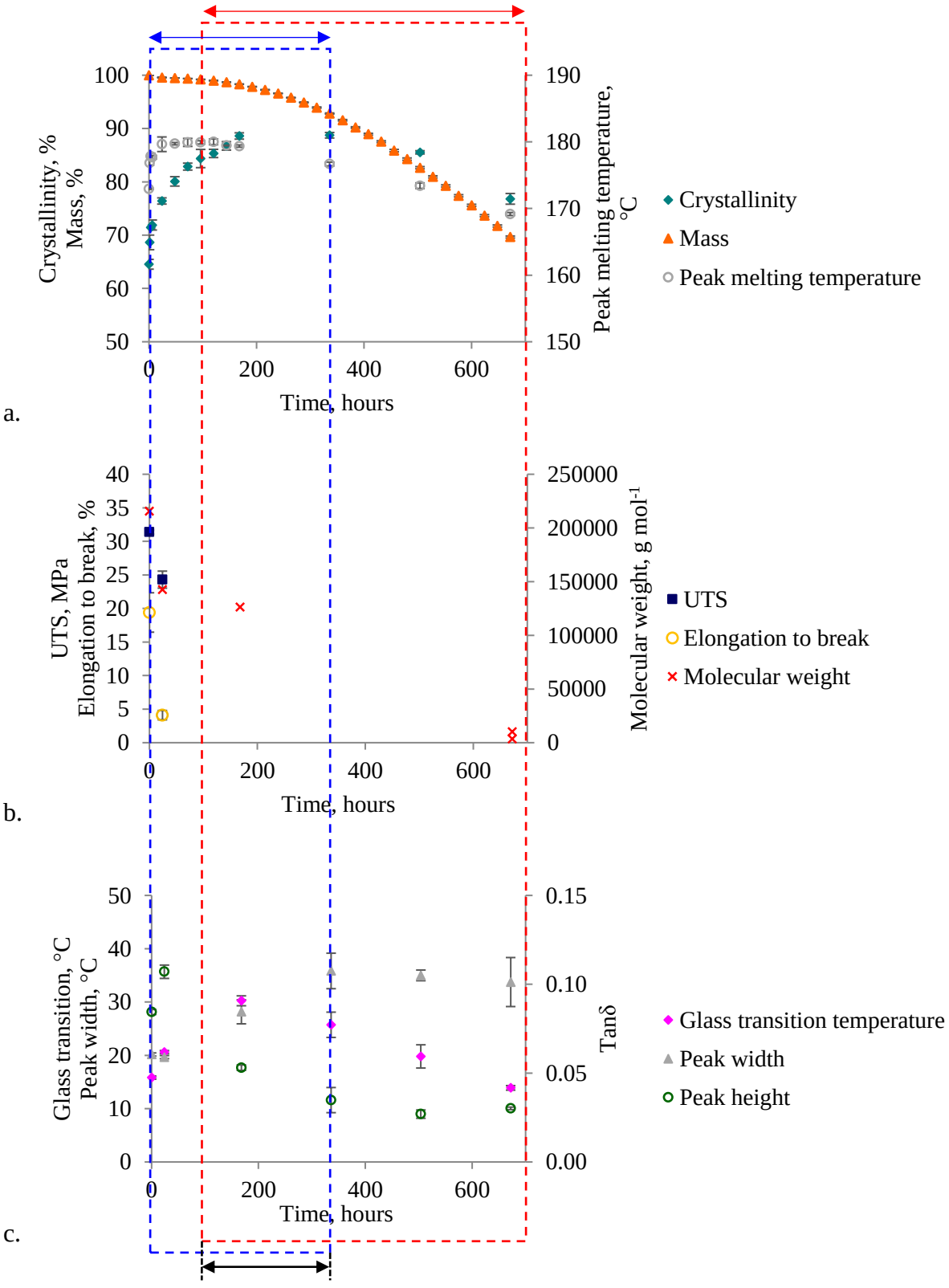

Figure 7.26. Change in sample properties over time at 150 °C. The blue and red dashed lines enclose the effects of secondary crystallisation and degradation respectively. The black dashed lines and arrow indicates the region of interplay between the two processes.

7.9 Conclusions

Many authors have reported or discussed the temperature dependence of thermal degradation of PHB and P(HB-co-HV) [54,63,65-68], and a thermal stability below the melting temperature and instability above the melting temperature is often noted [63,67,68]. At low temperatures, degradation is not possible, as mobility is too restricted to allow the cyclic ring to form, therefore chain scission cannot occur. This is evident in the lack of mass loss and discolouration of samples stored at -22 to 100 °C. However, at slightly higher temperatures, which are still below the melting temperature, it appears there is enough mobility in the polymer chains for the degradation process to occur if heated for extended times.

When stored at 125 °C there are indications that the chain scission process is active, towards the end of the storage duration. These include the deviation from trends in the mechanical properties observed at lower storage temperatures, the slight and gradual decrease in mass, minor discolouration after 504 hours of storage, and the emergence of small shoulder on the lower temperature side of the DSC endotherm. However, the T_g increased, the width of the tanδ peak was maintained, and there was no significant decrease in T_m or crystallinity (as observed by DSC and IR). Due to the interplay of secondary crystallisation and degradation processes, the crystallinity and T_m are initially maintained as the shorter, more mobile, chains created by chain scission are able to crystallise more easily. It is likely that a minor amount of degradation occurred with storage at 125 °C within the time limits of this work, and that degradation only affected the amorphous regions of the samples.

Storage at 150 °C resulted in a drastic change in mechanical properties within the first 24 hours, with large decreases in UTS and elongation to break corresponding to the rapid increase in crystallinity observed in both the DSC and IR data. These changes are commonly reported in

the current literature in terms of degradation, and while there is no decrease in crystallinity or significant decrease in mass after this length of storage, a corresponding decrease in M_w was observed. It is possible that chain scission was active within the amorphous regions at this time, which would cause the change in mechanical properties, and the emergence of the shoulder on the low temperature side of the DSC endotherm. However, due to the higher crystallinity of the samples there was incomplete dissolution meaning that the M_w, as determined by GPC, is likely to have been higher than detected. Degradation at this early stage is possible, but not certain, and the embrittlement caused by the extensive rise in crystallinity is likely to have dominated the change in mechanical properties.

There are clear signs of degradation in the samples stored at 150 °C after 96 hours. The most obvious being the increasing rate of mass loss from this point onwards, believed to be caused by the evaporation of crotonic acid (as identified in the IR spectra) formed during chain scission. The loss in mass is shortly followed by a large decrease in the T_m, T_g, and tanδ peak height, and an increase in the tanδ peak width (as shown by DSC and DMTA). All of which indicate a breakdown in constraints on the amorphous regions and, to some extent, the crystal structure. The interplay between the secondary crystallisation and degradation processes initially maintains the crystallinity, and masks the true onset of degradation, but this too decreased after 336 hours of storage.

After 672 hours of storage at 150 °C, the evidence for the degradation process being active below the T_m is overwhelming. Over 30 % of the original sample mass was lost, the M_w had decreased from a unimodal distribution peaking at 215 505 g mol^{-1} to bimodal peaks at 10 100 g mol^{-1} and 3373 g mol^{-1}, the crystallinity and T_m reduced from maximum values of 88.7 % and 180.0 °C, to 76.8 % and 169.2 °C, the tanδ peak collapsed, and the samples were dark brown in colour.

CHAPTER 8 – CONCLUSIONS AND FURTHER WORK

8.1 Conclusions

P(HB-co-HV) was stored at a range of temperatures and analysed over time to determine the effects of secondary crystallisation. Storage of samples at -22 °C did not cause a change in any of the properties measured in this work. This is due to the samples being held below the glass transition temperature of the polymer, where the chains in the amorphous regions are 'frozen' in place, and no movement is possible. Therefore, these samples acted as the control groups, and provided a measure of the degree of variation inherent to the samples prior to thermal conditioning.

At storage temperatures between 7 and 125 °C, the secondary crystallisation process was active, changing the properties of the material over time as the crystallinity increased. This increase in crystallinity was evident in the DSC data and trends in the crystallinity index, calculated from IR data. At lower storage temperatures, 20 to 50 °C, the onset of melting occurred at lower temperatures, indicating that less stable crystal structures may have formed within the amorphous regions during storage which melted out more easily (infill). At 7 and 20 °C a secondary relaxation in E′ was observed in the DMTA data. It is possible that the softening observed in the E′ curve also relates to the melting out of these smaller structures. At higher storage temperatures the onset of melting increased as a result of lamellar thickening. A corresponding increase in peak melting temperature was observed at storage temperatures of 75 °C and above. DMTA also revealed an increase in the T_g, and decrease in the height of the tanδ peak as chains from the amorphous phase crystallised, causing a reduction the amount of material in the amorphous phase, and increased constrictions on the remaining amorphous

phase. The result of these microstructural changes is seen as an increase in Young's modulus and UTS, as the material stiffened, as well as a decrease in the elongation to break, due to the increased brittleness. Higher storage temperatures provide the polymer chains with a greater amount of energy, increasing their mobility, and increasing the rate of secondary crystallisation. This results in greater rates of property change at higher storage temperatures.

The data obtained from samples stored at 125 °C suggests that, as well as the secondary crystallisation process, degradation may also have been active at extended storage times. While the DMTA and DSC data did not reveal any obvious signs of degradation, the Young's modulus increased to a lesser extent than the samples stored between 20 and 100 °C, and there was a decrease in the UTS observed after 120 hours of storage. There was also a slight and gradual decrease in mass throughout the storage duration, and after 504 hours of storage minor discolouration was detected. Small amounts of chain scission in the amorphous regions would have increased the rate of the secondary crystallisation process; as shorter chains have fewer entanglements, greater mobility, and can therefore pack more easily into the crystalline structure. This provides an explanation as to why the DMTA and DSC data did not exhibit any signs of degradation. It is likely that, within the time limits of this work, minor degradation occurred with storage at 125 °C, and that the degradation remained within the amorphous regions of the samples.

Analysis of data collected from samples stored at 150 °C clearly presents the effects of both secondary crystallisation and degradation. Which process dominated the overall change in properties was dependent on the length of storage time. UTS and elongation to break both experienced significant decreases within the first 24 hours of storage, and after 48 hours tensile testing was no longer possible as severe embrittlement of the samples caused them to fracture whist being clamped into the instrument. These changes correspond to a large, rapid increase

in the crystallinity observed in both the DSC and IR data. The effect of crystallinity increase also caused initial increases in the T_g and the position of the tanδ peak, as it constrained the amorphous material further. The interplay of secondary crystallisation and degradation was demonstrated by the increase in tanδ peak width over time, as the increased constraints caused by secondary crystallisation extended the peak to the high temperature side, and chain scission created shorter, less entangled chains which extended the peak to the low temperature side. Another feature seen to develop early on in the study was an increase in T_m, and the emergence of a prominent shoulder on the low temperature side of the DSC melting peak. Initially formed through the partial melting and recrystallisation of the least stable crystals during storage, the shoulder first shifted to higher temperatures, most likely caused by lamellar thickening, and began to merge with the main melting peak.

After 96 hours of storage at 150 °C, the effects of degradation began to be clearly expressed in the property changes. The rate of mass loss began to increase, due to the effects of crotonic acid formation and evaporation, along with a significant decrease in T_m and onset of melting, as the main melting peak and shoulder shifted to lower temperatures. At the same time the T_g and the tanδ peak height decreased, and the tanδ peak width increased. These factors indicate a breakdown in constraints on the amorphous regions and, to some extent, the crystal structure. A decrease in crystallinity did not occur until after 336 hours of storage, as the chain scission process initially increases the degree of crystallinity as it creates, shorter, less entangled chains which have greater mobility and can therefore pack more easily into the crystalline structure. In effect, this interplay between secondary crystallisation and degradation processes masks the start of the degradation process.

The effects of degradation are pronounced after 672 hours of storage at 150 °C. Over 30 % of the original sample mass was lost, the M_w had decreased from a unimodal distribution peaking

at 215 505 g mol^{-1} to bimodal peaks at 10 100 g mol^{-1} and 3373 g mol^{-1}, the crystallinity and T_m reduced from maximum values of 88.7 % and 180.0 °C, to 76.8 % and 169.2 °C, the tanδ peak had collapsed, and the samples became dark brown in colour.

8.2 Further work

Changes in properties were still being recorded at the end of the storage times examined in this work. Further work should extend the duration of the time-temperature studies, to 1 or more years, to fully explore the temperature dependence on the rates and limits of the secondary crystallisation process. Yet the upper temperature limit should be lowered, to avoid the complications caused by the interplay between the secondary crystallisation and degradation processes. Further IR work could aid in the determination of a suitable temperature limit.

The 150 °C IR isothermal study in this work had been intended to last significantly longer, in order to observe the primary crystallisation, secondary crystallisation and degradation processes. However, there were issues with maintaining the contact between the sample and the ATR crystal. Further work should develop the IR studies, using solution cast samples and performing experiments in the transmission mode to avoid this problem. This should allow the duration of the experimental run to be extended, and make investigation into the interplay of secondary crystallisation and degradation possible. IR isothermal studies could establish a link between the change in crystallinity and the development of crotonic acid at a temperature significantly below the melting point. If successful, transmission experiments could also be run at lower temperatures to discover the lower limits of the degradation process, as the current work suggests it may be active at temperatures as low as 125 °C.

SEM work could be carried out to examine any change in morphology which occurs over time due to secondary crystallisation. This line of investigation could be expanded to include WAXS and SAXS work, to analyse changes in lamellar thickness according to the length of storage time, over the expanded temperature range.

REFERENCES

[1] Cowie, J.M.G. (1991) *Polymers: Chemistry & physics of modern materials*. 2nd edn. Cheltenham: Nelson Thornes. pp. 231-259.

[2] Mandelkern, L. (2004) *Crystallisation of Polymers*. 2nd ed. Cambridge: Cambridge University Press (vol. 2). pp.80, 90.

[3] Mandelkern, L. (2004) 'The crystalline state' in Mark, J. (ed.) *Physical properties of polymers*. Cambridge: Cambridge University Press. pp.243-257.

[4] Young, R.J. and Lovell, P.A. (2011) *Introduction to polymers*. 3rd edn. Bosa Roca: CRC Press pp.432-441.

[5] Wilson, R.J. (2002) 'Calorimetry', in Haines, P.J. (ed.) *Principles of thermal analysis and calorimetry*. Cambridge: RSC Paperbacks. p.133.

[6] Hoffman, J.D. and Lauritzen, J.I. (1960) 'Theory of formation of polymer crystals with folded chains in dilute solution', *Journal of Research of the National Bureau of Standards Section A-Physics and Chemistry*, 64 (1), pp. 73-102.

[7] Hoffman, J.D. and Weeks, J.J. (1962a) 'Rate of spherulitic crystallization with chain folds in polychlorotrifluoroethylene', *The Journal of Chemical Physics*, 37 (8), pp. 1723-1741.

[8] Hoffman, J.D. and Lauritzen, J.I. (1973) 'Extension of theory of growth of chain-folded polymer crystals to large undercoolings', *Journal of Applied Physics***,** 44 (10), pp. 4340-4352.

[9] Hoffman, J.D., Guttman, C.M. and DiMarzio, E.A. (1979) 'On the problem of crystallisation of polymers from the melt with chain folding', *Faraday Discussions*, 68, pp. 177-197.

[10] Hoffman, J.D. (1982) ‘Role of reptation in the rate of crystallization of polyethylene fractions from the melt’, *Polymer*, 23 (5), pp. 656-670.

[11] Verhoyen, O., Dupret, F. and Legras, R. (1998) ‘Isothermal and non-isothermal crystallization kinetics of polyethylene terephthalate: mathematical modeling and experimental measurement’, *Polymer Engineering and Science*, 38 (9), pp. 1594-1610.

[12] Kolb, R., Wutz, C. and Stribeck, N. et al. (2001) ‘Investigation of secondary crystallization of polymers by means of microbeam X-ray scattering’, *Polymer*, 42 (12), pp. 5257-5266.

[13] de Koning, G.J.M., Scheeren, A.H.C. and Lemstra, P.J. et al. (1994) ‘Crystallization phenomena in bacterial poly[(R)-3-hydroxybutyrate] .3. Toughening via texture changes’, *Polymer*, 35 (21), pp. 4598-4605.

[14] Špitalský, Z. and Bleha, T. (2004) ‘Elastic properties of poly(hydroxybutyrate) molecules’, *Macromolecular Bioscience*, 4 (6), pp. 601-609.

[15] Bergmann, A. and Owen, A. (2004) ‘Dielectric relaxation spectroscopy of poly[(R)-3-hydroxybutyrate] (PHB) during crystallization’, *Polymer International*, 53 (7), pp. 863-86.

[16] Heo, K.Y., Yoon, J.W. and Jin, K.S. et al. (2008) ‘Structural evolution in microbial polyesters’, *Journal of Physical Chemistry*, 112 (15), pp. 4571-4581.

[17] Righetti, M.C. and Di Lorenzo, M.L. (2011) ‘Melting temperature evolution of non-reorganized crystals. Poly(3-hydroxybutyrate)’, *Thermochimica Acta*, 512 (1-2), pp. 59-66.

[18] Verlinden, R.A.J, Hill, D.J. and Kenward, M.A. et. al. (2007) 'Bacterial synthesis of biodegradable polyhydroxyalkanoates', *Journal of Applied Microbiology*, 102 (6), pp. 1437-1449.

[19] Rodríguez-Contreras, A., Calafell-Monfort, M. and Marqués-Calvo, M.S. (2012) 'Enzymatic degradation of poly(3-hydroxybutyrate) by a commercial lipase', *Polymer Degradation and Stability*, 97 (11), pp. 2473-2476.

[20] Sindhu, R., Ammu, B. and Binod, P. (2011) 'Production and characterization of poly-3-hydroxybutyrate from crude glycerol by Bacillus sphaericus NII 0838 and improving its thermal properties by blending with other polymers', *Brazilian Archives of Biology and Technology*, 54 (4), pp. 783-794.

[21] Holmes, P.A. (1985) 'Applications of PHB - a microbially produced biodegradable thermoplastic', *Physics in Technology*, 16 (1), pp. 32-36.

[22] Gunaratne, L.M.W.K. and Shanks, R.A. (2006) 'Thermal memory of poly(3-hydroxybutyrate) using temperature-modulated differential scanning calorimetry', *Journal of Polymer Science Part B – Polymer Physics*, 44 (1), pp. 70-78.

[23] You, J.W., Chiu, H.J., Shu, W.J. and Don, T.M. (2003) 'Influence of hydroxyvalerate content on the crystallization kinetics of poly(hydroxybutyrate-co-hydroxyvalerate)', *Journal of Polymer Reasearch*, 10 (1), pp. 47-54.

[24] Federov, M.B., Vikhoreva, G.A. and Kil'deeva, N.R. et al. (2007) 'Antimicrobial Activity of Core-Sheath Surgical Sutures Modified with Poly-3-hydroxybutyrate', *Applied Biochemistry and Microbiology*, 43 (6), pp. 611-615.

[25] Shishatskaya, E.I., Volova, T.G. and Puzyr, A.P. et al. (2004) ‘Tissue Response to the Implantation of Biodegradable Polyhydroxyalkanoate Sutures’, *Journal of Materials Science: Materials in Medicine,* 15 (6), pp. 719-728.

[26] Chen, G.Q. and Wu, Q. (2005) ‘The Application of Polyhydroxyalkanoates as Tissue Engineering Materials’, *Biomaterials,* 26 (33), pp. 6565-6578.

[27] Sun, X.L., Tokuda, A. and Oji, Y. et al. (2012) ‘Effects of molar mass of poly(L-lactide acid) on the crystallization of poly[(R)-3-hydroxybutyrate] in their ultrathin blend films’, *Macromolecules,* 45 (5) pp. 2485-2493.

[28] Liu, Q.S., Zhu, M.F. and Wu, W.H. et al. (2009) ‘Reducing the formation of six-membered ring ester during thermal degradation of biodegradable PHBV to enhance its thermal stability’, *Polymer Degradation and Stability,* 94 (1), pp. 18-24.

[29] Arakawa, K., Yokohara, T. and Yamaguchi, M. (2008) ‘Enhancement of melt elasticity for poly(3-hydroxybutyrate-co-3-hydroxyvalerate) by addition of weak gel’, *Journal of Applied Polymer Science*, 107 (2), pp. 1320-1324.

[30] Doi, Y. (1990) *Microbial Polyesters*. New York: VCH.

[31] Miguel, O. and Iruin, J.J. (1999) ‘Evaluation of the Transport Properties of Poly(3-hydroxybutyrate) and its 3-hydroxyvalerate Copolymers for Packaging Applications’, *Macromolecular Symposia,* 144, pp. 427-438.

[32] Biddlestone, F., Harris, A., Hay, J.N. and Hammond, T. (1996) ‘The physical ageing of amorphous poly(hydroxybutyrate)’, *Polymer International*, 39 (3), pp. 221-229.

[33] de Koning, G.J.M. and Lemstra, P.J. (1993) 'Crystallization phenomena in bacterial poly[(R)-3-hydroxybutyrate] .2. Embrittlement and rejuvenation', *Polymer*, 34 (19), pp. 4089-4094.

[34] Hong, S.G. and Chen, W.M. (2006) 'The attenuated total reflection infrared analysis of surface crystallinity of polyhydroxyalkanoates', *e-Polymers*, 024, pp. 1-17 [online]. Available at: https://www.degruyter.com/view/j/epoly.2006.6.issue-1/epoly. 2006.6.1.310/epoly.2006. 6.1.310.xml (Accessed: 10 September 2013).

[35] Bibers, I., Tupureina, V., Dzene, A. and Kalnins, M. (1999) 'Improvement of the deformative characteristics of poly-beta-hydroxybutyrate by plasticization', *Mechanics of Composite Materials*, 35 (4), pp. 357-364.

[36] Cyras, V.P., Fernández, N.G. and Vázquez, A. (1999) 'Biodegradable films from PHB-8HV copolymers and polyalcohols blends: crystallinity, dynamic mechanical analysis and tensile properties', *Polymer International*, 48 (8), pp. 705-712.

[37] Vogel, R., Tandler, B. and Voigt, D. et al. (2007) 'Melt spinning of bacterial aliphatic polyester using reactive extrusion for improvement of crystallization', *Macromolecular Bioscience*, 7 (6), pp. 820-828.

[38] Suttiwijitpukdee, N., Sato, H., Unger, M. and Ozaki, Y. (2012) 'Effects of hydrogen bond intermolecular interactions on the crystal spherulite of poly(3-hydroxybutyrate) and cellulose acetate butyrate blends: studied by FT-IR and FT-NIR imaging spectroscopy', *Macromolecules*, 45 (6), pp. 2738-2748.

[39] Hay, J.N. and Sharma, L. (2000) 'Crystallisation of poly(3-hydroxybutyrate)/polyvinyl acetate blends', *Polymer*, 41 (15), pp. 5749:5757.

[40] Withey, R.E. and Hay, J.N. (1999) 'The effect of seeding on the crystallisation of poly(hydroxybutyrate), and co-poly(hydroxybutyrate-co-valerate)', *Polymer,* 40 (18), pp. 5147-5152.

[41] Padermshoke, A., Katsumoto, Y. and Sato, H. et al. (2004) 'Surface melting and crystallisation behaviour of polyhydroxyalkanoates studied by attenuated total reflection infrared spectroscopy', *Polymer,* 45 (19), pp. 6547-6554.

[42] Fischer, J.J., Aoyagi, Y., Enoki, M., Doi, Y. and Iwata, T. (2004) 'Mechanical properties and enzymatic degradation of poly([R]-3-hydroxybutyrate-co-[R]-3-hydroxyhexanoate) uniaxially cold drawn films', *Polymer Degradation and Stability,* 83 (3), pp. 453-460.

[43] Zhao, Q., Cheng, G.X. and Song, C.J. et al. (2006) 'Crystallization behavior and biodegradation of poly(3-hydroxybutyrate) and poly(ethylene glycol) multiblock copolymers', *Polymer Degradation and Stability,* 91 (6), pp. 1240-1246.

[44] Peng, S.W., An, Y.X. and Chen, C. et al. (2003) 'Isothermal crystallization of poly(3-hydroxybutyrate-co-3-hydroxyvalerate)', *European Polymer Journal,* 39 (7), pp. 1475-1480.

[45] Savenkova, L., Gercberga, Z. and Bibers, I. et al. (2000) 'Effect of 3-hydroxy valerate content on some physical and mechanical properties of polyhydroxyalkanoates produced by Azotobacter chroococcum', *Process Biochemistry,* 36 (5), pp. 445-450.

[46] El-Hadi, A., Schnabel, R. and Straube, E. et al. (2002) 'Effect of melt processing on crystallization behavior and rheology of poly(3-hydroxybutyrate) (PHB) and its blends', *Macromolecular Materials and Engineering,* 287 (5), pp. 363-372.

[47] Roa, J.P.B., Patrício, P.S.D. and Oréfice, R.L. et al. (2013) 'Improvement of the thermal properties of poly(3-hydroxybutyrate) (PHB) by low molecular weight polypropylene glycol (LMWPPG) addition', *Journal of Applied Polymer Science,* 128 (5), pp. 3019-3025.

[48] Wei, L., Liang, S. and McDonald, A.G. (2015) 'Thermophysical properties and biodegradation behavior of green composites made from polyhydroxybutyrate and potato peel waste fermentation residue', *Industrial Crops and Products,* 69, pp. 91-103.

[49] Xu, J., Guo, B.H. and Yang. R. et al. (2002) 'In situ FTIR study on melting and crystallization of polyhydroxyalkanoates', *Polymer,* 43 (25), pp. 6893-6899.

[50] Yoshie, N., Oike, Y. and Kasuya, K. et al. (2002) 'Change of surface structure of poly(3-hydroxybutyrate) film upon enzymatic, hydrolysis by PHB depolymerase', *Biomacromolecules,* 3 (6), pp. 1320-1326.

[51] Phillipson, K., Jenkins, M.J. and Hay, J.N. (2015) 'The ageing of poly(ε-caprolactone)', *Polymer International,* 64 (12), pp. 1695-1705.

[52] Schwarz, I., Stranz, M., Bonnet, M. and Petermann, J. (2001) 'Changes of mechanical properties in cold-crystallized syndiotactic polypropylene during aging', *Colloid and Polymer Science,* 279 (5), pp. 506-512.

[53] Morales, E. and White, J.R. (2009) 'Effect of ageing on the mechanical properties and the residual stress distribution of hybrid clay-glass fibre-polypropylene injection mouldings', *Journal of Materials Science,* 44 (17), pp. 4734-4742.

[54] Chen, Y., Chou, I.N. and Tsai, Y.H. et al. (2013) 'Thermal degradation of poly(3-hydroxybutyrate) and poly(3-hydroxybutyrate-co-3-hydroxyvalerate) in drying treatment', *Journal of Applied Polymer Science,* 130 (5), pp. 3659-3667.

[55] Sadocco, P., Canetti, M. and Seves, A. et al. (1993) ‘Small-angle X-ray-scattering study of the phase-structure of poly(D-(-)-3-hydroxybutyrate) and atactic poly(epichlorohydrin) blends’, *Polymer*, 34 (16), pp. 3368-3375.

[56] Canetti, M., Urso. M. and Sadocco, P. (1999) ‘Influence of the morphology and of the supermolecular structure on the enzymatic degradation of bacterial poly(3-hydroxybutyrate)’, *Polymer*, 40 (10), pp. 2587-2594.

[57] Fujita, M., Sawayanagi, T. and Tanaka, T. et al. (2005) ‘Synchrotron SAXS and WAXS studies on changes in structural and thermal properties of poly[(R)3-hydroxybutyrate] single crystals during heating’, *Macromolecular Rapid Communications*, 26 (9), pp. 678-683.

[58] Mitomo, H. and Doi, Y. (1999) ‘Lamellar thickening and cocrystallization of poly(hydroxyalkanoate)s on annealing’, *International Journal of Biological Macromolecules*, 25 (1-3), pp. 201-205.

[59] Gunaratne, L.M.W.K., Shanks, R.A. and Amarasinghe, G. (2004) ‘Thermal history effects on crystallisation and melting of poly(3-hydroxybutyrate)’, *Thermochimica Acta*, 423 (1-2), pp. 127-135.

[60] Shanks, R.A. and Gunaratne, L.M.W.K. (2011) ‘Comparison of reversible melting behaviour of poly(3hydroxybutyrate) using quasi-isothermal and other modulated temperature differential scanning calorimetry techniques’, *Journal of Thermal Analysis and Calorimetry*, 104 (3), pp. 1117-1124.

[61] Ziaee, Z. and Supaphol, P. (2006) Non-isothermal melt- and cold-crystallization kinetics of poly(3-hydroxybutyrate), *Polymer Testing*, 25 (6), pp. 807-818.

[62] Aoyagi, Y., Yamashita, K. and Doi, Y. (2002) 'Thermal degradation of poly[(R)-3-hydroxybutyrate], poly[ε-caprolactone], and poly[(S)-lactide]', *Polymer Degradation and Stability*, 76 (1), pp. 53-59.

[63] Chan, C.H., Kummerlöwe, C. and Kammer, HW. (2004) 'Crystallization and melting behavior of poly(3-hydroxybutyrate)-based blends', *Macromolecular Chemistry and Physics*, 205 (5), pp. 664-675.

[64] Grassie, N., Murray, E.J. and Holmes, P.A. (1984a) 'The thermal-degradation of poly(-(D)-beta-hydroxybutyric acid) .1. Identification and quantitative-analysis of products', *Polymer Degradation and Stability*, 6 (1), pp. 47-61.

[65] Grassie, N., Murray, E.J. and Holmes, P.A. (1984b) 'The thermal-degradation of poly(-(D)-beta-hydroxybutyric acid) .2. Changes in molecular-weight', *Polymer Degradation and Stability*, 6 (2), pp. 95-103.

[66] Grassie, N., Murray, E.J. and Holmes, P.A. (1984c) 'The thermal-degradation of poly(-(D)-beta-hydroxybutyric acid) .3. The reaction mechanism', *Polymer Degradation and Stability*, 6 (3), pp. 127-134.

[67] Kunioka, M. and Doi, Y. (1990) 'Thermal degradation of microbial copolyesters - poly(3-hydroxybutyrate-co-3-hydroxyvalerate) and poly(3-hydroxybutyrate-co-4-hydroxybutyrate)', *Macromolecules*, 23 (7), pp. 1933-1936.

[68] Janigová, I., Lacík, I. and Chodák, I. (2002) 'Thermal degradation of plasticized poly(3-hydroxybutyrate) investigated by DSC', *Polymer Degradation and Stability*, 77 (1), pp. 35-41.

[69] Žagar, E. and Kržan, A. (2004) 'SEC-MALS characterization of microbial polyhydroxyalkanoates', *Biomacromolecules,* 5 (2), pp. 628-636.

[70] Xiang, H., Wen, X. and Miu, X et al., (2016) 'Thermal depolymerization mechanisms of poly (3-hydroxybutyrate-co-3-hydroxyvalerate)', *Progress in Natural Science-Materials International,* 26 (1), pp. 58-64.

[71] Yang, H. and Liu, J. (2004) 'Thermal analysis of poly(3-hydroxybutyrateco-3-hydroxyvalerate) irradiated under vacuum', *Polymer International,* 53 (11), pp. 1677-1681.

[72] Hoffmann, A., Kreuzberger, S. and Hinrichsen, G. (1994) 'Influence of thermal-degradation on tensile-strength and Young's modulus of poly(hydroxybutyrate)', *Polymer Bulletin,* 33 (3), pp. 355-359.

[73] Li, S.D., Yu, P.H. and Cheung, M.K. (2001) 'Thermogravimetric analysis of poly(3-hydroxybutyrate) and poly(3-hydroxybutyrate-co-3-hydroxyvalerate)', *Journal of Applied Polymer Science,* 80 (12), pp. 2237-2244.

[74] Nguyen, S., Yu, G.E. and Marchessault, R.H. (2002) 'Thermal degradation of poly(3-hydroxyalkanoates): preparation of well-defined oligomers', *Biomacromolecules,* 3 (1), pp. 219-224.

[75] Liu, Q., Shyr, T.W. and Tung, C.H. et al. (2012) 'Particular thermal properties of poly(3-hydroxybutyrate-co-3-hydroxyvalerate) oligomers', *Journal of Polymer Research,* 19 (1), pp. 9756.

[76] Leroy, E., Petit, I. and Audic, J.L. et al. (2012) 'Rheological characterization of a thermally unstable bioplastic in injection molding conditions', *Polymer Degradation and Stability,* 97 (10), pp. 1915-1921.

[77] Renstad, R., Karlsson, S. and Albertsson, AC. (1996) 'Influence of processing parameters on the molecular weight and mechanical properties of poly(3-hydroxybutyrate-co-3-hydroxyvalerate)', *Polymer Degradation and Stability*, 57 (3), pp. 331-338.

[78] Farmahini-Farahani, M., Xiao, H. and Khan, A. et al. (2015) 'Preparation and Characterization of Exfoliated PHBV Nanocomposites to Enhance Water Vapor Barriers of Calendared Paper', *Industrial & Engineering Chemistry Research*, 54 (45), pp. 11277-11284.

[79] Barham, P.J., Keller, A. and Otun, E.L. et al. (1984) 'Crystallization and morphology of a bacterial thermoplastic: poly-3-hydroxybutyrate', *Journal of Materials Science*, 19 (9), pp. 2781-2794.

[80] Hay, J. N. and Mills, P.J. (1982) 'The use of differential scanning calorimetry to study polymer crystallization kinetics', *Polymer*, 23 (9), pp. 1380-1384.

[81] Lorenzo, A. T., Arnal, M.L. and Albuerne. J. *et al*. (2007) 'DSC isothermal polymer crystallization kinetics measurements and the use of the Avrami equation to fit the data: Guidelines to avoid common problems', *Polymer Testing*, 26 (2), pp. 222-231.

[82] Thomson, W.T. (1993) *Theory of Vibration with Applications*. 4th edn. London: Chapman & Hall. pp.77-78.

[83] Peterlin, A. (1964) 'Secondary crystallization and annealing of polyethylene', *Journal of Applied Physics*, 35 (1), pp. 75-81.

[84] Marand, H. and Huang, Z. (2004) 'Isothermal lamellar thickening in linear polyethylene: correlation between the evolution of the degree of crystallinity and the melting temperature', *Macromolecules*, 37 (17), pp. 6492-6497.

[85] El-Taweel, S.H., Stoll, B. and Schick, C. (2011) 'Crystallization kinetics and miscibility of blends of polyhydroxybutyrate (PHB) with ethylene vinyl acetate copolymers (EVA)', *e-Polymers*, 018, pp. 1-16 [online]. Available at: https://www.degruyter.com/ view/j/epoly.2011 .11.issue- 1/epoly.2011.11.1.191/epoly.2011.11.1.191.xml (Accessed: 9 October 2012).

[86] Huang, Z., Marand, H. and Cheung, W. *et al*. (2004) 'Study of crystallization processes in ethylene-styrene copolymers by conventional DSC and temperature-modulated calorimetry: linear polyethylene and low styrene content copolymers', *Macromolecules*, 37 (26), pp. 9922-9932.

[87] Hoffman, J.D. and Weeks, J.J. (1962b) 'Melting process and equilibrium melting temperature of polychlorotrifluoroethylene', *Journal of Research of the National Bureau of Standards Section A-Physics and Chemistry*, 66 (1), pp. 13-28.

[88] Organ, S.J. and Barham, P.J. (1993) 'On the equilibrium melting temperature of polyhydroxybutyrate', *Polymer*, 34 (10), pp. 2169-2174.

[89] Wu, Q., Tian, G. and Sun, S. (2001) 'Study of microbial polyhydroxyalkanoates using two-dimensional Fourier-transform infrared correlation spectroscopy', *Journal of Applied Polymer Science*, 82 (4), pp. 934-940.

[90] Williams, D.H. and Fleming, I. (1989) *Spectroscopic methods in organic chemistry*. 4th ed., rev. Maidenhead, Berks: McGraw-Hill Book Company (UK) Limited. p. 2.

[91] Gunaratne, L.M.W.K. and Shanks, R.A. (2005) 'Thermal memory of poly(3-hydroxybutyrate) using temperature-modulated differential scanning calorimetry', *Journal of Polymer Science Part B-Polymer Physics*, 44 (1), pp. 70-78.

[92] Marand, H., Alizadeh, A. and Farmer, R. et al. (2000) ‘Influence of structural and topological constraints on the crystallization and melting behavior of polymers. 2. Poly(arylene ether ether ketone)’, *Macromolecules*, 33 (9), pp. 3392-3403.

[93] Vizcaino-Caston, I., Kelly, C.A. and Fitzgerald, A.V.L. *et al*. (2016) ‘Development of a rapid method to isolate polyhydroxyalkanoates from bacteria for screening studies’, *Journal of Bioscience and Engineering*, 121 (1), pp. 101-104.

[94] Galego, N., Rozsa, C. and Sánchez, R. et al. (2000) ‘Characterization and application of poly(β-hydroxyalkanoates) family as composite biomaterials’, *Polymer Testing*, 19 (5), pp. 485-492.

[95] Cambridge Polymer Group (2014) *Glass transition by DMA*. Available at: http://www.campoly.com/files/6114/2850/4047/035_Glass_Transition_by_DMA_ADMIN-0243_v2.0.pdf (Accessed: 20 October 2016).

[96] Lizundia, E., Petisco, S. and Sarasua JR. (2013) ‘Phase-structure and mechanical properties of isothermally melt-and cold-crystallized poly (L-lactide)’, *Journal of the Mechanical Behavior of Biomedical Materials*, 17, pp. 242-251.

[97] Zuza, E., Ugartemendia, J.M. and Lopez A. et al. (2008) ‘Glass transition behavior and dynamic fragility in polylactides containing mobile and rigid amorphous fractions’, *Polymer*, 49 (20), pp. 4427-4432.

[98] Modi, S.J. (2010) *Assessing the Feasibility of Poly-(3-hydroxybutyrate-co-3-hydroxyvalerate) (PHBV) and Poly-(lactic acid) for Potential Food Packaging Applications*. MSci. Thesis. The Ohio State University. Available at: https://etd.ohiolink.edu/rws_etd/document/get/osu1268921056/inline (Accessed: 06 May 2016).

[99] Wunderlich, B. (2003) ‘Reversible crystallization and the rigid-amorphous phase in semicrystalline macromolecules’, *Progress in Polymer Science*, 28 (3), pp. 383-450.

[100] Callister, W.D. Jr. and Rethwisch, D.G. (2008) *Fundamentals of Materials Science and Engineering: An Integrated Approach*. 3rd ed. Hoboken, N.J.: John Wiley & Sons. pp. 272-273.

[101] Gogolewski, S., Jovanovic, M. and Perren, S.M. *et al*. (1993) ‘Tissue response and in vivo degradation of selected polyhydroxyacids: Polylactides (PLA), poly(3-hydroxybutyrate) (PHB), and poly(3- ydroxybutyrate-co-3-hydroxyvalerate) (PHB/VA)’, *Journal of Biomedical Materials Research*, 27 (9), pp. 1135-1148.

[102] National Center for Biotechnology Information (2016) *PubChem compound database; Crotonic acid* Available at: https://pubchem.ncbi.nlm.nih.gov/compound/637090 (Accessed: 4 October 2016).

[103] Terada, M. and Marchessault, R.H. (1999) ‘Determination of solubility parameters for poly(3-hydroxyalkanoates)’, *International Journal of Biological Macromolecules*, 25 (1-3), pp. 207-215.

APPENDIX A

Poster presented at the Young Researchers Meeting, Nottingham (2013)

APPENDIX B

DSC Experimental Data

Table B1. Enthalpy of fusion. Experimental data for all storage temperatures over time.

Enthalpy of fusion, J/g								
Time, hours	Storage temperature, °C							
	-22	7	20	50	75	100	125	150
UC	89.27 (±0.53)	89.27 (±0.53)	89.27 (±0.53)	89.27 (±0.53)	91.86 (±4.32)	91.86 (±4.32)	94.22 (±1.33)	94.22 (±1.33)
1	*nt*	*nt*	*nt*	*nt*	100.70 (±1.14)	102.04 (±0.49)	102.52 (±1.14)	100.22 (±2.00)
3	*nt*	*nt*	*nt*	*nt*	*nt*	*nt*	104.45 (±0.18)	104.33 (±0.45)
6	*nt*	*nt*	*nt*	*nt*	103.02 (±0.64)	104.17 (±1.08)	107.03 (±1.35)	104.97 (±1.38)
12	*nt*	*nt*	*nt*	*nt*	*nt*	103.90 (±0.82)	*nt*	*nt*
24	89.59 (±1.61)	89.67 (±2.77)	85.55 (±4.67)	98.05 (±4.18)	104.90 (±2.38)	106.96 (±1.42)	107.87 (±0.85)	111.55 (±0.85)
48	92.50 (±2.06)	89.81 (±1.57)	90.16 (±4.21)	102.00 (±2.74)	107.43 (±1.25)	108.87 (±0.65)	108.33 (±1.56)	116.92 (±1.29)
72	91.19 (±2.43)	86.73 (±2.29)	93.14 (±2.48)	99.97 (±3.70)	102.31 (±5.74)	103.49 (±1.34)	107.69 (±2.17)	120.97 (±0.95)
96	90.18 (±2.61)	88.94 (±2.89)	95.79 (±1.48)	104.14 (±0.90)	105.71 (±3.58)	108.73 (±0.87)	109.50 (±0.83)	123.18 (±2.50)
120	92.40 (±2.35)	91.41 (±0.96)	98.29 (±1.01)	103.18 (±1.50)	106.04 (±3.31)	109.84 (±0.56)	107.70 (±1.84)	124.57 (±1.13)
144	88.95 (±2.27)	91.21 (±1.64)	96.42 (±3.20)	103.53 (±1.03)	106.93 (±1.30)	105.90 (±1.56)	109.09 (±0.55)	126.65 (±1.16)
168	88.10 (±0.91)	92.85 (±0.60)	97.09 (±2.89)	103.92 (±1.25)	108.90 (±1.72)	108.91 (±0.10)	108.83 (±3.02)	129.36 (±0.86)
336	92.04 (±1.68)	89.02 (±4.53)	100.75 (±2.42)	106.07 (±1.09)	107.56 (±0.74)	101.35 (±5.62)	113.19 (±1.39)	129.55 (±0.76)
504	87.84 (±0.77)	91.19 (±2.67)	96.08 (±3.06)	104.68 (±1.34)	108.13 (±2.52)	109.23 (±0.87)	115.12 (±0.89)	124.88 (±0.44)
672	85.66 (±3.35)	86.14 (±1.89)	95.85 (±2.13)	101.87 (±4.56)	107.90 (±1.18)	107.55 (±0.33)	114.81 (±0.24)	112.14 (±1.47)

**nt* = not tested.

**Error is to ± 1 standard deviation.

Table B2. Crystallinity. Experimental data for all storage temperatures over time.

Crystallinity, %								
Time, hours	Temperature, °C							
	-22	7	20	50	75	100	125	150
UC	61.14 (±0.37)	61.14 (±0.37)	61.14 (±0.37)	61.14 (±0.37)	62.92 (±2.96)	62.92 (±2.96)	64.53 (±0.92)	64.53 (±0.92)
1	*nt*	*nt*	*nt*	*nt*	68.98 (±0.78)	69.89 (±0.33)	70.22 (±0.78)	68.64 (±1.37)
3	*nt*	*nt*	*nt*	*nt*	*nt*	*nt*	71.54 (±0.12)	71.46 (±0.31)
6	*nt*	*nt*	*nt*	*nt*	70.56 (±0.43)	71.35 (±0.74)	73.31 (±0.93)	71.90 (±0.94)
12	*nt*	*nt*	*nt*	*nt*	*nt*	71.16 (±0.56)	*nt*	*nt*
24	61.37 (±1.10)	61.42 (±1.90)	61.13 (±2.33)	67.15 (±2.86)	71.85 (±1.63)	73.26 (±0.97)	73.88 (±0.58)	76.41 (±0.58)
48	63.35 (±1.42)	61.51 (±1.08)	61.75 (±2.88)	69.86 (±1.88)	73.58 (±0.86)	74.57 (±0.45)	74.20 (±1.07)	80.08 (±0.88)
72	62.46 (±1.66)	59.40 (±1.57)	63.80 (±1.70)	68.48 (±2.53)	70.08 (±3.93)	70.88 (±0.92)	73.76 (±1.49)	82.85 (±0.65)
96	61.77 (±1.79)	60.92 (±1.98)	65.60 (±1.02)	71.33 (±0.62)	72.40 (±2.45)	74.41 (±0.67)	75.00 (±0.57)	84.37 (±1.71)
120	63.28 (±1.61)	62.61 (±0.66)	67.32 (±0.70)	70.67 (±1.03)	72.63 (±2.27)	75.23 (±0.39)	73.77 (±1.26)	85.32 (±0.77)
144	60.93 (±1.55)	62.47 (±1.12)	66.04 (±2.19)	70.91 (±0.71)	73.24 (±0.89)	72.54 (±1.07)	74.72 (±0.38)	86.74 (±0.79)
168	60.34 (±0.62)	63.60 (±0.40)	66.50 (±1.98)	71.17 (±0.85)	74.59 (±1.18)	74.60 (±0.07)	74.54 (±2.07)	88.60 (±0.59)
336	63.04 (±1.15)	60.97 (±3.10)	69.01 (±1.66)	72.65 (±0.75)	73.67 (±0.50)	69.42 (±3.85)	77.53 (±0.96)	88.73 (±0.52)
504	60.16 (±0.52)	62.46 (±1.83)	65.81 (±2.10)	71.70 (±0.92)	74.06 (±1.72)	74.82 (±0.60)	78.85 (±0.61)	85.53 (±0.31)
672	58.67 (±2.29)	59.00 (±1.30)	65.65 (±1.46)	69.77 (±3.12)	73.90 (±0.81)	73.66 (±0.22)	78.64 (±0.17)	76.81 (±1.01)

**nt* = not tested.

**Error is to ± 1 standard deviation.

Table B3. Melting onset. Experimental data for all storage temperatures over time.

Melting onset								
Time, hours	Storage temperature, °C							
	-22	7	20	50	75	100	125	150
UC	100.52 (±3.89)	100.52 (±3.89)	100.52 (±3.89)	100.52 (±3.89)	97.68 (±11.68)	97.68 (±11.68)	92.81 (±2.76)	93.05 (±2.77)
1	*nt*	*nt*	*nt*	*nt*	90.27 (±1.46)	104.30 (±2.64)	104.13 (±2.98)	119.60 (±9.13)
3	*nt*	*nt*	*nt*	*nt*	*nt*	*nt*	110.07 (±11.47)	123.72 (±0.77)
6	*nt*	*nt*	*nt*	*nt*	92.67 (±4.01)	104.37 (±1.78)	108.49 (±13.22)	128.72 (±1.61)
12	*nt*	*nt*	*nt*	*nt*	*nt*	100.83 (±2.73)	*nt*	*nt*
24	98.63 (±4.79)	95.85 (±4.24)	103.94 (±18.71)	72.52 (±3.18)	94.51 (±3.19)	108.73 (±0.79)	106.85 (±4.20)	127.96 (±4.50)
48	97.36 (±7.76)	101.60 (±6.53)	89.02 (±17.29)	75.49 (±1.81)	91.98 (±2.83)	107.72 (±1.35)	102.93 (±4.89)	130.81 (±1.43)
72	94.33 (±4.43)	101.92 (±3.23)	52.93 (±1.48)	73.85 (±10.23)	96.53 (±3.64)	102.28 (±5.71)	110.58 (±5.77)	123.53 (±1.43)
96	92.12 (±0.96)	101.16 (±1.71)	50.46 (±2.09)	71.70 (±1.51)	92.88 (±4.47)	99.77 (±3.83)	118.73 (±1.71)	139.34 (±1.76)
120	92.94 (±0.57)	97.36 (±8.32)	50.84 (±2.48)	74.54 (±4.49)	94.88 (±4.46)	110.88 (±2.70)	111.40 (±9.33)	138.45 (±2.30)
144	102.30 (±4.38)	93.06 (±3.04)	50.77 (±5.15)	73.91 (±0.43)	96.09 (±2.96)	100.57 (±1.12)	109.88 (±5.13)	144.46 (±2.16)
168	109.69 (±5.63)	93.70 (±1.65)	50.08 (±3.83)	72.27 (±2.19)	88.94 (±8.18)	102.47 (±9.33)	123.22 (±3.44)	138.83 (±2.14)
336	96.23 (±3.91)	101.35 (±7.42)	49.83 (±1.54)	72.14 (±1.62)	96.40 (±2.36)	108.84 (±5.47)	122.08 (±2.08)	141.80 (±2.37)
504	101.35 (±1.11)	99.01 (±6.97)	59.94 (±4.45)	73.47 (±3.67)	94.39 (±4.39)	108.47 (±5.03)	123.22 (±1.70)	138.39 (±3.56)
672	104.57 (±11.65)	100.08 (±2.55)	55.58 (±3.55)	66.96 (±15.58)	97.40 (±1.07)	104.30 (±4.13)	125.23 (±1.48)	145.47 (±2.51)

**nt* = not tested.

***Error is to ± 1 standard deviation.

Table B4. Melting peak. Experimental data for all storage temperatures over time.

Melting peak (T_m)								
Time, hours	Storage temperature, °C							
	-22	7	20	50	75	100	125	150
UC	172.78 (±0.48)	172.78 (±0.48)	172.78 (±0.48)	172.78 (±0.48)	172.47 (±0.57)	172.47 (±0.57)	171.41 (±0.11)	172.94 (±0.10)
1	*nt*	*nt*	*nt*	*nt*	172.42 (±0.25)	172.94 (±0.34)	174.06 (±0.71)	176.83 (±0.34)
3	*nt*	*nt*	*nt*	*nt*	*nt*	*nt*	174.78 (±0.25)	177.83 (±0.47)
6	*nt*	*nt*	*nt*	*nt*	173.50 (±0.66)	173.67 (±0.50)	176.75 (±2.10)	177.69 (±0.27)
12	*nt*	*nt*	*nt*	*nt*	*nt*	174.17 (±0.14)	*nt*	*nt*
24	171.67 (±0.00)	171.39 (±0.48)	175.28 (±2.68)	174.17 (±0.00)	173.50 (±0.47)	174.36 (±0.63)	174.94 (±0.13)	179.64 (±1.10)
48	172.22 (±0.48)	171.39 (±0.96)	172.78 (±0.96)	173.05 (±0.48)	174.03 (±0.24)	174.70 (±0.21)	175.83 (±0.55)	179.72 (±0.18)
72	173.06 (±0.96)	172.22 (±0.96)	172.78 (±0.96)	174.44 (±0.96)	174.33 (±0.60)	174.81 (±0.13)	176.03 (±0.46)	179.92 (±0.60)
96	171.39 (±0.48)	172.50 (±0.83)	171.95 (±0.48)	172.22 (±0.48)	173.64 (±0.17)	174.86 (±0.17)	176.44 (±1.71)	179.92 (±0.25)
120	171.11 (±0.48)	171.39 (±0.48)	171.67 (±0.00)	172.78 (±1.27)	173.67 (±0.28)	176.00 (±1.80)	175.83 (±0.38)	180.00 (±0.43)
144	171.39 (±0.48)	171.39 (±0.48)	172.22 (±0.48)	172.22 (±0.96)	173.81 (±0.10)	175.06 (±0.78)	175.58 (±0.58)	179.45 (±0.05)
168	171.11 (±0.48)	173.06 (±1.73)	172.22 (±0.96)	173.61 (±0.48)	173.44 (±0.32)	174.58 (±0.34)	176.53 (±0.46)	179.36 (±0.17)
336	170.55 (±0.48)	171.11 (±0.48)	170.83 (±0.84)	172.78 (±0.48)	174.25 (±1.04)	176.06 (±1.42)	177.00 (±1.04)	176.67 (±0.29)
504	172.22 (±0.96)	171.67 (±0.84)	174.72 (±2.55)	173.05 (±0.48)	173.97 (±0.24)	174.53 (±0.18)	176.47 (±0.09)	173.42 (±0.42)
672	172.50 (±0.00)	172.50 (±0.83)	172.50 (±0.00)	173.61 (±0.48)	173.89 (±0.27)	176.03 (±1.21)	176.00 (±0.50)	169.17 (±0.22)

**nt* = not tested.
**Error is to ± 1 standard deviation.

Table B5. Last trace of crystallinity. Experimental data for all storage temperatures over time.

Last trace of crystallinity								
Time, hours	Storage temperature, °C							
	-22	7	20	50	75	100	125	150
UC	202.81 (±1.84)	202.81 (±1.84)	202.81 (±1.84)	202.81 (±1.84)	192.63 (±2.84)	192.63 (±2.84)	197.07 (±4.03)	197.47 (±4.05)
1	*nt*	*nt*	*nt*	*nt*	196.27 (±2.32)	203.92 (±4.56)	201.23 (±1.36)	200.44 (±1.85)
3	*nt*	*nt*	*nt*	*nt*	*nt*	*nt*	199.83 (±2.59)	204.13 (±2.01)
6	*nt*	*nt*	*nt*	*nt*	199.68 (±4.86)	203.98 (±0.86)	205.65 (±0.88)	205.46 (±4.92)
12	*nt*	*nt*	*nt*	*nt*	*nt*	198.99 (±4.47)	*nt*	*nt*
24	196.17 (±0.76)	195.41 (±2.66)	200.40 (±1.47)	202.80 (±8.27)	202.71 (±3.88)	200.32 (±5.73)	206.03 (±0.90)	206.09 (±0.76)
48	201.29 (±3.59)	200.72 (±5.60)	198.70 (±7.07)	200.03 (±5.55)	204.36 (±2.85)	202.90 (±0.34)	206.03 (±0.29)	201.76 (±4.94)
72	201.67 (±1.72)	197.30 (±0.94)	199.27 (±6.95)	202.49 (±8.35)	200.06 (±2.61)	201.77 (±2.77)	203.44 (±2.18)	204.77 (±1.80)
96	200.28 (±2.69)	200.21 (±4.44)	205.59 (±1.52)	206.79 (±5.68)	202.05 (±3.31)	197.22 (±1.77)	202.74 (±2.48)	205.65 (±3.69)
120	199.58 (±4.34)	200.03 (±4.39)	205.08 (±2.96)	205.52 (±2.95)	199.49 (±1.97)	199.87 (±2.00)	199.06 (±3.70)	204.89 (±3.80)
144	192.94 (±1.64)	196.04 (±3.27)	203.63 (±4.34)	204.07 (±3.13)	203.47 (±2.39)	198.42 (±1.92)	199.20 (±2.66)	202.81 (±2.52)
168	200.34 (±1.11)	200.28 (±0.87)	202.24 (±1.37)	206.98 (±4.18)	201.45 (±4.34)	203.73 (±0.81)	204.01 (±1.86)	205.97 (±4.12)
336	201.73 (±3.41)	200.85 (±3.98)	204.96 (±4.95)	207.93 (±2.90)	203.22 (±5.17)	205.36 (±1.52)	204.20 (±3.62)	207.23 (±2.03)
504	194.52 (±2.58)	200.09 (±3.66)	202.11 (±2.58)	202.80 (±5.33)	202.93 (±3.61)	201.26 (±5.62)	207.10 (±2.69)	203.18 (±1.98)
672	192.06 (±2.40)	193.77 (±0.61)	196.74 (±1.37)	201.16 (±5.85)	203.89 (±3.52)	202.78 (±2.60)	200.76 (±2.33)	190.79 (±1.68)

**nt* = not tested.

**Error is to ± 1 standard deviation.

APPENDIX C

IR Crystallinity Index Experimental Data

Table C1. Crystallinity index. Experimental data for all storage temperatures over time.

Crystallinity index																
Time, hours	Storage temperature, °C															
	-22		7		20		50		75		100		125		150	
UC	4.93	(±0.03)	4.93	(±0.03)	4.93	(±0.03)	4.93	(±0.03)	4.67	(±0.39)	4.67	(±0.39)	5.38	(±0.03)	5.38	(±0.03)
24	4.93	(±0.12)	4.78	(±0.07)	4.86	(±0.23)	4.96	(±0.24)	5.37	(±0.08)	5.27	(±0.17)	5.30	(±0.17)	5.66	(±0.21)
48	4.99	(±0.15)	4.74	(±0.07)	4.99	(±0.15)	4.97	(±0.15)	5.27	(±0.45)	4.92	(±0.18)	5.37	(±0.29)	5.49	(±0.05)
72	4.84	(±0.09)	4.57	(±0.23)	5.05	(±0.11)	4.81	(±0.09)	5.49	(±0.34)	5.32	(±0.20)	5.45	(±0.37)	5.85	(±0.14)
96	4.93	(±0.15)	4.88	(±0.06)	5.05	(±0.15)	4.95	(±0.26)	5.25	(±0.10)	5.47	(±0.20)	5.50	(±0.23)	6.03	(±0.07)
120	4.81	(±0.12)	5.00	(±0.04)	4.97	(±0.28)	4.78	(±0.41)	5.17	(±0.33)	5.31	(±0.41)	5.65	(±0.22)	6.27	(±0.04)
144	4.88	(±0.21)	5.07	(±0.05)	5.06	(±0.09)	5.04	(±0.13)	5.33	(±0.10)	5.10	(±0.09)	5.79	(±0.16)	6.21	(±0.25)
168	4.90	(±0.07)	4.91	(±0.05)	5.08	(±0.36)	5.29	(±0.06)	5.08	(±0.16)	5.27	(±0.07)	5.69	(±0.10)	5.95	(±0.19)
192	4.64	(±0.49)	4.95	(±0.04)	5.18	(±0.21)	5.13	(±0.07)	5.42	(±0.11)	5.47	(±0.22)	5.63	(±0.24)	6.33	(±0.06)
216	5.02	(±0.17)	5.04	(±0.10)	5.08	(±0.11)	5.40	(±0.13)	5.55	(±0.22)	5.37	(±0.20)	5.70	(±0.10)	6.36	(±0.38)
240	5.09	(±0.23)	4.97	(±0.26)	5.21	(±0.12)	5.26	(±0.17)	5.14	(±0.25)	5.30	(±0.22)	5.67	(±0.49)	6.06	(±0.60)
264	5.03	(±0.16)	5.10	(±0.08)	5.12	(±0.17)	5.07	(±0.15)	5.41	(±0.25)	5.42	(±0.11)	5.72	(±0.28)	6.70	(±0.30)
288	4.91	(±0.05)	5.12	(±0.16)	5.26	(±0.04)	5.24	(±0.07)	5.45	(±0.13)	5.43	(±0.18)	5.82	(±0.26)	6.13	(±0.21)
312	5.22	(±0.06)	5.02	(±0.23)	5.01	(±0.50)	5.17	(±0.23)	5.33	(±0.01)	5.53	(±0.12)	5.98	(±0.28)	6.37	(±0.45)
336	5.04	(±0.20)	4.89	(±0.32)	5.24	(±0.20)	5.17	(±0.32)	5.14	(±0.19)	5.64	(±0.02)	5.60	*na*	5.99	*na*

*Error is to ± 1 standard deviation.
***na* = not applicable. Single sample run.
****nt* = not tested.

Table C1 continued. Crystallinity index. Experimental data for all storage temperatures over time.

Crystallinity index														
Time, hours	Storage temperature, °C													
	-22		7		20		50		75		100		125		150	
360	4.60	(±0.54)	4.54	(±0.35)	5.02	(±0.27)	5.36	(±0.19)	5.15	(±0.43)	5.33	(±0.15)	5.72	(±0.19)	6.69	(±0.13)
384	4.76	(±0.35)	4.48	(±0.15)	4.79	(±0.35)	5.14	(±0.15)	5.38	(±0.29)	5.51	(±0.19)	5.85	(±0.28)	6.42	(±0.31)
408	4.89	(±0.18)	4.74	(±0.08)	5.15	(±0.21)	5.17	(±0.30)	5.20	(±0.44)	5.17	(±0.27)	5.77	(±0.31)	6.48	(±0.22)
432	4.74	(±0.15)	4.71	(±0.64)	5.20	(±0.17)	5.27	(±0.24)	5.15	(±0.43)	5.21	(±0.31)	5.46	(±0.38)	6.51	(±0.41)
456	4.99	(±0.03)	4.88	(±0.15)	4.75	(±0.54)	5.13	(±0.11)	5.35	(±0.15)	5.27	(±0.25)	5.77	(±0.21)	6.82	(±0.25)
480	5.02	(±0.24)	5.17	(±0.29)	4.61	(±0.59)	5.18	(±0.24)	4.94	(±0.16)	5.10	(±0.37)	6.00	(±0.13)	6.70	(±0.33)
504	4.69	(±0.47)	5.01	(±0.31)	4.98	(±0.36)	5.05	(±0.32)	5.37	(±0.18)	5.49	(±0.15)	6.33	*na*	6.68	*na*
528	4.72	(±0.17)	4.59	(±0.49)	4.87	(±0.13)	5.29	(±0.29)	5.18	(±0.07)	5.25	(±0.38)	5.47	(±0.08)	6.38	(±0.31)
552	4.66	(±0.28)	4.77	(±0.24)	5.05	(±0.04)	4.93	(±0.43)	5.17	(±0.28)	5.42	(±0.27)	5.38	(±0.10)	6.15	(±0.23)
576	4.78	(±0.33)	4.70	(±0.10)	4.72	(±0.14)	5.00	(±0.24)	5.13	(±0.12)	5.64	(±0.12)	5.57	(±0.24)	6.14	(±0.35)
600	4.84	(±0.12)	4.62	(±0.15)	5.00	(±0.22)	5.08	(±0.18)	5.02	(±0.33)	5.08	(±0.31)	6.02	(±0.08)	6.13	(±0.10)
624	4.75	(±0.19)	4.83	(±0.21)	4.92	(±0.23)	5.11	(±0.31)	5.17	(±0.24)	5.20	(±0.29)	5.84	(±0.33)	5.87	(±0.74)
648	4.90	(±0.22)	5.03	(±0.17)	4.67	(±0.10)	4.85	(±0.35)	5.36	(±0.24)	5.37	(±0.37)	5.82	(±0.27)	5.83	(±0.34)
672	4.91	(±0.15)	4.95	(±0.33)	4.90	(±0.11)	5.30	(±0.34)	5.54	(±0.15)	5.36	(±0.11)	5.46	*na*	*nt*	

*Error is to ± 1 standard deviation.
***na* = not applicable. Single sample run.
****nt* = not tested.

APPENDIX D

DMTA Experimental Data

Table D1. T_g from tanδ. Experimental data for all storage temperatures over time.

T_g, °C									
Time, hours	Storage temperature, °C								
	-22	7	20	50	75	100	125	150	
UC	16.50	16.50	16.50	15.90	15.10	15.10	15.80	15.83	(±0.30)
24	17.00	17.50	19.10	21.00	23.90	24.70	23.50	20.60	(±0.30)
168	16.20	15.60	16.90	22.30	23.80	25.70	24.70	30.23	(±0.32)
336	16.50	16.60	18.60	23.10	24.10	23.90	25.30	25.73	(±1.58)
504	16.20	17.60	20.20	24.10	24.00	25.90	25.30	19.80	(±0.76)
672	17.60	18.50	21.40	24.10	27.60	27.20	29.70	13.90	(±0.42)

*Error is to ± 1 standard deviation.

Table D2. Tanδ peak height. Experimental data for all storage temperatures over time.

Tanδ peak height									
Time, hours	Storage temperature, °C								
	-22	7	20	50	75	100	125	150	
UC	0.087	0.087	0.092	0.083	0.079	0.079	0.076	0.084	(±0.0014)
24	0.083	0.079	0.075	0.061	0.067	0.081	0.095	0.107	(±0.0038)
168	0.085	0.072	0.064	0.063	0.065	0.075	0.083	0.053	(±0.0015)
336	0.092	0.071	0.061	0.053	0.065	0.077	0.081	0.035	(±0.0071)
504	0.086	0.071	0.057	0.056	0.058	0.071	0.072	0.027	(±0.0023)
672	0.086	0.063	0.051	0.052	0.063	0.072	0.063	0.030	(±0.0007)

*Error is to ± 1 standard deviation.

Table D3. Tanδ peak width. Experimental data for all storage temperatures over time.

Tanδ peak width, °C								
Time, hours	Storage temperature, °C							
	-22	7	20	50	75	100	125	150
UC	20.5	20.5	20.5	20.0	19.5	19.5	18.5	20.17 (±0.29)
24	20.0	21.5	20.5	20.0	20.5	21.0	22.0	19.67 (±0.29)
168	20.5	18.0	18.5	20.5	20.5	21.0	20.5	28.17 (±2.25)
336	21.0	18.5	18.5	19.0	20.0	20.5	21.0	35.83 (±3.33)
504	20.5	18.5	20.0	20.0	19.5	20.5	21.5	35.00 (±1.00)
672	21.0	18.0	18.0	19.5	19.5	19.5	20.5	33.75 (±4.60)

*Error is to ± 1 standard deviation.

Table D4. Distribution of the tanδ peak area. Experimental data for all storage temperatures over time.

Distribution of the tanδ peak area, %								
Time, hours	Storage temperature, °C							
	-22	7	20	50	75	100	125	150
UC	60.1	60.1	60.1	57.2	58.7	58.7	55.7	60.8 (±0.91)
24	59.1	57.2	55.2	51.7	53.7	54.8	59.1	56.6 (±1.18)
168	60.1	57.6	53.2	51.1	53.5	54.8	52.7	50.8 (±2.75)
336	58.7	53.2	53.4	55.1	52.5	53.0	56.5	54.6 (±3.17)
504	60.1	53.2	54.4	49.9	53.6	58.3	51.1	56.3 (±2.27)
672	59.1	54.9	54.8	49.9	51.4	50.6	50.8	57.7 (±3.73)

*Error is to ± 1 standard deviation.

Table D5. T_g from E′. Experimental data for all storage temperatures over time.

T_g, °C									
Time, hours	Storage temperature, °C								
	-22	7	20	50	75	100	125	150	
UC	0.30	0.30	0.30	-0.40	-0.40	-0.40	1.50	0.30	(±0.12)
24	0.50	0.30	2.30	4.50	4.80	8.10	6.00	5.63	(±1.07)
168	0.60	0.00	2.60	5.00	5.30	7.60	5.80	4.20	(±0.47)
336	2.00	0.30	2.00	4.50	6.00	5.30	7.00	-3.63	(±2.45)
504	0.50	1.30	2.50	5.30	4.60	9.00	8.50	-7.63	(±2.06)
672	1.30	3.00	5.30	3.30	9.00	9.30	7.50	-14.25	(±5.30)

*Error is to ± 1 standard deviation.

Table D6. Secondary relaxation peak temperature. Experimental data for samples stored at 7 and 20 °C over time.

Secondary relaxation peak temperature, °C		
Time, hours	Storage temperature, °C	
	7	20
UC	-	-
24	-	49.3
168	32	46.6
336	35.8	49
504	41.3	51.5
672	43.5	55.3

APPENDIX E

Mechanical Testing Experimental Data

Table E1. Young's Modulus. Experimental data for all storage temperatures over time.

Young's Modulus, MPa								
Time, hours	Storage temperature, °C							
	-22	7	20	50	75	100	125	150
UC	1346 (±70)	1346 (±70)	1346 (±70)	1346 (±70)	1375 (±46)	1168 (±133)	1302 (±37)	1236 (±37)
24	1367 (±42)	1406 (±23)	1644 (±56)	1793 (±41)	1806 (±27)	1633 (±52)	1458 (±20)	1224 (±9)
48	1292 (±17)	1361 (±37)	1614 (±23)	1801 (±53)	1729 (±110)	1721 (±24)	1469 (±29)	*nt*
72	1227 (±39)	1399 (±10)	1657 (±42)	1840 (±21)	1926 (±30)	1677 (±87)	1454 (±42)	*nt*
96	1377 (±55)	1458 (±8)	1810 (±14)	1942 (±14)	1878 (±41)	1772 (±34)	1550 (±40)	*nt*
120	1320 (±37)	1506 (±14)	1773 (±13)	1950 (±29)	2008 (±29)	1736 (±43)	1536 (±16)	*nt*
144	1266 (±32)	1541 (±47)	1801 (±22)	2060 (±85)	2062 (±14)	1779 (±73)	1554 (±47)	*nt*
168	1338 (±48)	1596 (±7)	1869 (±16)	2067 (±49)	1955 (±45)	1859 (±30)	1599 (±27)	*nt*

*nt = not tested.
**Error is to ± 1 standard deviation.

Table E2. UTS. Experimental data for all storage temperatures over time.

UTS, MPa								
Time, hours	Storage temperature, °C							
	-22	7	20	50	75	100	125	150
UC	31.41 (±1.34)	31.41 (±1.34)	31.41 (±1.34)	31.41 (±1.34)	31.96 (±0.33)	31.46 (±0.79)	31.60 (±0.86)	31.38 (±0.29)
24	32.28 (±0.64)	31.57 (±0.49)	32.73 (±0.88)	34.49 (±1.06)	35.60 (±0.74)	34.11 (±0.62)	33.36 (±0.31)	24.30 (±1.27)
48	31.32 (±0.95)	31.50 (±0.35)	31.69 (±0.54)	34.98 (±0.78)	33.85 (±2.32)	34.83 (±0.76)	33.61 (±0.15)	*nt*
72	30.51 (±0.79)	32.08 (±0.63)	32.67 (±0.66)	36.43 (±0.41)	36.50 (±1.30)	35.70 (±1.48)	33.62 (±0.44)	*nt*
96	31.55 (±0.06)	31.76 (±0.51)	33.38 (±0.88)	37.73 (±0.73)	37.23 (±0.80)	35.06 (±1.49)	33.68 (±0.14)	*nt*
120	30.74 (±0.99)	31.55 (±0.30)	32.47 (±0.57)	36.25 (±1.50)	37.39 (±0.47)	35.58 (±1.43)	32.89 (±0.60)	*nt*
144	30.60 (±0.18)	31.69 (±1.10)	33.62 (±0.46)	37.32 (±0.84)	37.99 (±0.50)	34.82 (±0.78)	32.32 (±0.96)	*nt*
168	30.54 (±0.21)	31.65 (±0.95)	33.83 (±0.31)	37.68 (±0.26)	36.65 (±0.80)	35.39 (±1.03)	32.45 (±0.46)	*nt*

*nt = not tested.
**Error is to ± 1 standard deviation.

Table E3. Elongation to break. Experimental data for all storage temperatures over time.

Elongation to break, %								
Time, hours	Storage temperature, °C							
	-22	7	20	50	75	100	125	150
UC	16.9 (±6.70)	16.9 (±6.70)	16.9 (±6.70)	16.9 (±6.70)	13.2 (±1.48)	11.9 (±3.30)	14.6 (±3.22)	19.4 (±2.94)
24	16.9 (±0.86)	15.8 (±3.98)	13.1 (±3.90)	8.2 (±3.02)	6.1 (±0.49)	7.7 (±1.48)	9.7 (±0.34)	4.1 (±0.69)
48	21.6 (±6.69)	12.2 (±3.65)	9.2 (±1.36)	6.7 (±0.94)	6.2 (±1.54)	6.9 (±0.18)	12.1 (±2.77)	*nt*
72	13.8 (±7.40)	14.4 (±4.66)	11.1 (±4.37)	6.9 (±1.63)	6.1 (±1.57)	7.4 (±1.38)	10.7 (±1.40)	*nt*
96	14.6 (±1.91)	16.7 (±2.44)	6.2 (±0.40)	6.7 (±1.11)	8.0 (±2.05)	6.7 (±1.30)	10.3 (±0.72)	*nt*
120	17.2 (±8.02)	11.2 (±1.53)	9.9 (±6.85)	6.3 (±1.96)	7.8 (±1.43)	7.5 (±1.04)	8.3 (±2.22)	*nt*
144	19.1 (±4.96)	12.7 (±3.87)	10.9 (±1.48)	6.3 (±0.94)	5.8 (±1.22)	5.9 (±1.33)	6.9 (±0.82)	*nt*
168	13.8 (±5.52)	10.1 (±1.88)	9.3 (±3.80)	7.0 (±0.29)	5.8 (±0.99)	5.9 (±1.46)	6.8 (±0.97)	*nt*

*nt = not tested.
**Error is to ± 1 standard deviation.

APPENDIX F

Mass Loss Experimental Data

Table F1. Sample mass as a percentage of the unconditioned values. Experimental data from hot pressed samples for all storage temperatures over time.

Mass, %								
Time, hours	Storage temperature, °C							
	-22	7	20	50	75	100	125	150
UC	100.00 (±0.00)	100.00 (±0.00)	100.00 (±0.00)	100.00 (±0.00)	100.00 (±0.00)	100.00 (±0.00)	100.00 (±0.00)	100.00 (±0.00)
24	100.00 (±0.00)	100.01 (±0.02)	100.00 (±0.00)	99.87 (±0.00)	99.79 (±0.02)	99.73 (±0.00)	99.74 (±0.02)	99.57 (±0.00)
48	99.98 (±0.02)	100.01 (±0.02)	100.00 (±0.00)	99.87 (±0.00)	99.81 (±0.02)	99.77 (±0.00)	99.70 (±0.00)	99.47 (±0.00)
72	100.00 (±0.00)	100.03 (±0.00)	100.00 (±0.00)	99.87 (±0.00)	99.83 (±0.00)	99.78 (±0.02)	99.69 (±0.02)	99.37 (±0.00)
96	99.99 (±0.02)	100.03 (±0.00)	100.00 (±0.00)	99.87 (±0.00)	99.81 (±0.02)	99.76 (±0.02)	99.67 (±0.04)	99.21 (±0.04)
120	99.97 (±0.00)	100.04 (±0.02)	100.00 (±0.00)	99.86 (±0.02)	99.83 (±0.03)	99.77 (±0.00)	99.65 (±0.02)	98.99 (±0.04)
144	99.98 (±0.02)	100.04 (±0.02)	100.00 (±0.00)	99.87 (±0.00)	99.81 (±0.02)	99.74 (±0.02)	99.64 (±0.04)	98.69 (±0.04)
168	99.98 (±0.02)	100.04 (±0.02)	100.00 (±0.00)	99.86 (±0.02)	99.82 (±0.02)	99.72 (±0.02)	99.63 (±0.04)	98.33 (±0.04)
192	*nt*	*nt*	*nt*	*nt*	*nt*	*nt*	99.60 (±0.04)	97.84 (±0.05)
216	*nt*	*nt*	*nt*	*nt*	*nt*	*nt*	99.61 (±0.02)	97.26 (±0.06)
240	*nt*	*nt*	*nt*	*nt*	*nt*	*nt*	99.59 (±0.02)	96.59 (±0.05)
264	*nt*	*nt*	*nt*	*nt*	*nt*	*nt*	99.57 (±0.04)	95.79 (±0.06)
288	*nt*	*nt*	*nt*	*nt*	*nt*	*nt*	99.55 (±0.02)	94.89 (±0.09)
312	*nt*	*nt*	*nt*	*nt*	*nt*	*nt*	99.59 (±0.02)	93.93 (±0.11)

**nt* = not tested.
**Error is to ± 1 standard deviation.

Table F1 continued. Sample mass as a percentage of the unconditioned values. Experimental data from hot pressed samples for all storage temperatures over time.

Mass, %								
Time, hours	Storage temperature, °C							
	-22	7	20	50	75	100	125	150
336	99.97 (±0.00)	100.03 (±0.00)	99.97 (±0.00)	99.86 (±0.02)	99.81 (±0.04)	99.72 (±0.02)	99.54 (±0.04)	92.81 (±0.11)
360	*nt*	*nt*	*nt*	*nt*	*nt*	*nt*	99.48 (±0.04)	91.55 (±0.13)
384	*nt*	*nt*	*nt*	*nt*	*nt*	*nt*	99.48 (±0.04)	90.19 (±0.14)
408	*nt*	*nt*	*nt*	*nt*	*nt*	*nt*	99.48 (±0.04)	88.93 (±0.17)
432	*nt*	*nt*	*nt*	*nt*	*nt*	*nt*	99.48 (±0.04)	87.53 (±0.17)
456	*nt*	*nt*	*nt*	*nt*	*nt*	*nt*	99.45 (±0.06)	85.86 (±0.22)
480	*nt*	*nt*	*nt*	*nt*	*nt*	*nt*	99.44 (±0.04)	84.26 (±0.22)
504	99.89 (±0.02)	100.01 (±0.02)	99.93 (±0.00)	99.87 (±0.00)	99.80 (±0.03)	99.73 (±0.03)	99.44 (±0.04)	82.65 (±0.20)
528	*nt*	*nt*	*nt*	*nt*	*nt*	*nt*	99.44 (±0.04)	80.93 (±0.20)
552	*nt*	*nt*	*nt*	*nt*	*nt*	*nt*	99.44 (±0.04)	79.24 (±0.20)
576	*nt*	*nt*	*nt*	*nt*	*nt*	*nt*	99.44 (±0.04)	77.39 (±0.20)
600	*nt*	*nt*	*nt*	*nt*	*nt*	*nt*	99.41 (±0.05)	75.59 (±0.20)
624	*nt*	*nt*	*nt*	*nt*	*nt*	*nt*	99.40 (±0.06)	73.65 (±0.20)
648	*nt*	*nt*	*nt*	*nt*	*nt*	*nt*	99.41 (±0.05)	71.71 (±0.20)
672	99.94 (±0.02)	100.07 (±0.00)	99.92 (±0.02)	99.86 (±0.02)	99.77 (±0.03)	99.67 (±0.03)	99.38 (±0.05)	69.65 (±0.19)

**nt* = not tested.

***Error is to ± 1 standard deviation.

Table F2. Sample mass as a percentage of the unconditioned values. Experimental data from the P(HB-co-HV) pellets, as supplied, for all storage temperatures over time.

Mass, %					
Time, hours	Storage temperature, °C				
	-22	7	20	50	150
UC	100.00 (±0.00)	100.00 (±0.00)	100.00 (±0.00)	100.00 (±0.00)	100.00 (±0.00)
24	100.01 (±0.02)	100.04 (±0.00)	99.96 (±0.10)	99.86 (±0.02)	99.55 (±0.04)
48	100.05 (±0.02)	100.05 (±0.02)	99.99 (±0.12)	99.86 (±0.02)	99.50 (±0.04)
72	100.05 (±0.02)	100.05 (±0.02)	99.96 (±0.10)	99.83 (±0.02)	99.48 (±0.04)
96	100.03 (±0.02)	100.05 (±0.02)	99.95 (±0.12)	99.85 (±0.04)	99.40 (±0.04)
120	100.05 (±0.02)	100.05 (±0.02)	99.97 (±0.11)	99.85 (±0.04)	99.31 (±0.05)
144	100.05 (±0.02)	100.08 (±0.00)	99.95 (±0.12)	99.86 (±0.02)	99.22 (±0.04)
168	100.05 (±0.02)	100.09 (±0.02)	99.97 (±0.11)	99.86 (±0.02)	99.09 (±0.06)
192	*nt*	*nt*	*nt*	*nt*	98.92 (±0.04)
216	*nt*	*nt*	*nt*	*nt*	98.70 (±0.04)
240	*nt*	*nt*	*nt*	*nt*	98.36 (±0.03)
264	*nt*	*nt*	*nt*	*nt*	98.01 (±0.06)
288	*nt*	*nt*	*nt*	*nt*	97.58 (±0.03)
312	*nt*	*nt*	*nt*	*nt*	97.09 (±0.03)
336	100.09 (±0.02)	100.10 (±0.02)	100.00 (±0.10)	99.86 (±0.02)	96.49 (±0.06)
504	100.09 (±0.02)	100.13 (±0.02)	100.00 (±0.10)	99.83 (±0.02)	89.50 (±0.09)
672	100.09 (±0.02)	100.13 (±0.02)	100.00 (±0.10)	99.86 (±0.02)	80.94 (±0.11)

*_nt_ = not tested.
**Error is to ± 1 standard deviation.